The photoconductive and luminescent properties of cadmium sulphide

M. A. Carter

THE PHOTOCONDUCTIVE AND LUMINESCENT PROPERTIES OF CADMIUM SULPHIDE

by

M.A. Carter, B.Sc.

A thesis presented to the UNIVERSITY OF DURHAM in support of the author's candidature for the degree of Doctor of Philosophy.

August 1971

ABSTRACT

An evaluation is presented of some of the photoconductive and luminescent properties of CdS crystals grown by sublimation in sealed tubes under excess pressures of cadmium and sulphur. It is demonstrated that the use of impure starting material, for crystal growth, can lead to anomalous results.

Eight discrete sets of electron traps were found in the present samples using the thermally stimulated current technique. The trapping parameters and the variation of trap density with growth conditions are given in the text. It is suggested that one of these traps, which had a thermal activation energy of 0.15 eV, is associated with cadmium interstitials. The densities of two traps, with activation energies of 0.53 eV and 0.60 eV, changed in magnitude when differing conditions of illumination were used prior to measurement. Such changes are shown to be commensurate with traps of a photochemical nature. Three and four probe measurements are also described, which were made to determine how the crystal surface and the indium contacts modify the thermally stimulated current.

Considerable differences were found in the spectral response and infrared quenching of photocurrent measured on cadmium and sulphur rich samples. A disparity was found between the thermal and optical separations of the sensitising Class 11 centres from the valence band, which indicates that these centres are singly negatively charged when occupied by electrons.

The structured luminescence, in the region 1.6 μm to 2.0 μm, has been attributed to radiative recombination of electrons from the sensitising Class 11 centres with holes in the upper branches of the valence band.

ACKNOWLEDGEMENTS

The author is indepted to Professor D.A. Wright for providing the laboratory facilities and to the U.K. Ministry of Defence for the financial support, without which this research would not have been possible.

The author would like to express his sincere thanks to Dr. J. Woods for his help, guidance and encouragement throughout the work.

The author also wishes to acknowledge the assistance and co-operation of his colleagues in the Department of Applied Physics, and to thank Mr. F. Spence and his staff for their help in the construction and development of the apparatus.

INDEX OF CONTENTS

CHAPTER 1

DEVICE APPLICATIONS AND BAND STRUCTURE OF CdS

1.1. Introduction

CdS is a member of the II-VI family of compound semiconductors, occurring naturally in the form of Greenockite. Growth of CdS from the melt requires high temperatures and pressures (of the order of 1500°C and 50 atmospheres respectively (Fahrig 1963)), so that early work was carried out on powders or on the scarce and impure natural ore. Although Lorentz (1891) reported that 'relatively large' CdS crystals could easily be grown by reacting cadmium vapour and hydrogen sulphide, it was not until Frerichs (1947) modified this method that satisfactory electrical and optical measurements were made on large numbers of synthetic CdS crystals.

In recent years the majority of synthetic CdS crystals have been grown by vapour phase techniques, either by sublimation of CdS using a carrier gas or by pulling a sealed tube containing CdS powder through a temperature gradient. Bulk CdS crystals grown in this manner are n-type and grow with the hexagonal wurtzite structure.

In this chapter some of the possible device applications of CdS will be discussed together with some of the basic physical properties such as the band structure, and the effective mass and mobility of the charge carriers.

1.2. Device Applications of CdS

The devices described in this section depend to a greater or lesser extent on the crystal quality and the concentrations of

defects in the CdS used. The major limitations to the performance of these devices are the lack of reproducibility from device to device, the time dependent variation of device characteristics which is sometimes observed, and in some cases the low device efficiency. The growth of CdS in a reproducible manner, with controlled electrical and optical properties, is of major importance when considering the manufacture of useful devices.

To achieve this end the processes involved in each device must be understood and the physical properties of the defects present under the particular conditions of manufacture should be known. Defect centres may both enhance or decrease device efficiency. A better understanding of the chemical and physical nature of the defects present in CdS should lead to the determination of the optimum conditions for device production.

The present work is concerned with the investigation of the defect structure in CdS crystals, grown by the sublimation of CdS powder in sealed tubes as described in Chapter 4. Although some of the devices discussed in this section are based on evaporated films, which have not been studied in the present work, a fuller understanding of the defect structure of single crystals is essential to the production of material, with the required properties, manufactured in different ways.

1.2.(a). CdS as a Photoconductor

Suitably prepared CdS is a sensitive photoconductor. Its resistivity may also be decreased by irradiation with alpha and beta particles, X-rays and gamma rays. The applications of CdS as a light detector are numerous. It has been used as a light meter in cameras, and also in burglar alarm systems where a constant beam of light would be interrupted by an intruder.

CdS may also be used for chart recording densitometer traces, such as those obtained from a spectrograph or electron micrograph. One of the main limitations to the use of CdS as a photoconductor is that more sensitive material has a slower response time, as is demonstrated in Chapter 2.

1.2.(b). The CdS Solar Cell

The fact that CdS samples are always n-type indicates that the observation of a photovoltaic effect requires either a heterojunction or a surface barrier contact to separate free carriers. A suitable heterojunction can be prepared by dipping an evaporated film of CdS, on its substrate, into a solution of cuprous ions for a few seconds. The film is then washed and dried at temperatures of approximately 250^{o}C for a few minutes. The result of these operations is the production of a thin film of Cu_2S on the CdS. Contact is then made to the Cu_2S and CdS layers, and in direct sunlight conversion efficiencies of 6% may be realised. The manufacture of reproducible cells is, at present, not possible. Shirland (1966) has given a comprehensive review of CdS solar cells describing their history, manufacture and performance.

Where reproducible cells are obtained, they would have the advantage of cheapness, plus the possibility that large area devices could be fabricated. The space application is perhaps obvious, where large area cells may be made on a thin plastic sheet, which could then be unfurled after the satellite cleared the Earth's atmosphere. It is also possible that the solar cell might prove an economical proposition in desert land, where conventional production of power is expensive and where the loss of power due to cloud cover would be expected to be minimal.

1.2.(c). The Thin Film Transistor

The CdS thin film transistor, Figure 1.2.1, is similar in operation to a M.O.S.T. Weimer (1962) gave a detailed account of the design considerations and potential of such devices. Thin film transistors have been manufactured by de Graaff and Koelmans (1966) by the evaporation of a 10μm wide strip of CdS onto a glass substrate. Source and drain contacts were evaporated on to either side of the CdS strip and a gate electrode was separated from the CdS by a silicon monoxide film. De Graaff and Koelmans produced devices with imput impedances of 10^4MΩ, and power amplification was obtained up to 200 Mc/sec. Two unfortunate disadvantages were found with these transistors, i.e. the device characteristics were not reproducible, and hysteresis effects were obtained.

The electrode configuration of the thin film transistor has proved, however, to be a useful tool for studying surface effects (see for example Waxman et al. (1965)).

1.2.(d). The Acousto-electric Amplifier

The principle of the acousto-electric amplifier depends on the interaction of acoustic waves travelling through a piezo-electric material with electrons driven by an external electric field. Certain acoustic waves create strong longitudinal electric fields, of piezoelectric origin, in CdS and the electrons interact with the acoustic waves via these fields. Hutson et al. (1961) first demonstrated the effect using shear waves travelling perpendicular to the c axis of CdS. They showed that for electron drift velocities less than the velocity of sound the acoustic wave was attenuated, and for drift velocities greater than the velocity of sound acoustic gain was achieved.

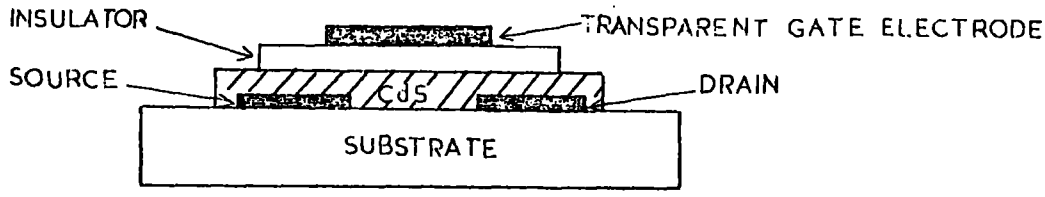

FIGURE 1.2.1 THIN FILM TRANSISTOR [WAXMAN ET AL.1966]

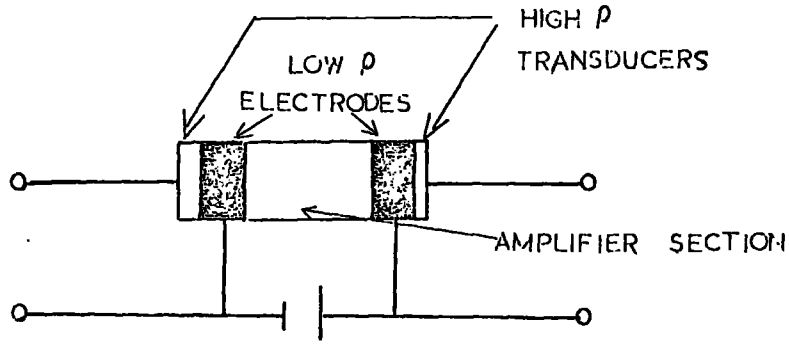

FIGURE 1.2.2 INTEGRAL STRUCTURE CdS PIEZOELECTRIC AMPLIFIER [MAY 1965]

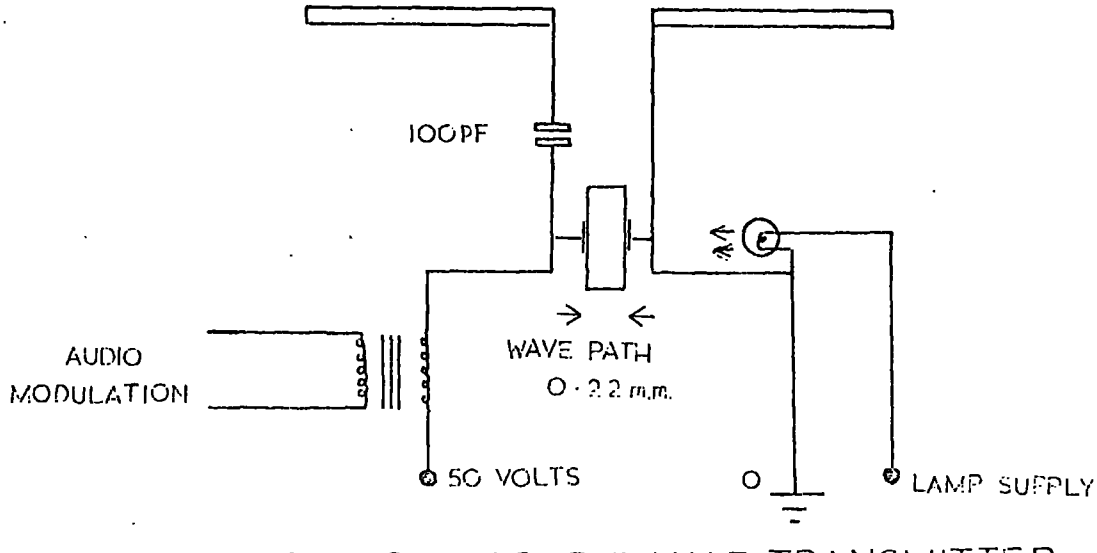

FIGURE 1.2.3 ACOUSTO-ELECTRIC V.H.F. TRANSMITTER [WIRELESS WORLD 1968]

Although acoustic gain has been observed by many workers, the main problem (apart from material control) is the loss incurred in the coupling between the transducers and the CdS sample. The best coupling has been obtained by using evaporated high resistivity CdS layers to form the transducers.

May (1965) has described the design considerations for a CdS acousto-electric amplifier. A typical device is shown in Figure 1.2.2. The electrodes are formed by evaporation of indium on to the ends of a suitable CdS bar. The transducers are formed by evaporation of high resistivity CdS on to the electrodes, which also act as the inner contacts to the transducers. It is also possible that such a device might be made by first diffusing indium in to the bar to form a low resistivity contact zone, followed by the careful diffusion of copper to form a high resistivity transducer zone. This second method has the advantage that the transducer orientation is better, and with the diffusion technique developed on other semiconductors this might well prove a viable proposition.

1.2.(e). The Acousto-electric Oscillator

Maines and Paige (1969) discuss current oscillations in thin CdS plates, from which an extremely simple acousto-electric oscillator may be fabricated. This device is illustrated in Figure 1.2.3. The 0.2 mm. CdS platelet oscillated at a frequency of 100 MHz. The signal was frequency modulated using transformer coupling, and the CdS platelet was illuminated to obtain the required resistivity of 10^3 Ωcm. Proper control of the material would mean that the sample could be suitably treated to obtain the optimum resistivity. To date, the output power of these devices has been only a few microwatts.

1.2.(f). The CdS Laser

Laser action of CdS under electron bombardment with current densities in the order of amps/cm^2, and accelerating voltages of tens or hundreds of kilovolts was first observed in 1965. Basov et al. (1965) found three sharp peaks at 5035 A^o, 4966 A^o and 4891 A^o at helium temperatures using an accelerating voltage of 200 KV and electron beam densities of about 1 amp/cm^2. They obtained a superlinear variation of emission intensity and line narrowing with increasing beam intersity. Increased directionality of the emitted light was also observed, although the Fabry-Perot cavity modes expected from a laser were not resolved. Benoit and Deverber (1965) working at helium temperatures observed the four criteria for lasing, namely those recorded by Basov et al., together with the resolution of the Fabry-Perot modes. The maximum emission was found in the region of 4910 A^o, with current densities of about 5 amps/cm^2, and accelerating voltages of 20 KV.

Nicoll (1967) has produced laser emission from CdS at room temperatures with a wavelength of 5280 A^o. The electron beam accelerating voltage and current were similar to those used by Benoit and Deverber, and the efficiency was found to be 0.1% for a beam current of 5 amp/cm^2 at 24 KV. Basov et al. (1966) reported optically stimulated laser emission from CdS at liquid nitrogen temperatures using ruby laser excitation.

1.2.(g). Anti-Stokes Emission from CdS

The excitation of green edge emission from CdS at nitrogen temperatures with photons of less than band gap energy was first reported by Halsted et al. (1959). They obtained an efficiency of 0.5% for conversion of light with wavelengths greater than 7000 A^o to edge emission, though correction for reflection gave

an internal efficiency of 5%. Such anti-Stokes luminescence has been investigated by a number of workers and is usually interpreted in terms of a two step process via an acceptor level lying close to the middle of the forbidden gap (Halsted et al. 1961, and Broser-Warminsky 1962). The introduction of copper impurities has been shown to enhance the anti-Stokes luminescence, though the observation of the process in undoped crystals indicates that either copper is not necessary for anti-Stokes emission or all CdS samples so far investigated contain copper as an impurity. Braunstein and Ockman (1964) used a ruby laser to excite edge emission and concluded that the excitation was due to the simultaneous absorption of two photons, as the samples they investigated were not intentionally doped.

There are two possible applications of anti-Stokes emission in CdS. The use of CdS as a red or near infrared image converter would be possible if the conversion efficiency could be increased, though the efficiency is inherently limited by the low absorption by CdS of long wavelength radiation.

Another possible application is the quantum counter discussed by Halsted et al. (1961). Figure 1.2.4 shows the energy level diagram, proposed by these workers, for photon amplification in both CdS and ZnS. They found that the rate of recombination R_{21} from the intermediate levels to the shallow acceptors is greater than the rate R_{32} at which electrons return from the conduction band to the intermediate levels. Thus, where the intermediate levels are filled by continuous excitation of energy E_{12}, a signal photon of energy E_{23} will allow a number of E_{12} photons to be absorbed.

Halsted et al. found photon amplification factors of 3 and 10 for copper doped CdS, where the optimum doping was of the order

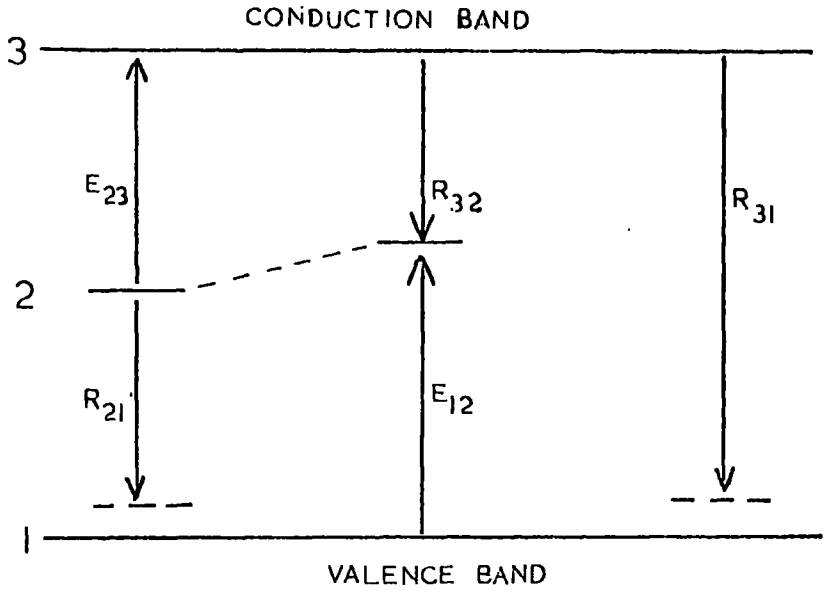

FIGURE 1.2.4. ANTISTOKE'S EMISSION—ENERGY LEVEL DIAGRAM [HALSTED ET AL. 1961]

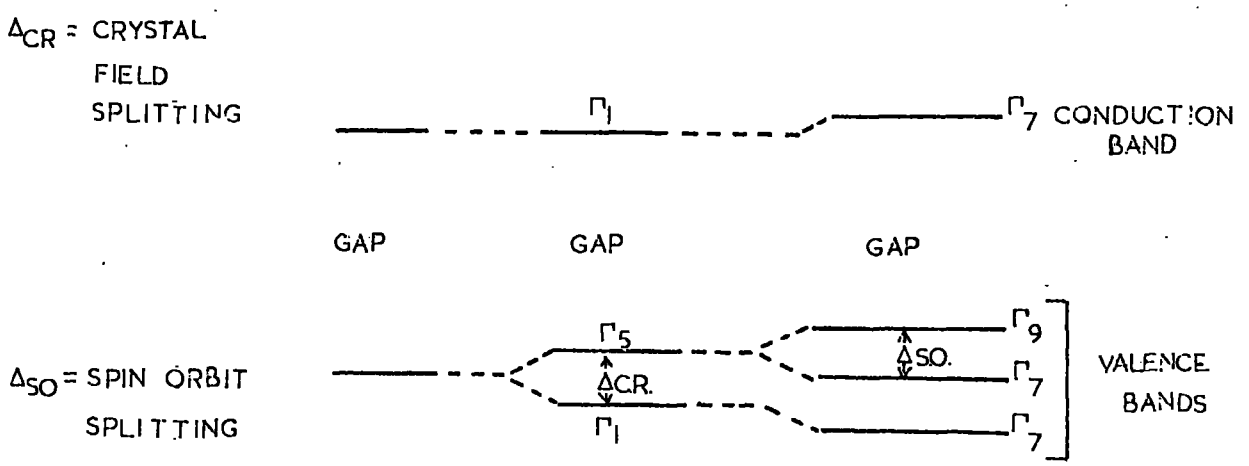

FIGURE 1.3.1. SYMMETRY AND BAND STRUCTURE OF WURTZITE [BIRMAN 1959]

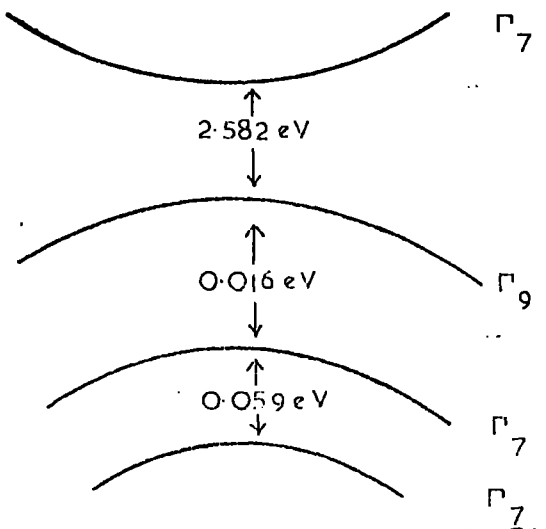

FIGURE 1.3.2 ENERGY SEPARATION OF CONDUCTION AND VALENCE BANDS IN CdS [THOMAS AND HOPFIELD 1959]

of 10 p.p.m. They confirmed that the analogous process occurs in ZnS, with higher amplification factors. They irradiated the ZnS with a continuous source of photons of energy E, where $E_{23} < E < E_{12}$, and found that the incidence of one photon of energy greater than E_{23} corresponded to the emission of 160 R_{21} photons. This output signal of 160 R_{21} photons was measured with a background 'noise' of $1.7.10^4$ photons generated by the pumping light of energy E_{12}. The rise time of R_{32} associated with the increase of the input signal E_{23} was of the order of seconds and was attributed to the influence of trapping.

1.3. The Band Structure of CdS

It was pointed out in Section 1.1 that synthetic crystals of CdS grow with a wurtzite structure. The conduction band of II-VI compounds with this crystal structure is formed from the s orbitals of the cations, and the valence band from the p orbitals of the anions. An ideal wurtzite lattice has nearest neighbour atoms in the same relative positions as the simpler zinc blende lattice. The next nearest neighbour configuration is very similar for the two structures. Differences arise for atoms at greater than next neighbour distances.

Birman (1959) obtained a qualitative picture of the conduction and valence bands at k = 0 (Γ) from considerations of the symmetry properties of these bands and the similarity between the wurtzite and zinc blende structures. He applied a perturbation to the zinc blende band structure, by considering a small non-cubic field due to atoms at distances greater than next nearest neighbour. Figure 1.3.1(a) shows the band structure in the absence of crystal field and spin orbit interactions. In Figure 1.3.1(b) the crystal field is introduced, and in

Figure 1.3.1(c) both spin orbit and crystal field splitting are considered. Birman also showed that the transition $\Gamma_7 \rightarrow \Gamma_9$ is allowed only for light polarised with its electric vector perpendicular to the c axis, though the $\Gamma_7 \rightarrow \Gamma_7$ transitions are allowed for both the electric victor parallel and perpendicular to the c axis.

Verification of this model has been obtained from the exciton structure of 'edge' emission and reflection in CdS by Thomas and Hopfield (1959). These workers observed three exciton absorption peaks at liquid nitrogen and liquid helium temperatures, which they associated with the ground states of excitons formed from the conduction band electrons and holes from the three valence bands. At helium temperature they observed two further absorption peaks due to the first excited states of two of the excitons. The lowest energy exciton absorption occurred only for $E \perp^{r}$ to the c axis and was assigned to the $\Gamma_7 \rightarrow \Gamma_9$ transition. Using Thomas and Hopfield's data, the band structure of CdS at helium temperatures is shown in Figure 1.3.2.

Balkanski and des Cloizeaux (1960) postulated a more complex band structure for wurtzite crystals. From group theoretical arguments they deduced that the conduction band would have six minima near k = 0. They calculated the energy difference between the conduction band minima and the conduction band at k = 0 and found this to be 10^{-3}eV. The results obtained by Thomas and Hopfield and the galvomagnetic measurements of Zook and Dexter (1963) are both consistent with Birman's single valleyed model of the conduction band, though the multi-valleyed model could equally well be applied. The experimental resolution necessary to distinguish these models has not yet been achieved.

The band gap of CdS decreases with increasing temperature and increases with increasing pressure. The temperature variation of the band gap is given by Bube (1960) as

$$E_G = G_0 - \lambda T \qquad (\text{where } \lambda = 5.2.10^{-4} \text{eV}/^{\circ}\text{K}) \qquad 1.3.1$$

Höhler (1949) showed that, for CdS, the temperature variation of the band gap due to thermal dilation of the lattice is about one fifth of the total variation.

CdS undergoes a phase change to the rock salt structure at about $2.4.10^4$ atmospheres (Corll 1964). Below this transition pressure the band gap, at constant temperature, is related to the pressure by

$$E_G = E_G(P = 0) + \rho P \qquad 1.3.2$$

where $\rho = 3.3.10^{-6}$ eV/atoms (Edwards et al. 1959).

1.4. Effective Masses of the Charge Carriers in CdS

The effective mass of electrons, m_e', in CdS has been measured by Baer and Dexter (1964) and Sawamoto (1964) using cyclotron resonance techniques at liquid helium temperatures. Baer and Dexter obtained values of m_e' $\perp^r$ and $||^l$ to the c axis of 0.171 m_e and 0.153 m_e respectively. These are in reasonable agreement with the mean value of 0.17 m_e found by Sawamoto.

The effective mass may also be estimated from other experiments where it is contained in the equations governing the experimentally measured quantities. As will be shown in the next section, the effective mass may be used as an adjustable parameter to fit theoretical variations of mobility to those obtained experimentally. Piper and Halsted (1961) fitted the theoretical

values for piezoelectric and polar optical mode scattering to their Hall effect measurements using $m_e' = 0.16\ m_e$. They also obtained an effective mass from a set of shallow donors, which had a thermal activation energy of 0.032 eV. Assuming these centres to be hydrogenic in nature, they estimated an effective mass of $0.20\ m_e$.

Piper and Marple (1961) studied the contribution of free electrons to the infrared absorption of gallium doped CdS. Their results yielded a value of $m_e' = 0.22\ m_e$, which was slightly anisotropic, though the anisotropy was of the same order as their experimental error. Hopfield and Thomas (1961) obtained a value of $m_e' = 0.205\ m_e$, from their studies of the exciton structure of CdS, which was anisotropic by about 5%.

Thus, the effective mass of a free electron in CdS is approximately $0.2\ m_e$ and is also slightly anisotropic.

Little information is available on the effective mass, m_h, of holes in CdS. Sawamoto found an absorption in his cyclotron resonance data consistent with an effective mass of $0.81\ m_e$. He assigned this to a heavy hole. Hopfield and Thomas estimated considerable anisotropy of hole effective masses, in the upper (Γ_7) valence band, from their exciton measurements yielding values of $m_h(\|^l \text{ to } c) = 5\ m_e$ and $m_h(\perp^r \text{ to } c) = 0.7\ m_e$. The average effective mass for a hole from these values is $1.87\ m_e$, which is in considerable disagreement with Sawamoto's result. From this limited information it may be concluded that the hole effective mass is larger than that for the electron, and is also quite anisotropic. However, as CdS grows as an n-type material, the hole effective mass is not required to understand the majority of transport processes.

1.5. Carrier Mobilities in CdS

The mobility of a free carrier is defined as its drift velocity per unit applied field. As a carrier moves through a material under the influence of an external field it will be scattered by any region where deviations from the ideal lattice occur. Such deviations can be caused by impurities, vacancies and interstitials in the host lattice, dislocations and inhomogeneities due to lattice vibrations. The carrier mobility and its variation with temperature reflects these deviations from the ideal, and it is for this reason that the value of carrier mobility is sometimes used as a measure of crystal perfection.

The mobility of free electrons in CdS has been investigated by a number of workers using Hall measurements. Most of the results are consistent with the free electron mobility being dominated by polar optical mode scattering at temperatures above about 150°K, and piezoelectric and ionised impurity scattering below this temperature.

Polar optical mode scattering occurs in the partially ionic CdS when the electrons interact with the dipoles produced where longitudinal optical phonons disturb the crystal lattice. The mobility, μ_{op}, in this case may be expressed as

$$\mu_{op} \propto \theta^{-1/2}(m_e/m_e')^{3/2}(e^{\theta/T} - 1) \qquad 1.5.1$$

where θ is the Debye temperature (Zook and Dexter 1963).

Acoustic phonons in CdS would be expected to create a deformation potential which would scatter electrons. Bardeen and Shockley (1950) showed that the mobility, μ_d, limited by deformation potential scattering is given by

$$\mu_d \propto m_e'^{-5/2}T^{-3/2} \qquad 1.5.2$$

These workers were considering monatomic, covalent, semiconductors where the effect of a deformation potential would be dominant. In piezoelectric materials, the acoustic phonons can also induce a potential of piezoelectric origin which will scatter electrons. According to Hutson (1960) piezoelectric scattering leads to a mobility variation of the form

$$\mu_p \propto (m_e/m_e')^{3/2} T^{-1/2} \qquad 1.5.3$$

Impurity scattering by ionised centres has been considered by Brooks (1955) and is given by

$$\mu_i = (m_e/m_e') \frac{T^{3/2}}{N_i Z^2} \log \frac{AT^2 m_e'/m_e}{n} \qquad 1.5.4$$

where N_i is the number of ionised impurity scattering centres with charge Z, n is the free electron density, and A is a constant. The weaker unionised impurity scattering was investigated by Erginsoy (1950) who found it to be almost temperature independent.

Figure 1.5.1 shows a typical plot of Hall mobility versus temperature measured by Subhan (1969) on a CdS sample cut from a boule crystal grown in this department. It was possible to fit the theoretical values for polar optical mode, piezoelectric, and ionised impurity scattering to these results using a value of $0.19\ m_e$ for the effective mass of the electron. No contribution from unionised impurity or deformation potential scattering could be estimated from the Hall data, so that it may be concluded that such effects are small in comparison with the other scattering mechanisms.

A value for the mobility of holes in CdS is difficult to obtain directly, because for most transport phenomena conduction

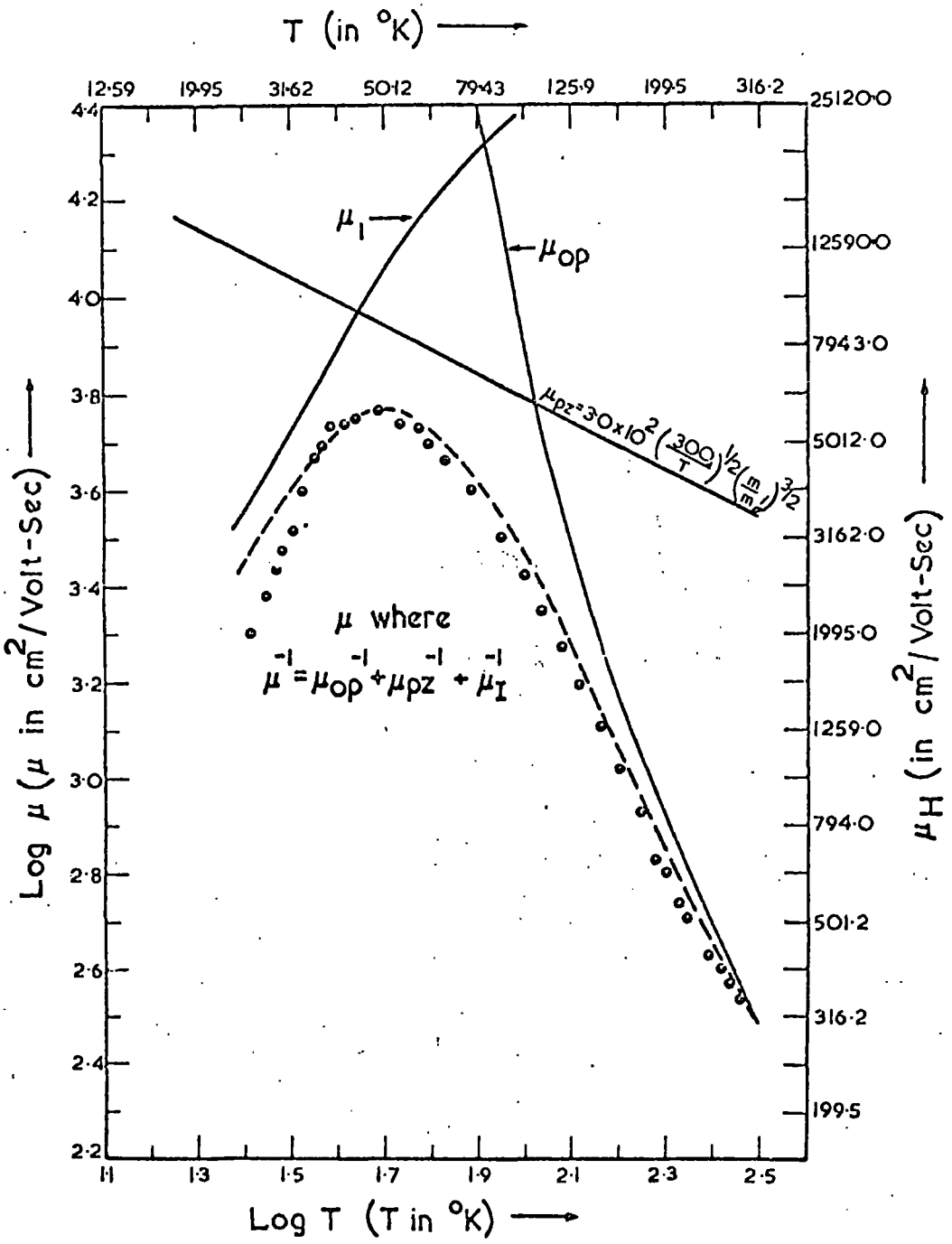

FIGURE 1.5.1. Temperature variation of the Hall mobility for crystal 183. The broken curve shows the theoretically computed values of the electrical mobility μ due to the combined effects of the polar optical mode (μ_{op}), piezoelectric (μ_{pz}) and ionized impurity scattering (μ_I) assuming $m_e'/m = 0.19$. μ_{pz} was calculated from the relation:

$$\mu_{pz} = 3.0 \times 10^2 \left(\frac{300}{T}\right)^{1/2} \left(\frac{m}{m_e'}\right)^{3/2}$$

is predominantly via free electrons. Spear and Mort (1963) measured a mean value of 15 cm^2/volt-sec. for the room temperature drift mobility of holes in CdS using pulsed electron beam excitation and a pulsed electric field. They found that the drift mobility at near liquid nitrogen temperatures increased exponentially with temperature yielding an activation energy of 0.019 $\pm$ 0.002 eV. They interpreted this in terms of hole mobility governed by holes in the upper two valence bands (Γ_9 and Γ_7), and the variation in mobility as due to the change in occupancy of these levels with temperature. Their value of 0.019 eV is close to that found by Thomas and Hopfield (see Figure 1.3.1) for the separation of the upper two valence bands.

Onuki and Hase (1965) measured the a.c. photo-Hall mobility at different excitation energies and found that the Hall mobility decreased at wavelengths less than 5300 A^o. Assuming this decrease to be due to a contribution from hole mobility, they deduced a value of 48 cm^2/volt-sec. for the hole mobility. Lecomber et al. (1966) measured a drift mobility of 23 cm^2/volt-sec. on one of their CdS samples, when they were studying the acousto-electric interaction of carriers with acoustic waves. Recently, Islam and Woods (1969) observed a second current saturation in measurements of acoustic wave-carrier interaction, when the sample was illuminated with infrared quenching radiation. Assuming this saturation to be due onset of acousto-electric interaction with holes, they calculated the room temperature hole mobility to be 48 cm^2/volt-sec.

References to Chapter 1

Balkanski, M. and J. des Cloizeaux, 1960, J. Phys. Radium 21, 825.

Bardeen, F. and W. Shockley, 1950, Phys. Rev. 77, 407.

Baer, W.S. and R.N. Dexter, 1964, Phys. Rev. 135, A1388.

Basov, N.G., O.V. Bogdankevich and A.G. Devyatkov, 1965, Soviet Phys. JEPT 20, 1067.

Basov, N.G., A.Z. Grasyuk, I.G. Zubaren and V.A. Kayulin, 1966, Soviet Phys. Solid State 7, 2932.

Benoit a la Guillaume, C. and J. Deverber, 1965, Compt. Rend. 261, 5428.

Birman, J.L., 1959a, Phys. Rev. 115, 1493.

Birman, J.L., 1959b, Phys. Rev. Letters 2, 157.

Braunstein, R. and N. Ockman, 1964, Phys. Rev. 134, 449.

Brooks, H., 1955, Advan. Electron. Electron Phys. 15, 85.

Broser, I. and R. Broser-Warminsky, 1962, in: Kallmann, H.P. and G.M. Spruch, eds. Luminescence of Organic and Inorganic Materials, Proc. of Intern. Conf. held in New York in 1962 (John Wiley and Sons, New York) p. 402.

Bube, R.H., 1960, Photoconductivity of Solids (John Wiley and Sons New York) p. 237.

Corll, J.A., 1964, J. Appl. Phys. 35, 3032.

Edwards, A.L., T.E. Slykhouse and H.G. Drickamer, 1959, J. Phys. Chem. Solids 11, 140.

Erginsoy, C., 1950, Phys. Ref. 79, 1013.

Fahrig, R.H., 1963, Electrochem. Tech. 1, 362.

Frerichs, R., 1947, Phys. Rev. 72, 494.

De Graaff, H.C. and H. Koelmans, 1966, Philips Tech. Rev. 17, 200.

Halsted, R.E., E.F. Apple and J.S. Prener, 1959, Phys. Rev. Letters 2, 420.

Halsted, R.E., E.F. Apple, J.S. Prener and W.W. Piper, 1960, in: Proc. of Intern. Conf. on Semiconductor Phys. held in Prague in 1961 (Publishing House of the Czechoslovak Academy of Sciences, Prague) p. 776.

Höhler, G., 1949, Ann. Physik 4, 371.

Hopfield, J.J. and D.G. Thomas, 1961, Phys. Rev. 122, 35.

Hutson, A.R., J.H. McFee and D.L. White, 1961, Phys. Rev. Letters 7, 237.

Hutson, A.R., 1960, Phys. Rev. Letters 4, 505.

Islam, M.N. and J. Woods, 1969, Solid State Communications 7, 1457.

Le Comber, P.G., W.E. Spear and A. Weinmann, 1966, Brit. J. Appl. Phys. 17, 467.

Lorentz, R., 1891, Chem. Ber. 24, 1501.

Maines, J.D. and E.G.S. Paige, 1969, J. Phys. C. 2, 175.

May, J.E., 1965, Proc. Inst. Elect. Electron Engrs. 53, 1465.

Nichol, F.H., 1967, Appl. Phys. Letters 10, 69.

Onuki, M, and H. Hase, 1965, J. Phys. Soc. Japan 20, 171.

Piper, W.W. and R.E. Halsted, 1960, in: Proc. of Intern. Conf. on Semiconductor Phys. held in Prague in 1961 (Publishing House of the Czechoslovak Academy of Sciences, Prague) p. 1046.

Piper, W.W. and D.F.T. Marple, 1961, J. Appl. Phys. 32, 2237.

Sawamoto, K., 1964, J. Phys. Soc. Japan 19, 318.

Shirland, F.A., 1966, Advanced Energy Conversion 6, 201.

Spear, W.E. and J. Mort, 1963, Proc. Phys. Soc. 81, 130.

Subhan, M.A., 1969, Thesis, Durham University, submitted Dec. 1969.

Thomas, D.G. and J.J. Hopfield, 1959, Phys. Rev. 116, 573.

Waxman, A., 1966, Solid State Electronics 9, 303.

Weimer, P.K., 1962, Proc. Inst. Radio Engrs 50, 1462.

Wireless World, 1968, Febuary, p. 685.

Zook, J.D. and R.N. Dexter, 1963, Phys. Rev. 129, 1980.

CHAPTER 2

PHOTOCONDUCTIVITY PHENOMENA IN CdS

2.1. Introduction

When photosensitive CdS is illuminated with radiation which creates electron-hole pairs, the free holes are rapidly captured at recombination centres and the current is carried mainly by the free electrons. Where uniform irradiation creates F free electrons per second in the whole crystal, the total number of free electrons, n, under steady state conditions is given by

$$n = F\tau_n \qquad 2.1.1$$

where τ_n is the free electron lifetime.

If ohmic contact is now made to the material and a voltage, V, applied the photocurrent, I, will be

$$I = ne/T_r \qquad 2.1.2$$

where T_r is the transit time of an electron between the electrodes and e is the electronic charge.

From Equations 2.1.1 and 2.1.2,

$$I = Fe\tau_n/T_r = GeF \qquad 2.1.3$$

where G is the photoconductive gain factor.

The transit time is determined by the free electron mobility μ_n, the electrode spacing L and the applied voltage, such that

$$T_r = L^2/V\mu_n \qquad 2.1.4$$

so that the photocurrent may be expressed as

$$I = \frac{F\tau_n e\mu_n V}{L^2} \qquad 2.1.5$$

2.2. The Free Electron Lifetime

From Equations 2.1.3 and 2.1.5 it can be seen that the photoconductive gain is governed by the two material parameters μ_n and τ_n. The variation of the electron mobility from sample to sample of CdS does not usually exceed an order of magnitude at room temperature. The variation of μ_n with temperature, in the range 100°K to 400°K, is again about one order of magnitude. The free electron lifetime can, however, vary by as much as eight orders of magnitude depending on the method of growth and sample preparation. Under certain conditions τ_n can change considerably with temperature and the intensity of illumination. The free electron lifetime is thus a key parameter for determining photoconductive gain.

If the lifetime of a free electron is terminated by recombination with a free hole trapped in a set of recombination centres with density N_R and capture cross-section S_R

$$\tau_n = (N_R S_R v)^{-1} \qquad 2.2.1$$

where v is the velocity of a free electron.

For a trap free material with a density of n free electrons under illumination

$$\tau_n = (nS_R v)^{-1} \quad \text{and} \quad I \propto F^{1/2} \qquad 2.2.2$$

because the number of free electrons is equal to the number of

empty recombination centres.

Where n_t trapping levels are introduced into the material and are filled with electrons, and where $n_t >> n$, the free electron lifetime becomes

$$\tau_n = (n_t S_R v)^{-1} \quad \text{and } I \propto F \qquad 2.2.3$$

and the sensitivity of the material is reduced by a factor n/n_t.

2.3. The Response Time

The response time t_o is the time for the photocurrent to decay to 1/e of its value under steady state conditions following the removal of the illumination. In a trap free material, or at high light intensities, the response time is equal to the free electron lifetime. Where there are trapping centres present, the observed decay is modified by the thermal emptying of these traps. The theoretical form of the isothermal decay of a single set of discrete traps is discussed in Section 3.9, and experimental results showing such a decay can be seen in Figure 5.6.6. The response time is typically of the order of minutes.

For a continuum of traps, with density $(n_t)_{kT}$, within a KT band near the steady state Fermi level for electrons, and where $(n_t)_{kT} >> n$, then

$$t_o = \frac{(n_t)_{kT}\tau_n}{n} \qquad 2.3.1$$

2.4. Space Charge Limited Currents

It would appear that the photoconductive gain, according to Equation 2.1.5, can be increased indefinitely by increasing the applied voltage or decreasing the electrode spacing. However,

at sufficiently high fields (but below those at which dielectric breakdown or impact ionisation would occur) a space charge is injected from the cathode into the bulk of the material. Thus, the photocurrent is obscured by the resulting space charge limited current (S.C.L.C.). The S.C.L.C. varies with a power of voltage of the order of two or greater, and when fields sufficiently great to inject a space charge are reached, an increase in field will produce a S.C.L.C. which rapidly swamps the photocurrent.

The limit is reached when the S.C.L.C. is of the same order as the photocurrent, or using the analogy with conventional amplification, when the signal (photocurrent) to noise (S.C.L.C.) is equal to unity. Under S.C.L.C. conditions the transit time T_r' of injected charge passing through the material is equal to the dielectric relaxation time, which is effectively the resistance-capacitance product for a particular sample. The space charge occurs because the material cannot dissipate the injected charge.

The transit time T_r' is governed by the drift mobility, μ_d, and

$$T_r' = L^2/V\mu_d \qquad 2.4.1$$

For a trap free photoconductor, the drift mobility and free electron mobility are equal, so that

$$T_r' = \tau_r = T_r \qquad 2.4.2$$

where τ_r is the dielectric relaxation time.

The gain G_{max} obtained when the S.C.L.C. is equal to the photocurrent can be derived from Equations 2.1.5, 2.4.1 and 2.4.2

and is

$$G_{max} = \tau_n/\tau_r' \qquad 2.4.3$$

The photoconductive gain will be larger at fields for which the injected space charge is greater than the photocurrent, because τ_r is inversely proportional to the conductivity. However, in the above equation τ_r' is the dielectric relaxation time found for the situation where the photocurrent and S.C.L.C. are equal. This is the approximate limit for practical measurement.

When $(n_t)_{kT}$ shallow traps are introduced into the photoconductor, and $(n_t)_{kT} >> n$, the drift mobility of free electrons is related to the free electron mobility, so that

$$\mu_d = \frac{\mu_n n}{(n_t)_{kT}} \qquad 2.4.4$$

Thus

$$T_r = \frac{T_r' n}{(n_t)_{kT}} = \frac{\tau_r' n}{(n_t)_{kT}} \qquad 2.4.5$$

and

$$G_{max} = \frac{\tau_n (n_t)_{kT}}{\tau_r' n} \qquad 2.4.6$$

Hence from Equations 2.3.1 and 2.4.6

$$G_{max} = t_o/\tau_r' \qquad 2.4.7$$

Therefore, the introduction of shallow traps into CdS decreases the effective maximum gain.

In practice, maximum gains in CdS have been observed where

$$G_{max} = (t_o/\tau_r')M \qquad 2.4.8$$

and M is of the order of hundreds. If $(n_t)_d$ deep trapping levels are present together with $(n_t)_{kT}$ shallow traps, and where the density of both these sets of traps is greater than n, μ_d becomes

$$\mu_d = \frac{\mu_n n}{(n_t)_{kT} + (n_t)_d} \qquad 2.4.9$$

so that the free electron transit time is given by

$$T_r = \frac{\tau_r' n}{(n_t)_{kT} + (n_t)_d} \qquad 2.4.10$$

The expression for G_{max} in this case is

$$G_{max} = \frac{\tau_n[(n_t)_{kT} + (n_t)_d]}{\tau_r' n} \qquad 2.4.11$$

The response time is still dependent on the traps in thermal equilibrium with the conduction band, i.e.

$$t_o = \frac{\tau_n (n_t)_{kT}}{n} \qquad 2.4.12$$

hence, the maximum photoconductive gain can be written

$$G_{max} = (t_o/\tau_r')M \qquad 2.4.13$$

where

$$M = 1 + (n_t)_d/(n_t)_{kT} \qquad 2.4.14$$

2.5. Demarcation Levels

The preceding discussion has shown that the photoconductive properties of a material are determined by the trapping levels and recombination centres present. Whether a centre acts as a trap or recombination centre can be determined by using the concept of demarcation levels.

Figure 2.5.1 shows the steady state Fermi levels and demarcation levels for electrons and holes in an insulator. At the demarcation level for electrons (holes), the electron (hole) has an equal probability of being thermally excited to the conduction band (valence band) or of acting as a recombination centre for a carrier of the opposite charge. Above the electron demarcation level the centres are predominantly electron traps, and below the hole demarcation level the centres are predominantly hole traps. The region between the demarcation levels contains recombination centres. Trapping centres lying above the electron demarcation level but below the electron Fermi level will be substantially filled with electrons. Although these centres have a greater probability of acting as trapping centres than recombination centres, the relatively large percentage occupancy by electrons will allow some recombination of holes.

The probability, q, of thermal release of an electron from a trap with activation energy, E_t, and capture cross-section, S_n, for electrons is

$$q = \nu \exp(-E_t/kT) \qquad 2.5.1$$

where ν is the attempt to escape frequency. From considerations of detailed balance it can be shown that

$$\nu = S_n v N_c \qquad 2.5.2$$

where v is the thermal velocity of a free electron and N_c is the density of states in the conduction band.

If the concentration of free holes is p, and S_p is the hole capture cross-section for holes by centres, containing electrons, which lie at the electron demarcation level, D_n, then

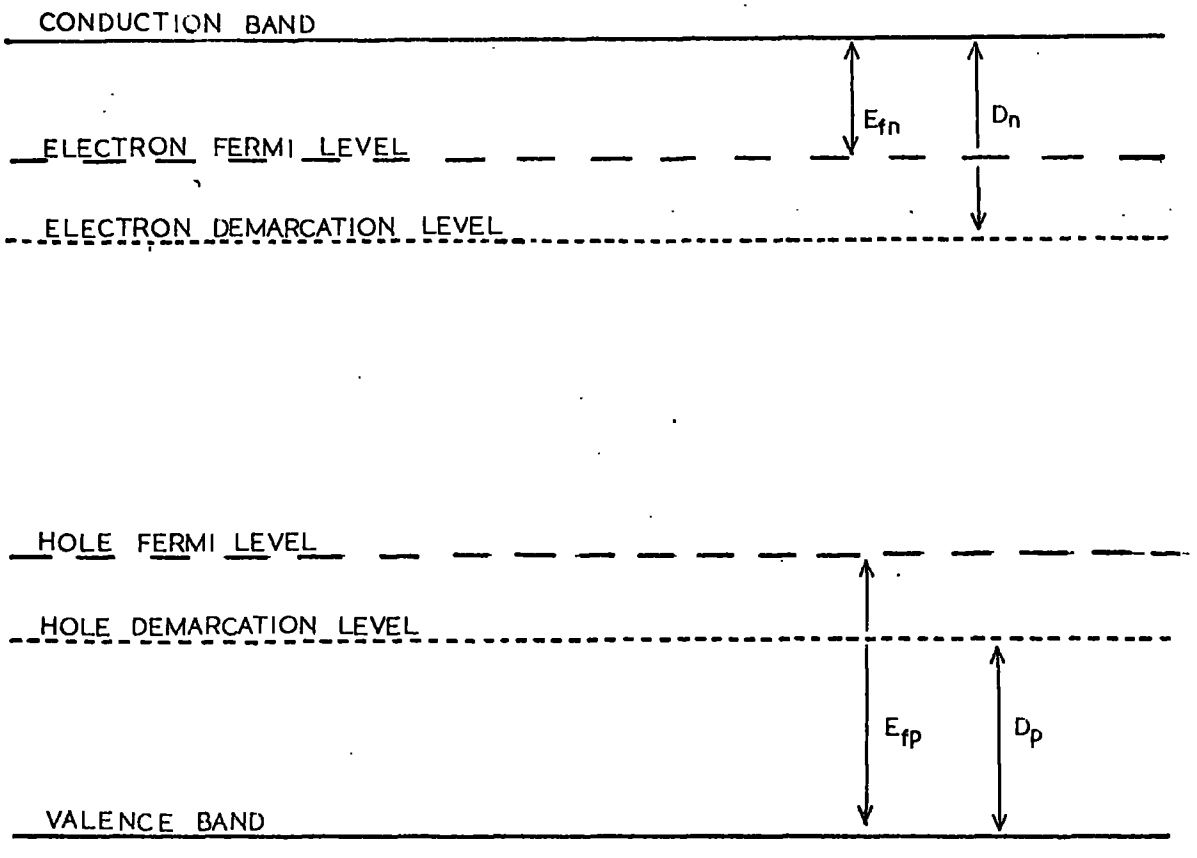

FIGURE 2.5.1. FERMI LEVELS AND DEMARCATION LEVELS FOR AN INSULATOR

$$S_n v N_c \exp(-D_n/kT) = pvS_p \qquad 2.5.3$$

The concentrations of free electrons and holes can be found from expressions similar to Equations 2.1.1 and 2.2.3. Thus

$$n = F/vS_n p_r \qquad 2.5.4$$

where S_n is the capture cross-section for electrons by empty recombination centres with a density p_r. Also

$$p = F/vS_p n_r \qquad 2.5.5$$

where S_p is the capture cross-section for holes of filled recombination centres with a density n_r, and where the velocity of the electrons and holes are equal. It follows that

$$p/n = S_n p_r / S_p n_r \qquad 2.5.6$$

From Equations 2.5.3 and 2.5.6 the electron demarcation level can be rewritten

$$D_n = kT\log(N_c n_r / n p_r) \qquad 2.5.7$$

Now the Fermi level for electrons, E_{fn}, is defined by

$$n = N_c \exp(-E_{fn}/kT) \qquad 2.5.8$$

therefore

$$D_n = E_{fn} + kT\log(n_r/p_r) \qquad 2.5.9$$

By a similar argument

$$D_p = E_{fp} - kT\log(n_r/p_r) \qquad 2.6.10$$

Here D_p and E_{fp} are the hole demarcation level and Fermi level respectively.

2.6. Sensitisation

Pure, stoichiometric crystals of CdS are usually poor photoconductors. The photosensitivity may often be increased markedly by incorporating donors such as the halogens or the Group IIIB metals. The introduction of these donors would be expected to be accompanied by an equal concentration of cadmium vacancies for charge compensation.

The process of sensitisation can be explained as follows. The lifetime of both free electrons and holes is of the order of 10^{-6} seconds in insensitive CdS. The introduction of compensated acceptors in the form of cadmium vacancies, as described above or by suitable impurity doping, leads to recombination centres yielding free electron lifetimes and free hole lifetimes of 10^{-2} and 10^{-8} respectively. The recombination centres found in insensitive photoconductors are termed Class I centres, the sensitising centres are called Class II centres.

Figure 2.6.1(a) shows the recombination processes in an insensitive material. The recombination centres have a large capture cross-section for both electrons and holes, leading to a small free electron lifetime and hence an insensitive material.

When Class II centres are introduced into the sample, their effectiveness in increasing the free electron lifetime will depend on whether or not they lie above or below the hole demarcation level. In Figure 2.6.1(b) the Class II centres lie below the hole

FIGURE 2.6.1 SENSITISATION BY INCORPORATION OF CLASS II CENTRES.

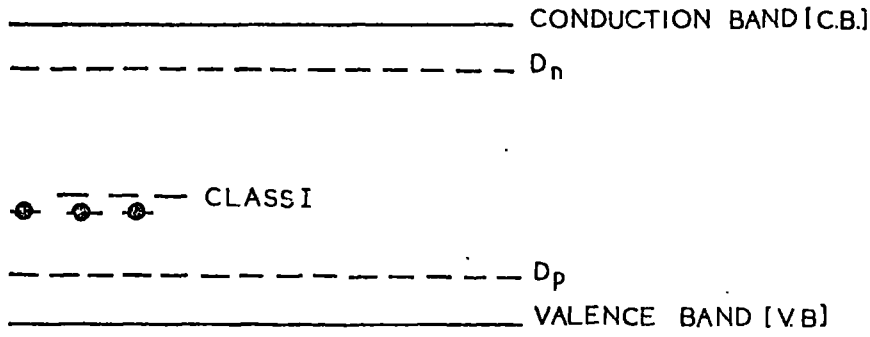

a] INSENSITIVE, CONTAINING ONLY FAST RECOMBINATION CLASS I CENTRES

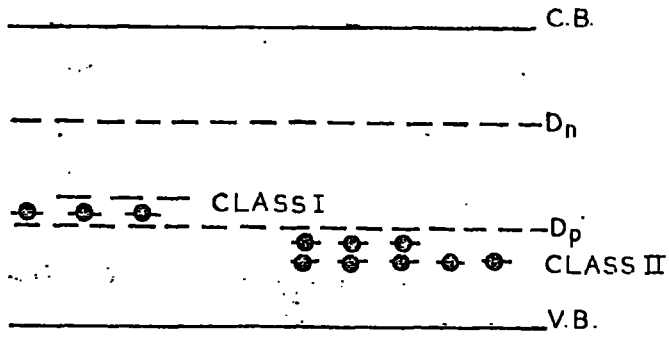

b] INSENSITIVE, BECAUSE CLASS II CENTRES LIE BELOW D_p.

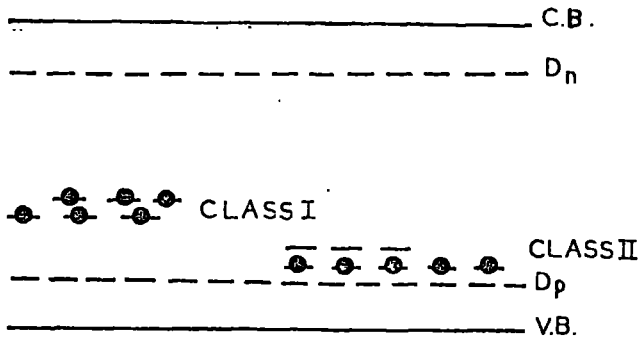

c] SENSITIVE, RECOMBINATION OCCURRING MAINLY AT CLASS II CENTRES

demarcation level where they act as trapping levels and so do not affect the recombination traffic significantly.

At lower temperatures and/or higher light intensities the hole demarcation level will move towards the valence band. When the hole demarcation level falls below the Class 11 centres, they may now function as recombination centres. As the capture cross-section for free electrons by the Class 1 centres is much greater than the capture cross-section for electrons of the Class 11 centres, the Class 1 centres will be predominantly filled with electrons. Under these conditions the recombination of free electrons is governed by the Class 11 centres, as shown in Figure 2.6.1(c), leading to an increase in free electron lifetime and a more photosensitive material.

2.7. Superlinearity

Under certain conditions a superlinear variation of photocurrent with light intensity may be observed in CdS. Both above and below the levels of light intensity yielding this superlinear behaviour, the photocurrent dependence on light intensity is found in practice to be approximately linear.

A simple model to explain the phenomenon of superlinearity can be obtained by considering a trap free photoconductor containing Class 1 and Class 11 centres as shown in Figures 2.6.1(b) and (c). At low light intensities the Class 1 centres lie between the demarcation levels for electrons and holes and act as recombination centres. The Class 11 centres lie well below the hole demarcation level, as shown in Figure 2.6.1(b), and behave as hole traps. When the illumination intensity is increased, the hole demarcation level moves towards the valence band, and the photocurrent will vary as the one half power of light intensity (for

this simple model) as will be demonstrated later in this section.

When the hole demarcation level passes through the Class 11 centres they will be converted from their role as hole traps to recombination centres. During this sensitisation process the free electron lifetime will increase rapidly with increasing light intensity, and the resultant photocurrent will be super-linear.

After the sensitisation has been completed, the variation of photocurrent with light intensity will again be sublinear and the free electron lifetime is determined by recombination at the Class 11 centres as shown in Figure 2.6.1(c).

In the above discussion it was stated that a variation of photocurrent with a one half power of light intensity would be expected from this simple model outside the region of super-linearity. Equating Equations 2.1.1 and 2.2.2, for a photo-conductor with a single set of recombination centres, gives

$$F = n^2 S_R v \qquad 2.8.1$$

for the situation where the density of empty recombination centres is equal to the free electron density. Thus

$$I \propto F^x \qquad 2.8.2$$

where $x = 1/2$. In practice there will also be trapping levels present which can change the value of x so that $1 > x > 1/2$. The value of x depends on the number and distribution of the traps as shown by Rose (1951).

Superlinearity depends essentially on the sensitisation process though the lower and upper breakpoints, as shown in

Figure 2.7.1, will be modified by the addition of trapping levels. Dussel and Bube (1966) have considered a four centre model which contains Class 1 and Class 11 centres together with a set of deep traps and a set of shallow traps, and give the criteria for the two breakpoints under these conditions. From the variation of the breakpoints with illumination intensity and temperature it is possible to estimate the thermal ionisation energy and the ratio S_p/S_n for the Class 11 centres and also the ratio of the density of the Class 1 centres to the density of the Class 1 centres.

2.8. Thermal Quenching

The photocurrent of CdS crystals is often independent of temperature in the range up to 300^{o}K. A characteristic decrease in photocurrent is usually observed at temperatures in the region of room temperature. This phenomenon is called thermal quenching.

The mechanism of thermal quenching can be regarded as the thermal desensitisation of a sensitised photoconductor containing Class 1 and Class 11 centres. As the temperature is raised, at constant light intensity, the hole demarcation level will move away from the valence band. In passing through the Class 11 centres there will be a decrease in the free electron lifetime and a quenching of the photocurrent. At higher light intensities the quenching described above would occur at higher temperatures as is found in practice.

The measurement of superlinearity, described in the last section, is usually derived from point to point measurement of photocurrent with temperature where a number of different light intensities is used. The superlinear variation of photocurrent with light intensity occurs in the region of thermal quenching.

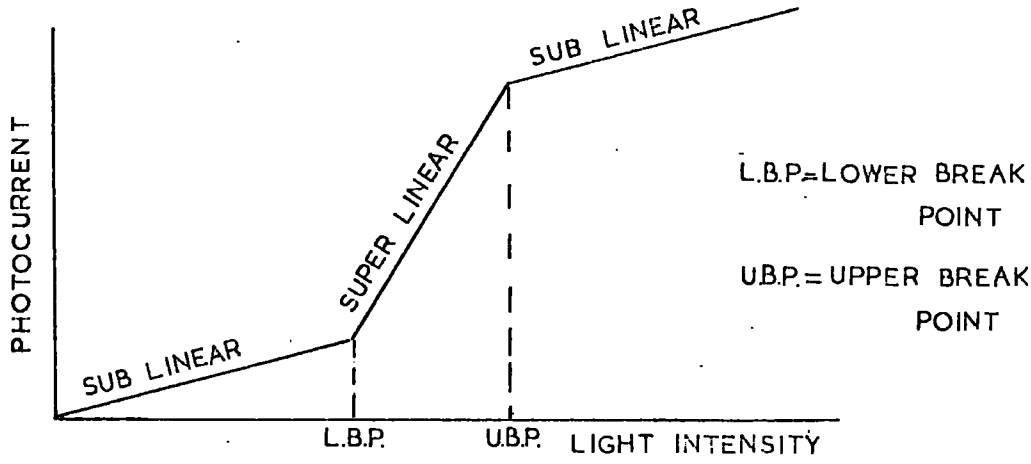

FIGURE 2.7.1. VARIATION OF PHOTOCURRENT WITH LIGHT INTENSITY FOR A SENSITIVE PHOTOCONDUCTOR

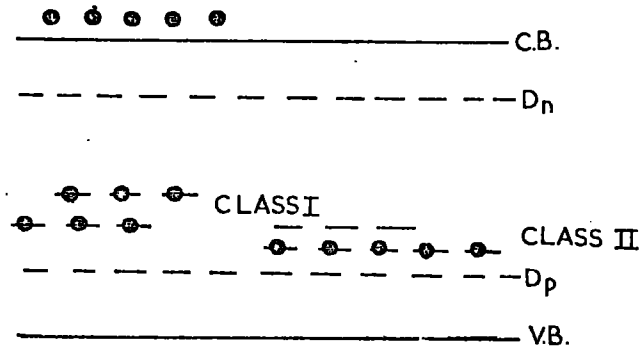

a] SENSITISED PHOTOCONDUCTOR CONTAINING CLASS I AND CLASS II CENTRES

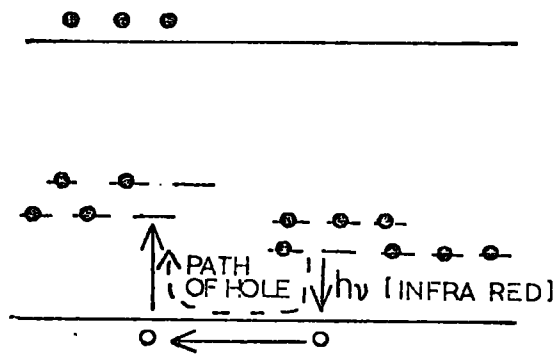

b] INFRA RED QUENCHING TRANSITIONS FOR A SENSITISED PHOTOCONDUCTOR

FIGURE 2.9.1. INFRA-RED QUENCHING OF PHOTOCURRENT.

2.9. Infrared Quenching

Infrared quenching occurs when the photocurrent of a sensitised CdS crystal, irradiated with visible light, is reduced by infrared illumination from a second source. Figure 2,9.1 shows the model which will account for this phenomenon. Under visible irradiation alone, electron recombination proceeds via the Class 11 centres and the Class 1 centres are filled and inoperative (Figure 2.9.1(a)). Irradiation with infrared photons of suitable energy lifts electrons from the valence band to the Class 11 centres. The resulting free holes are captured by the Class 1 centres which now become active in recombination with a subsequent decrease in the photocurrent (Figure 2.9.1(b)). Infrared quenching is essentially an optical switching of the recombination path for free electrons from Class 11 to Class 1 centres in a sensitised photoconductor.

By studying the spectral distribution of photocurrent with differing infrared wavelengths from the secondary source, it is possible to estimate the energetic separation of the Class 11 centres from the valence band. Figures 9.3.1 to 9.3.5 show the typical quenching spectra for samples investigated during the course of the present work. The energy threshold for the onset of infrared quenching is the height of the Class 11 centres above the valence band.

2.10. Thermoelectric Power Measurements

It was stated, in the introduction to the present chapter, that current is carried mainly by free electrons in CdS when the crystal is illuminated with radiation which creates electron-hole pairs. Where the crystal is thermally or optically quenched, and also when it is irradiated with infrared radiation alone,

a greater contribution to the current is expected from the freed holes.

Recently, Lawrance and Bube (1968) have measured the thermoelectric power, on bar shaped CdS samples oriented with the c axis lying parallel to the longest dimension of the bar, under the same conditions of illumination and temperature as are usual for spectral response, infrared quenching and thermally stimulated current measurements. They showed that the spectral response of thermoelectric power (T.E.P.) changes from positive to negative with increasing photon energy in the range 1.0 to 1.5eV indicating a significant contribution from free holes when the samples were illuminated with infrared photons. The spectral response of T.E.P. also showed fine structure which was interpreted in terms of a multi-level recombination centre.

The optical quenching T.E.P. measurements were characterised by two broad bands at room temperature, which were similar in basic structure to the infrared quenching of photocurrent, though the T.E.P. quenching bands showed an increase in negative T.E.P. (compared with the expected more positive contribution from freed holes). There was also considerable fine structure in the T.E.P. quenching 'maxima'. To explain the fine structure and the large negative values of the 'maxima', Lawrance and Bube tentatively proposed that the sensitising centres were associated pairs of intrinsic defects which could exist in various charge states. Such centres were assumed to be dipoles having a preferred crystallographic orientation. Excitation with infrared quenching radiation causes a change in the state of polarisation of the dipoles which results in an increase in the negative T.E.P. The fine structure was associated with the vibrational modes of the dipoles.

Where the T.E.P. was monitored under similar conditions as those used for thermally stimulated current measurement positive T.E.P. maxima were observed at temperatures of approximately 150°K 150°K, 280°K, and 360°K. The highest temperature maximum was assumed to be caused by polar defects.

The T.E.P. measurements made by Lawrance and Bube indicate that both the optical and thermal quenching of photocurrent are more complex than would be expected from a simple model, and also that hole traps may contribute significantly to thermally stimulated current measurements. The polarisation and space charge effects which they reported, however, suggest that a more detailed program of work is required before an unambiguous interpretation can be made from T.E.P. data.

References to Chapter 2

Dussel, G.A. and R.H. Bube, 1966, J. Appl. Phys. 37, 13.

Rose, A., 1951, Concepts in Photoconductivity and Allied Problems, published by John Wiley and Sons, Inc. New York.

Lawrance, R. and R.H. Bube, 1968, J. Appl. Phys. 39, 1807.

CHAPTER 3

THERMALLY STIMULATED CONDUCTIVITY

3.1. Introduction

When a photoconducting material containing trapped electrons or holes is heated in the dark, the conductivity shows structure which is dependent on the thermal release of the trapped carriers. This variation of conductivity with temperature is called thermally stimulated conductivity. The study of thermally stimulated conductivity has been widely used to determine thermal activation energies, capture cross-sections, and densities of trapping centres in photoconductors.

In this chapter an elementary model for describing electron trapping phenomena is presented together with some of the analytical techniques derived from it, which are applicable to thermally stimulated conductivity. Although the following treatment is limited to electron trapping in n-type photoconductors, it could equally well be applied to the trapping of holes in p-type materials. The thermal release of charge carriers in both cases is characterised by an increase in free carrier density. (The thermal release of holes in a n-type crystal yields a decrease in free electron density, because when the hole is removed at the cathode an electron must also be removed from the conduction band for charge conservation.)

3.2. An Elementary Model for Describing Electron Trapping Phenomena

The model consists of a single set of discrete trapping levels, with thermal activation energy, E_t, and a single set of

recombination centres. S_t and S_r are the capture cross-sections for electrons by the trapping and recombination centres respectively.

The probability, q, of an electron escaping from a trap at temperature T is

$$q = \nu \exp(-E/kT) \qquad 3.2.1$$

where ν is the attempt to escape frquency and k is Boltzmann's constant.

The rate of change of trapped electron density, n_t, is

$$dn_t/dt = -n_t \nu \exp(-E/kT) + n_c(N_t - n_t)S_t v \qquad 3.2.2$$

where n_c is the free electron density, v is the thermal velocity of free electrons and N_t is the total density of traps.

The rate of change of n_c is given by

$$dn_c/dt = - dn_t/dt - n_c/\tau_n \qquad 3.2.3$$

where τ_n is the free electron lifetime. It is found in practice that $n_c/\tau_n >> dn_c/dt$, so that Equation 3.2.3 may be expressed as

$$n_c = -\tau_n dn_t/dt \qquad 3.2.4$$

The heating rate, β, is usually arranged to be linear so that

$$\beta = dT/dt \qquad 3.2.5$$

The conductivity, σ, can be found from the relationship

$$\sigma = n_c e \mu_n \qquad 3.2.6$$

where e and μ_n are the electronic charge and the free electron mobility respectively.

Solutions to the above equations, which give the conductivity as a function of temperature for the thermally stimulated emptying of traps, are found in the three limiting cases:-

(a) Monomolecular Recombination or No Retrapping, where $S_t << S_r$

(b) Fast Retrapping, where $S_t >> S_r$

(c) Bimolecular Recombination, where $S_t = S_r$

3.2(a). No Retrapping

Under these conditions, Equation 3.2.2 may be simplified to

$$dn_t/dt = - n_t \nu \exp(-E/kT) \qquad 3.2.7$$

n_t is found by integration of Equation 3.2.7 between the limits T_o and T, where T_o is the temperature at the beginning of the thermally stimulated current run. Substitution of n_t in Equation 3.2.7 gives dn_t/dt which is inserted into Equation 3.2.4 and leads to the conductivity, σ, where

$$\sigma = n_o \tau_n e \mu_n \nu \exp\left[-E/kT - \int_{T_o}^{T} (\nu/\beta)\exp(-E/kT)dT\right] \qquad 3.2.8$$

Here n_o is the initial density of trapped electrons. In this analysis it is assumed that μ_n, τ_n and ν are temperature independent.

3.2(b). Fast Retrapping

In this case it is usual to assume that the traps are in thermal equilibrium with the conduction band, thus

$$n_c/N_c = (n_t/N_t)\exp(-E/kT) \qquad 3.2.9$$

where N_c is the effective density of states in the conduction band. If the value of n_c, from Equation 3.2.9, is substituted in Equation 3.2.4 then

$$dn_t/dt = -(N_c n_t/N_t \tau_n)\exp(-E/kT) \qquad 3.2.10$$

From Equations 3.2.4 and 3.2.10 the variation of conductivity with temperature is given by

$$\sigma = (N_c e\mu_n n_o/N_t)\exp\left[-E/kT - (e/N_t\beta\tau_n)\int_{T_o}^{T} N_c \exp(-E/kT)\,dT\right] \qquad 3.2.11$$

which holds when μ_n and τ_n are independent of temperature.

The expressions for no retrapping and fast retrapping may both be written in the form

$$\sigma = A\exp\left[-E/kT - B\int_{T_o}^{T} \exp(-E/kT)\,dT\right] \qquad 3.2.12$$

where A and B are often treated as constants. The only difference between Equations 3.2.8 and 3.2.11 expressed in the above manner is that for fast retrapping the terms A and B carry the temperature dependence of N_c. This may be regarded as negligible compared with the integral, which is a rapidly varying function of temperature.

The reason for the similarity of no retrapping and fast retrapping thermally stimulated conductivity curves is the assumption that trapping is a dominant process throughout the emptying of fast retrapping centres. For this to be true, the centres would have to be only partially filled. Since the probability of

thermal release (which contains an implicit dependence on capture cross-section) is greater for fast retrapping than for slow, monomolecular recombination, then fast traps would be expected to give a measurable thermally stimulated conductivity at lower temperatures than for monomolecular recombination. Where fast traps are initially full, the effect of retrapping is at first small. As the traps empty retrapping will cause an effective lessening of the probability of thermal release and so the thermally stimulated conductivity curve will broaden out at higher temperatures. Where retrapping is predominant thoughout the emptying process, then no broadening ensues and the variation of conductivity is similar to that observed under monomolecular recombination.

3.2(c). Bimolecular Recombination

Garlick and Gibson (1948) first proposed a solution to the allied problem of thermoluminescence as a function of temperature under bimolecular conditions. They assumed that the density of filled trapping centres was equal to the density of empty recombination centres (i.e. $n_c << n_t$). The probability of a released electron recombining at an empty recombination centre is thus

$$n_t/[(N_t - n_t) + n_t] = n_t/N_t \qquad 3.2.13$$

This modifies Equation 3.2.2 giving

$$dn_t/dt = -(n_t^2/N_t)\nu\exp(-E/kT) \qquad 3.2.14$$

Thus the conductivity under bimolecular recombination may be expressed as

$$\sigma = \frac{n_o^2 \tau_n \mu_n \nu \exp(-E/kT)}{N_t\left[1 + (n_o\nu/N_t\beta)\int_{T_o}^{T}\exp(-E/kT)\right]^2} \qquad 3.2.15$$

Although μ_n and ν are assumed to be temperature independent, τ_n will depend strongly on temperature. As pointed out by Saunders (1967), the density of recombination centres varies during the emptying of the trapping centres. Because $S_t = S_r$ for bimolecular recombination, the free electron lifetime is

$$\tau_n = (S_t n_t v)^{-1} \qquad 3.2.16$$

Substitution of this value of τ_n into Equation 3.2.15 yields

$$\sigma = \frac{n_o e \mu_n N_c \exp(-E/kT)}{N_t\left[1 + (n_o \nu / N_t \beta)\int_{T_o}^{T} \exp(-E/kT)\right]} \qquad 3.2.17$$

3.3. Methods of Evaluating Trapping Parameters

Equations 3.2.8, 3.2.11 and 3.2.17 represent the variation of conductivity with temperature to be expected in practice under the conditions stated. Obtaining a 'best fit' between practical and theoretical curves, as described in Section 3.7, would seem to be the most accurate method of using these equations. However, the calculations involved are tedious so that other approximate expressions have been used in the past. Nicholas and Woods (1964) reviewed these approximations, which fall into three groups.

3.3(a). Methods Utilising the Curve Geometry

These methods use the half heights and the temperature maximum of the curve together with empirically determined constants to obtain the thermal activation energy and in some cases the capture cross-section.

Grossweiner's Method for monomolecular recombination provides a typical example. If T' and T^* are the temperatures of the low

temperature half height and the maximum of the curve respectively, the Grossweiner thermal activation energy is

$$E_G = 1.51kT^*T'/(T^* - T') \qquad 3.3.1$$

Provided that $E_G/kT > 20$ and $N_c\nu S_t > 10^7$ then E_G is accurate to better than 10%.

Grossweiner also gave an expression for capture cross-section namely

$$S_t = \frac{3T'\beta\exp(E/kT^*)}{2N_c\nu T^*(T^* - T')} \qquad 3.3.2$$

3.3(b). Variation of Heating Rate Methods

These methods rely on the fact that the temperature, T^*, of the maximum changes with different heating rates. If Equation 3.2.8 is differentiated with respect to temperature, then it is found that

$$\exp(E/kT^*) = N_c\nu S_t T^{*2}/E \qquad 3.3.3$$

Booth (1954) considered two heating rates with maxima at T_1^* and T_2^* and obtained the expression

$$E = [kT_1^*T_2^*/(T_1^* - T_2^*)]\log(T_2^{*2}/T_1^{*2}) \qquad 3.3.4$$

Hoogenstraaten (1958) used a number of heating rates and plotted $\log(T^{*2}/\beta)$ against $1/T^*$. The slope of this line gives the thermal activation energy.

3.3(c). Garlick and Gibson's Method

Garlick and Gibson (1948) considered the initial rise of the conductivity curve. Under these conditions the integrals in

Equations 3.2.8, 3.2.11 and 3.2.17 are assumed to be negligible so that the conductivity may be expressed as

$$\sigma \propto \exp(-E/kT) \qquad 3.3.5$$

The integrals, in the expressions for conductivity with temperature, are significant for values of conductivity greater than 10% of the peak maximum value (Land 1969).

3.4. Keating's Method

Apart from the assumption that the free electron lifetime and electron mobility are temperature independent, Equations 3,2.8 and 3.2.17 also assume that the attempt to escape frequency, ν, does not vary with temperature. Implicit in this assumption is that the capture cross-section $S_t \propto T^{-2}$. Lax (1960) reviewed the measured temperature dependences of capture cross-section, S, for a number of impurity defects in silicon and found variations of the form

$$S \propto T^{-n} \qquad 3.4.1$$

with the value of n in the range 0 to 4.

Keating (1961) introduced the temperature dependence of S_t by substituting Equation 3.4.1 into the expression for monomolecular recombination. He obtained the following solution for thermal activation energy

$$kT^*/E = ((T'' - T')/T^*)(1.2\gamma - 0.54) + 5.5.10^{-3} - (\gamma/2 - 0.75/2)^2 \qquad 3.4.2$$

where T'' is the temperature at half height on the high

temperature side of the maximum, and

$$\gamma = (T'' - T^*)/(T^* - T') \qquad 3.4.3$$

Keating also found that the relationship held in the case of fast retrapping where the determination of thermal activation energies was accurate to 3.5 % or better.

Recently Chen (1969) has considered the temperature dependence of S_t by substituting $\nu = \nu' T^{-2}$ and $\nu = \nu' T^{2}$ into the equation for monomolecular recombination, and $\nu = \nu' T^{2}$ into the equation for bimolecular recombination. He estimated that the error in the value of thermal activation energy, by assuming ν to be be temperature independent, was 10% or less in these extreme cases.

3.5. Bube's Fermi Level Analysis

Bube (1955) assumed that quasi Fermi level at the maximum of the conductivity curve corresponds to the thermal activation energy. Thus

$$n_c/N_c = \exp(-E/kT)) \qquad 3.5.1$$

This relationship holds only when the traps are in quasi thermal equilibrium with the conduction band (i.e. under fast retrapping conditions).

3.6. Haine and Carley-Read Analysis

Using somewhat different notation for Equations 3.2.2 and 3.2.3, Haine and Carley-Read (1968) expressed the rate of change of the free electron density as

$$dn_c/dT = n_t\theta/\tau_t - n_c(1 - n_t/N_t)/\tau_t - n_c/\tau_n \qquad 3.6.1$$

where

$$\theta = N_c/N_t \exp(-E/kT) \qquad 3.6.2$$

and the trapping time, τ_t, is given by

$$\tau_t = (N_t S_t v)^{-1} \qquad 3.6.3$$

Haine and Carley-Read assumed, as in Section 2.2, that $dn_c/dt << n_c/\tau_n$ so that Equation 3.6.1 may be rewritten as

$$n_c = n_t\theta/(1 + \tau_t/\tau_n - n_t/N_t) \qquad 3.6.4$$

3.6(a). Slope and Peak Maximum Expressions

If Equation 3.6.4 is differentiated with respect to temperature, then

$$dn_c/dT = \frac{n_t(d\theta/dT) + (dn_t/dT)\theta}{(1 + \tau_t/\tau_n - n_t/N_t)} + \frac{n_t\theta(dn_t/dT)}{N_t(1 + \tau_t/\tau_n - n_t/N_t)^2} \qquad 3.6.5$$

From Equations 3.2.4 and 3.2.5 it follows that

$$dn_t/dT = - n_c/(\tau_n\beta) \qquad 3.6.6$$

and

$$d\theta/dT = \theta(E/kT + 3/2)/T \qquad 3.6.7$$

In practice it is found that $E >> kT$, so the temperature dependence of N_c may be neglected and Equation 3.6.7 approximates to

$$d\theta/dT = \theta E/kT^2 \qquad 3.6.8$$

Substituting Equations 3.6.6 and 3.6.8 into Equation 3.6.5, and using the value of n_t from Equation 3.6.4 we obtain the relationship

$$dn_c/dT = n_c/(\tau_n + \tau_t)[E(\tau_n + \tau_t)/kT^2 - (n_c + N_t\theta)^2/(\beta N_t{}^2\theta)] \qquad 3.6.9$$

When θ from Equation 3.6.2 is substituted in the above equation

$$(1/n_c)dn_c/dT = E/kT^2 - \frac{(n_c + N_c\exp(-E/kT))^2}{\beta N_t(\tau_n + \tau_t)N_c\exp(-E/kT)} \qquad 3.6.10$$

Rearrangement of Equation 3.6.10 gives

$$N_t(\tau_n + \tau_t) = \frac{(n_c + N_c\exp(-E/kT))^2}{\beta N_c[E/kT^2 - (1/n_c)dn_c/dT]\exp(-E/kT)} \qquad 3.6.11$$

As $dn_c/dT = 0$ at the peak maximum, then

$$N_t(\tau_n + \tau_t) = (kT^{*2}N_c/E\beta)\exp(-E/kT^*)[1 + (n_c/N_c)\exp(E/kT^*)]^2 \qquad 3.6.12$$

In principle, solutions to Equation 3.6.11 may be obtained by considering two points on a single thermally stimulated conductivity curve. However, Haine and Carley-Read found that the most convenient method of evaluation was to use two heating

rates. The factor $N_t(\tau_n + \tau_t)$ can be eliminated when points on the two curves with the same temperature are used. Thus

$$\frac{[n_{c1} + N_c\exp(-E/kT)]^2}{\beta_1[E/kT^2 - (1/n_{c1})dn_{c1}/dT]} =$$

$$\frac{[n_{c2} + N_c\exp(-E/kT)]^2}{\beta_2[E/kT^2 - (1/n_{c2})dn_{c2}/dT]} \qquad 3.6.13$$

from which the thermal activation energy can be calculated. Equation 3.6.13 may be simplified when the parameters of the peak maximum are used for one of the heating rates.

3.6(b). Integral Expression

Haine and Carley-Read also proposed an integral expression for determining thermal activation energies. The density of trapped electrons can be wtitten as

$$n_t = n_o - \int_o^t (n_c/\tau_n)dt \qquad 3.6.14$$

Substituting n_t from equation 3.6.14 and θ from Equation 3.6.2 into Equation 3.6.4

$$n_c = \frac{n_o - \int_o^t (n_c/\tau_n)dt\ N_c\exp(-E/kT)}{N_t(1 + \tau_t/\tau_n) - n_o + \int_o^t (n_c/\tau_n)dt} \qquad 3.6.15$$

This last equation may be rewritten as

$$N_t(1 + \tau_t/\tau_n) - n_o = n_o - \int_o^t (n_c/\tau_n)dt$$

$$(N_c/n_c)\exp(-E/kT) - \int_o^t (n_c/\tau_n)dt \qquad 3.6.16$$

Again, in principle, Equation 3.6.16 can be used to obtain

activation energies by employing two integration limits. Where the left hand sides of the resulting two equations are eliminated

$$\exp(-E/kT) = \frac{n_{c1}n_{c2}\left[\int_o^{t_1}(n_c/\tau_n)dt - \int_o^{t_2}(n_c/\tau_n)dt\right]}{n_{c2}\left[n_o - \int_o^{t_1}(n_c/\tau_n)dt\right] - n_{c1}\left[n_o - \int_o^{t_2}(n_c/\tau_n)dt\right]} \qquad 3.6.17$$

Haine and Carley-Read suggest that a simpler method is to use two heating rates.

3.6(c). Capture Cross-sections

Assuming that the initial trap occupancy is governed by a Fermi distribution, then after equilibrium has been reached in the presence of exciting radiation at the lowest temperature attained during a thermally stimulated conductivity measurement

$$n_o/N_t = \left[1 + (N_c/n_{co})\exp(-E/kT)\right]^{-1} \qquad 3.6.18$$

Thus for all but the shallowest traps the probability of occupancy will be unity.

The capture cross-section can be obtained from the value of τ_t in the factor $N_t(\tau_n + \tau_t)$ from Equations 3.6.11 and 3.6.12 or from the value of τ_t in the factor $N_t(1 + \tau_t/\tau_n)$ from Equation 3.6.16. The free electron lifetime is found from photoconductive measurement, and N_t is obtained from Equation 3.6.18, where n_o is determined by the method described in Section 3.8. A value of capture cross-section cannot be found for fast traps, as in this case the ratio τ_t/τ_n is small.

3.7. Curve Fitting Technique

This technique was proposed by Cowell and Woods (1967).

The theoretical expressions for thermally stimulated conductivity derived in Section 3.2 are normalised to the experimental curves. The value of thermal activation energy is then varied until a 'best fit' is found beteeen theory and practice.

3.7(a). Monomolecular Recombination

Following the argument of Cowell and Woods, the conductivity in the case of monomolecular recombination may be expressed as

$$\sigma = A\exp(-t + B\int_{t_o}^{t}\exp(-t)t^{-2}dt) \qquad 3.7.1$$

where $t = E/kT$, and A and B are constants such that

$$A = n_t\tau_n e\mu_n\nu \qquad 3.7.2$$

and

$$B = \nu E/\beta k \qquad 3.7.3$$

An exact solution of the integral in Equation 3.7.1 cannot be obtained, but by successive integration by parts a convergent series is found and Equation 3.7.1 may be rewritten as

$$\sigma = A\exp[-t - B\exp(-t)t^{-2}(1 - 2t^{-1} + 6t^{-2} - 24t^{-3} .....)]\Big|_{t_0}^{t} \qquad 3.7.4$$

The lower limit of integration may be ignored, as in practice its contribution to the thermally stimulated curve is less than 1% provided that $t_o < 1.5t$.

The values of the constants, A and B, may be determined by considering the peak maximum expression for conductivity. By

differentiating the peak maximum expression for Equation 3.7.1 and equating it to zero, the constant B is given by

$$B = \exp(t^*)t^{*2} \qquad 3.7.5$$

The normalisation constant, A, may be found from Equation 3.7.3 where

$$A = \sigma^*/[\exp(-t^*) - B\exp(-t^*)t^{*-2}(1 - 2t^{*-1} + 6t^{*-2} - 24t^{*-3} \ldots\ldots)] \qquad 3.7.6$$

3.7(b). Fast Retrapping

The thermally stimulated conductivity in the case of fast retrapping was expressed by Cowell and Woods as

$$\sigma = C\exp[-t - D\exp(-t)t^{-3.5}(1 - 3.5t^{-1} + 15.75t^{-2} - 86.625t^{-3} \ldots\ldots)] \qquad 3.7.7$$

where D is found from the peak maximum relationship to be given by

$$D = \frac{N_c^* E^{5/2}}{N_t \beta T^{*3/2} k^{5/2} \tau_n} = \exp(t^*)t^{*7/2} \qquad 3.7.8$$

The normalisation constant, C, is

$$C = N_c e \mu_n n_o / N_t \qquad 3.7.9$$

and may also be found from Equation 3.7.7 at the peak maximum.

In the expression for fast retrapping, Cowell and Woods consider that the temperature dependence of N_c is significant in the constant D, but negligible in the constant C. If it may be

regarded as negligible in both cases then, as demonstrated in Section 3.2(b), the equations for monomolecular recombination and fast retrapping are identical. The assumption that N_c is constant is reasonable, as μ_n is assumed also to be temperature independent though is known to vary in the form $\mu_n \propto T^{-3/2}$.

If the temperature dependence of N_c is included for both constants, the equation for fast retrapping becomes

$$\sigma = Xt^{-3/2}\exp[-t - Y\exp(-t)t^{-2}(1 - 3.5t^{-1} + 15.75t^{-2} - 86.625t^{-3} \ldots\ldots)] \qquad 3.7.10$$

where the normalisation constant is

$$X = \frac{N_c^* e\mu_n n_o}{T^{*3/2} N_t}(E/k)^{3/2} \qquad 3.7.11$$

and

$$Y = \frac{3 + 2t^*}{2t^*}(\exp(t^*)t^{*2}) \qquad 3.7.12$$

In practice $t^* > 10$, so that to a first approximation

$$Y = \exp(t^*)t^{*2} = B \qquad 3.7.13$$

and the expressions for fast and no retrapping are again identical.

3.7(c). Bimolecular Recombination

In this case, which Cowell and Woods did not consider, the conductivity (from Equation 3.2.17) may be rewritten as

$$\sigma = A_1 t^{-3/2}\exp(-t)/[1 + B_1\exp(-t)t^{-2}(1 - 2t^{-1} + 6t^{-2} - 24t^{-3} \ldots\ldots)] \qquad 3.7.14$$

where the normalisation constant, A_1, is given by

$$A_1 = \frac{n_o e \mu_n N_c^*}{N_t T^{*3/2}} (E/k)^{3/2} \qquad 3.7.15$$

and can also be determined from Equation 3.7.14 at the peak maximum where

$$B_1 = \frac{n_o \nu E}{N_t \beta k} = t^{*2} \exp(t^*)[-3/(2t^* + 3) + 2t^{*-1} - 6t^{*-2} + 24t^{*-3} \ldots\ldots]^{-1} \qquad 3.7.16$$

3.7(d). Capture Cross-sections

The capture cross-section cannot be determined from the equation for fast retrapping because it does not contain the parameter ν. For monomolecular and bimolecular recombination, the value of ν may be obtained from the constants B and B_1 respectively. The capture cross-section is then calculated using the relationship

$$\nu = N_c S_t v \qquad 3.7.17$$

which is found by consideration of detailed balance.

3.8. Trap Densities

The charge, Q, passing through a sample as a set of traps empty may be found by integrating the total thermally stimulated conductivity curve with respect to time. Where the photoconductive gain, G, is determined from Equation 2.1.3 and V_o is the volume of the sample, then

$$n_o = Q/eV_oG \qquad 3.8.1$$

3.9. Constant Temperature Method of Thermally Stimulated Conductivity

If a photoconductor is held at constant temperature in the temperature range of the thermal emptying for a particular trap, but below its peak maximum temperature, then a decay in conductivity will be observed. From this variation of conductivity with time it is possible to evaluate the parameters of the trap which is emptying. To describe this variation, Haine and Carley-Read (1968) rewrote Equation 3.6.4 as

$$n_c = n_t \theta \tau_n / \tau_t \qquad 3.9.1$$

where $n_t \simeq N_t$. Now

$$dn_t/dt = - n_c/\tau_n \qquad 3.9.2$$

and so

$$n_c = n_o \theta (\tau_n/\tau_t) \exp(-t\theta/\tau_t) \qquad 3.9.3$$

Where $n_t << N_t$, Equation 3.6.2 may be expressed as

$$n_c = n_t \theta \tau_n / (\tau_n + \tau_t) \qquad 3.9.4$$

and from Equations 3.7.2 and 3.7.4

$$n_c = \frac{n_o \theta \tau_n}{\tau_n + \tau_t} \exp -t\theta/(\tau_n + \tau_t) \qquad 3.9.5$$

Where $\log(n_c)$ is plotted against time for a trap obeying monomolecular recombination kinetics ($\tau_t >> \tau_n$), then a single straight line of slope θ/τ_t is obtained regardless of occupancy. For fast retrapping ($\tau_t << \tau_n$) and high initial occupancy, a plot of $\log(n_c)$

versus time yields at first a line of slope θ/τ_t (Equation 3.9.3) which changes via a curve of variable slope to a straight line of slope θ/τ_n (Equation 3.9.5).

Figure 5.6.6 shows a double exponential decay of current with time for a set of traps which emptied with a thermally stimulated current maximum at approximately 115°K. (Although the capture cross-section for this set of traps was about $10^{-20}cm^2$, their relatively high density ($\sim 10^{15}/cm^3$) yielded a value of 40 for the ratio τ_n/τ_t and so they satisfied the criterion for fast retrapping. τ_t was found from Equation 3.6.3 and τ_n from photoconductivity measurements).

When a single exponential decay is observed it is not possible to differentiate between monomolecular recombination and fast retrapping with initial low occupancy unless the ratio τ_n/τ_t is known. However the thermal activation energy and capture cross-section may easily be determined from a double exponential decay.

References to Chapter 3

Booth, A.H., 1954, Can. J. Phys. 32, 214.

Bube, H.R., 1955, J. Chem. Phys. 23, 18.

Chen, R., 1969, J. Appl. Phys. 40, 570.

Cowell, T.A.T. and J. Woods, 1967, Brit. J. Appl. Phys. 18, 1045.

Dussel, G.A. and R.H. Bube, 1967, Phys. Rev. 155, 764.

Garlick, G.F.J. and A.F. Gibson, 1948, Proc. Phys. Soc. 60, 574.

Grossweiner, L.I., 1953, J. Appl. Phys. 24, 1306.

Haine, M.E. and R.E. Carley-Read, 1968, J. Phys. D. (Brit. J. Appl. Phys.) Series 2, 1, 1257.

Hoogenstraaten, W., 1958, Thesis, University of Amsterdam, submitted February 1958.

Keating, P.N., 1961, Proc. Phys. Soc. 78, 1408.

Land, P.L., 1969, J. Phys. Chem. Solids 30, 1681.

Lax, M., 1960, Phys. Rev. 119, 1502.

Nicholas, K.H. and J. Woods, 1964, Brit. J. Appl. Phys. 15, 783.

Saunders, I.J., 1967, Brit. J. Appl. Phys. 18, 1219.

CHAPTER 4

CRYSTAL GROWTH AND EXPERIMENTAL APPARATUS

4.1. Introduction

In this chapter the growth of CdS boule crystals is described together with the preparation of samples for electrical and optical measurement and the apparatus used. The method of growth is particularly relevant because one of the main objects of the present work was to compare the properties of samples grown in partial pressures of cadmium with those grown in partial pressures of sulphur.

For boule crystals grown in this manner, measurements were made of thermally stimulated current, photocurrent with temperature, spectral response of photocurrent, infrared quenching, and electron bombardment induced photocurrent using a two probe configuration of electrodes. Thermally simulated current, photocurrent with temperature and spectral response were also monitored for selected samples both for three probe and four probe electrode arrangements so that the effects of the crystal surfaces and the contacts might also be studied. Infrared luminescence from boule crystals was investigated by irradiating cleaved crystal faces.

4.2. Growth of CdS Boule Crystals

Boule crystals of CdS were grown in this department using the method described by Clark and Woods (1968). The undoped samples were grown from 'Optran' Grade powder supplied by B.D.H. Chemicals Ltd. Two boule crystals were grown from 'Electronic' Grade powder supplied by Derby Luminescents Ltd. One of these boules was intentionally doped with sodium and the other, although nominally pure, showed similar properties to that which was sodium doped.

In the majority of cases the powder supplied was used as the charge from which boules were grown. However, for the two 'Derby' crystals and for two of the 'Optran' crystals the powder was used to grow small CdS crystals using an argon flow process. (The purpose of this treatment was to purify the starting material by removing volatile impurities with the gas stream.) The flow crystals were then crushed and used as the charge from which the larger boule crystals were grown.

Mass spectrographic analysis of the 'Optran' powder showed that most impurities were present in concentrations of < 0.1 p.p.m. Recrystallisation of this powder, using the argon flow process, did not appear to significantly decrease the impurity concentrations except for a decrease in the copper concentration by a factor of two.

'Derby' starting material was found to be contaminated with zinc, phosphorus, silicon, aluminium and manganese in concentrations of 30 - 90 p.p.m. Chlorine was also shown to be present in concentrations of 150 p.p.m., though prior to the mass spectrographic analysis the samples had been etched in a solution of hydrochloric acid. Recrystallisation did effect a reduction in the concentrations of impurities, though they were still present at levels of 1 - 10 p.p.m.

Figure 4.2.1 shows the furnace arrangement and the growth tube used to grow the boule crystals. The upper and lower furnaces were of conventional design and resistance heated. The temperature of each furnace was recorded and controlled by a Pt-PtRh thermocouple. A spacer was placed between the furnaces to prevent excessive heat transfer. The growth tube was constructed from quartz glass and comprised a 4.0 mm diameter tube joined coaxially to a 1.5 cm diameter growth chamber which was approximately 15 cm

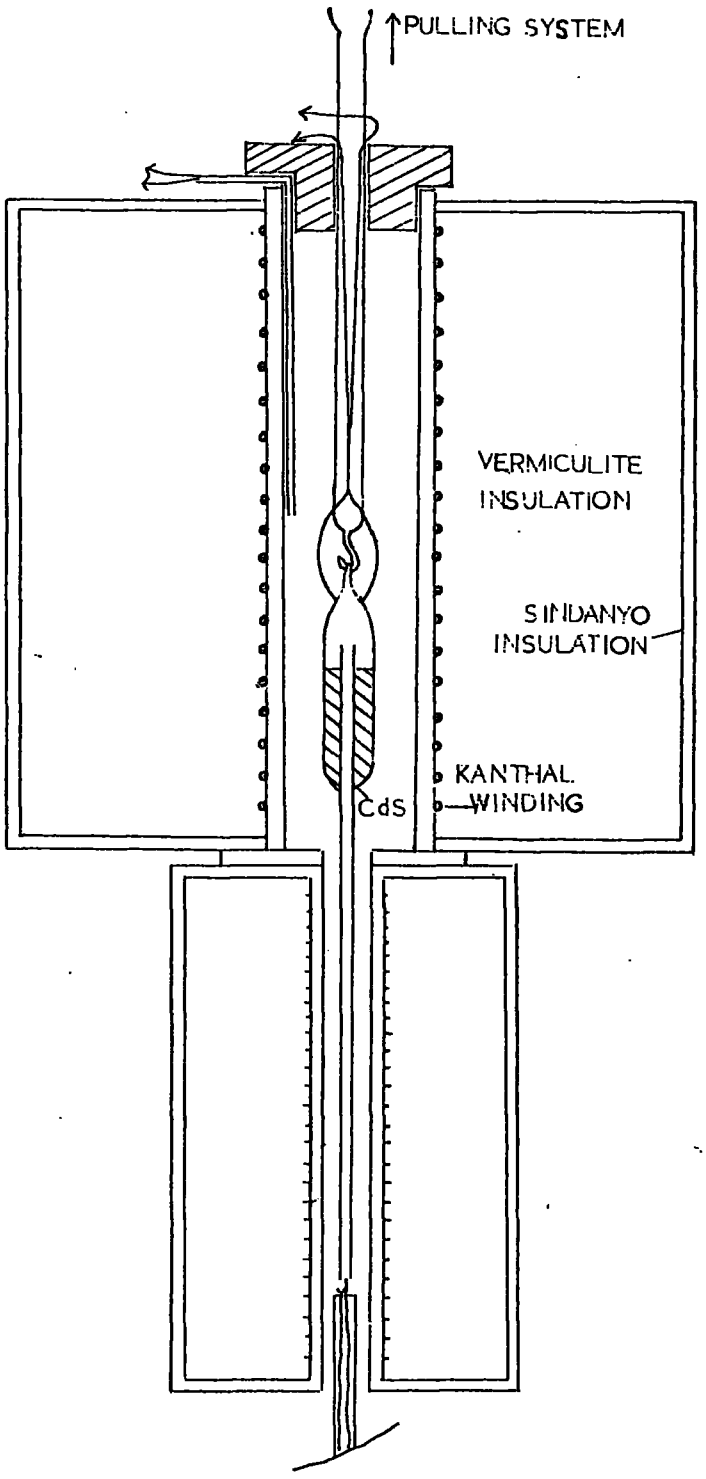

FIGURE 4.2.1. FURNACE ARRANGEMENT SHOWN WITH GROWTH TUBE IN INITIAL POSITION.

long.

The procedure used for the crystal growth was as follows. 0.1 gm of sulphur (cadmium) was placed in the growth chamber, which had previously been evacuated and baked. The sulphur (cadmium) was then melted under vacuum to remove volatile impurities. On cooling, approximately 30 gm of CdS was added to the growth chamber. The growth tube was evacuated for a few hours and sealed. The growth tube was placed in the furnace system, as shown in Figure 4.2.1, and both furnaces were brought to their operating temperatures of 1150°C for the upper furnace and 50°C to 775°C for the lower (reservoir) furnace. The growth tube was pulled vertically at a rate of either 0.6 mm/hr or 1.2 mm/hr, and the excess sulphur (cadmium) distilled into the 'tail' of the growth tube which was situated in the reservoir furnace. The partial pressure of sulphur (cadmium) could be controlled, during the growth of the CdS boule, by adjusting the temperature of the reservoir furnace.

The boule grew from the apex at the top of the growth tube. To avoid polycrystallinity the semi-angle of the conical apex had to be about 30°. With a greater or lesser angle, multiple nucleation occurred. A boule took between 3 to 6 days to grow. After growth it was slowly brought to room temperature over a period of three days.

In the following chapters the notation T_S = X°C (T_{Cd} = X°C) will be used to denote a boule crystal grown in a partial pressure of sulphur (cadmium), where the reservoir furnace was held at a temperature of X°C.

4.3. Electrical Contacts

Samples used for the electrical measurements were usually cut from the boules using a diamond impregnated wheel on a Meyer and Burger Ltd. cutting machine Type T.S3, although in some cases the samples were cleaved from the boules and ground to the size required with carborundum powder (grit size 600). In both cases the samples were subsequently etched in chromic acid and washed in distilled water. The chromic acid etch was made by dissolving 70 gm of chromic oxide in 200 cc of distilled water. 10 cc of concentrated sulphuric acid was then added, and after the resulting solution had cooled it was diluted by the addition of three parts of water to one part of chromic acid.

Electrical contact to the samples was made using indium metal which forms an ohmic contact to CdS (Smith 1955). Three types of contact arrangements were used, which involved two, three and four probe contact to the sample as described in Sections 4.3(a), 4.3(b) and 4.3(c) respectively. The majority of samples were studied using the two probe configuration of electrodes and selected samples were investigated with the three and four probe arrangements. With a three electrode configuration, where a guard ring is used as the third contact, it is possible to monitor the current flowing in the surface region of the sample and compare this with the current travelling through the bulk material. The four probe electrode configuration allows the potential between two central electrodes on a bar of CdS (Figure 4.3.3) to be monitored whilst the current through the two end contacts is measured. In this way the conductivity of the sample can be compared with the current flowing through it, and hence the contact resistance may be investigated.

In all cases, the contacts were made by the evaporation of

1 - 2 μm thick indium layers on to the samples in a conventional evaporator unit evacuated by a water cooled mercury diffusion pump which was backed by an oil rotary pump. A liquid nitrogen 'cold trap' was interposed between the evaporating chamber and the diffusion pump. The indium was evaporated from a molybdenum boat held at 850°C when the evaporating chamber had reached a pressure of about 10^{-5} torr.

4.3(a). Two Probe Configuration of Electrodes

Samples for two probe measurement had dimensions which were typically 1x2x5 mm^3 (Figure 4.3.1(a)). Indium was evaporated onto the four sides of the CdS bar near to its ends (Figure 4.3.1 (b)) using a mask to maintain the centre portion of the bar free from evaporant. The crystal was placed on a glass cover slip, which had two copper wires fixed to it by means of silver filled epoxy resin (Figure 4.3.1(c)). Two small pieces of indium sheet had also been placed in the resin. A strip of indium sheet was laid between each of the evaporated layers on the sample and the indium fixed to the slide (Figure 4.3.1(d)).

The slide was placed on a heater strip mounted under a small bell jar. A chromel-alumel thermocouple was held in contact with the heater strip so that its temperature could be monitored. A positive pressure of oxygen free nitrogen gas was maintained in the bell jar to prevent oxidation of the indium and the CdS. The bell jar was flushed out with nitrogen for five minutes and then the heater strip was raised to a temperature of 200°C and maintained at this temperature until the molten indium sheet wetted the evaporated layers. After cooling to room temperature, the cover slip was removed from the heater and a robust sample was available for measurement.

a]

b]

c]

d]

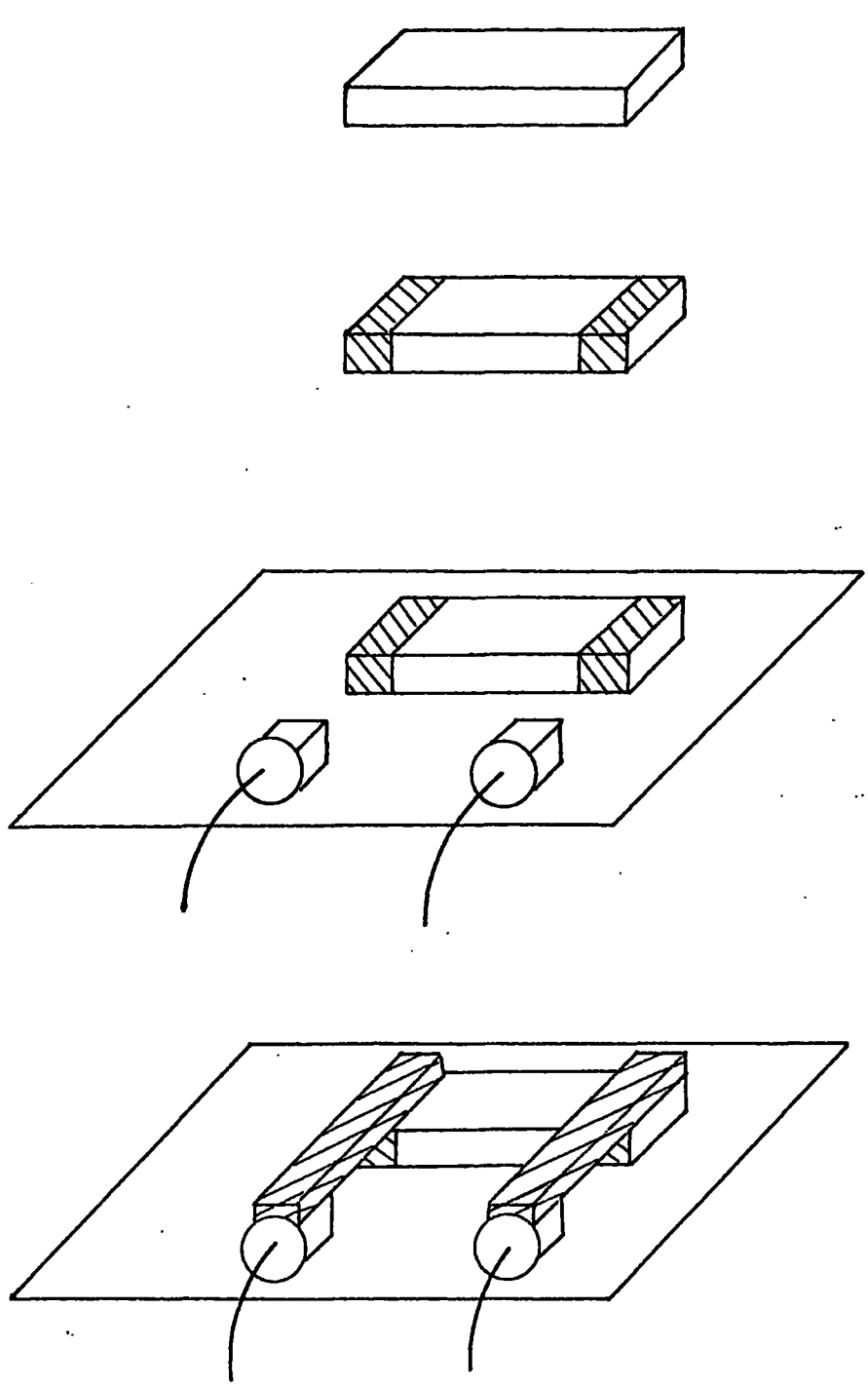

FIGURE 4.3.1. TWO PROBE CONFIGURATION OF ELECTRODES

a] INITIAL SAMPLE

b] SAMPLE WITH EVAPORATED INDIUM CONTACTS

c] SAMPLE ON GLASS SLIDE TOGETHER TWO COPPER WIRES AND TWO PIECES OF INDIUM SHEET FIXED WITH SILVER FILLED EPOXY RESIN

d] FINAL ARRANGEMENT BEFORE MELTING INDIUM

4.3(b). Three Probe Configuration of Electrodes

Irregular shaped CdS plates, as shown in Figure 4,3.2(a), were used for this electrode configuration. The plates were taken from boule crystals both by sawing and by grinding cleaved pieces. The samples were again etched in chromic acid and washed in distilled water prior to the evaporation of indium. The thickness of the plates varied from 0.5 to 1.0 mm. The surface area (about 25 mm^2) was sufficient to allow a guard ring, which was 0.6 mm wide and had an outside diameter of 3.5 mm, to be evaporated on to one surface. At the centre of this ring a spot of indium, 1.2 mm in diameter, was also evaporated (Figure 4.3.2 (b)). An indium disc of diameter 3.5 mm (bottom contact) was evaporated onto the face of the crystal opposite to that on which the guard ring had been deposited.

A disc of indium sheet of the same size as the bottom contact was cemented to a cover slip, using silver filled epoxy resin, together with two copper wires which were used as connections to the guard ring and centre spot. A further disc of indium sheet the same size as the bottom contact was gently pressed against the evaporated bottom contact, and two small pieces of indium were pressed onto the guard ring and the centre spot. The resulting sample, with the attached indium, was placed on the cover slip so that the indium disc on the sample and that on the cover slip were completely in contact. The cover slip was heated in an oxygen free nitrogen gas flow until the indium melted. On cooling, the samples connections were completed by attaching the two free copper wires on the cover slip to the dots of indium on the guard ring and centre spot (Figure 4.3.2(c) and (d)).

A guard ring arrangement was also used on bar shaped samples approximately 6 mm long and 1 mm^2 in cross-sectional area. Two

a)

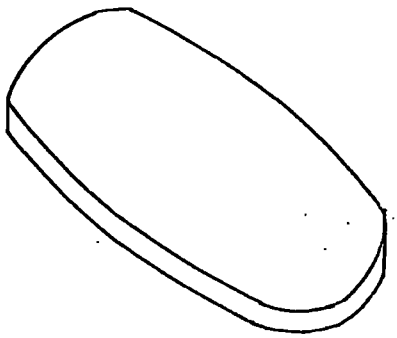

b)

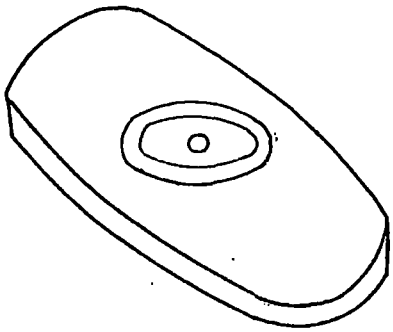

c)

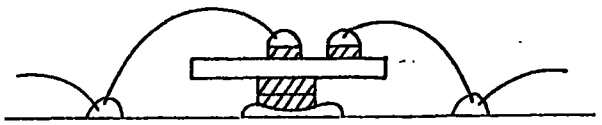

d)

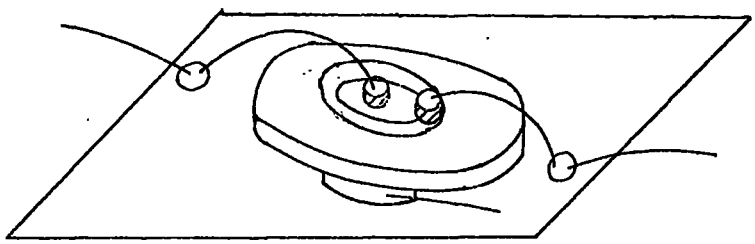

FIGURE 4.3.2. THREE PROBE CONFIGURATION OF ELECTRODES.

a) INITIAL SAMPLE.

b) SAMPLE WITH EVAPORATED INDIUM CONTACTS.

c) SIDE ELEVATION BEFORE MELTING INDIUM.

d) PERSPECTIVE VIEW OF COMPLETED SPECIMEN.

end contacts were evaporated in a similar manner to that employed for electrical contact to two probe samples. In addition, a ring of indium (0.5 mm wide) was deposited near to one of the end contacts by performing four separate evaporations through a metal mask.

4.3(c). Four Probe Configuration of Electrodes

Some of the techniques developed for the two and three probe samples were used in attaching four probes to a CdS bar. Typical dimensions of the samples were 1x2x8 mm^3. The end contacts were formed in exactly the same manner as those for a two probe sample. The wires to the two evaporated spots between the end contacts were fixed in the same way as the wires to the guard ring and centre spot of a three probe specimen.

Figure 4.3.3 shows the steps in the manufacture of a four probe sample. In Figure 4.3.3(a) the initial sample is shown, and in Figure 4.3.3(b) the evaporated indium layers can be seen. Figure 4.3.3(c) and (d) shows the side elevation and perspective view of the finished specimen.

4.4. D.C. Current Measurement

The currents measured during the study of thermally stimulated current, spectral response and infrared quenching lay in the range 10^{-3} to 10^{-13} amperes. Figure 4.4.1(a) shows the circuit diagram of the voltage supply together with a block diagram of the amplifiers and the chart recorders. Non-microphonic cable and B.N.C. plugs and sockets were used for all external electrical coupling on the low current side of the d.c. amplifier. The voltage supply was powered by a 120 volt 'Winner' battery, which was contained in an earthed metal box. The positive side of the

a)

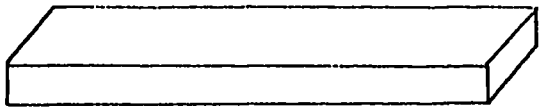

b)

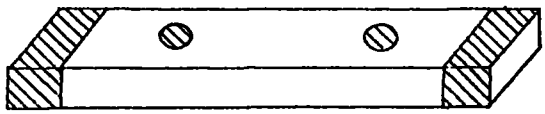

c)

d)

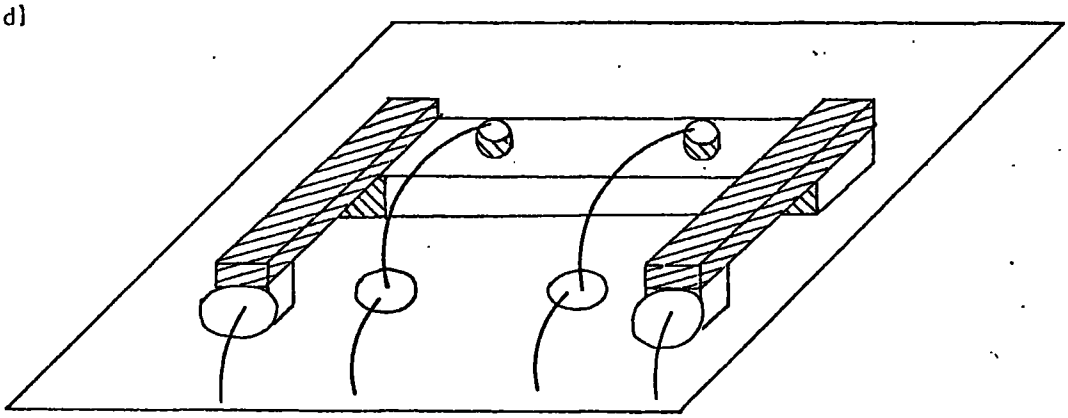

FIGURE 4.3.3. FOUR PROBE CONFIGURATION OF ELECTRODES

a) INITIAL SAMPLE.

b). SAMPLE WITH EVAPORATED CONTACTS.

c) SIDE ELEVATION OF COMPLETED SPECIMEN.

d) PERSPECTIVE VIEW OF COMPLETED SPECIMEN.

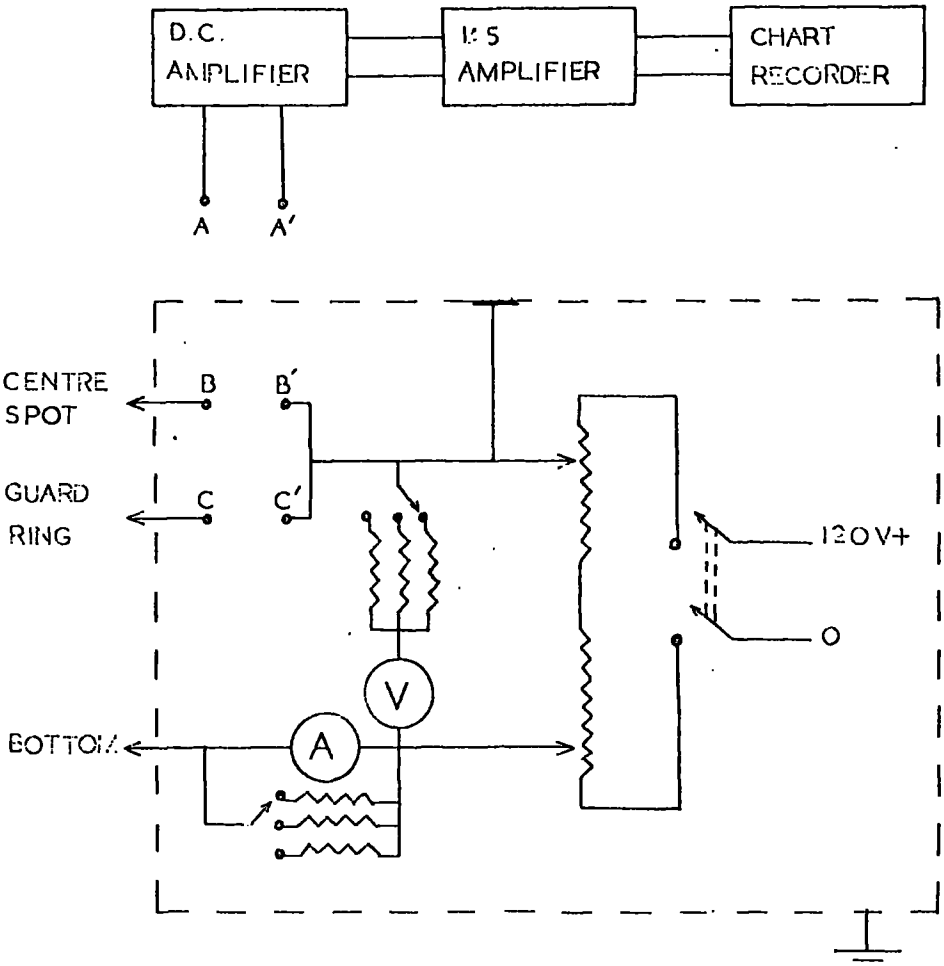

FIGURE 4.4.1.(a) CIRCUIT DIAGRAM FOR D.C. CURRENT MEASUREMENT.

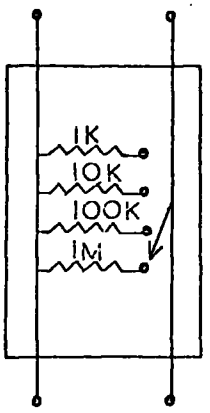

FIGURE 4.4.1.(b) SWITCHABLE RESISTORS USED FOR MEASUREMENT OF CURRENT IN THE RANGE 10^{-3} TO 10^{-6} AMPERES

voltage supply was maintained at earth potential.

For three probe measurement a coaxial lead from the d.c. amplifier, shown as A-A' in Figure 4.4.1(a), could either be plugged into the current lead from the guard ring (B-B') or into the current lead from the centre spot (C-C'). A plug was used to short out C-C' (B-B') when it was required to monitor the centre spot (guard ring) current while the guard ring (centre spot) was held at substantially the same potential.

For two and four probe measurements the leads marked 'spot' and 'bottom' in Figure 4.4.1(a) were connected to the ends of the sample and the current measured by joining A-A' to B-B'.

The d.c. amplifier was a Type NE 503B model manufactured by Rank Nucleonics and Control Ltd. which was designed to measure current in the range 10^{-6} to 10^{-13} amperes. Where continuous monitoring of higher currents in the range 10^{-3} to 10^{-6} amperes was required switchable resistors (Figure 4.4.1(b)) were placed in series with the current lead and the voltage across these resistors measured on the 0 - 1 volt range of the d.c. amplifier. Accurate point to point measurement in the higher current range was made using a Sangamo and Weston d.c. microammeter Model S82.

The output of the d.c. amplifier was from 0 - 1 milliamperes. The output was fed to a 5 milliampere full scale deflection Record chart recorder (Type M/A DC MC) via a 1:5 amplifier the gain of which was linear in the required range. The chart recorder input leads could be shorted out using a push button switch. This enabled calibration marks to be placed on the recorder trace at convenient temperatures as the current was being measured as a function of temperature.

A Sweeney E.S.T.V. Model 1170 was used to measure the

potential between electrodes during four probe studies. The input impedance of this instrument was greater than 10^{13} ohms.

4.5. Cryostat Design and Specimen Mounting

Two cryostats were used during the course of the measurements to be described in Chapters 5 to 9. These were similar as may be seen from Figures 4.5.1 and 4.5.2, which show the cryostats used for the measurement of (1) thermally stimulated current and infrared luminescence and (2) spectral response and infrared quenching. In both cases, the sample was mounted on a copper block at the end of the nitrogen 'tank'. The copper block was cooled by pouring liquid nitrogen into the central tube. Heating was achieved by placing a resistance heater inside this tube. The cryostat used for the spectral response and infrared quenching had a 0.7 litre capacity tank above the specimen block. It was therefore possible to maintain liquid nitrogen temperatures for some three hours from a single filling.

During the majority of measurements, the cryostat inner was surrounded by a vacuum jacket which had 'O' ring sealed quartz windows placed in positions appropriate to the measurement required. The vacuum interspace could be maintained at either rotary oil pump pressures, or at diffusion pump pressures by means of a conventional water cooled oil diffusion pump backed by a rotary pump. A liquid nitrogen 'cold trap' was situated between the diffusion pump and the cryostat so that condensible vapours could be removed when required.

The specimens were mounted on the copper block of the cryostat in the following manner. A small quantity of Edwards high

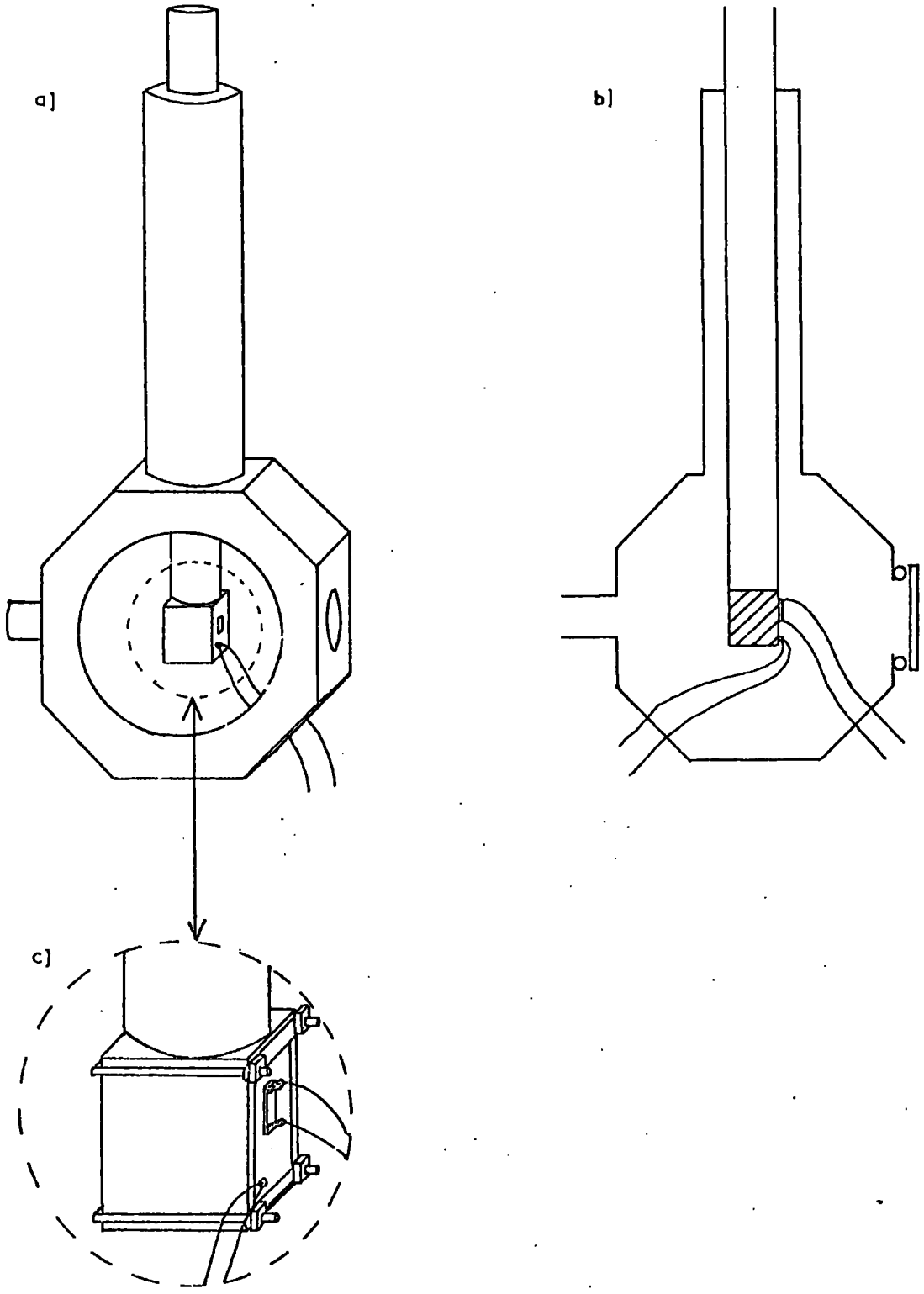

FIGURE 4.5.1. CRYOSTAT FOR THERMALLY STIMULATED CURRENT AND INFRARED LUMINESCENCE MEASUREMENTS

a] PERSPECTIVE VIEW WITH SAMPLE MOUNTED FOR INFRARED LUMINESCENCE.

b] SIDE ELEVATION WITH SAMPLE MOUNTED FOR THERMALLY STIMULATED CURRENT MEASUREMENT.

c] ARRANGEMENT OF SAMPLE ON THE COPPER BLOCK FOR TWO PROBE THERMALLY STIMULATED CURRENT MEASUREMENT.

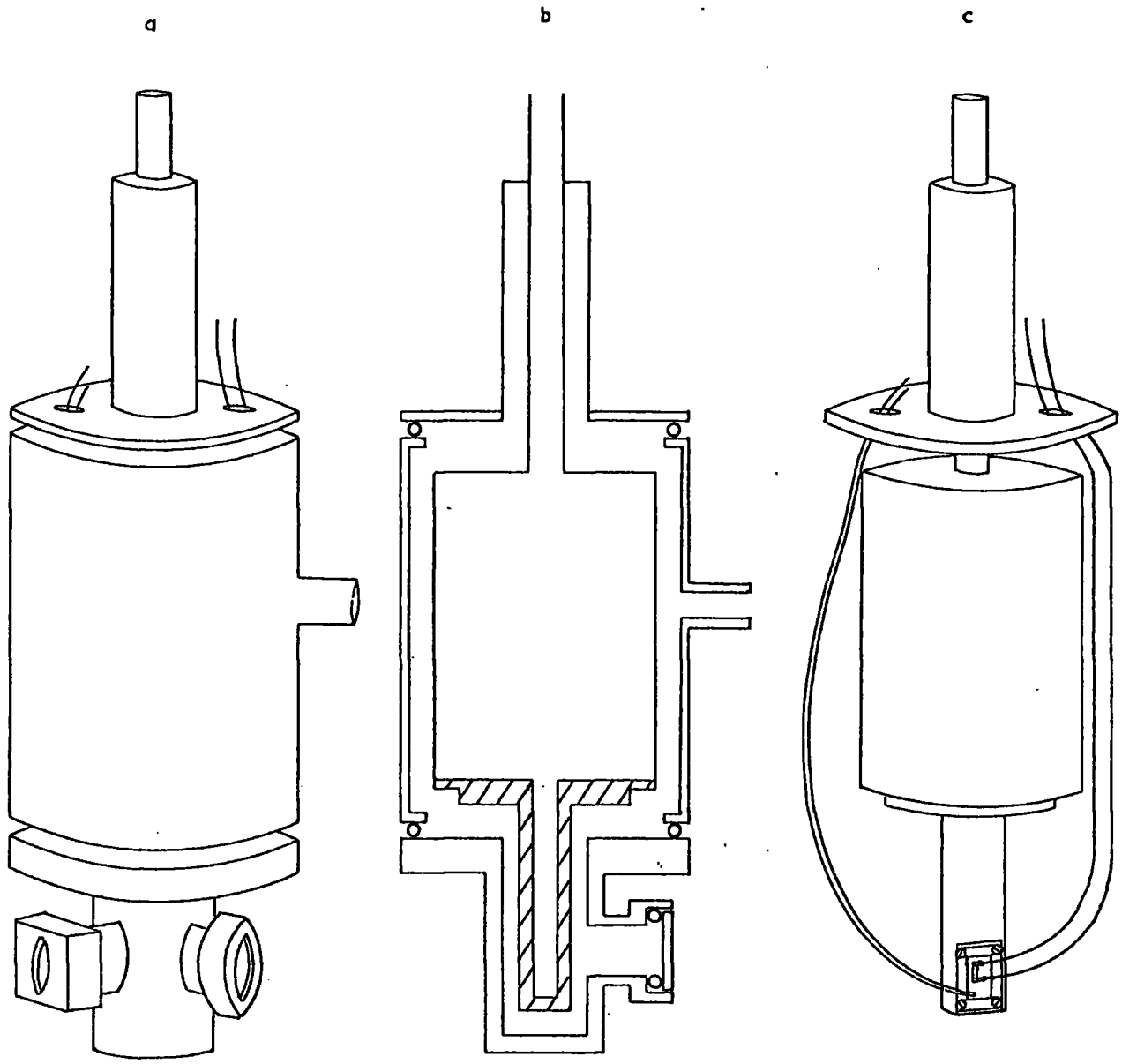

FIGURE 4.5.2. CRYOSTAT FOR SPECTRAL RESPONSE AND INFRARED QUENCHING MEASUREMENTS.

a) PERSPECTIVE VIEW.

b) SIDE ELEVATION.

c) PERSPECTIVE VIEW OF CRYOSTAT INNER.

vacuum silicone grease was smeared under the cover slip to ensure reasonable thermal contact to the block. The cover slip was secured rigidly to the block by two phosphor bronze straps. These straps were either held against the block by two small 'U' bolts (Figure 4.5.1(b)) or bolted to it (Figure 4.5.2(c)).

Electrical connections from the mounted sample to the exterior of the cryostat were made by means of a glass to metal seal soft soldered to the outside wall of the cryostat. The leads entering the body of the cryostat were electrically screened by a metal cap bolted over the glass to metal seal. B.N.C. sockets mounted on the cap were used for coaxial wire connection to the power supply and the amplifier.

A copper/constantan thermocouple was soldered to the cover slip with indium. The wires also passed to the cryostat exterior via the glass to metal seal. The reference junction of the thermocouple was placed in a beaker of water at room temperature, and the thermocouple potential was measured using a portable potentiometer (Cat. No. 7569P) manufactured by W.G. Pye and Co. Ltd.

The samples for infrared luminescence measurement were attached to the copper block with indium. The temperature was again measured by a copper/constantan thermocouple soldered to the block.

4.6. Thermally Stimulated Current Measurements

Thermally stimulated current measurements were made using the cryostat shown in Figure 4.5.1, with the sample attached as shown in Figure 4.5.1(b) and (c). The larger opening was closed by means of a flat plate and an 'O' ring seal. The sample could be

illuminated through the smaller window using a 750 watt tungsten lamp, which was filtered with a one centimetre path length of 10% copper sulphate solution and two Chance HA1 filters where this was required. For measurements in the dark, a light-tight cap was placed over the smaller window.

The details of the illumination schedule, heating rate and applied voltage used during the course of thermally stimulated current measurement are given in Section 2 of the following chapter.

4.7. Infrared Luminescence

The samples for infrared luminescence were mounted on the copper block of the cryostat as shown in Figure 4.5.1(a). A schematic diagram of the experimental arrangement can be seen in Figure 4.7.1. Radiation from a 250 watt mercury lamp was filtered with a one centimetre path length of 10% copper sulphate solution and two Chance HA1 infrared absorbing filters. The filtered light was focussed onto the sample by a lens. The luminescence emission from the sample, which was chopped at 800 cycles per second, was collected onto the input slits of a Barr and Stroud monochromator Type VL2 using two front silvered concave mirrors. The output of the monochromator was measured with a PbS cell, which was connected to a Barr and Stroud amplifier Type 7909 tuned to the chopping frequency. The output signal from the amplifier was recorded on a Honeywell Electronik 15* strip chart recorder.

The monochromator wavelength control was driven by a synchonous motor via a seven speed gear box (Barr and Stroud Type SQ20). The control operated a switch which closed at intervals of four minutes to record the rotation of the quartz prisms.

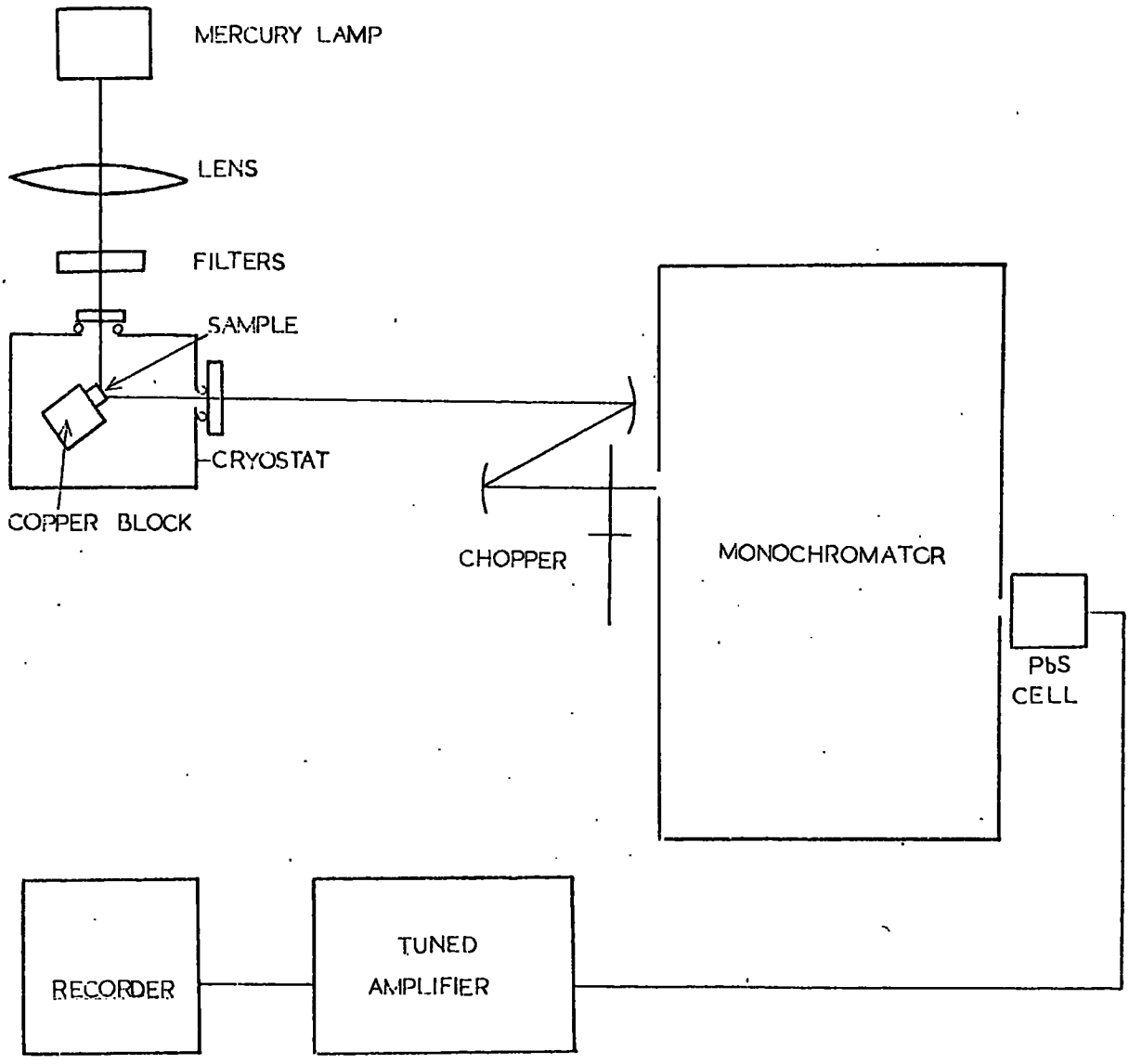

FIGURE 4.7.1. ARRANGEMENT FOR MEASUREMENT OF INFRARED LUMINESCENCE.

This switch was used to activate a solenoid in the chart recorder which caused a subsiduary pen to trace out a short line perpendicular to the edge of the chart.

The PbS cell was calibrated against a thermopile using a tungsten lamp. The output of the thermopile was again amplified using the Barr and Stroud amlifier. The chopping frequency in this case was 10 cycles per second.

Measurements of infrared luminescence, which are discussed in Chapter 9, were made in the spectral range 0.6 - 2.5 μm. This range represented the effective limits of the above system. The infrared filters passed light of wavelength less than 0.6 μm, and radiation passing through the monochromator was 'cut off' at 2.5 μm.

4.8. Spectral Response and Infrared Quenching of Photocurrent

Spectral response and infrared quenching measurements were made using the cryostat shown in Figure 4.5.2. The left hand window (Figure 4.5.2(a)) of the cryostat was clamped against the output slits of the monochromator with a special adaptor. This adaptor allowed for vertical movement of the cryostat relative to the output slits. A 250 watt tungsten lamp was focussed on the input slits of the monochromator using the two front silvered mirrors. The sample was set at 45° to the two windows by rotating the inner section of the cryostat (Figure 4.5.2(c)). The cryostat was then lifted vertically using a screw type 'jack' until the maximum response of the sample was obtained with light coming from the output slits of the monochromator.

For spectral response measurements, the right hand window shown in Figure 4.5.2(a) was closed by means of a brass cap, so that the only exciting radiation came from the output slits of the

monochromator.

When infrared quenching was to be studied illumination from a 750 watt tungsten lamp, filtered with copper sulphate solution and two Chance HA 1 filters, was also incident on the sample via the right hand window. The quenching radiation was then supplied from the output slits of the monochromator.

The spectral response and infrared quenching radiations were arranged so that their energy density, in the region of the sample, were constant for all the wavelengths examined. This was achieved by measuring the output of the monochromator with a thermopile, as described in Section 4.7, and adjusting the current passing through the tungsten lamp to give constant energy output at the wavelength band widths used.

Spectral response and infrared quenching will be discussed in Chapter 8. Response measurements were made in the spectral range 0.44 μm to 2.50 μm at 90°K, room temperature and 388°K. Infrared quenching was measured at 90°K and at room temperature, for wavelengths from 0.7 μm to 2.0 μm.

References to Chapter 4

Clark, L. and J. Woods, 1968, J. Cryst. Growth 3, 4, 126.

Smith, R.W., 1955, Phys. Rev. 97, 1525.

CHAPTER 5

TWO PROBE THERMALLY STIMULATED CURRENT MEASUREMENT

5.1. Introduction

A theoretical discussion of thermally stimulated conductivity was presented in Chapter 3. In practice the quantity measured is the thermally stimulated current (T.S.C.) which is monitored while the trapping centres are emptying. The form of an isolated T.S.C. curve is the same as that for thermally stimulated conductivity, though the normalisation constant for the particular type of recombination kinetics considered must be modified using the relationship

$$\sigma = IL/VA_r \qquad 5.1.1$$

where V is the voltage applied to a sample of length L and cross-sectional area A_r. (A computor programme is given in Appendix 1, which was used to generate theoretical T.S.C. curves for mono-molecular recombination, fast retrapping and bimolecular recombination. The equations for conductivity as a function of temperature in these three cases, Equations 3.7.4, 3.7.7 and 3.7.14 respectively, were modified using Equation 5.1.1 to give the expressions for T.S.C.)

Samples cut from 'Optran' boule crystals, grown with varying cadmium and sulphur reservoir temperatures as described in Chapter 4, showed eight T.S.C. peaks in the temperature range 95°K to 388°K. In this chapter the values of the trapping parameters of these eight traps will be discussed together with the variation of trap density with growth conditions. The T.S.C. curves for two samples obtained from boule crystals grown from Derby Luminescent material are presented in Section 5.11.

In some samples the magnitude of the T.S.C. associated with some of the peaks was seen to vary with the temperature of illumination prior to measurement. However, these phenomena will be discussed in the following chapter.

5.2. Experimental Procedure

Each sample investigated was mounted on a pyrex slide as described in Chapter 4. The slide was attached to the tail of a liquid nitrogen cryostat, together with a copper constantan thermocouple. In order that reproducible measurements could be obtained a strict heating and cooling cycle was followed. The sample was first heated in the dark to a temperature of 388°K and on cooling was illuminated from any desired intermediate temperature T_i. When the lowest temperature, approximately 95°K, was attained the illumination was continued for a further five minutes. Where T.S.C. measurement was required the illumination was removed. A fixed voltage of 100 volts was then applied to the sample, and the T.S.C. was monitored while the sample was heated from liquid nitrogen temperatures to 388°K. To record the photocurrent as a function of temperature, the illumination was maintained during the heating from low temperature.

Illumination was carried out using a 750 watt tungsten lamp, which was filtered using two Chance HA 1 infrared filters and a one centimeter path length of 10% copper sulphate solution contained in a pyrex cell.

It was not found possible to maintain a heating rate which was constant over the range 95°K to 388°K, but within the temperature region of a particular peak the deviation from linearity was small. Figure 5.2.1 shows a typical plot of temperature versus time during a T.S.C. run. The heating rate in this case varied between an initial rate of 0.53°K/sec and a final rate of 0.31°K/sec.

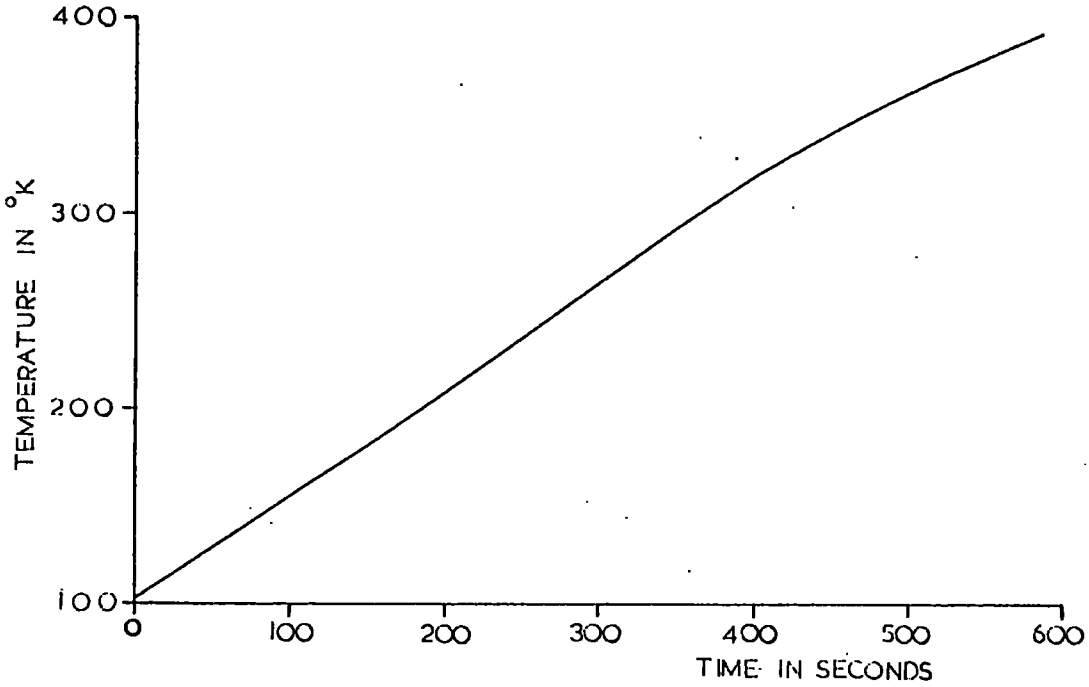

FIGURE 5.2.1 TEMPERATURE VERSUS TIME FOR A TYPICAL T.S.C. RUN

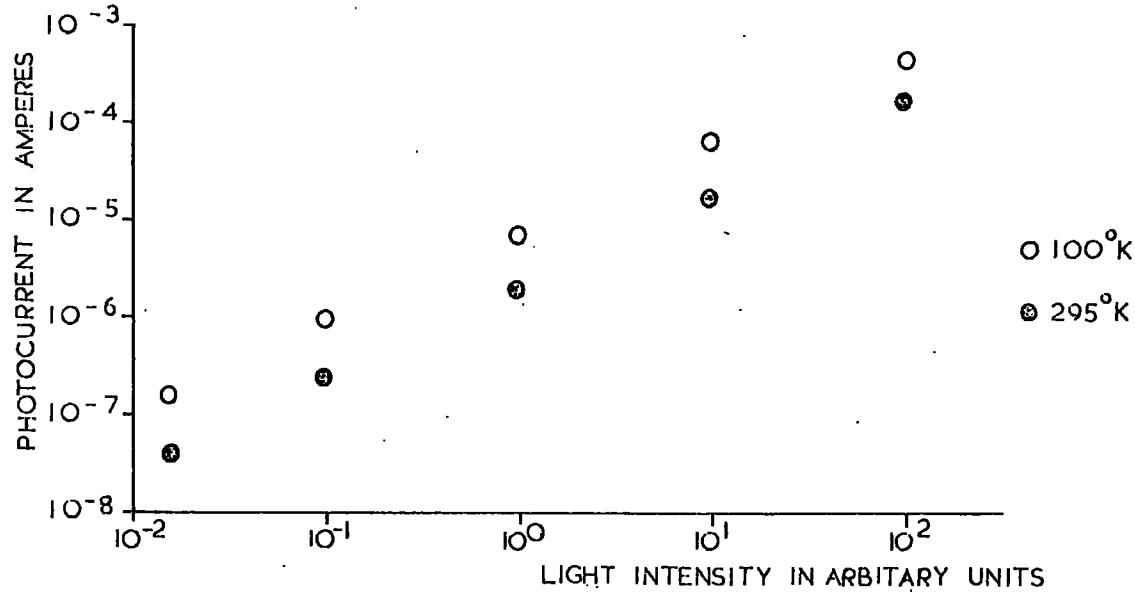

FIGURE 5.3.1 PHOTOCURRENT VERSUS LIGHT INTENSITY FOR A T_{Cd} = 550°C SAMPLE

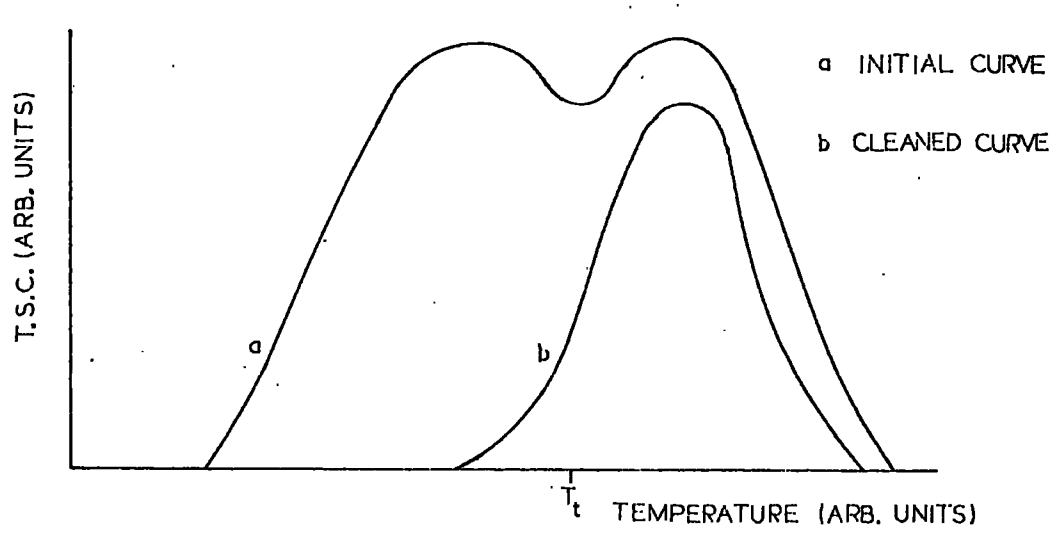

FIGURE 5.4.1 THERMAL CLEANING OF A T.S.C. CURVE

5.3. Measurement of Photocurrent

The variation of the photocurrent with temperature was measured on all samples examined using the T.S.C. technique, in order that the variation of the free electron lifetime, τ_n, might be estimated. The theoretical expressions for T.S.C. are valid only when the free electron lifetime is independent of temperature. If τ_n varies with temperature either a correction must be applied or the T.S.C. data must be disregarded. A knowledge of the value of the free electron lifetime is also essential for the determination of the photoconductive gain, which must be known if the density of trapping centres is to be calculated from the T.S.C. data.

The free electron lifetime cannot be obtained from photocurrent measurements made under the same conditions as those which prevail during a T.S.C. run. If the photocurrent is measured, with the temperature varying, at the same current level as the T.S.C. then the thermal emptying of the traps will modify the photocurrent observed. Similarly, measurement of the photocurrent at a number of fixed temperatures over the temperature span of a T.S.C. run can only be used if it is assumed that the lifetime under equilibrium conditions is equivalent to that where the temperature is varying.

In fact, the temperature variation of the photocurrent was measured using the same intensity of illumination as that used to excite the sample. Measurements of photocurrent versus light intensity, at both liquid nitrogen and room temperatures, were found to be reasonably linear down to current levels some two orders of magnitude greater than the T.S.C. (Typical results of photocurrent versus light intensity are shown in Figure 5.3.1 for a sample grown with $T_{Cd} = 550^{o}C$). It was therefore assumed that

the photocurrent at high light intensity reflects the variation of lifetime at a current level similar to that experienced during a T.S.C. run, at least for temperatures between liquid nitrogen and room temperatures.

In this chapter the T.S.C. results reported are those obtained when the temperature variation of lifetime was small.

5.4. Thermal Cleaning

Where a T.S.C. measurement yields two or more overlapping peaks, the analysis of each peak is simplified by emptying the traps lying on the low temperature side of the peak considered. Figure 5.4.1 curve (a) is a complete T.S.C. curve containing two such overlapping peaks. By heating the sample to a temperature T_t the low temperature trap is emptied, and on cooling and subsequent reheating curve (b) is obtained, which is the T.S.C. contribution due to the higher temperature trap. It should be noted that the magnitude of the T.S.C. of the higher temperature trap is decreased by this cleaning process.

5.5. Variation of the T.S.C. Spectrum with Growth Conditions

The variation of T.S.C. with temperature yields a structured curve which is analagous to optical absorption spectra. As the absorption versus wavelength shows a number of absorption bands, so the T.S.C. versus temperature curve shows band-like structure due to the thermal emptying of different traps. The term 'T.S.C. spectra' will be used to denote T.S.C. versus temperature curves.

Two basic forms of T.S.C. spectra were found in undoped 'Optran' samples grown with various over pressures of cadmium and sulphur. Figure 5.5.1 shows the T.S.C. spectra as samples grown with $T_{Cd} = 350^{o}C$ (two samples), $T_S = 50^{o}C$ and $T_S = 150^{o}C$. The

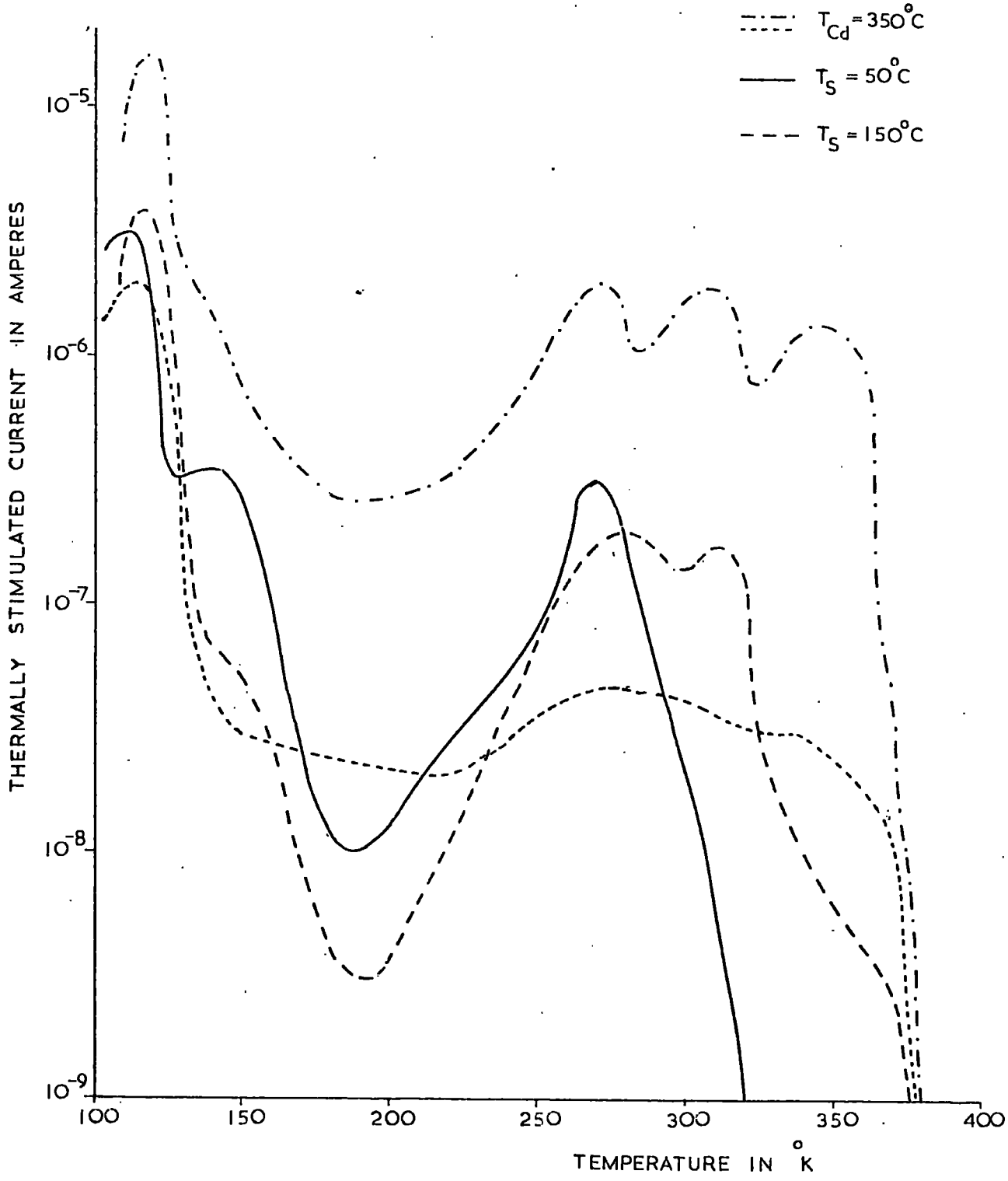

FIGURE 5.5.1. THERMALLY STIMULATED CURRENT SPECTRA OF FOUR CADMIUM RICH SAMPLES

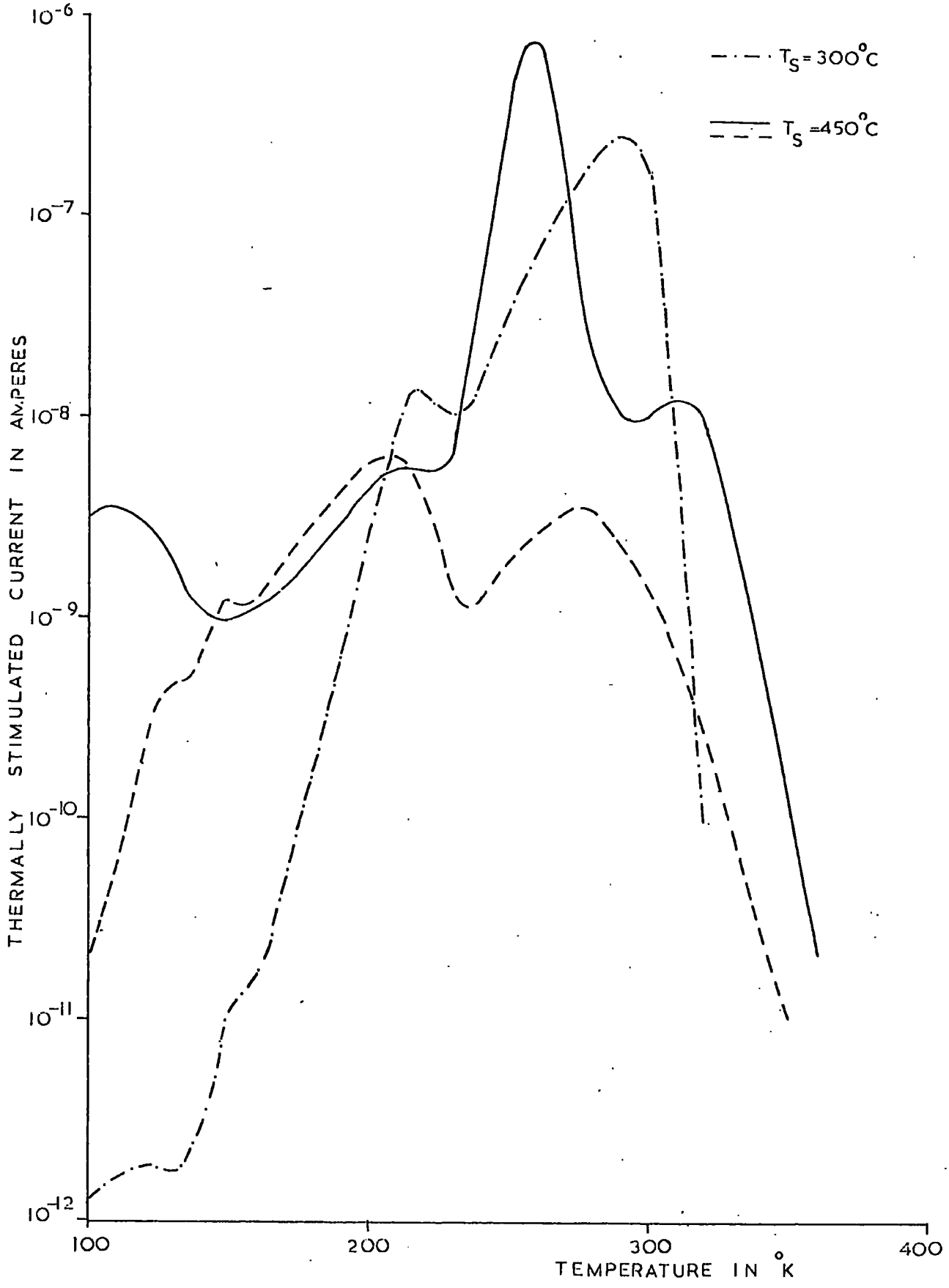

FIGURE 5.5.2. THERMALLY STIMULATED CURRENT SPECTRA OF THREE SULPHUR RICH SAMPLES

spectra in Figure 5.5.2 were found in samples grown with T_S = 300°C (two samples) and T_S = 450°C. In both Figures 5.5.1 and 5.5.2 the dark current has been subtracted from the spectra. To simplify description of the various samples investigated, the term 'cadmium rich' will be used when referring to samples showing T.S.C. spectra similar to those shown in Figure 5.5.1 and the term 'sulphur rich' when the T.S.C. is similar to that shown in Figure 5.5.2.

In most cases the T.S.C. spectra measured on samples cut from the same boule were similar. Figures 5.5.3 and 5.5.4 show the T.S.C. spectra of samples cut from boule crystals grown with T_{Cd} = 350°C and T_s = 300°C respectively. The magnitude of the T.S.C. in both figures indicates a maximum variation in trap density of approximately one order of magnitude for samples taken from the same boule. (This observation is made directly from the T.S.C. levels in Figures 5.5.3 and 5.5.4 as all four samples were of similar dimensions (about 1x1x4 mm^3) and the free electron lifetime was similar when the samples were obtained from the same boule).

When the T.S.C. spectrum was remeasured on a sample, which had been etched in orthophosphoric acid at 150°C, it was found to be similar to that measured previously. This may appear to be a trivial observation, but it does indicate defect stability at 150°C and also reproducibility of contact phenomena.

5.6. The Thermal Activation Energies and Capture Cross-sections of the Low Temperature Traps

Five trapping centres were found which yielded peak maxima in the temperature range 95°K to 230°K. These traps will be denoted by the letters A, B, C, D and E. Their peak maximum temperatures

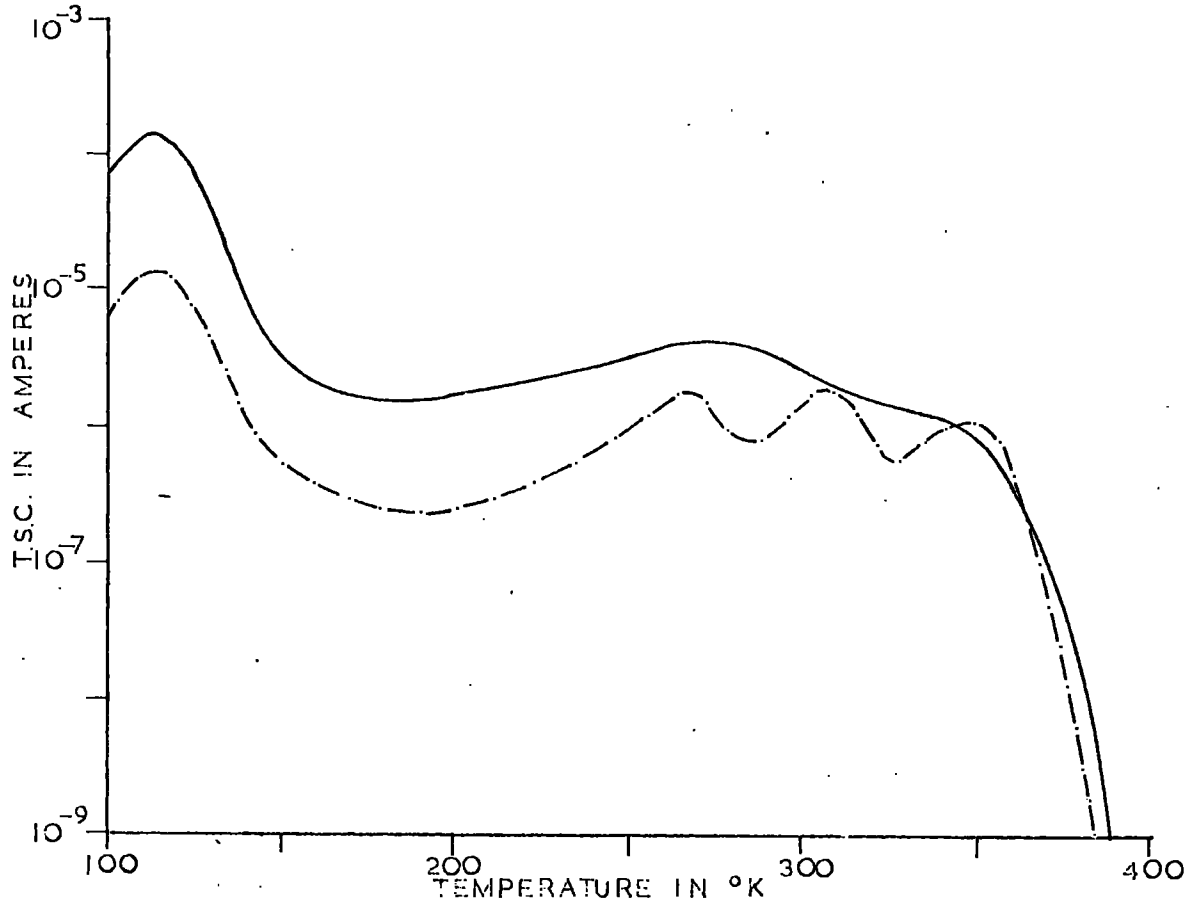

FIGURE 5.5.3. T.S.C. SPECTRA FOR TWO SAMPLES TAKEN FROM A BOULE GROWN WITH $T_{Cd} = 350\,^{\circ}C$

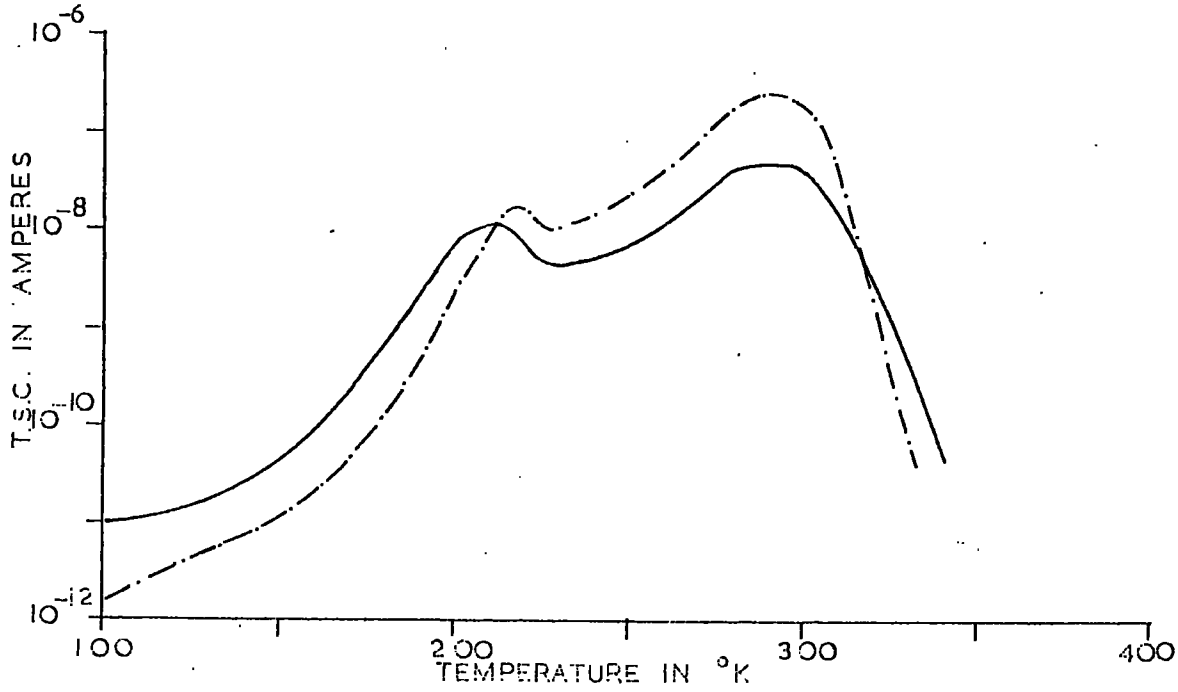

FIGURE 5.5.4. T.S.C. SPECTRA FOR TWO SAMPLES TAKEN FROM A BOULE GROWN WITH $T_S = 300\,^{\circ}C$

were approximately 115°K, 138°K, 158°K, 190°K and 212°K respectively, using heating rates in the range 0.1°K/sec to 0.5°K/sec. As can be seen in Figure 5.5.1, traps A, B, and C are predominant in crystals grown either in excess pressures of cadmium or in low pressures of sulphur. With crystals prepared under higher sulphur pressures, the fourth lowest maximum (which in one sample comprised two peaks due to traps D and E) was more prominent as may be seen in Figure 5.5.2.

The values of thermal activation energy, E_t, and capture cross-section, S_t, for traps A, B, and C were, in most cases, found from samples grown in cadmium rich conditions, where thermal cleaning gave reasonable curves. The trapping parameters of traps D and E were obtained from samples grown in sulphur rich conditions. It was found that a good fit was obtained using the theoretical slow retrapping formula applied to each of the five lowest T.S.C. peaks. Figures 5.6.1 to 5.6.3 show typical cleaned peaks for traps A, B, and C, together with the points of the theoretical curves which give the best fit.

The fourth lowest maxima, found in a sample grown with T_S = 450°C, could be fitted to a theoretical slow retrapping curve with an activation energy of 0.27 eV. However, careful thermal cleaning of this peak led to a trap depth of 0.43 eV, indicating that the initial 'trap' was in fact a doublet comprising traps D and E. Figure 5.6.4 shows the doublet and the theoretical slow retrapping curves the sum of which forms the envelope of the doublet, E_t = 0.31 eV for trap D and E_t = 0.44 eV for trap E.

Trap E, found in a sample grown with T_S = 300°C, is shown in Figure 5.6.5. A good fit was obtained with a theoretical slow retrapping curve, where E_t = 0.44 eV, though trap D could not be detected.

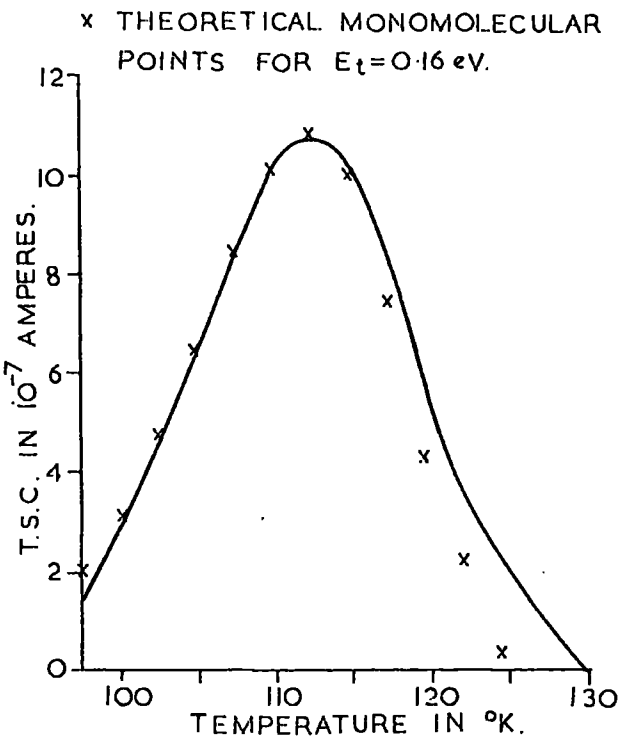

FIGURE 5.6.1 T.S.C. CURVE FOR TRAP A [FROM A T_S=150°C SAMPLE].

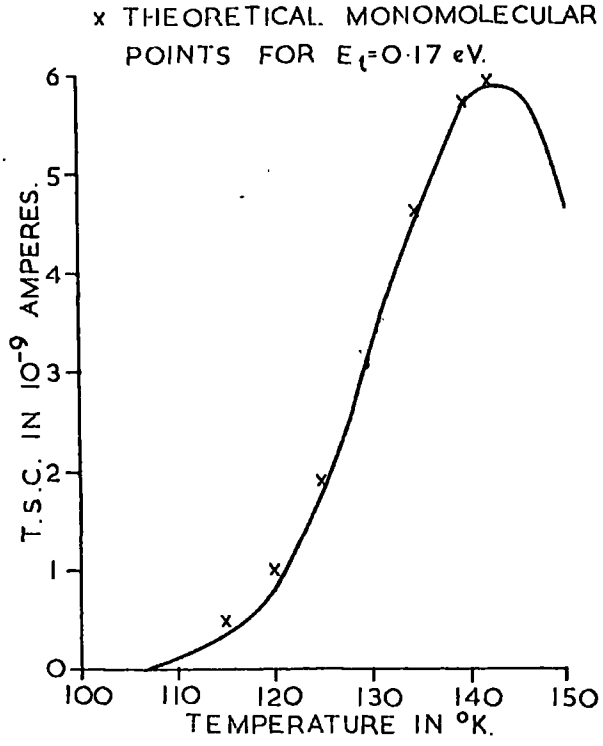

FIGURE 5.6.2 T.S.C. CURVE FOR TRAP B [FROM A T_S=150°C SAMPLE].

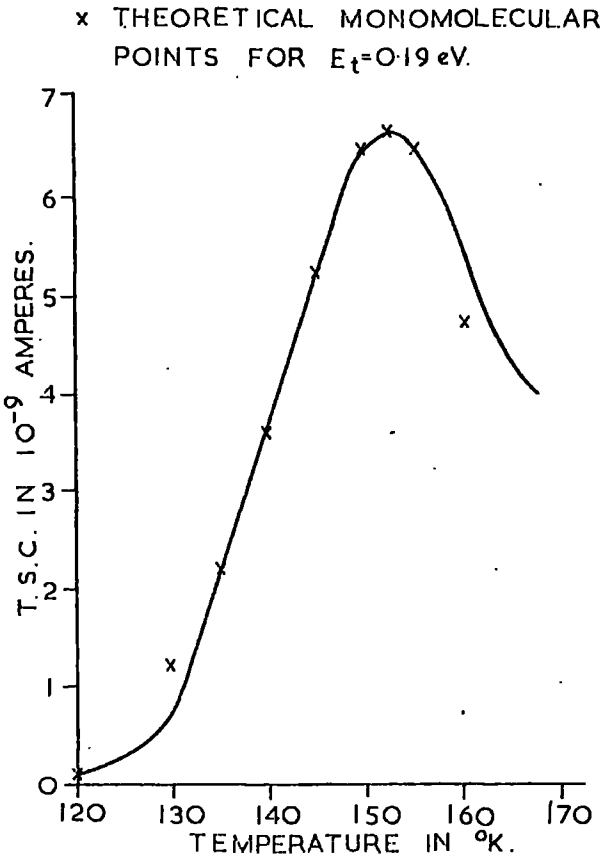

FIGURE 5.6.3 T.S.C. CURVE FOR TRAP C [FROM A T_S=150°C SAMPLE].

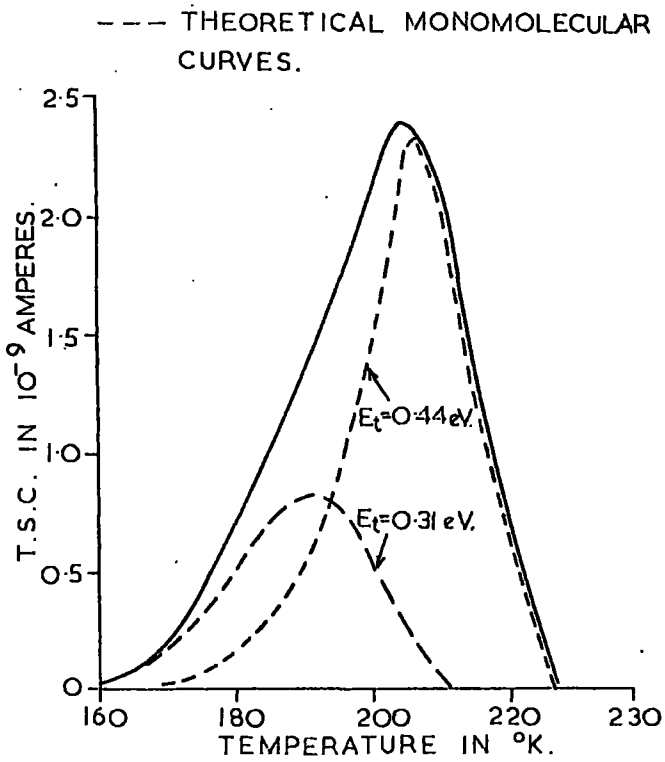

FIGURE 5.6.4 T.S.C. CURVE FOR DOUBLET COMPRISING TRAPS D AND F [FROM A T_S 450°C SAMPLE].

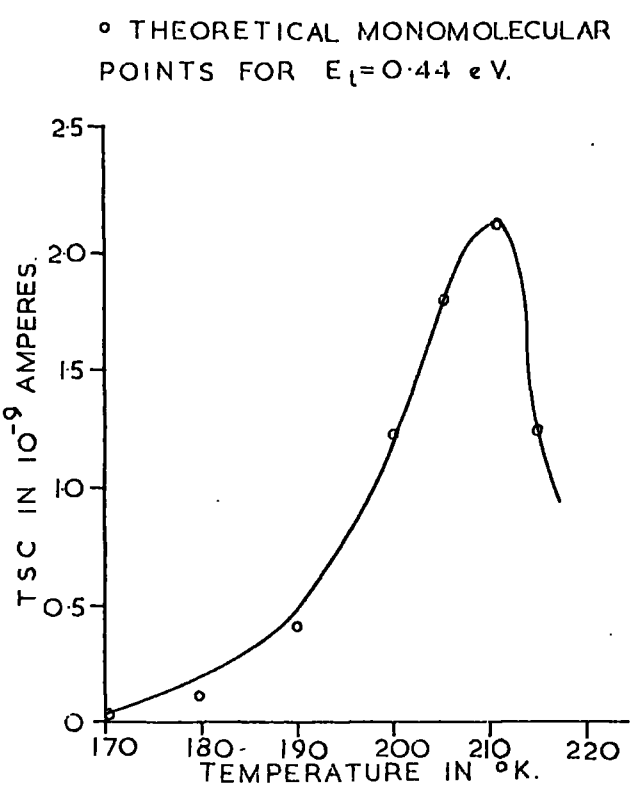

FIGURE 5.6.5 T.S.C. CURVE FOR TRAP A [FROM A T_S=300°C SAMPLE].

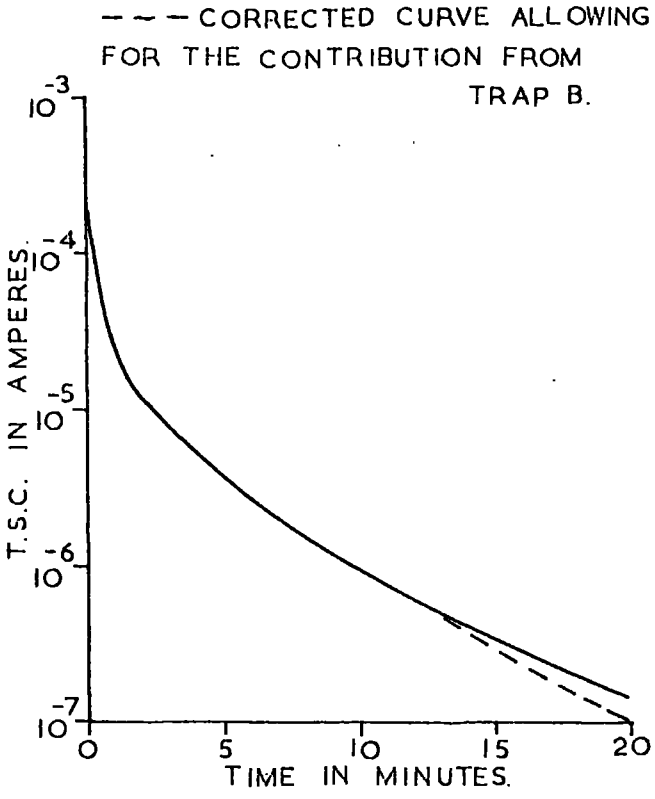

FIGURE 5.6.6 ISOTHERMAL DECAY OF T.S.C. FOR TRAP A [FROM A T_{Cd}=350°C SAMPLE].

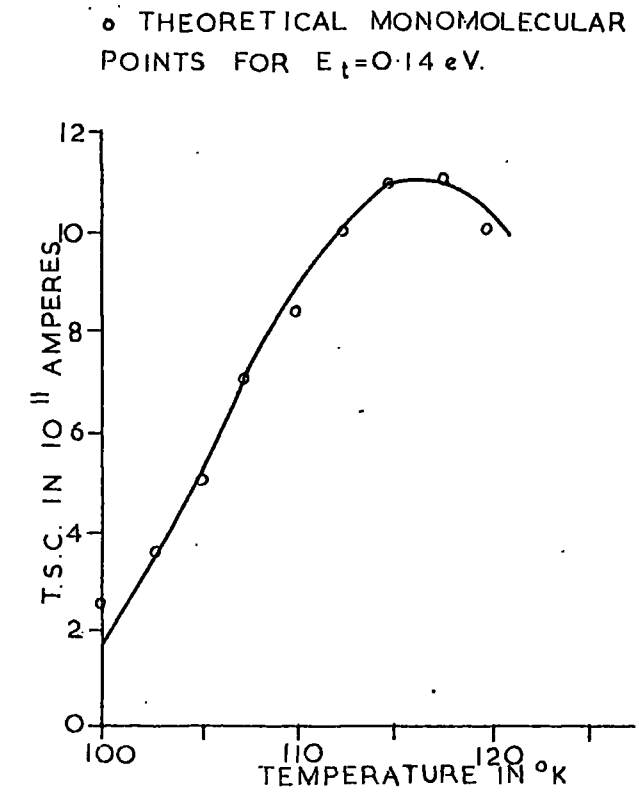

FIGURE 5.6.7 T.S.C. FOR TRAP A [T_S=450°C SAMPLE].

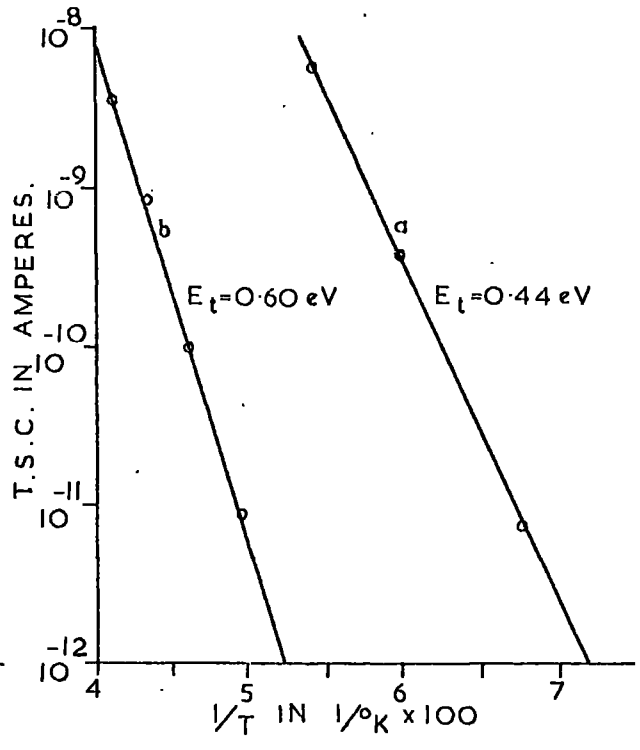

FIGURE 5.6.8 INITIAL RISE OF T.S.C. IN A T_{Cd} 350°C SAMPLE.
a WITH SHOULDER AT 210°K PRESENT.
b WITH SHOULDER REMOVED BY THERMAL CLEANING.

Table 5.6.1 shows the mean values of temperature maximum, thermal activation energy and capture cross-section obtained from the best fit monomolecular curves using the curve fitting method described in Chapter 3. The table also contains the mean values of thermal activation energies calculated using Bube's method (1955), which is the value to be expected in the case of fast retrapping. (It was pointed out in Section 3.2(b) that the expression used in curve fitting for fast retrapping is similar to that for slow retrapping, provided that the fast traps are only partially filled at the beginning of the T.S.C. run. As the cleaning of the five low temperature peaks meant that they must satisfy this criterion then one would expect that were they fast traps there would be agreement between their thermal activation energies derived by Bube's method and those obtained from the monomolecular curve fitting technique.)

It can be seen, from Table 5.6.1, that the Bube value of E_t differs from that found from monomolecular curve fitting for traps A, B, C and D and thus it may be assumed that these traps empty with negligible retrapping. The similarity of the monomolecular and Bube thermal activation energies for trap E suggests that it is a fast trap. A value of $S_t = 10^{-17} cm^2$ was found from the best fitting monomolecular curve. This value is certainly in error, if trap E is a fast trap, because the theoretical expression for fast retrapping does not contain the implicit dependence on capture cross-section which occurs in the expression for monomolecular recombination.

Isothermal current decays of trap A in cadmium rich samples were analysed using Haine and Carley-Read's method, which is described in Section 3.9. Using this method, log(current) is plotted against time. For slow retrapping ($\tau_t >> \tau_n$, where $\tau_t = (N_t S_t v)^{-1}$ and τ_n is the free electron lifetime) a single straight

TABLE 5.6.1

Trapping Parameters of the Low Temperature Traps

Trap	A	B	C	D	E
T^* in ^oK	115	138	158	190	212
E_t in eV	0.15	0.16	0.18	0.31	0.44
Bube E_t in eV	0.22	0.26	0.29	0.46	0.48
S_t in cm^2 assuming slow retrapping	10^{-20}	10^{-22}	10^{-22}	10^{-20}	10^{-17} *

* fast retrapping centre

TABLE 5.6.2

Comparison of Isothermal Decay and T.S.C. Values for the Trapping Parameters of Trap A

	E_t in eV	S_t in cm^2	N_t in no./cm^3
Isothermal Decay	0.125	6.4×10^{-20}	2.9×10^{15}
T.S.C.	0.15	10^{-20}	2×10^{15}

line is obtained whose slope depends on τ_t. Fast retrapping ($\tau_t << \tau_n$), where the initial trap occupancy is high, yields at first a straight line dependent on τ_t which changes via a variable slope to a second straight line governed by τ_n.

Figure 5.6.6 shows a typical plot of the isothermal of trap A in a sample grown with $T_{Cd} = 350^{o}C$. Analysis of such curves led to values of thermal activation energy of 0.125 eV and a capture cross-section of $6.10^{-20} cm^2$, which are in substantial agreement with those found from the curve fitting technique assuming conditions of slow retrapping. The values of thermal activation energy, capture cross-section and trap density obtained from the decay are included in Table 5.6.2. For comparison, Table 5.6.2 also gives the trapping parameters of trap A obtained from slow retrapping curve fitting.

It can be seen in Figure 5.6.6 that the isothermal decay leads to a double exponential variation with temperature. This may seem somewhat surprising at first sight, as the capture cross-section of the trap is small and a double decay indicates some retrapping. However, for the double decay shown in Figure 5.6.6 $\tau_n/\tau_t = 40$, which satisfies the criterion for fast retrapping that $\tau_t << \tau_n$.

A correction was made to the lower current region of the isothermal decay of trap A, and is shown as a dotted line in Figure 5.6.6. This allowed for the influence on the decay due to trap B. In the present case the activation energy was only changed from 0.125 eV to 0.12eV. (The interference of one trap on the isothermal decay of another will be discussed in Section 5.12, where the correction described above is used as an example.)

The assumption that traps A, B and C found in cadmium rich conditions are identical with those seen in sulphur rich samples is, in part, justified by the similarity of peak position with

respect to temperature. It was found possible to isolate trap A in one of the sulphur rich crystals sufficiently well to apply the curve fitting technigue. Figure 5.6.7 shows the T.S.C. curve for trap A in a sample grown with T_S = 450°C, and the points for the best fitting theoretical slow retrapping curve. The value of 0.14 eV is in reasonable agreement with the trap depth of 0.15 eV found in cadmium rich samples, especially as the T.S.C. from trap A is only a shoulder on the T.S.C. curve under sulphur rich conditions.

It has also been assumed that the shoulder on the T.S.C. curve found at about 210°K in cadmium rich samples is due to trap E, which empties in this temperature region in sulphur rich samples. It was not possible to isolate a peak at 212°K in cadmium rich samples, but plots of log(T.S.C.) versus 1/T (Garlick and Gibson's method, see Section 3.3(c)) were obtained with the shoulder present and also with the shoulder removed using the thermal cleaning technique. Figure 5.6.8 shows these plots for a sample grown with T_{Cd} = 350°C. Where the shoulder was present a value of activation energy of 0.44 eV was found, and when the shoulder was removed by thermal cleaning an activation energy pf 0.60 eV was obtained. The value of 0.44 eV is in agreement with the slow retrapping value of 0.44 eV found for the 212°K peak (trap E) in sulphur rich samples. The large difference in activation energy before and after cleaning indicates that the shoulder is due to a trap emptying in the region of 210°K.

5.7. Trap Densities of the Low Temperature Traps

The trap density of a single set of traps, which yields an isolated T.S.C. curve, can be calculated from Equation 3.8.1. The total charge passing through the sample, during the emptying

of the traps, is obtained from the area under the T.S.C. curve. Because of the overlapping nature of the five lowest temperature maxima this simple method could not always be used. When peak overlap occurred, the effective area under each T.S.C. maximum was estimated using the best fitting monomolecular curve, normalised to the uncleaned value of T.S.C. at the temperature maximum. Such monomolecular curves were computed from the values of thermal activation energy and temperature maximum presented in Table 5.6.1.

The values of trap densities are given in Table 5.7.1 for samples grown in both cadmium rich and sulphur rich conditions. The table also contains the reservoir temperatures and saturated vapour pressures of cadmium and sulphur used during the growth of the crystals. More exact values of density were calculated for trap E, where an isolated, cleaned T.S.C. curve could be obtained in sulphur rich samples. Trap D, which was found in one of the samples grown with $T_S = 450^{\circ}C$, could not be detected in samples taken from other boule crystals.

From Table 5.7.1 the marked decrease in the density of trap A, from $10^{16}/cm^2$ to $10^{12}/cm^2$, with increasing sulphur pressure during growth indicates that this trap is associated with cadmium rich conditions. If it were a simple native defect, it would be supposed that it was a cadmium interstitial or a sulphur vacancy. Boyn (1968) has studied the optical absorption of CdS heat treated in cadmium and sulphur, and concluded that cadmium interstitials and vacancies are the dominant native defects. He observed two absorption bands at 0.32 eV and 0.4 eV in samples heat treated in cadmium, and associated these with singly ionised cadmium interstitials because the bands were not seen in samples heat treated in sulphur. It seems reasonable to associate trap A with cadmium interstitials. Further support for this hypothesis may be found in the work of Arkad'eva (1964), who observed an optical threshold

TABLE 5.7.1

The Densities of the Low Temperature Traps (number/cm^3)

Growth Conditions	Saturated Vapour Pressure in torr	Boule Number	Trap A	Trap B	Trap C	Trap D	Trap E
T_{Cd} = 350°C	4.0×10^{-1}	78	10^{15}	10^{13}	10^{13}	—	10^{13}
T_{Cd} = 350°C	4.0×10^{-1}	79	10^{16}	10^{15}	10^{13}	—	10^{13}
T_S = 50°C	4.0×10^{-5}	70	10^{15}	10^{14}	10^{13}	—	10^{13}
T_S = 150°C	1.5×10^{-1}	76	10^{15}	10^{14}	10^{14}	—	10^{14}
T_S = 300°C	5.0×10^{1}	190	10^{11}	10^{11}	10^{12}	—	10^{14}
T_S = 450°C	7.6×10^{2}	94	10^{12}	10^{13}	10^{14}	10^{14}	10^{14}
T_S = 450°C	7.6×10^{2}	100	10^{12}	10^{11}	10^{12}	—	10^{12}

of 0.32 eV for the emptying of a trap which had a thermal activation energy of 0.18 eV, calculated from T.S.C. measurements. The optical trap depth of 0.32 eV, found by Arkad'eva, is the same as the lower energy absorption band which Boyn reported. The thermal activation energy of 0.18 eV is close to the value of 0.15 eV found for trap A during the course of the present work.

No distict variation with growth conditions was indicated for the other low temperature traps. From this it may be inferred that these traps are either due to impurities, or to complexes of native defects not strongly affected by variations in the growth conditions suffered, at least over the range of samples investigated.

5.8. Anomalous Low Temperature Traps

The three lowest temperature traps were well defined in samples cut from a boule crystal grown with $T_{Cd} = 550^{o}C$. Figure 5.8.1 shows the T.S.C. spectrum obtained from one of these samples, after continuous illumination from $388^{o}K$. The T.S.C. curves for traps A, B, and C were extremely narrow. Consequently, monomolecular curve fitting yielded values of E_t, of 0.35 eV, 0.38 eV and 0.40 eV respectively, which were larger than those previously encountered for these traps. (The reason for a large value of E_t for a narrow T.S.C. curve is demonstrated most easily by reference to Grossweiner's method for monomolecular recombination (Section 3.3(a)). The Grossweiner thermal activation energy is given in Equation 3.3.1, where the difference between the peak maximum temperature, T^*, and the low temperature half height, T', is contained in the denominator. $T^* - T'$ will be small for a narrow T.S.C. curve, and hence leads to a large value of E_t.)

The sample shown in Figure 5.8.1 was also excited with monochromatic light centred on 4335 A^{o} and 7700 A^{o}, using Barr and

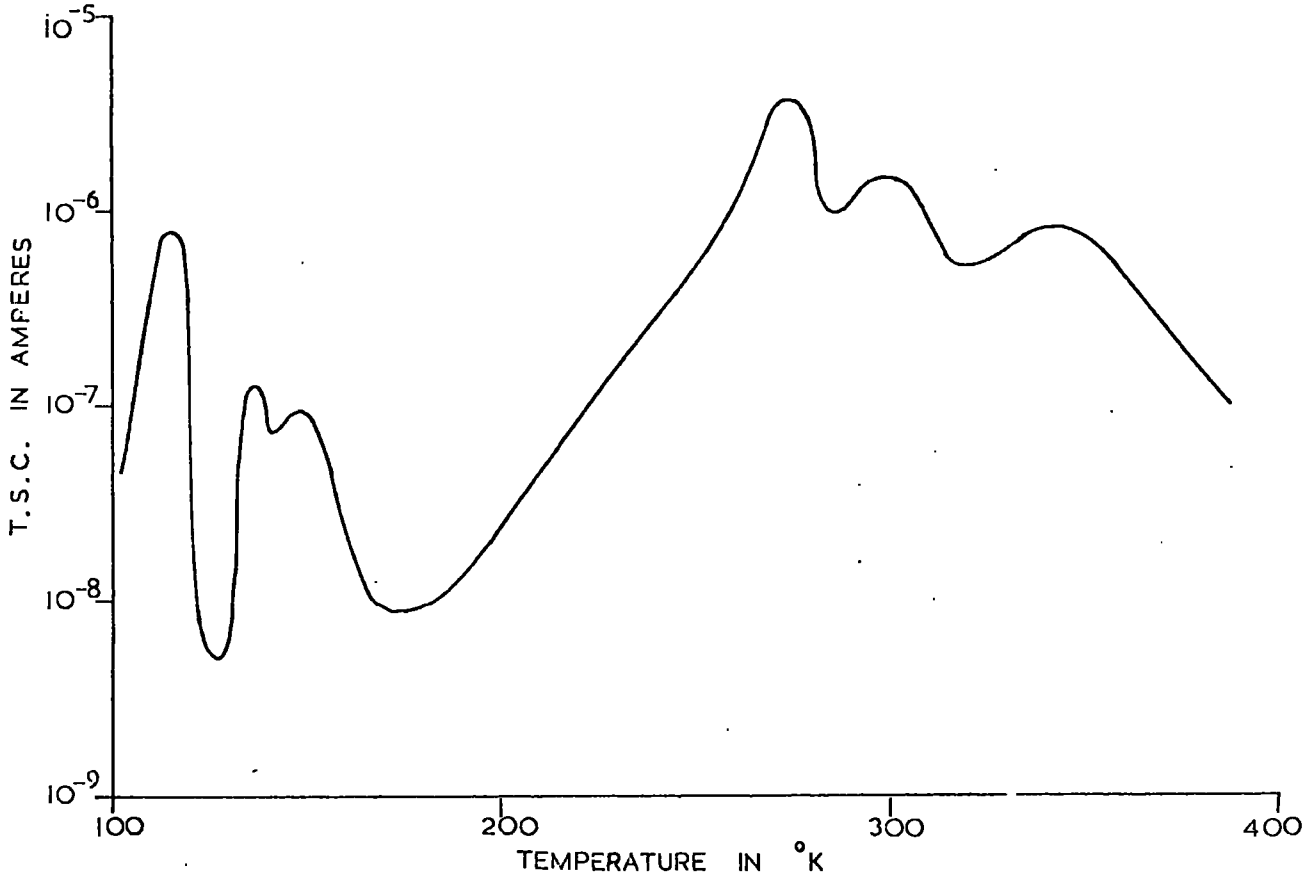

FIGURE 5.8.1 T.S.C. SPECTRA FOR A T_{Cd} = 550 °C SAMPLE

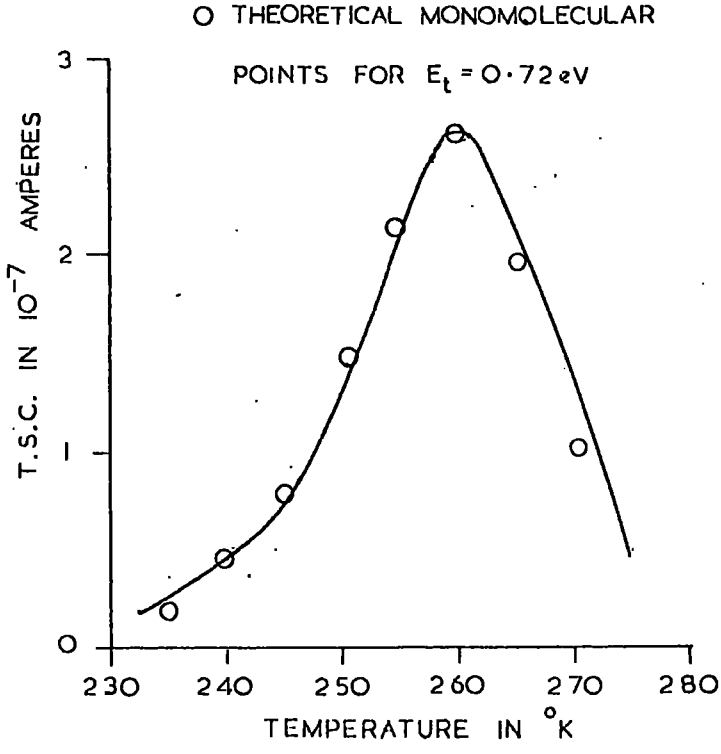

FIGURE 5.9.1 T.S.C. CURVE FOR TRAP F

[FROM A T_S = 450 °C SAMPLE]

Stroud interference filters, to determine whether or not the usual broader peaks could be obtained. In both cases the sharp structure was observed. A similar spectrum was also obtained when the indium contacts were renewed.

5.9. The High Temperature Traps

Three maxima were observed in the T.S.C. curves in the temperature region from 250°K to 388°K, with values of T* of approximately 270°K, 300°K and 350°K, using heating rates in the range 0.1°K/sec to 0.5°K/sec. These traps are denoted by the letters F, G and H respectively. The calculation of the trapping parameters of these traps was difficult for three reasons.

(a) Because of the overlap of the peaks, careful thermal cleaning was required in order to obtain meaningful results.

(b) The onset of thermal quenching occurs in this temperature region. Although the high intensity photocurrent showed little decrease with increasing temperature below 350°K, in most samples, the quenching at photocurrent levels of the same order as the T.S.C. was considerable (see Figure 5.9.4) for trap H.

(c) Under conditions where traps F and G varied with the temperature of illumination, T_i, prior to the T.S.C. run, their T.S.C. curves were sharpened, leading to erroneous values of E_t in some cases as high as 1.10 eV.

In all cases a theoretical slow retrapping curve could be fitted to the experimental data.

Trap F gave values of E_t in the range 0.7 eV to 0.8 eV where it suffered minimal interference from trap G, and where there was no apparent change in density with change in T_i. The mean value of E_t was 0.75 eV, with a capture cross-section of $6.10^{-14} cm^2$. A typical curve, together with the points for the best fitting

theoretical curve with E_t = 0.72 eV, is shown in Figure 5.9.1.

Trap G gave values of E_t in the range 0.47 eV to 0.57 eV, with a mean value of E_t = 0.53 eV and $S_t = 10^{-19} cm^2$, where there was no variation of peak height with change in T_i.

Trap H, in many cases, yielded a narrow T.S.C. curve which gave a high value of E_t (see Section 5.8) calculated by curve fitting on the assumption of slow retrapping. The narrowness of the T.S.C. curve can be explained in terms of thermal quenching, which causes a rapid change in lifetime during the emptying of trap H. Figure 5.9.2 shows a cleaned T.S.C. curve for trap H, in a sample grown with $T_{Cd} = 350^{o}C$. The sample was cooled after passing the peak maximum temperature. On reheating, the curve in Figure 5.9.3 was obtained. The best fit to the first curve yielded a value of E_t = 0.60 eV. From the second curve E_t = 1.06 eV.

In order that the variation of the free electron lifetime might be estimated in the temperature region in which trap H emptied, the photocurrent for the above sample was measured at fixed temperature for a number of different light intensities (Figure 5.9.4). The photocurrent measurements were made in the temperature range from $329^{o}K$ to $388^{o}K$. It was found that at low light intensities equilibrium was reached only after 30 to 60 minutes. The thermal quenching at a current level corresponding to that of the T.S.C. maximum in Figure 5.9.2 was comparatively small. At a current level corresponding to the T.S.C. maximum in Figure 5.9.3, the quenching caused a change of three orders of magnitude in the photocurrent. This large change in photocurrent demonstrates that a significant variation in the free electron lifetime would be expected for the corresponding T.S.C. curve (Figure 5.9.3). As the sample responded slowly to thermal quenching

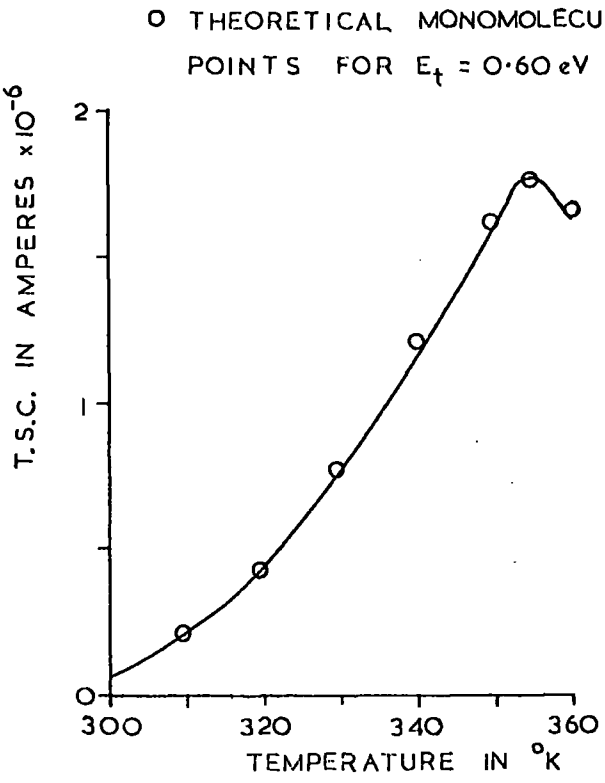

FIGURE 5.9.2 T.S.C. FOR TRAP H [FROM A T_{Cd} = 350 °C SAMPLE]

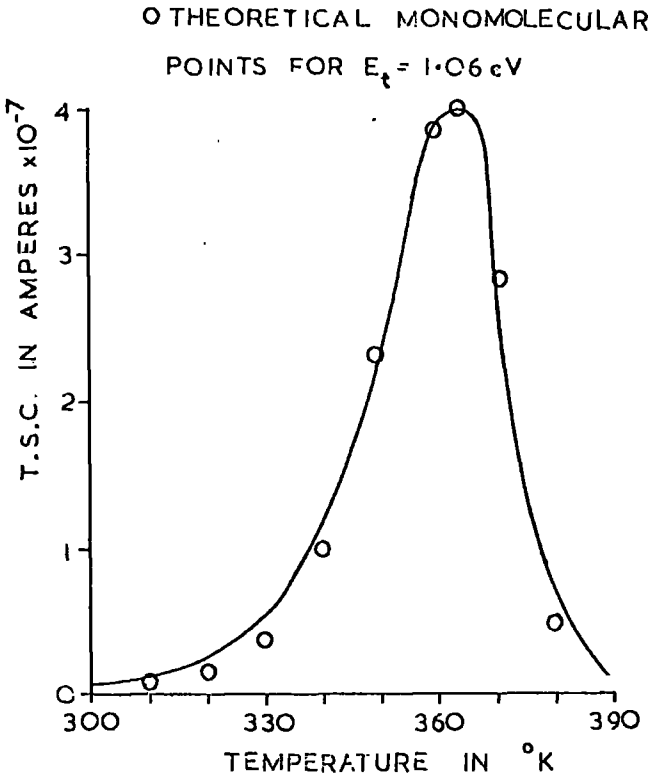

FIGURE 5.9.3 T.S.C. FOR TRAP H [FROM THE SAME SAMPLE AS FIGURE 5.9.2]

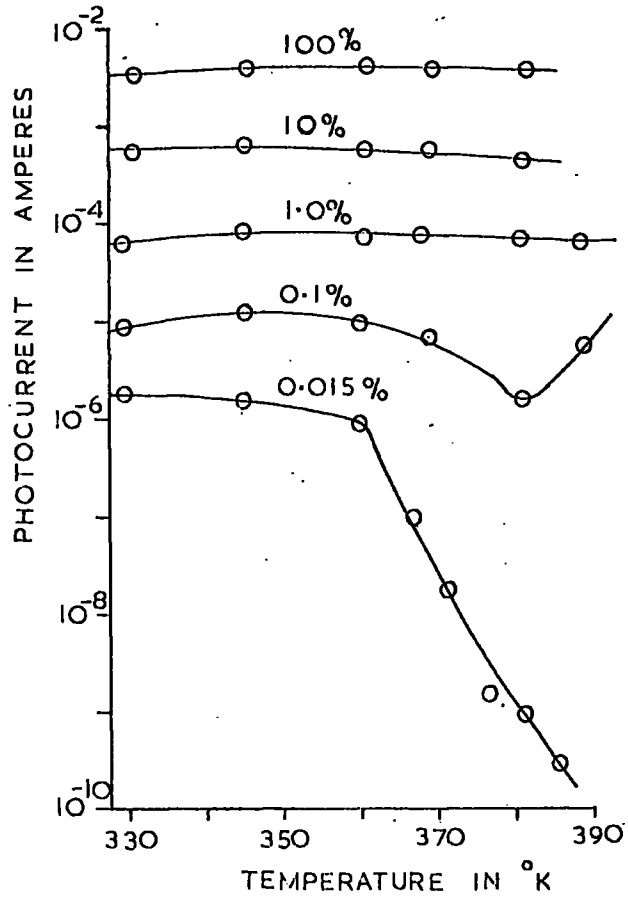

FIGURE 5.9.4 PHOTOCURRENT VERSUS TEMPERATURE FOR THE SAME SAMPLE AS FIGURE 5.9.2 [LIGHT INTENSITY IN %]

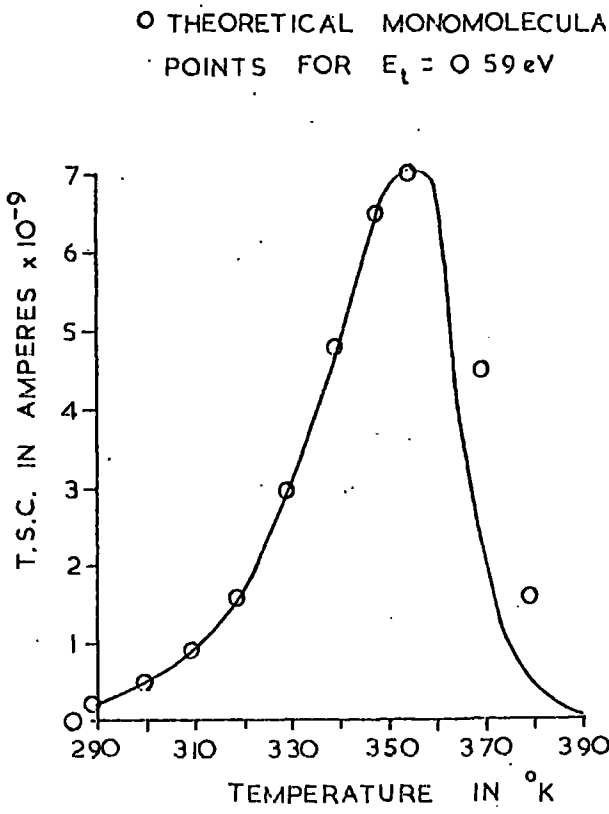

FIGURE 5.9.5 T.S.C. FOR TRAP H [FROM A T_{Cd} = 350 °C SAMPLE]

it is incorrect to modify the T.S.C. curve shown in Figure 5.9.3 using the variation in lifetime deduced from photocurrent measurements. However, the large value of E_t obtained from the T.S.C. curve shown in Figure 5.9.3 is certainly explicable in terms of thermal quenching.

Figure 5.9.5 shows the thermally cleaned T.S.C. curve for trap H, found in another sample grown with $T_{Cd} = 350^{o}C$. A good fit was obtained for the first part of this curve with a slow retrapping thermal activation energy of 0.59 eV. The disagreement with this theoretical value for the high temperature wing of the curve was almost certainly due to the thermal quenching effect discussed above. From these results a value of 0.60 eV was assigned to trap H, the corresponding capture cross-section is $2.0 \times 10^{-20} cm^2$.

Table 5.9.1 gives the thermal activation energies, Bube thermal activation energies and the capture cross-sections, on the assumption of slow retrapping, for traps F, G and H. With trap F the disagreement between the slow retrapping value of E_t and that obtained using Bube's method indicates that although trap F has a large capture cross-section it empties under slow retrapping conditions. Trap G shows good agreement between the activation energies calculated by both methods, though the variation of T^* with the T.S.C. level, which is expected for a fast trap, was not found (see Figures 6.3.1 and 6.3.2).

For trap H there was again agreement between the two methods of evaluating E_t. Reference to Figures 6.3.1 and 6.3.2 shows that there is a variation of T^* with the magnitude of the T.S.C. for this trap, which also indicates that it is a fast retrapping centre. The small value of S_t ($\sim 10^{-20} cm^2$), obtained from curve

TABLE 5.9.1

Trapping Parameters of the High Temperature Traps

Trap	T^* in ^oK	E_t in eV	Bube E_t in eV	S_t in cm^2 assuming slow retrapping
F	270	0.75	0.49	10^{-13}
G	300	0.53	0.56	10^{-19} *
H	350	0.60	0.61	10^{-20} *

*fast retrapping centres

TABLE 5.10.1

Trap Densities of the High Temperature Traps (number/cm^3)

Growth Conditions	Boule Number	Trap F	Trap G	Trap H
T_{Cd} = 350°C	78	10^{14}	10^{14}	10^{14}
T_{Cd} = 350°C	79	10^{14}	10^{14}	10^{14}
T_S = 50°C	70	10^{14}	10^{13}	10^{12}
T_S = 150°C	76	10^{14}	10^{14}	10^{13}
T_S = 300°C	190	10^{16}	10^{16}	*
T_S = 450°C	94	10^{14}	10^{15}	—
T_S = 450°C	100	10^{15}	10^{13}	—

* A large variation in N_t for trap H was found in samples taken from this boule. The maximum value was $N_t = 10^{16}/cm^3$.

fitting on the assumption of slow retrapping, is certainly erroneous if trap H is a fast trap. The change in the magnitude of the T.S.C. with T_i will be further discussed in the following chapter.

5.10. The Densities of the High Temperature Traps

Because of the variation of the densities of these trapping centres with T_i, the values of trap density given in this section are the maximum found. The approximate method, described at the beginning of Section 5.7, was used to estimate the trap densities. Table 5.10.1 gives the densities found together with the temperature of the cadmium or sulphur reservoir used in the growth of the samples investigated.

Trap H was present in all samples grown under cadmium rich conditions. It was also found in two samples taken from a boule crystal grown with $T_S = 300^oC$, although it was not observed in four other samples from this boule. Trap H could not be detected in samples grown with $T_S = 450^oC$, however the dark current was high in these samples and may have obscured it if its density was low.

There is a general trend of the density of trap H to decrease with increasing sulphur richness, although its occurrence in the two samples grown with $T_S = 300^oC$ is anomalous in this respect. Woods and Nicholas (1964) studied a number of CdS samples, grown by vapour phase recrystallisation in an argon gas flow, and found that trap H occurred only in samples annealed in sulphur. (The trapping parameters of Woods and Nicholas' 'trap H', which had $T^* = 330^oK$ and $E_t = 0.63$ eV, are sufficient justification for associating it with trap H found in the present work. Woods

and Nicholas also found that their trap H varied with T_i in a similar manner to the present trap H.) Thus it would appear that trap H can exist under both cadmium and sulphur rich conditions, and hence it seems reasonable to propose that it is more likely to be due to a complex of native defects and/or impurities rather than a simple native defect.

The relatively constant values of the densities of traps F and G indicate that these also may be due complex native defects or impurites, not substantially affected by the changes in the conditions of growth of the present samples.

5.11. T.S.C. from two Derby Luminescent Samples

The T.S.C. spectra of two samples grown from Derby Luminescent powder were investigated. In both cases, the T.S.C. curves were not substantially affected by the temperature of illumination prior to measurement. Figure 5.11.1, curves (a) and (b), shows the spectra for these samples, grown with T_{Cd} = 300°C and T_S = 350°C, following illumination from 388°K. The T_S = 350°C sample (curve (b)) did show a well defined T.S.C. curve at low temperature (T^* = 130°K), which yielded a value of E_t = 0.09 eV by the slow retrapping curve fitting technique. Although the T_{Cd} = 300°C sample showed some structure at low temperatures, it was not possible to isolate a T.S.C. curve.

Attempts were made to thermally clean the broad structure in both samples, which occurred above 150°K. It was found that cleaning yielded the same structure at a lower T.S.C. level, suggesting that the high temperature T.S.C. was due to a continuum of traps. (From the analysis of Optran samples one would expect to find a number of traps in the temperature region 150°K to 388°K.)

The Derby starting powder was found, by mass spectrographic

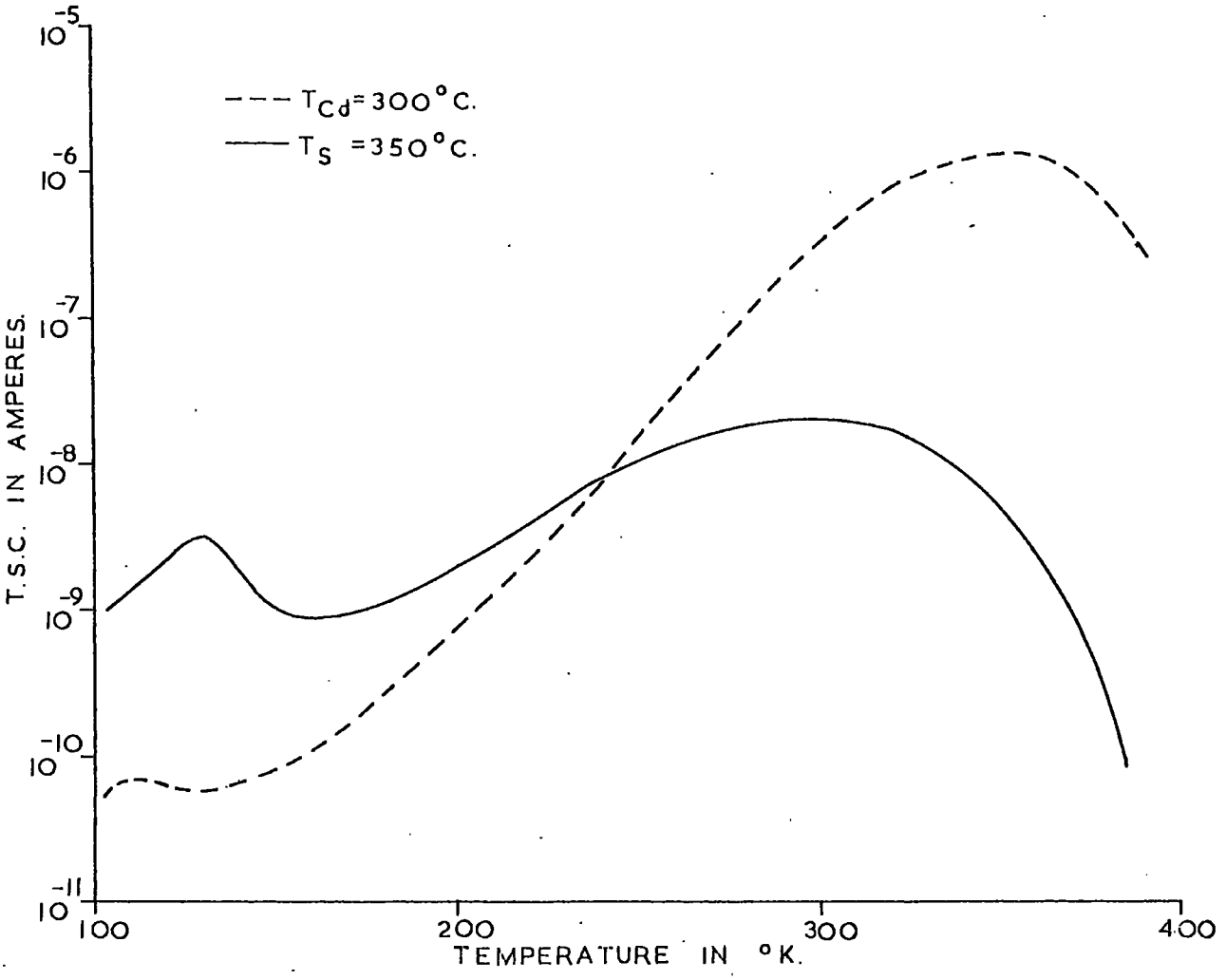

FIGURE 5.II.I THERMALLY STIMULATED CURRENT SPECTRA FOR TWO SAMPLES GROWN FROM DERBY LUMINESCENT MATERIAL.

TABLE 5.12.1

Comparison of E_t and T^* for the Low Temperature Traps and the traps found by Cowell and Woods (1967)

Present Work	T^* in °K	115	138	158	190	212
	E_t in eV	0.15	0.16	0.18	0.31	0.44
Cowell and Woods	T^* in °K	103	130	162	205	240
	E_t in eV	0.20	0.16	0.25	0.38	0.42

analysis, to contain impurities whose densities were one to two orders of magnitude greater than those found in Optran material (see Section 4.2). The anomalous T.S.C. spectra of the Derby samples, compared with Optran samples, may well be due to complexes formed by these impurities.

5.12. Discussion

Eight discrete trapping levels (denoted by the letters A to H) have been found in Optran boule crystals grown in cadmium and sulphur overpressures. The trapping parameters of these centres are presented in Tables 5.6.1 and 5.9.1. The trap densities, for samples grown under both cadmium and sulphur rich conditions, can be found in Tables 5.7.1 and 5.10.1.

Trap A, which decreased in density by four orders of magnitude with increasing sulphur pressures during growth, has been associated with a singly ionised cadmium interstitial. Trap D was only detected in one boule crystal grown with T_S = 450°C, and occurred as a doublet with trap E. Trap H decreased in density from $10^{14}/cm^3$ to $10^{12}/cm^3$ for samples grown with T_{Cd} = 350°C to T_S = 150°C. However, trap H was found in densities of the order of $10^{16}/cm^3$ in two samples taken from a boule grown with T_S = 300°C, which indicates that it can occur under both cadmium and sulphur rich conditions.

The relatively constant values of densities for the other traps suggests that, as they were unaffected by the conditions of growth suffered during the present investigations, they are likely to be due to impurities or native defect complexes.

Cowell and Woods (1967) discussed the evaluation of a T.S.C. spectrum in a sample grown by the modified Piper and Polich method described by Clark and Woods (1966). They used the curve fitting

technique to estimate trapping parameters. The results in this thesis are in reasonable agreement with their work. (Table 5.12.1 shows, for comparison, the values of E_t and T^* determined for traps A to E and the values of E_t and T^* found by Cowell and Woods.) Cowell and Woods found four T.S.C. maxima at 103°K, 130°K, 162°K and 230°K. The thermal activation energies of the three lowest temperature traps were 0.20 eV, 0.16 eV and 0.25 eV respectively, though in some cases the lowest maximum yielded a value of 0.16 eV.

During the course of the present work, trap D was found as a doublet with trap E. Cowell and Woods (1967) also discovered a doublet, with a maximum at approximately 230°K, which gave thermal activation energies of 0.38 eV and 0.42 eV for the two components. There is sufficient evidence from the work described here to assign a value of 0.44 eV to the high temperature component (trap E). Had this value been applied to their doublet, then the lower component would have been broader. This would have led to a value lower than 0.38 eV for the activation energy.

Cowell and Woods (1969) also discussed two traps, which emptied with $T^* = 275$°K and 325°K respectively, found in rods which had been grown by the flow process and subsequently annealed in sulphur vapour. The thermal activation energies of these traps were 0.85 eV and 0.63 eV respectively. The agreement between the value of $E_t = 0.60$ eV for trap H and the value of $E_t = 0.63$ eV, reported by Cowell and Woods, is good. Trap F ($E_t = 0.75$ eV and $T^* = 270$°K) and Cowell and Woods' lower temperature trap do not compare so favourably. However, trap F was found to yield higher values ot E_t when the T.S.C. level varied with the temperature, T_i, of illumination prior to measurement. The trap 'F' discussed by Cowell and Woods changed considerably in density with change in T_i,

and may therefore have given a large value of E_t for this reason.

Nicholas (1963) presented a number of T.S.C. spectra, measured on flow crystals, which showed seven maxima which were similar to those found in this work. Nicholas' analysis of the data obtained from these spectra was somewhat dubious, as he assumed that a trap could empty and lead to a value of T* which varied by as much as 100°K. Nicholas found traps with thermal activation energies of 0.05 eV at low temperatures, and 0.25 eV at approximately 300°K. These were not found in the present work, although overlapping curves in the same temperature regions did yield similar values.

The general shape of the T.S.C. spectra found both by Cowell and Woods and by Nicholas, from investigations of flow crystals, indicates that their samples were grown under cadmium rich conditions. This is not surprising, as no attempt was made to maintain stoichiometry during the growth of the flow crystals.

The method of Haine and Carley-Read (1968) was not used to analyse the T.S.C. curves because of the overlapping nature of the contributions from each trap. The thermal cleaning process decreases the occupancy of the trap investigated, as described in Section 5.4. In order to apply the Haine and Carley-Read T.S.C. technique it would be necessary to obtain cleaned curves at different heating rates with the same density of filled traps. This would have been very difficult to attain.

The trap depths obtained by Haine and Carley-Read from their T.S.C. analysis are almost certainly in error, since none of their curves was thermally cleaned. In both the spectra presented in their paper, they assume only two traps in the temperature range 80°K to 360°K whereas eight have been detected in the present work. Comparison of their T.S.C. spectra with those shown in Figures

5.5.1 and 5.5.2 indicates that their samples were also grown under cadmium rich conditions.

The constant temperature decay method advocated by Haine and Carley-Read also requires careful application. From Equation 3.9.3, the decay at constant temperature for a trap emptying under slow retrapping conditions may be written in the form

$$n_c = n_o N_c \tau_n S_t v [\exp(-E_t/kT) \exp(-tN_c v S_t \exp(-E/kT))] \qquad 5.12.1$$

where the contribution to the free electron density at t = 0 is

$$n_c = n_o N_c \tau_n S_t v [\exp(-E/kT)] \qquad 5.12.2$$

Thus the initial free electron density from each of the full or partially full traps present in the sample is governed by the factor $n_o S_t \exp(-E/kT)$. A similar factor is found in the case of fast retrapping.

Where trapping centres of similar density, capture cross-section and thermal activation energy occur, as was the case with the low temperature traps found in the present work, it is not safe to assume that the interference from other traps is negligible. Also, the decay of one set of traps may be modified by a contribution from a second set of traps whose density is greater than the first.

In the present work the decay method was used to analyse trap A (E_t = 0.15 eV and T^* = 115^{o}K), which was two orders of magnitude greater in density than trap B. The expected contribution from trap B (E_t = 0.16 eV and T^* = 138^o) to the decay at 100^{o}K would be 5.0×10^{-8} amperes at t = 0, using Equation 5.12.2 and assuming the trapping parameters found from T.S.C. curves. After 10^3 seconds

the contribution from trap B would have decreased by less than 0.1%, so the contribution to the decay is essentially a constant 5.0×10^{-8} amperes. The isothermal decay of trap A is shown in Figure 5.6.6, where the above correction for trap B is marked with a dotted line. The curve shown in Figure 5.6.6 yielded a value of E_t = 0.125 eV, which was decreased to 0.12 eV when trap B was considered. The correction is small in this case because trap A was of much greater density than trap B. Had traps A and B been of equal density, the uncorrected decay would have yielded a value of E_t which was considerably larger.

Haine and Carley-Read found values of E_t = 0.18 eV and E_t = 0.24 eV for isothermal decays measured at 104°K and 103°K respectively, in two different CdS samples. The large disparity between these two results and also the value of E_t = 0.12 eV from the present work may well be explained in terms of interference from other traps. (As Haine and Carley-Read did not thermally clean their T.S.C. spectra it is not possible to apply a correction to their values. However, comparison of the T.S.C. spectra shown in Figure 5.5.1 with their spectra indicates that trap B may well have been present.)

The method of analysis advocated by Bube (1955) does lead to fairly reproducible values of E_t for a given trap in different samples. There is, however, no reason to suppose that these are the true values. Equation 3,5.1 may be rewritten to yield a Bube thermal activation energy given by

$$E_t = kT^* \log(N_c/n_c^*) \qquad 5.12.3$$

In the T.S.C. curves reported here the value of $\log(N_c/n_c^*)$ varied from 18 to 26, depending on the density of filled trapping centres. This leads to a mean value Bube thermal activation energy, such that

$$E_t = 22kT^* \qquad 5.12.4$$

with an error of about 20%. This error is considerably smaller than that incurred by curve fitting or allied techniques, where lifetime variation is disregarded or insufficient thermal cleaning is carried out. Thus the Bube value gives a thermal activation factor which may be used to describe a T.S.C. curve in a similar manner to the approximation $E_t = 25kT^*$ used by early workers on thermoluminescence.

The initial rise method first proposed by Garlick and Gibson (1948), although basically sound, was not often used in the present work because of the overlap of the peaks investigated. When the second of three overlapping peaks is thermally cleaned, great care is required to ensure that this trap is not emptied to the extent that it becomes only a shoulder on the next highest peak. Inherently, there may be a small contribution left from the lowest peak, which would affect the second mainly in the initial rise region.

References to Chapter 5

Arkad'eva, E.N., 1964, Sov. Phys. Solid State 6, 798.

Boyn, R., 1968, Phys. Stat. Sol. 19, 307.

Bube, H.R., 1955, J. Chem. Phys. 23, 18.

Clark, L. and J. Woods, 1966, Brit. J. Appl. Phys. 17, 319.

Cowell, T.A.T. and J. Woods, 1967, Brit. J. Appl. Phys. 18, 1045.

Garlick, G.F.J. and A.F. Gibson, 1948, Proc. Phys. Soc. 60, 574.

Haine, M.E. and R.E. Carley-Read, 1968, J. Phys. D. (Brit. J. Appl. Phys.) Series 2, 1, 1257.

Nicholas, K.H., 1963, Thesis, University of Durham, submitted August 1963.

Woods, J. and K.H. Nicholas, 1964, Brit. J. Appl. Phys. 15, 1361.

CHAPTER 6

VARIATION OF THERMALLY STIMULATED CURRENT LEVEL WITH CONDITIONS OF ILLUMINATION

6.1. Introduction

In the last chapter, the values of thermal activation energy, capture cross-section and trap density were determined under conditions which yielded a maximum in trap density and a minimum in the variation of the free electron lifetime with temperature. For the majority of samples investigated, a change in the magnitude of the T.S.C. was found with the temperature at which the illumination was switched on during cooling, prior to the T.S.C. measurement.

The results presented in this chapter are for measurements made using a two probe electrode configuration as described in Section 4.3(a), so that the observed changes in the magnitude of the T.S.C. might be caused by contact effects or by trapping centres lying near to the surface of the CdS samples. A more detailed investigation of contact and surface effects is given in Chapter 7. The phenomena reported here are confined to those which have no apparent association with effects due to surface traps or the contacts.

A variation of the T.S.C. due to bulk effects can be explained in terms of a change in the free electron lifetime. The magnitude of the T.S.C. can also vary due to a change in the density of photochemical centres, or due to the change in the occupancy of traps surrounded by a potential barrier.

6.2. Variation of the Free Electron Lifetime

As described in Chapter 5, an estimate of the variation of the free electron lifetime with temperature was obtained by measuring the photocurrent as a function of temperature, at a current level approximately two orders of magnitude greater than that of the T.S.C. From Equation 2.1.5 it can be seen that the value of photocurrent is a direct measure of the product of the free electron lifetime and mobility. This product is of paramount importance in determining the shape of the T.S.C. curve for an isolated trapping centre, and hence the spectrum which is the sum of such curves.

For samples investigated in this thesis, the illumination could be switched on at any desired temperature, T_i, during cooling to liquid nitrogen temperatures prior to the measurement of either the T.S.C. or the photocurrent as a function of temperature. By comparing the measurements of the photocurrent and the T.S.C., made under the same conditions of pre-illumination, it is possible to differentiate between variations of the T.S.C. due to the lifetime-mobility product and those due to a real variation of trap density or occupancy. The free electron mobility would not be expected to vary greatly for different illumination treatments to the sample in the temperature range of the T.S.C. measurements, and in consequence changes in the photocurrent level with illumination schedule can be attributed mainly to lifetime effects.

With most samples, the magnitudes of the T.S.C. and photocurrent were larger when the illumination was switched on at higher temperatures, though in the majority of cases the maximum change was by a factor two or less. These changes can be explained in terms of an increase in free electron lifetime. Three samples investigated showed variations of photocurrent of a

few orders of magnitude, depending on the value of T_i used.

Figure 6.2.1 shows the T.S.C. spectra for sample grown with $T_S = 50^oC$. The sample was cooled and illuminated with a tungsten lamp from 388^oK, 200^oK and 90^oK. The photocurrent versus temperature curves, shown in Figure 6.2.2, were obtained for the same sample using a number of values of T_i between 388^oK and 90^oK. The large variation of free electron lifetime is reflected in both sets of curves. Similar changes in the free electron lifetime were observed in samples grown with $T_{Cd} = 550^oC$ and $T_S = 450^oC$, so that no correlation can be made between the growth conditions and the observation of this phenomenon.

The thermal sensitisation can be seen to be associated with a comparatively small temperature region. From Figure 6.2.2, it is clear that the photocurrent, and hence the lifetime, is very sensitive to illumination for values of T_i between 168^oK and 202^oK. For the samples grown with $T_{Cd} = 550^oC$ and $T_S = 450^oC$ the rapid increase in photocurrent with increasing temperature also occurred at a temperature of about 200^oK. This suggests that the sensitisation process is associated with a definite thermal step. As the free electron lifetime is inversely proportional to the density of Class 11 centres filled with holes (Equation 2.2.1), the sensitive state occurs when the Class 11 centres are occupied in lesser density by holes than when the sample is insensitive. The sensitisation of samples discussed in this section may be explained in terms of hole traps, each of which is surrounded by a potential barrier. When the sample is illuminated whilst cooling from high temperatures (Figure 6.2.2 curve (a)), the free holes so created may be captured by the hole traps. The occupancy of the Class 11 centres by holes is reduced, because some of the holes are captured at the trapping centres, and the sample is in its sensitive state. Excitation at low temperatures after

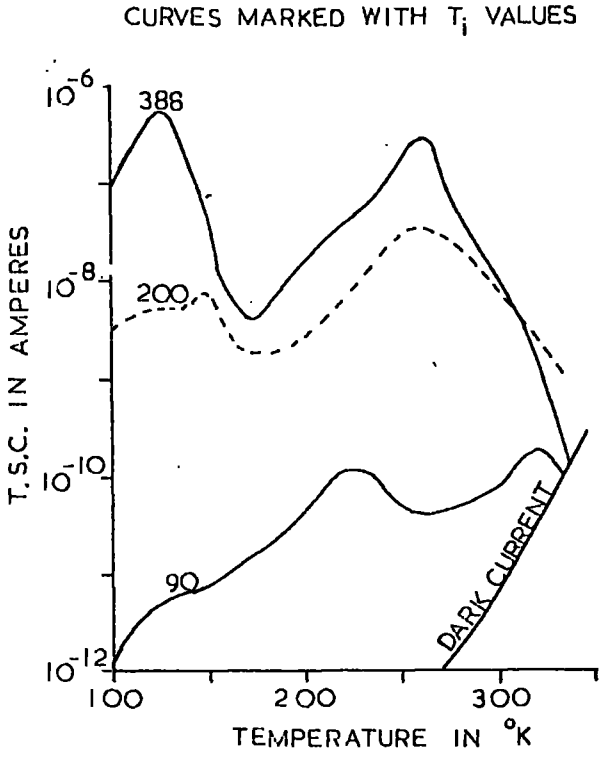

FIGURE 6.2.1 T.S.C. SPECTRA FOR A $T_S = 50^{\circ}C$ SAMPLE

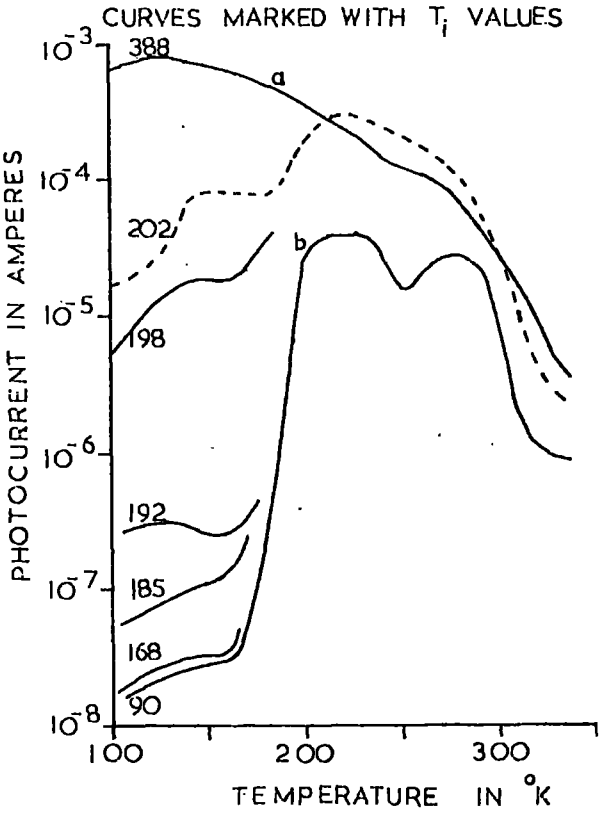

FIGURE 6.2.2 PHOTOCURRENT VERSUS TEMPERATURE FOR A $T_S = 50^{\circ}C$ SAMPLE

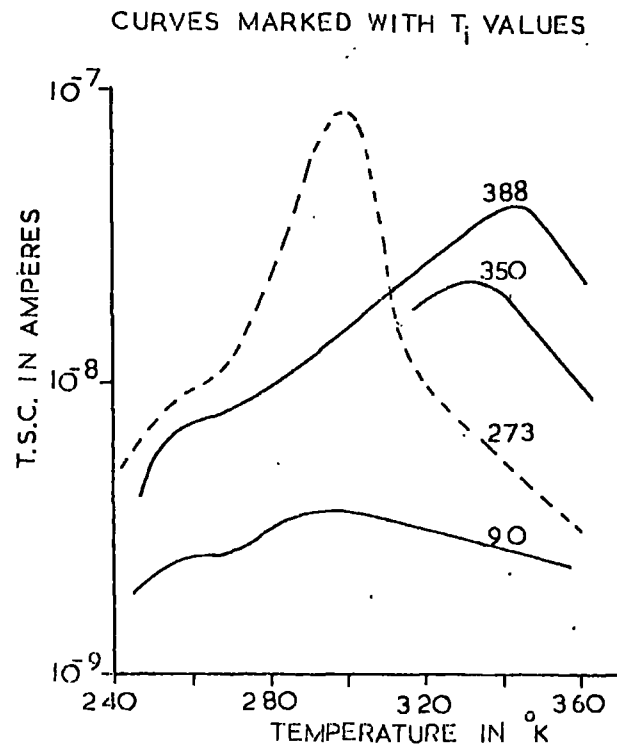

FIGURE 6.3.1 T.S.C. FOR A $T_{Cd} = 350^{\circ}C$ SAMPLE FOLLOWING ILLUMINATION WITH A TUNGSTEN LAMP (FILTERED TO REMOVE INFRARED)

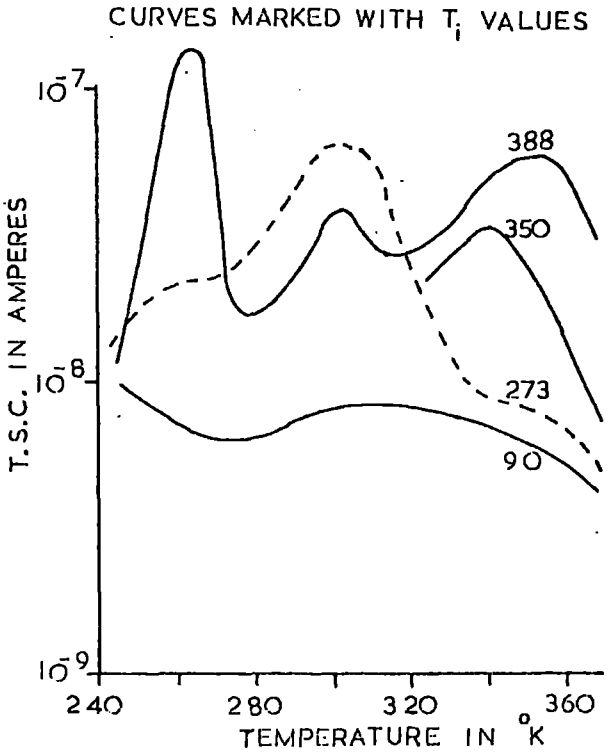

FIGURE 6.3.2 T.S.C. FOR A $T_{Cd} = 350^{\circ}C$ SAMPLE FOLLOWING ILLUMINATION WITH AN UNFILTERED TUNGSTEN LAMP

cooling in the dark creates free holes, though they connot surmount the barriers surrounding the traps. As the temperature is raised under illumination (Figure 6.2.2 curve (b)), the thermal energy of holes in the valence band becomes sufficient to surmount the barriers and the traps are filled with holes. The occupancy of the Class 11 centres by holes is reduced, because some of the holes are captured at the traps, and this leads to a higher free electron lifetime.

Four Chance coloured filters peaking in the blue, green, yellow and orange regions of the spectrum (filters OB 10, OY 12, OY 18 and OY 1 respectively) were individually interposed between the tungsten lamp and the T_S = 50°C sample during illumination, together with two Chance HA 1 filters and a one centimetre path length of 10% copper sulphate solution. The photocurrent was also monitored using a tungsten lamp from which the infrared had been removed. No significant change in the general shape of the photocurrent versus temperature curves was found under these conditions.

The large change in the free electron lifetime will be discussed in the later chapters dealing with infrared quenching and spectral response, and infrared luminescence. Particular emphasis should be placed on the observation of luminescence changes which occur in the same temperature region as that for the photocurrent rise, thus indicating that the effect cannot be attributed to contacts. This was further confirmed in the contact measurements which are described in the following chapter.

Variations in the level of the photocurrent with time under constant illumination and temperature have been reported by a number of workers (e.g. Zomov and Serdyuk 1969). In only two cases were such effects observed in the present work. The first

is discussed in connection with the traps which empty at approximately 270°K and 300°K in a sample grown with T_S = 300°C (Section 6.3(b)). The other was observed during four probe measurements. This is described in Section 7.3(c).

6.3. Photochemical and Potential Barrier Trapping Centres

The last section demonstrated that some of the variations of the T.S.C. spectrum can be explained in terms of a change in the free electron lifetime. Where a variation of T.S.C. occurs, with no corresponding change in the photocurrent, it must be assumed that the density or occupancy of the traps varies with the temperature of illumination. Two possible models may be used to explain such phenomena.

Trapping centres which are observed only following illumination at high temperatures may be created under these conditions, and may not exist following illumination at lower temperatures. Where native defects, such as vacancies or interstitial atoms, occur close to one another in the host lattice, then at sufficiently high temperatures these may associate or dissociate to form a trapping centre. Thus, they will only be observed when there is sufficient lattice thermal energy to create the centres. Traps of this nature are called photochemical traps, and the change in magnitude of the T.S.C. with temperature of illumination corresponds to a change in the density of these centres.

Another possible explanation of the observation of particular trapping centres following high temperature treatment, is that each centre is surrounded by a potential barrier. At elevated temperatures, the free electrons in the conduction band have sufficient thermal energy to surmount the barriers surrounding such centres, so that their occupancy increases with increasing

temperature of illumination.

In both cases, the peak height of the T.S.C. would be expected to increase exponentially with increasing temperature of illumination. For the photochemical centre this exponent is associated with the activation energy required to create the trap, and for the potential barrier trap the exponent is determined by the barrier height.

Two variations in the density of trapped electrons were observed during the course of the present work. These variations were associated with

(a) trap H ($T^* = 350^oC$ and $E_t = 0.60$ eV) and

(b) trap F ($T^* = 270^oK$ and $E_t = 0.75$ eV) and trap G ($T^* = 300^oK$ and $E_t = 0.53$ eV).

6.3(a). Trap H

The trapping parameters for this centre are given in Table 5.9.1. The agreement between the Bube thermal activation energy and that found from monomolecular curve fitting, and also the change in T^* with the magnitude of the T.S.C. (see Figures 6.3.1 and 6.3.2), indicates that trap H is a fast trap. The capture cross-section of $2.0 \times 10^{-20} cm^2$, which was calculated on the assumption of monomolecular recombination is therefore open to question.

Although trap H was observed in two samples grown with $T_S = 300^oC$, it was not detected in any other sulphur rich sample ($T_S \geq 300^oC$). In all but one cadmium rich sample investigated, the density of these traps decreased with decreasing T_i. Figures 6.3.1 and 6.3.2 show the T.S.C. of traps F, G and H in a sample grown with $T_{Cd} = 350^oC$, for different values of T_i under illumination by infrared filtered and unfiltered tungsten radiation

respectively. Trap H can be seen on the right hand side of these figures.

If it is assumed that the variation in the height of the T.S.C. curve is associated with the creation of trapping centres of density N_t, then

$$N_t = N_o \exp(-E_a/kT_i) \qquad 6.3.1$$

where E_a is the activation energy for the photochemical creation of the trapping centres, and T_i is the temperature at which the illumination of the sample was begun during the cooling cycle of the T.S.C. schedule. A similar relationship is obtained for a trap surrounded by a potential barrier, where E_a represents the barrier height. A more detailed appraisal of the two models will be given in the discussion at the end of this chapter, where the results of other workers will be considered.

Figure 6.3.3 shows a plot of I^* (which is proportional to trap density) versus the reciprocal of T_i, for illumination with an infrared filtered tungsten lamp. An activation energy of 0.27 eV was obtained. Similar values were found for four other samples showing the effect.

In addition to the change in I^* with T_i, a variation of T^* was observed with the T.S.C. level. Such an observation is consistent with that expected from a fast retrapping centre. Using the notation defined in Chapter 3, the expression

$$t^{*2}\exp(t^*) = N_c E_t / N_t \beta \tau_n k \qquad 6.3.2$$

is obtained from Equation 3.7.8 for a fast trap, where $T = T^*$. Equating Equations 6.3.1 and 6.3.2, and eliminating N_t, leads to

$$N_c E_t / \beta \tau_n k t^{*2} \exp(t^*) = N_o \exp(-E_a/kT_i) \qquad 6.3.3$$

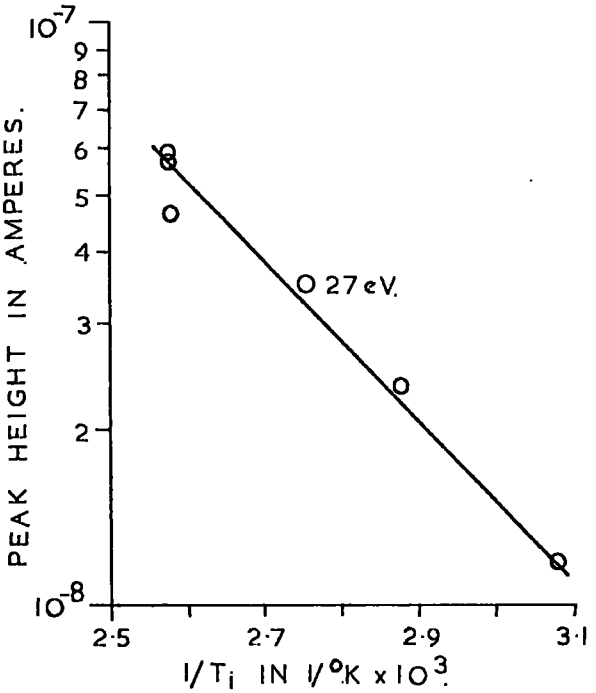

FIGURE 6.3.3 PEAK HEIGHT OF TRAP H VERSUS $1/T_i$ (FROM A $T_{cd}=350°C$ SAMPLE).

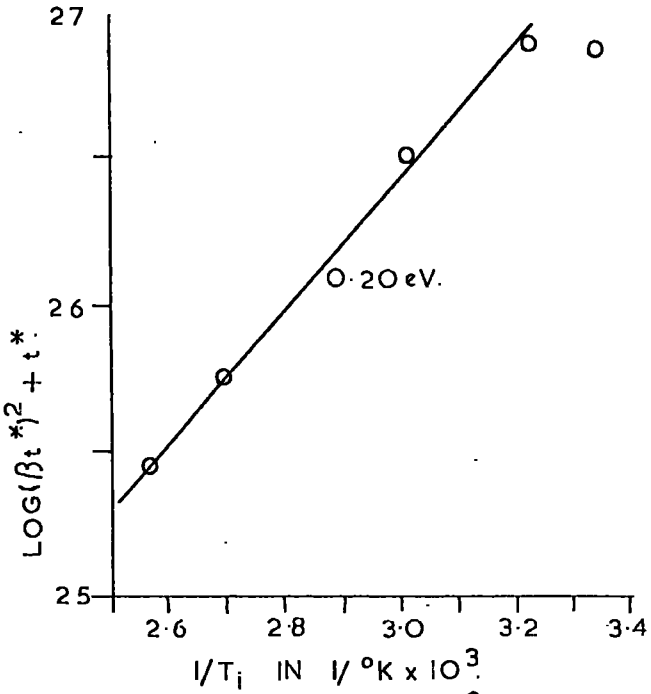

FIGURE 6.3.4 $LOG(\beta t^*)^2 + t^*$ VERSUS $1/T_i$ FOR TRAP H (FROM A $T_{Cd}=350°C$ SAMPLE).

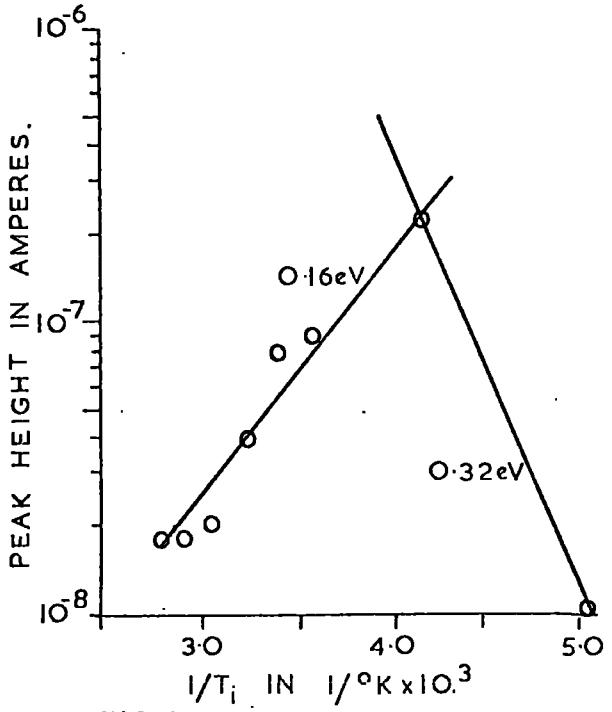

FIGURE 6.3.5 PEAK HEIGHT OF TRAP G VERSUS $1/T_i$ (FROM A $T_{Cd}=350°C$ SAMPLE).

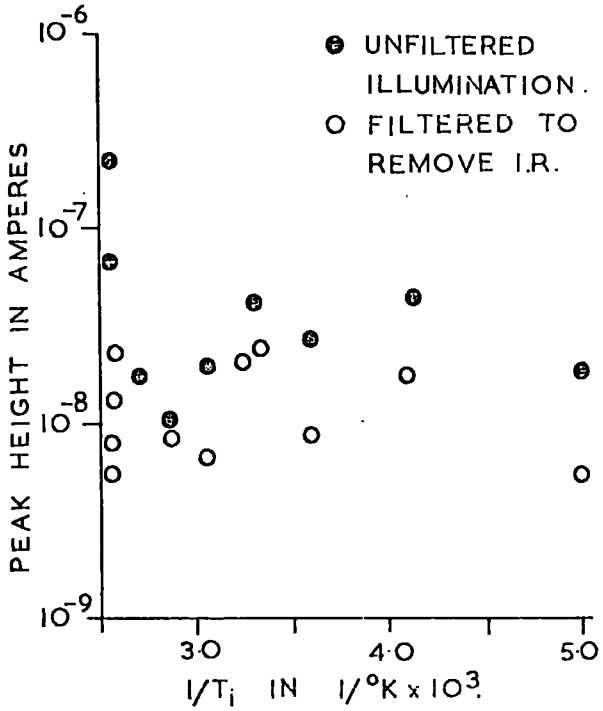

FIGURE 6.3.6 PEAK HEIGHT OF TRAP F VERSUS $1/T_i$ (FROM A $T_{Cd}=350°C$ SAMPLE).

This simplifies to

$$\log(\beta t^{*2}) + t^{*} + \text{const} = E_a/kT_i \qquad 6.3.4$$

A plot of $\log(\beta t^{*2}) + t^{*}$ versus $1/T_i$ is drawn in Figure 6.3.4, yielding an activation energy of 0.20 eV. The difference between this value of E_a and that found above (0.27 eV) may be explained in terms of the considerable scatter of experimental points for the two methods of evaluating E_a.

Trap H was also studied using filtered light in the blue, green and red regions of the visible spectrum. Barr and Stroud interference filters centred on 4380 A^{o}, 5460 A^{o} and 7700 A^{o} were individually interposed between the tungsten lamp and the sample; the two shorter wavelength filters were accompanied by a one centimetre path length of 10% copper sulphate solution and two Chance HA 1 filters. Where the 4380 A^{o} and 7700 A^{o} filters were used for trap filling, only a small variation of T.S.C. level was observed following illumination at temperatures of 388°K, 270°K and 95°K. The green 5460 A^{o} radiation caused an order of magnitude variation, similar to that observed under broad band illumination.

6.3(b). Traps F and G

The trapping parameters for these traps are given in Table 5.9.1. The T.S.C. associated with these traps were observed to vary with T_i in both cadmium and sulphur rich samples, though the change with T_i was not as simple as that for trap H. In cadmium rich samples the changes in the T.S.C. curves for traps F, G and H occurred simultaneously.

Only two cadmium rich samples showed a significant variation

of traps F and G with a change in T_i. Figure 6.3.1 shows the T.S.C. curves for a T_{Cd} = 350°C sample illuminated with T_i = 388°K, 350°K, 270°K and 90°K, where the illumination was an infrared filtered tungsten lamp. The curves in Figure 6.3.2 were obtained using the same values of T_i and an unfiltered tungsten lamp. With both types of illumination, a decrease in the width at half height of the T.S.C. curve for trap G (Figure 6.3.1) and trap F (Figure 6.3.2) was observed, as compared with the T.S.C. of traps F and G in other samples where there was little variation of peak height with T_i. As explained in Section 5.9, the sharpening of the T.S.C. curves means that analysis yields a high value of E_t. Thus values of E_t = 1.0 eV were obtained for trap G (E_t = 0.53 eV) in Figure 6.3.1 and for trap F (E_t = 0.75 eV) in Figure 6.3.2, using the curve fitting technique described in Chapters 3 and 5.

The peak height of trap G, following infrared filtered illumination, is plotted against $1/T_i$ in Figure 6.3.5, and an activation energy of 0.16 eV is derived from the line of positive slope. A line of negative slope has been drawn through the two lowest temperature points in Figure 6.3.5, yielding an activation energy of 0.32 eV. This last value is only approximate, but it indicates the order of magnitude of the negative activation energy. A similar variation with T_i was observed for trap G after the sample was irradiated with unfiltered tungsten light. The line of positive slope gave an activation energy of 0.14 eV and that of negative slope an activation energy of 0.21 eV. The line of positive slope may be considered to yield the activation energy to destroy these centres, and the line of negative slope the activation energy to create or fill the traps.

Figure 6.3.6 shows the variation of the peak maximum current, I^*, of trap F versus $1/T_i$, where points are given both for

filtered and unfiltered tungsten irradiation. I^* for trap F can be seen to be relatively constant, except for T_i = 388°K with unfiltered tungsten radiation. The photocurrent was also monitored for the same values of T_i as the T.S.C., and an increase in photocurrent was observed for unfiltered tungsten illumination at T_i = 388°K. This corresponds with the increase in the general level of the T.S.C. The density of trap F may therefore be considered to remain unchanged with variation of T_i.

A similar change of traps F and G was observed in another T_{Cd} = 350°C sample. The main difference in the T.S.C. of the two samples was that in the first sample described the maximum T.S.C. for traps F, G and H were similar in magnitude. The second sample showed a maximum value of T.S.C. for traps F and G which was two orders of magnitude greater than that observed for trap H.

A number of samples were taken from a T_S = 300°C boule, which showed considerable changes in the T.S.C. levels of traps F and G with T_i, although trap H was not detected. The changes in the T.S.C. level were in qualitative agreement with that observed in the two cadmium rich samples. Figure 6.3.7 shows the T.S.C. from F and G for one sample cut from this boule, using a number of values of T_i.

Difficulty was experienced in finding a consistent variation of trap F and G in the T_S = 300°C samples for a number of reasons.

(a) The resolution of traps F and G was much better for cadmium rich samples than sulphur rich samples. In Figures 6.3.1 and 6.3.2, the maxima of trap F and trap G can be clearly seen. Figure 6.3.7 shows the T.S.C. in the temperature region at which traps F and G empty, in a T_S = 300°C sample. Although the two traps cannot be resolved, thermal cleaning indicated that both

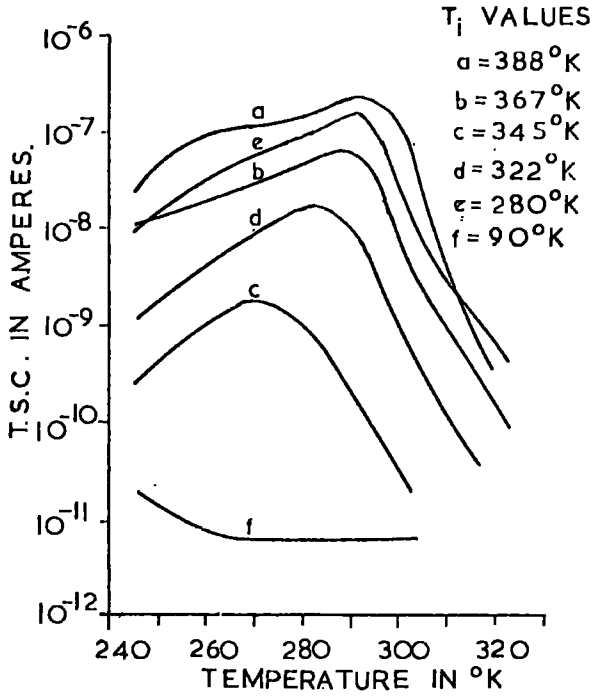

FIGURE 6.3.7 T.S.C. FOR TRAPS F AND G (FROM A T_S = 300°C SAMPLE) USING A NUMBER OF VALUES OF T_i

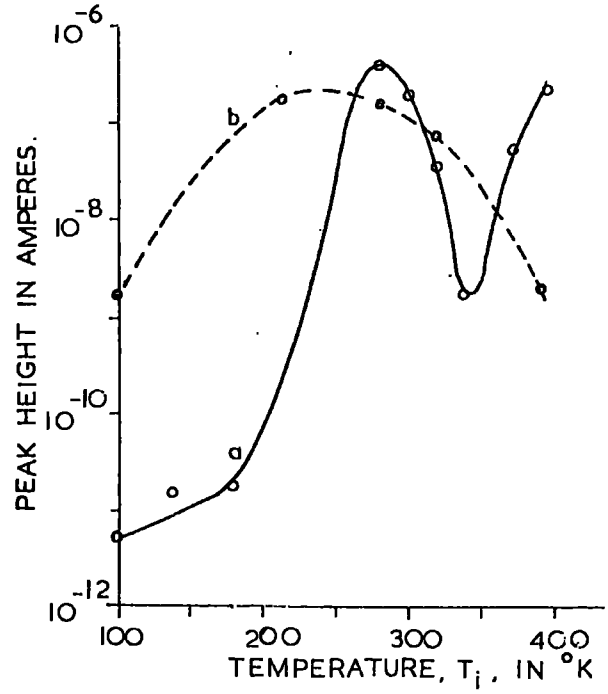

FIGURE 6.3.8 PEAK HEIGHT VERSUS TEMPERATURE, T_i, (a) FROM FIGURE 6.3.7, (b) FOR TRAP G IN ANOTHER T_S = 300°K.

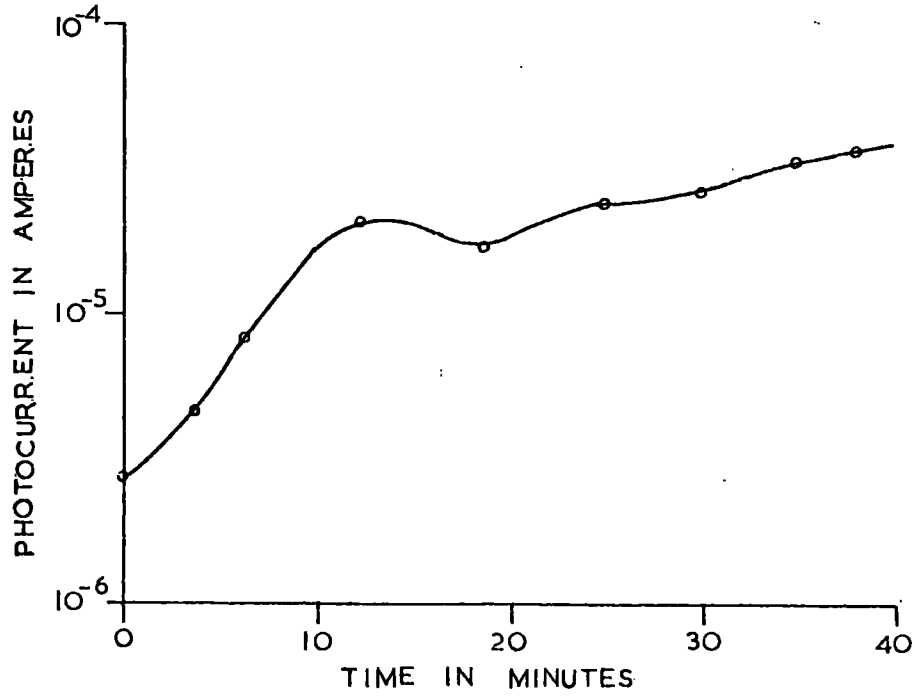

FIGURE 6.3.9 PHOTOCURRENT VERSUS TIME FOR A T_S = 300°C SAMPLE ILLUMINATED AT 388° K

traps were present.

(b) There were considerable differences, from sample to sample, in the variation with T_i. Figure 6.3.8 shows the maximum current for the doublet, comprising traps F and G, for the sample shown in Figure 6.3.7, and for trap G in another sample taken from the same boule. In both cases an infrared filtered tungsten lamp was used to fill the traps.

(c) In sulphur rich samples the dark current in the region of traps F and G is in some cases comparable in magnitude to the T.S.C.

(d) Variation of lifetime occurred in some samples, which was not always reproducible. In one sample a decrease in lifetime was observed, as measured by the current level of the T.S.C., from one T.S.C. run to the next. In another sample continuous illumination at 388°K led to a rise in photocurrent with time, as shown in Figure 6.3.9.

Under these conditions widely differing values of activation energies were obtained, from sample to sample, by plotting I^* against $1/T_i$. A qualitative agreement with the variation observed in cadmium rich samples can be seen in Figure 6.3.8, where a maximum in I^* was obtained for values of T_i in the region 200°K to 300°K.

6.4. Discussion

In this chapter it has been demonstrated that variation of lifetime can have a very significant effect on the observed T.S.C. measured after differing conditions of illumination. Measurements of photocurrent under the same conditions of pre-illumination can be used to show where such lifetime effects occur. The

author knows of no report of a rapid increase in photocurrent with increasing temperature, similar to that observed (see Figure 6.2.2) during the course of the present work.

The variation in the magnitude of the T.S.C. for traps F, G and H has been described in this chapter. Trap H was observed mainly in cadmium rich samples, and increased exponentially with increasing T_i. Trap G was observed to have a maximum in T.S.C. for T_i in the range 200°K to 300°K, for both cadmium and sulphur rich samples, where a change in the T.S.C. level was found. Trap F varied with T_i in sulphur rich samples, although it was relatively constant in cadmium rich samples for $T_i < 388$°K.

Woods and Nicholas (1964), and Cowell and Woods (1969) have observed variations of the high temperature traps which are very similar to those observed here. In both papers it was noted that the density of trap H reached a maximum under illumination at high temperature. Cowell and Woods also found an exponential increase of trap H with T_i, although their value of activation energy (0.07 eV) does not agree with the values of between 0.20 eV and 0.27 eV obtained from the present results.

Cowell and Woods also reported a variation of I^* for a trap with $T^* = 275$°K, and a thermal activation energy of 0.85 eV. This variation with T_i is almost identical to that observed for trap G ($E_t = 0.53$ eV) in cadmium rich samples. They found a maximum in density for $T_i = 200$°K, and a plot of I^* versus $1/T_i$ gave activation energies of 0.18 eV and 0.32 eV for the lines of negative and positive slope repectively. These values agree well with the values of 0.16 eV and 0.32 eV, found in the present work for illumination of a $T_{Cd} = 350$°C sample with an infrared filtered tungsten lamp.

A large disparity can be seen between the values of E_t found

for trap G (0.53 eV) and that reported by Cowell and Woods (0.85 eV). This may well be due to the sharpening of the T.S.C. curve (yielding a high value of E_t) which occurs when there is a variation of the T.S.C. with T_i. Trap G gave values which were as large as 1.0 eV under these conditions. When no significant change in the T.S.C. level was observed, thermal activation energies between 0.47 eV and 0.57 eV were obtained.

Trap F yielded values of E_t = 0.75 eV and T^* = 270°K, which are comparable to the parameters found by Cowell and Woods. In most cases trap F gave high values of E_t (1.0 eV) where the T.S.C. spectrum changed with T_i. As described earlier (see Figure 6.3.6), the magnitude of trap F remained relatively constant for values of T_i < 388°K, and so does not behave similarly to Cowell and Woods' 'trap F'.

Bube et al. (1966) observed a T.S.C. curve with T^* = 289°K in mixed CdS:Se crystals. The trap responsible for this curve had a thermal activation energy of 0.73 eV, using a best fit monomolecular curve. The magnitude of the T.S.C. varied with T_i such that it was essentially constant for values of T_i below 180°K and above 210°K. Bube et al. interpreted the change in the level of the T.S.C. in terms of a trap surrounded by a potential barrier. Where tunnelling through the barrier is considered negligible, the cross-section for capture of carriers, S_{tc}, is related to the effective cross-section for escape of carriers, S_{te}, by the relationship

$$S_{te} = S_{tc}\exp(E_b/kT) \qquad 6.4.1$$

where E_b is the barrier height. The results of Bube et al. were consistent with a barrier height of approximately 0.3 eV, and values of S_{te} and S_{tc} of approximately 10^{-14}cm^2 and 10^{-19}cm^2

respectively.

The value of 0.32 eV, found in the present work for the exponential increase in I^* for trap G with T_i, is in good agreement with the value of Bube et al, although the values of E_t were completely different. Another significant difference is that Bube et al. did not observe a maximum for I^* with T_i, but reported a saturation of trap filling for $T_i > 210^oK$.

Cowell and Woods postulated that their traps, which compare in T^* and E_t with traps F and H, varied in a photochemical manner. They also proposed that their traps were associated. In the present work, traps G and H behaved in a similar manner to the traps reported by Cowell and Woods. Traps G and H do not appear to be associated for three reasons.

(a) In most cadmium rich samples the variation of trap H was not accompanied by a change of trap G.

(b) Trap H was not observed in most of the sulphur rich samples, although a variation in trap G was observed.

(c) In the two cadmium rich samples investigated, the ratios of the maximum value of I^* for traps G and H was two orders of magnitude. (The photocurrent versus temperature measurements made on these samples indicated that the differences in the T.S.C. could not be explained in terms of the free electron lifetime.)

Woods and Nicholas, and Cowell and Woods observed variations of the high temperature traps in flow crystals annealed in sulphur vapour, which were similar to those observed in the two cadmium rich samples. Nicholas and Woods also found that trap G occurred only in sulphur annealed flow crystals. In this thesis trap H was detected mainly in cadmium rich crystals, but was also found

in two sulphur rich samples. Traps F and G were observed in the majority of samples investigated. Thus it would appear that the high temperature traps can exist under both cadmium and sulphur rich conditions. It seems reasonable to propose that they are likely to be due to complex assocations of native defects and/or impurities than to simple native defects.

Equation 6.3.2, for a fast trap at T^*, shows that T^* depends on the two material parameters τ_n and N_t (the trap density). Because τ_n was found from photocurrent measurement to be relatively constant for the cadmium rich sample described in Section 6.3(a), the variation in T^* for trap H suggests that it is caused by a change in N_t. Such a change in density of a set of traps is commensurate with centres of a photochemical nature. The relatively good agreement between values of E_a for trap H of 0.20 eV and 0.27 eV, deduced from the variations of I^* and respectively, also favour a variation in density rather than occupancy. As trap H behaves as a fast trap it is difficult to equate a large capture cross-section with a centre surrounded by a potential barrier. The behaviour of trap H therefore strongly suggests that it is a photochemical centre, whose activation energy for creation is approximately 0.24 eV.

Trap G gave values of E_t which were similar for both monomolecular curve fitting and Bube's method. This indicates that trap G is also a fast retrapping centre. Again the large capture cross-section is not compatible with a potential barrier centre. The more complex variation of trap G with T_i, yielding both an activation energy for creation and destruction does not fit the model propsed by Bube et al. Thus, the variation of trap G with T_i favours a photochemical centre.

References to Chapter 6

Bube, H.R., G.A. Dussel, C.-T. Ho and L.D. Miller, 1966, J. Appl. Phys. 37, 21.

Cowell, T.A.T. and J. Woods, 1969, J. Phys. D. (Brit. J. Appl. Phys.) Series 2, 2, 1053.

Woods, J. and K.H. Nicholas, 1964, Brit. J. Appl. Phys. 15, 1361.

Zomov, V.V. and V.V. Serdyuk, 1969, Sov. Phys. Solid State 10, 1936.

CHAPTER 7

CONTACTS AND SURFACE EFFECTS

7.1. Introduction

The T.S.C. measurements described in Chapters 5 and 6 were made on rod shaped samples with indium contacts made to each end, as described in Section 4.3(a). With such a configuration of electrodes it is not possible to determine how the T.S.C. is modified by contact effects or to determine whether some of the trapping centres observed are associated with the surfaces of the samples.

In this chapter experiments are described in which a four electrode arrangement was used to investigate the uniformity of the potential distribution along a crystal. A three probe configuration of electrodes was used to determine whether there was a significant contribution to the T.S.C. from surface traps. The effects of ambient pressure on the T.S.C. measurements, made on samples with two probes, is also discussed.

7.2. Contacts

Indium and gallium have been used extensively to make contacts to CdS, and Smith (1955) showed that both were ohmic. The indium contacts used for the two probe measurements made during the present work were tested against the following criteria:-

(a) Linearity of current-voltage curves under illumination.

(b) Reproducibility of T.S.C. on reversing the current through the sample.

(c) The absence of noise during T.S.C. measurement.

All samples were etched before contact was made, so that the

the anomalous dark current effects, reported by Verdyuk and Bube (1967), were rarely encountered.

It was considerably more difficult to make ohmic contacts to sulphur rich than to cadmium rich samples. This observation is in agreement with the work of Stewart and Wilson (1967) who found a similar difficulty. They found a correlation between the ease of making ohmic contacts and the density of etch pits which could be produced. They concluded that ohmic contact was made by diffusion of the contact material into dislocations.

7.3. Four Probe Measurements

For this mode of measurement, the samples were provided with contacts and mounted as described in Section 4.3(c). The experimental arrangement used for the electrical measurements has also been described earlier in Section 4.4. A side elevation of a typical specimen with four electrodes (numbered 1 to 4) is shown in the insert on Figure 7.3.1.

A potential of 100 volts was applied across the two end contacts (1 and 4) and the T.S.C. or photocurrent was monitored with the current flow via these contacts. The potential between the central electrodes (2 and 3) was also recorded during the T.S.C. or photocurrent run. Where a large variation of potential occurred, further measurement was made between either of the end electrodes and its nearest neighbour electrode (1 and 2 or 3 and 4). This electrode number notation will be followed in the text below, since it simplifies the description of the pairs of electrodes used for potential or other measurement.

Four samples were investigated in the manner described above. Three of these (A, B and C) were grown under cadmium rich conditions and the fourth (D) was sulphur rich. Using the three

criteria listed in Section 7.2, the contacts to sample A were non-ohmic whereas the contacts to samples B, C and D were ohmic.

7.3(a). Sample A

This sample was obtained from a boule grown with $T_S = 50^{\circ}C$. Figure 7.3.1 shows the T.S.C. curves ((a) and (b)) for both directions of current through the sample after illumination with an infrared filtered tungsten lamp during cooling from $388^{\circ}K$ to $95^{\circ}K$. Figure 7.3.2 shows (i) the potential developed between electrodes 2 and 3, and (ii) the potential occurring between electrode 1 (the cathode) and electrode 2, during the observation of the T.S.C. curve Figure 7.3.1 (a). Figure 7.3.1 curve (c) shows the thermally stimulated conductance derived from Figure 7.3.1 (a) and the potential measurements in Figure 7.3.2 (ii). (A thermally stimulated conductance curve corresponding to the T.S.C. shown in curve (b) Figure 7.3.1 has not been presented, because the T.S.C. measurement was extremely noisy and so casts some doubt on the reliability of the conductance values.)

From Figure 7.3.1 it is quite clear that the end contacts cannot be regarded as ohmic (from the second criterion in Section 7.2) since there is a considerable difference between the T.S.C. for the two directions of current flow. For both directions of flow, the majority of the applied potential was dropped between the negative end electrode and its nearest neighbour electrode. Such an observation is consistent with a rectifying or non-ohmic contact. The distortion of the T.S.C. curves, due to the imperfect contacts, can be clearly seen by comparing the T.S.C. and thermally stimulated conductance values given in Figure 7.3.1.

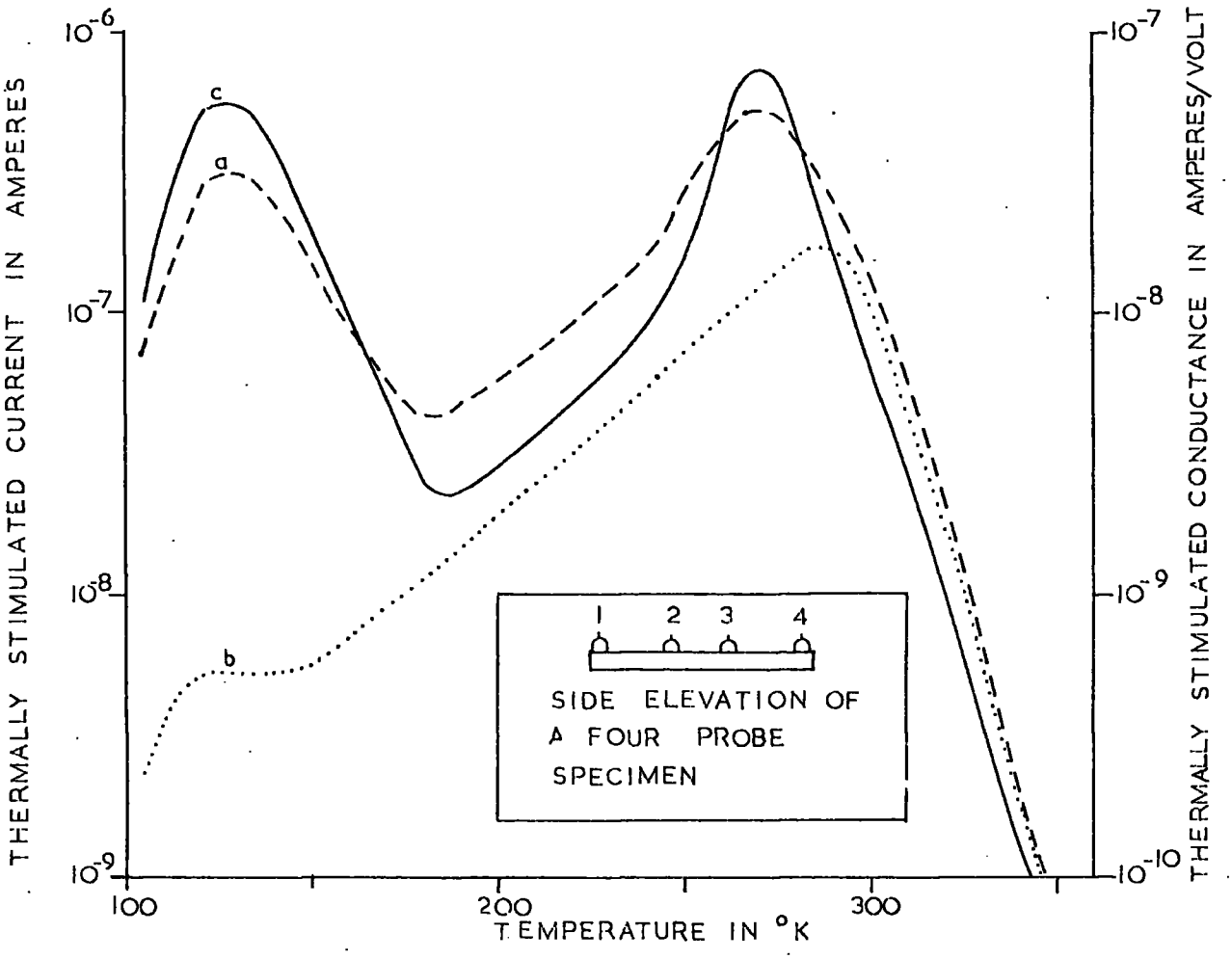

FIGURE 7.3.1 T.S.C. AND THERMALLY STIMULATED CONDUCTANCE FOR SAMPLE A

a AND b T.S.C. FOR BOTH DIRECTIONS OF CURRENT THROUGH SAMPLE

c THERMALLY STIMULATED CONDUCTANCE CORRESPONDING TO CURVE (a)

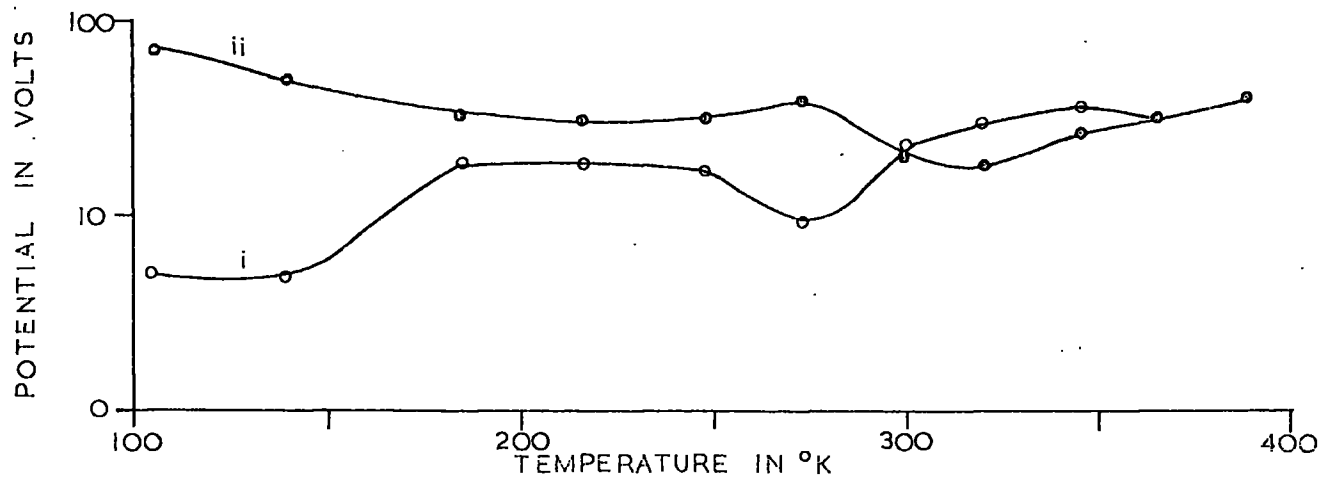

FIGURE 7.3.2 THE POTENTIAL MEASURED BETWEEN ELECTRODES 2 AND 3 (CURVE [i]) AND 1 AND 2 (CURVE [ii]) DURING T.S.C. CURVE (a) ABOVE.

7.3(b). Sample B

Sample B was taken from a boule grown with T_{Cd} = 350°C. When the electrodes were applied, all three criteria for ohmic contact were obeyed. Figure 7.3.3 shows the T.S.C., curve (a), measured after cooling from 388°K to 95°K under illumination, whereas curve (b) was monitored after cooling in the dark and illuminating at 95°K for five minutes. The excitation radiation was provided by an infrared filtered tungsten lamp. The T.S.C. curves were characteristic of cadmium rich samples, showing the variations associated with the highest temperature trap which were discussed in Chapter 6.

Figure 7.3.4 shows the potential dropped between electrodes 2 and 3 during the course of both the T.S.C. runs illustrated in Figure 7.3.3. The magnitude and temperature variation of the potential dropped between electrodes 2 and 3 were the same when the current was reversed in direction through the sample. The minimum in potential can be seen to correspond to the maximum of the trap emptying at 300°K. As described in Chapter 6, this centre can vary in density with differing illumination treatment, and it would seem that the emptying of this trap is associated with a space charge built up at the end contacts. The potential between electrodes 2 and 3 remained practically constant when the photocurrent was monitored as a function of temperature following either of the two standard cooling schedules.

For completeness, the thermally stimulated conductance curves are shown in Figure 7.3.3, for comparison with the corresponding T.S.C. curves also shown in this figure. The T.S.C. and thermally stimulated conductance spectra, made for the same illumination schedule, can be seen to be very similar.

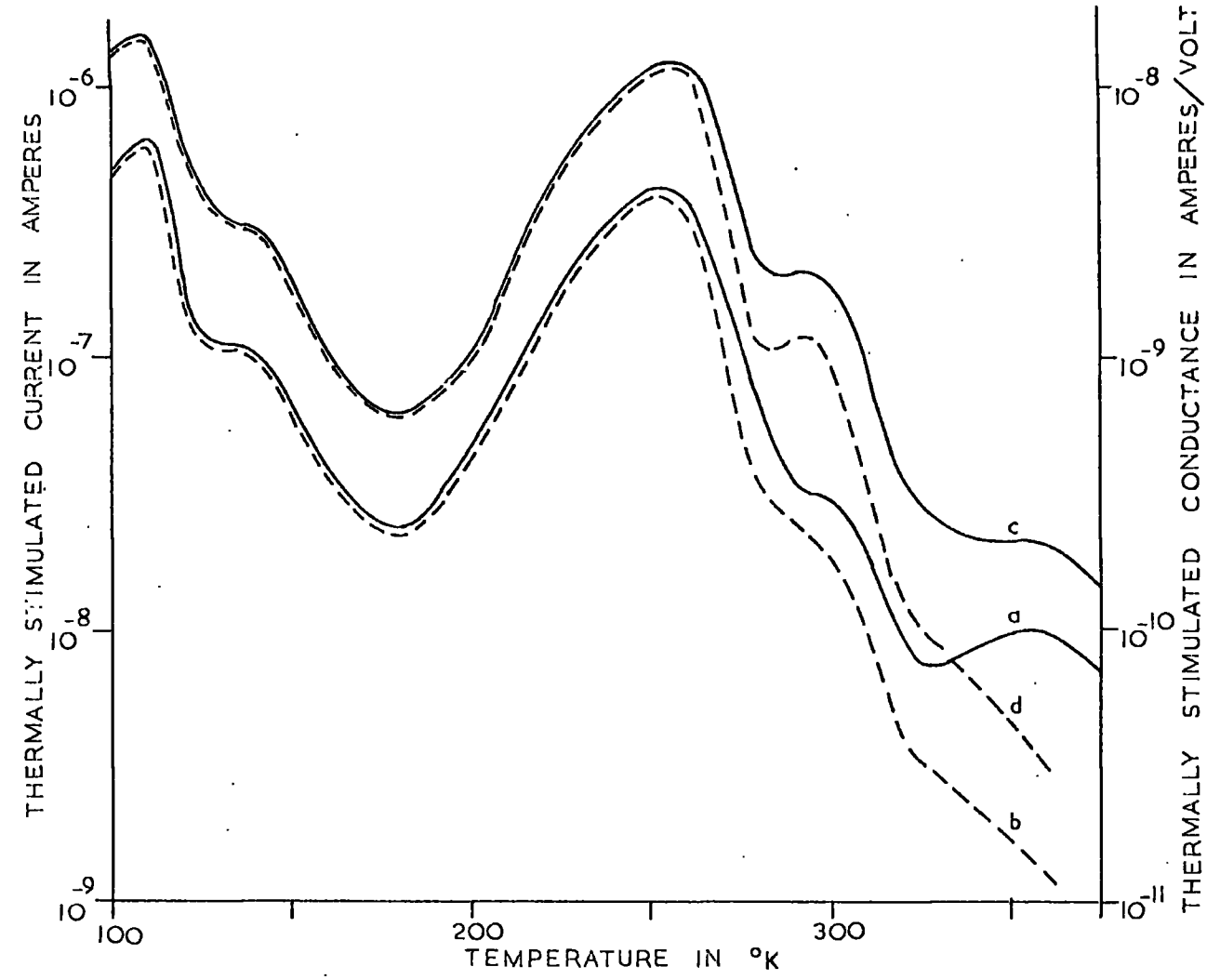

FIGURE 7.3.3 T.S.C. AND THERMALLY STIMULATED CONDUCTANCE FOR SAMPLE B

a T.S.C. AFTER COOLING FROM 388°K UNDER ILLUMINATION
b T.S.C. AFTER ILLUMINATION AT 95°K ONLY
c AND d THERMALLY STIMULATED CONDUCTANCE CORRESPONDING TO T.S.C. CURVES (a) AND (b)

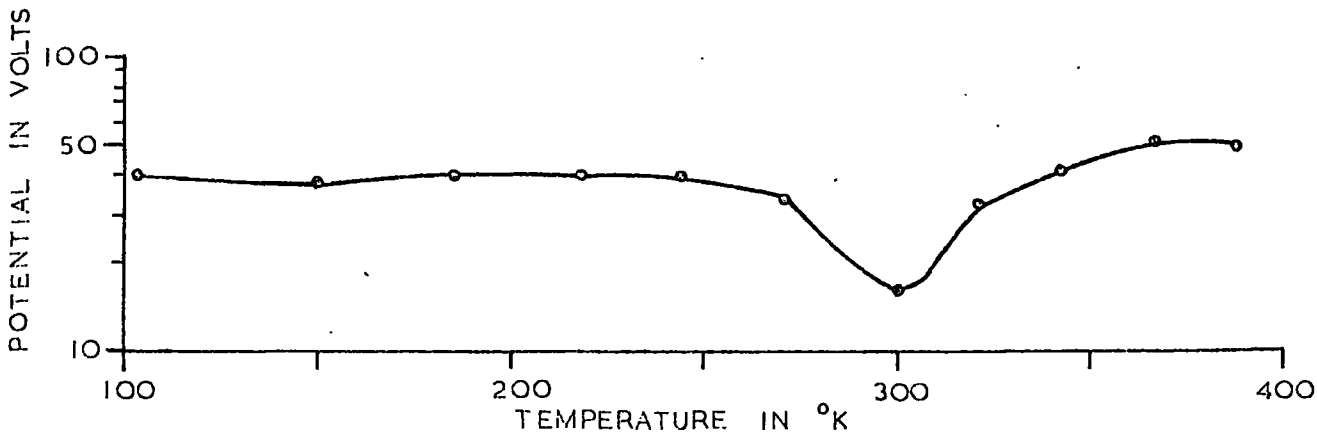

FIGURE 7.3.4 POTENTIAL MEASURED BETWEEN ELECTRODES 1 AND 2 FOR THE ABOVE T.S.C. CURVES

7.3(c). Sample C

This sample was obtained from a boule grown with T_{Cd} = 550°C. According to the three criteria, the indium contacts were ohmic. Under continuous illumination at room temperature a decay in photocurrent was observed. Figure 7.3.5 shows the photocurrent as a function of time during irradiation at 295°K, with an infra-red filtered tungsten lamp.

Figure 7.3.6 curve (a) shows the T.S.C. measured after a schedule of illumination at room temperature for 25 minutes, followed by cooling to 95°K under illumination. Curve (b) shows the T.S.C. measured after a schedule of illumination whilst cooling from room temperature as soon as the illumination was switched on. Two main features are evident from these curves, i.e. the magnitude of the T.S.C. associated with the low temperature traps decreased while that of the highest temperature trap increased, after illumination for 25 minutes at room temperature.

Figure 7.3.7 shows the potentials, as measured between electrodes 2 and 3, which correspond to the T.S.C. curves (a) and (b) in Figure 7.3.6. Using these values of potential as a function of temperature, the thermally stimulated conductance curves, corresponding to the T.S.C. measurements, are also presented in Figure 7.3.6.

Where the sample was illuminated during cooling from 388°K, the resultant T.S.C. curve was essentially the same as that observed after 25 minutes illumination at room temperature (Figure 7.3.6 curve (a)). Figure 7.3.8 curve (i) shows the potential measured between electrodes 1 and 2, curve (ii) shows the potential measured between electrodes 2 and 3 and curve (iii) shows the potential measured between electrodes 3 and 4 during a T.S.C. run made after illumination while cooling from 388°K.

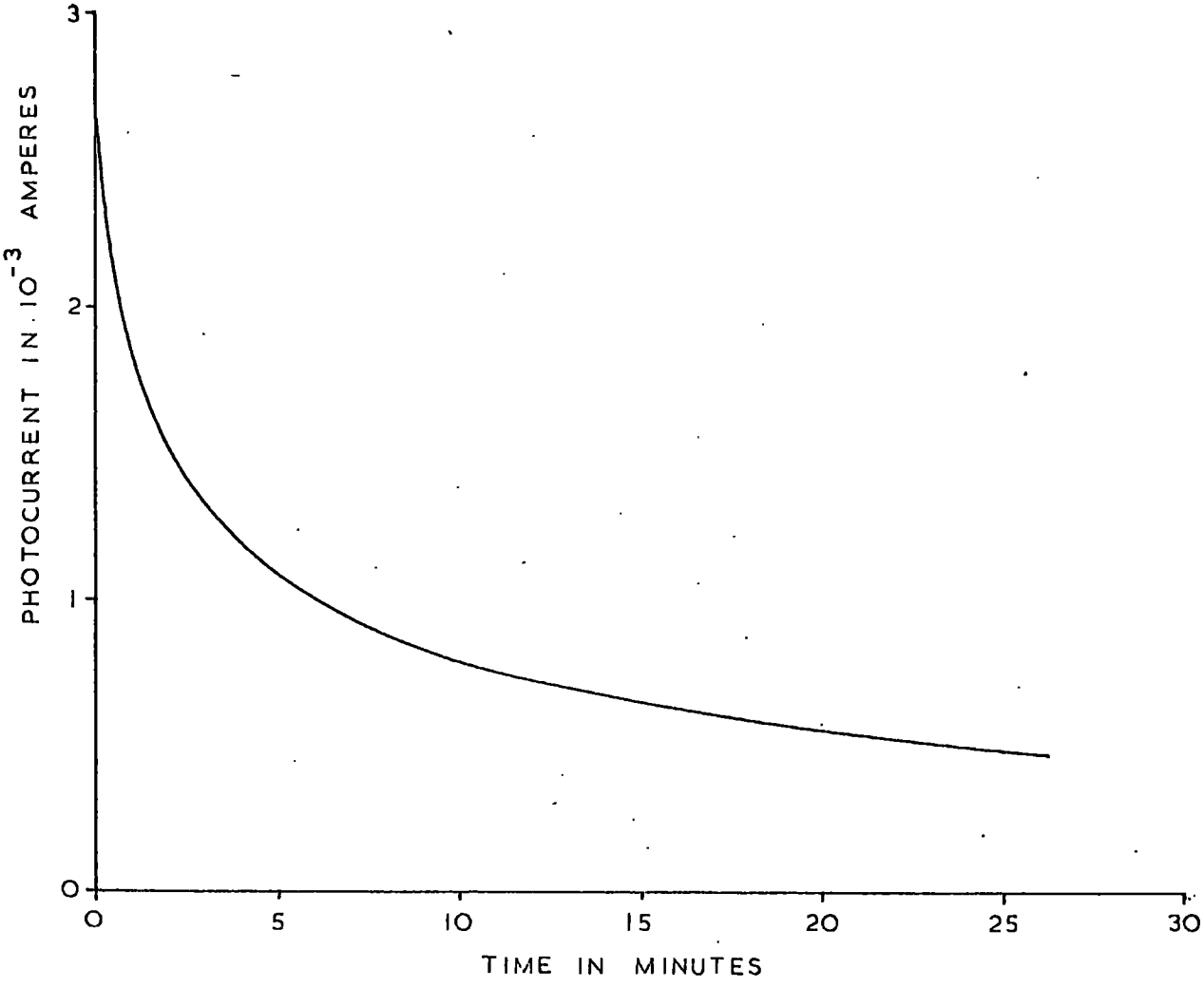

FIGURE 7.3.5 PHOTOCURRENT VERSUS TIME FOR SAMPLE C, AT 295°K

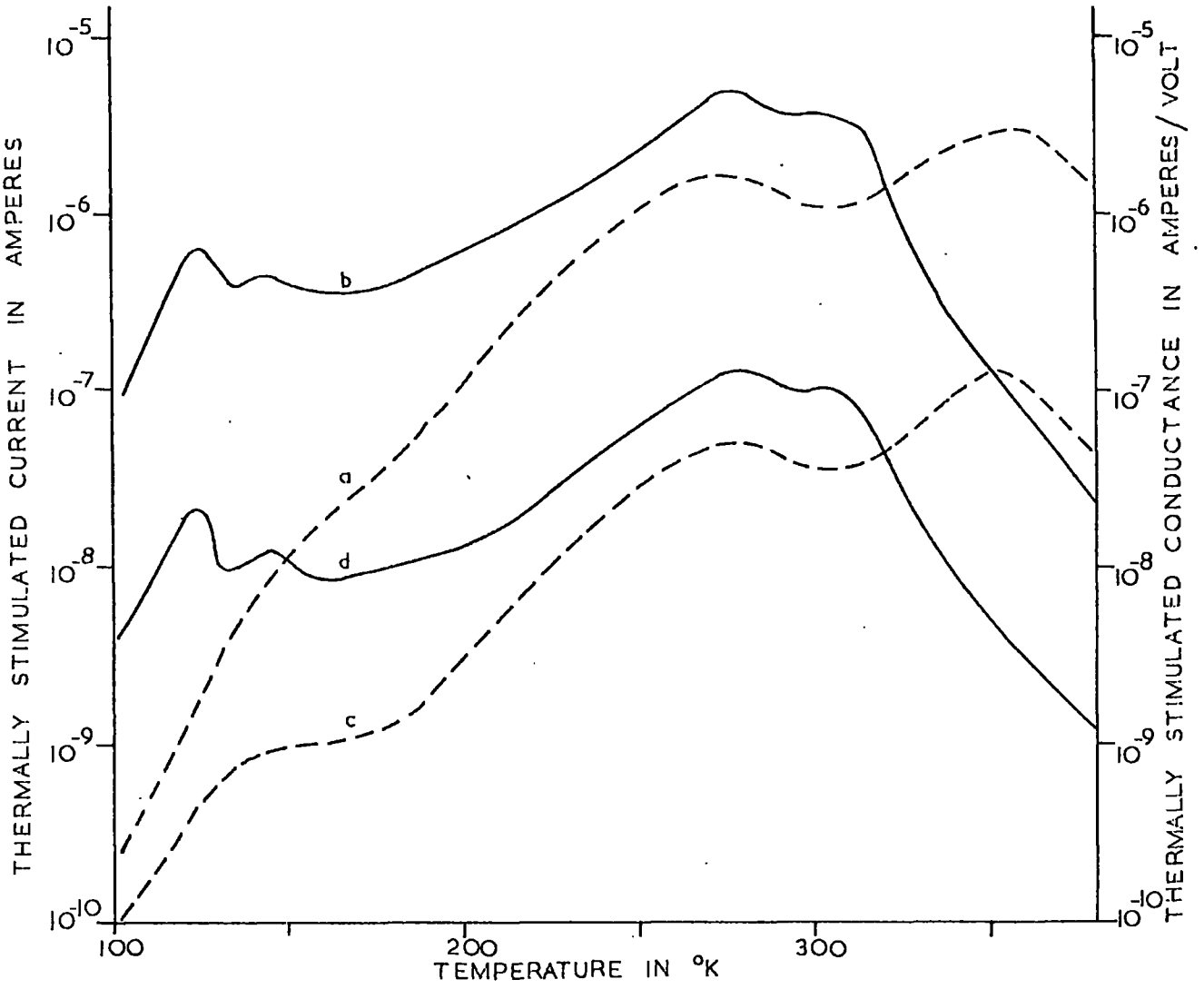

FIGURE 7.3.6 T.S.C. AND THERMALLY STIMULATED CONDUCTANCE FOR SAMPLE C

a T.S.C. AFTER 25 MINUTES ILLUMINATION AT ROOM TEMPERATURE

b T.S.C. AFTER COOLING UNDER ILLUMINATION FROM ROOM TEMPERATURE

c AND d THERMALLY STIMULATED CONDUCTANCE CORRESPONDING TO T.S.C. CURVES (a) AND (b)

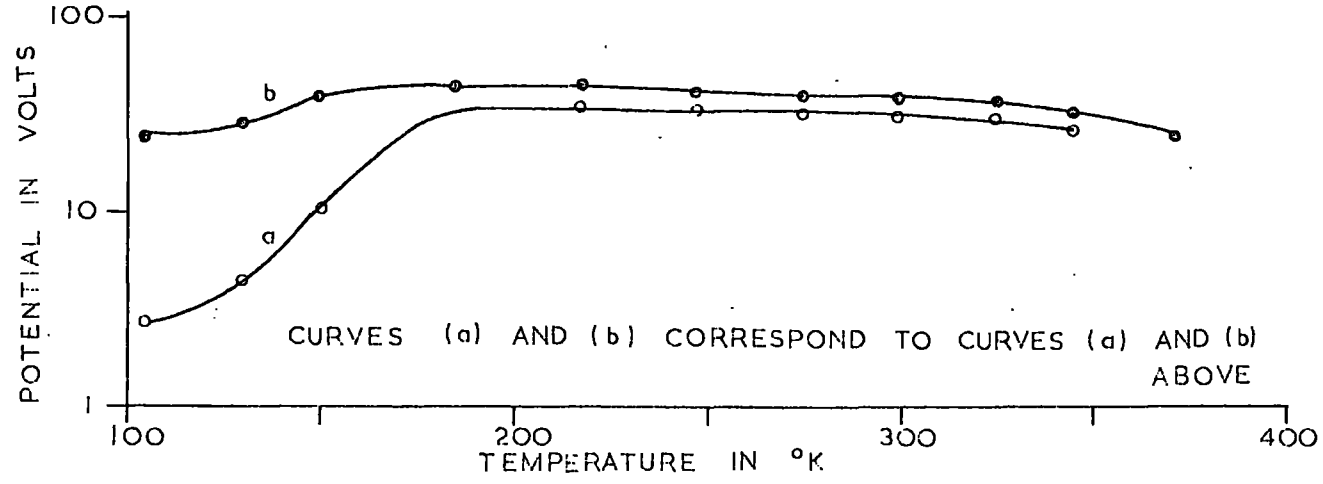

FIGURE 7.3.7 POTENTIAL MEASURED BETWEEN ELECTRODES 1 AND 2 DURING THE ABOVE T.S.C. MEASUREMENTS

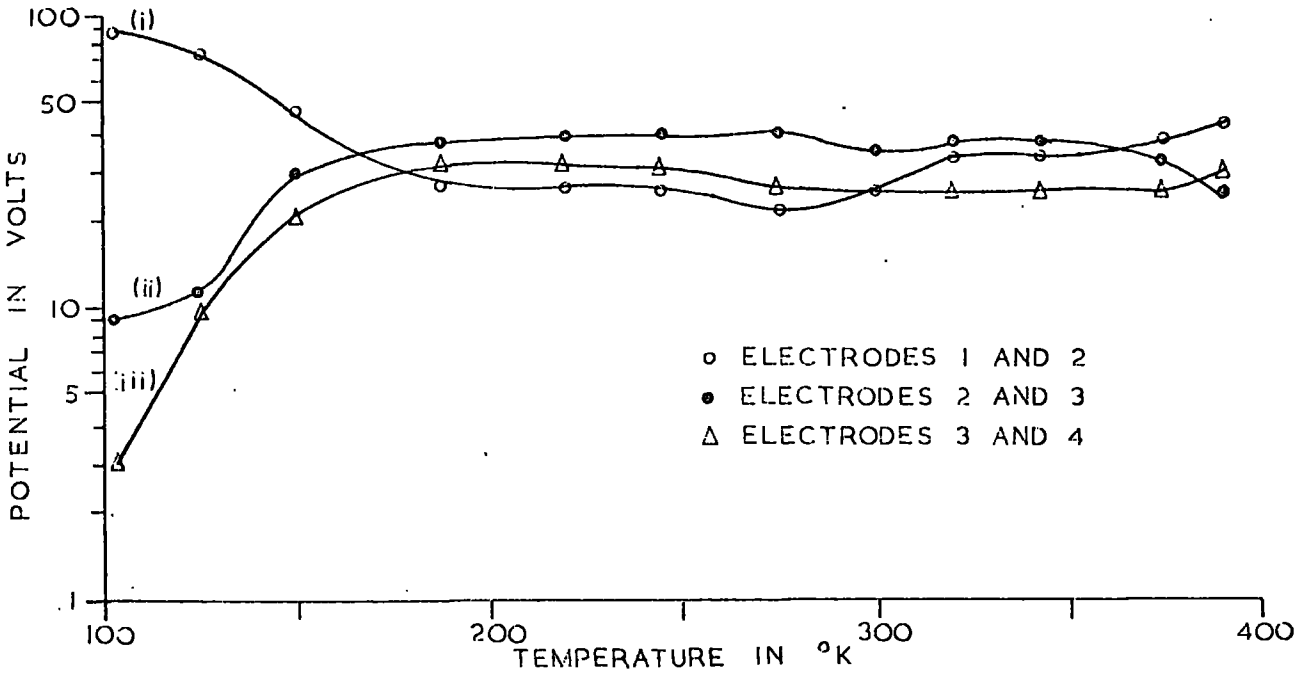

FIGURE 7.3.8 POTENTIAL MEASURED BETWEEN ELECTRODES DURING A T.S.C. RUN ON SAMPLE C, FOLLOWING ILLUMINATION FROM 388 °K

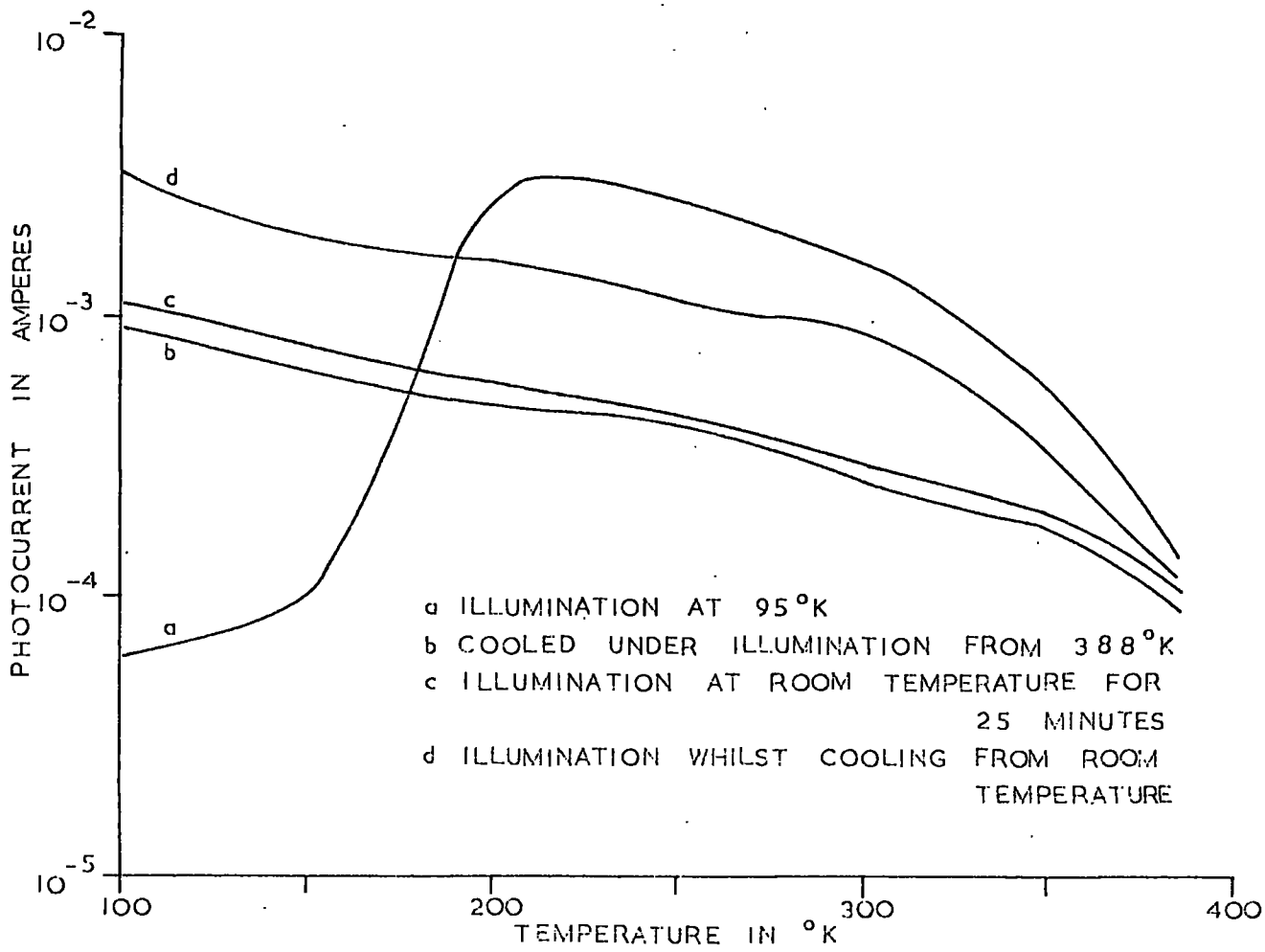

FIGURE 7.3.9 PHOTOCURRENT VERSUS TEMPERATURE FOR SAMPLE C, FOLLOWING DIFFERENT ILLUMINATION TREATMENTS PRIOR TO MEASUREMENT

The apparent decrease in the density of the low temperature traps is therefore associated with a build up of potential between electrodes 1 and 2. When the current through the sample was reversed while the crystal was illuminated, there was a decay in the photocurrent. Under the reverse potential there was also a decrease in the apparent density of the low temperature traps and an increase in the T.S.C. associated with the highest temperature trap, following the schedule which involved illumination at room temperature for 25 minutes. The potentials measured between electrodes 1 and 2, 2 and 3 and 3 and 4 were the same as those observed before current reversal, for T.S.C. curves recorded using the same illumination conditions.

Thus, the potential build up was associated with the same electrodes (1 and 2) for both directions of current flow through the sample. Such an observation is not compatible with any theory, known to the author, which describes a rectifying or non-ohmic contact. It would seem most probable that the sample was not homogeneous, and that part of the sample lying in the region of the end contact (1) could suffer a large change in resistivity under certain conditions of illumination.

Two probe T.S.C. measurements were also made between electrodes 2 and 3, after irradiation while cooling from 388^{o}K. The magnitude of the T.S.C. of the low temperature traps was approximately a factor 4 smaller than that observed during four probe measurements after cooling from room temperature under illumination, although the T.S.C. curves at high temperature were similar in both cases. This indicates that part of the inhomogeneous region lay between electrodes 2 and 3. Such an observation is consistent with the thermally stimulated conductance curves shown in Figure 7.3.6. Here the apparent density of the low

temperature traps is an order of magnitude smaller, following illumination at room temperature for 25 minutes (curve (c)), compared with the conductance monitored after illumination while cooling from room temperature (curve (d)).

The density of the low temperature traps was again low according to the T.S.C. monitored following five minutes irradiation at 95°K. This, however, was not unexpected as other samples cut from the T_{Cd} = 550°C boule had previously shown the same phenomenon, see Section 6.2, where there is a decrease in the apparent density of the low temperature traps, following irradiation at low temperature, due to a decrease in the free electron lifetime. The photocurrent was similarly decreased at low temperatures following a similar illumination schedule.

Figure 7.3.9 curve (a) shows the photocurrent as a function of temperature following five minutes illumination at 95°K. There is the anticipated rise in photocurrent at approximately 200°K. It should be emphasised that the isothermal decay in photocurrent and the sharp rise in photocurrent with temperature appear to be two separate phenomena. No large change in the potential between electrodes 2 and 3 was detected during the T.S.C. run following low temperature irradiation of the sample. Figure 7.3.9 also shows the photocurrent versus temperature for three other relevant illumination treatments. It can be seen that illumination during cooling from 388°K (curve (b)) and illumination for 25 minutes at room temperature (curve (c)) both cause a decrease in the photocurrent level compared with the situation following illumination whilst cooling from room temperature (curve (d)). The structure of curve (a) is different from that of curves (b), (c) and (d), and it should be noted that the sharp rise in photocurrent with temperature is associated with the low

temperature illumination treatment.

The isothermal decay of photocurrent in the region of room temperature has been reported by a number of workers on CdS. Recently, Zomov and Serdyuk (1969) observed a variation of photocurrent similar to that reported here. They explained the effect in terms of a model with a single set of traps, of density N_t and capture cross-section S_t, and a single set of recombination centres. They assumed that the occupancy of the traps increased with time, and so decreased the density of recombination centres occupied by electrons. This leads to a reduction in the free electron lifetime with time, and hence an isothermal decay of photocurrent. (It will be shown later in this section that the present isothermal decay is commensurate with a photochemical increase in the density of traps, and is not due to a change in their occupancy. The arguments of Zomov and Serdyuk will however be followed, as the decay observed here may be expressed in a similar form to theirs.)

If it is assumed that the traps are initially empty and that the density of recombination centres occupied by holes is N_R, under illumination which creates F free electrons per second, then the free electron density is given by

$$n_c = F/N_R S_R v \qquad 7.3.1$$

where S_R is the capture cross-section for electrons by recombination centres containing holes, and v is the thermal velocity of the free electron. When n_t traps are filled with electrons, the free electron density becomes

$$n_c = F/(N_R + n_t)S_R v \qquad 7.3.2$$

For an order of magnitude change in the free electron

lifetime $N_R << n_t$, and the free electron density can be expressed as

$$n_c = F/n_t S_r v \qquad 7.3.3$$

The equation for the kinetics of trap occupancy, Equation 3.2.2, may be rewritten so that

$$dn_t/dt = S_t v n_c N_t - n_t S_t v N_{ct} \qquad 7.3.4$$

where the substitutions $\nu = N_c S_t v$ and $N_c \exp(-E_t/kT) = N_{ct}$ are made, and where it is assumed that $N_{ct} >> n_c$. Integration of Equation 7.3.4 yields the relationship

$$n_t = [n_c N_t / N_{ct}](1 - \exp(-S_t v N_{ct} t)) \qquad 7.3.5$$

and when this value of n_t is substituted in Equation 7.3.3 we obtain the following expression

$$1/n_\infty^2 - 1/n^2 = (1/n_\infty^2)\exp(-S_t v N_{ct} t) \qquad 7.3.6$$

where the value of n_c at $t \rightarrow \infty$ is given by

$$n_\infty = (N_{ct} F / S_t v N_t)^{1/2} \qquad 7.3.6$$

As the isothermal decay is attributed to a change in free electron lifetime and not to a change in mobility, a plot of $\log(1/I_\infty^2 - 1/I^2)$ versus time should yield a straight line. Here I is the photocurrent at time t. Figure 7.3.10 shows the isothermal decay of photocurrent for sample C, measured at 303°K, 308.5°K, 322°K and 334°K, plotted in the form of $\log(1/I_\infty^2 - 1/I^2)$ versus time. The initial part of each of these curves conforms to a straight line, although they deviate from the ideal relationship after some 10 to 20 minutes. This indicates that the

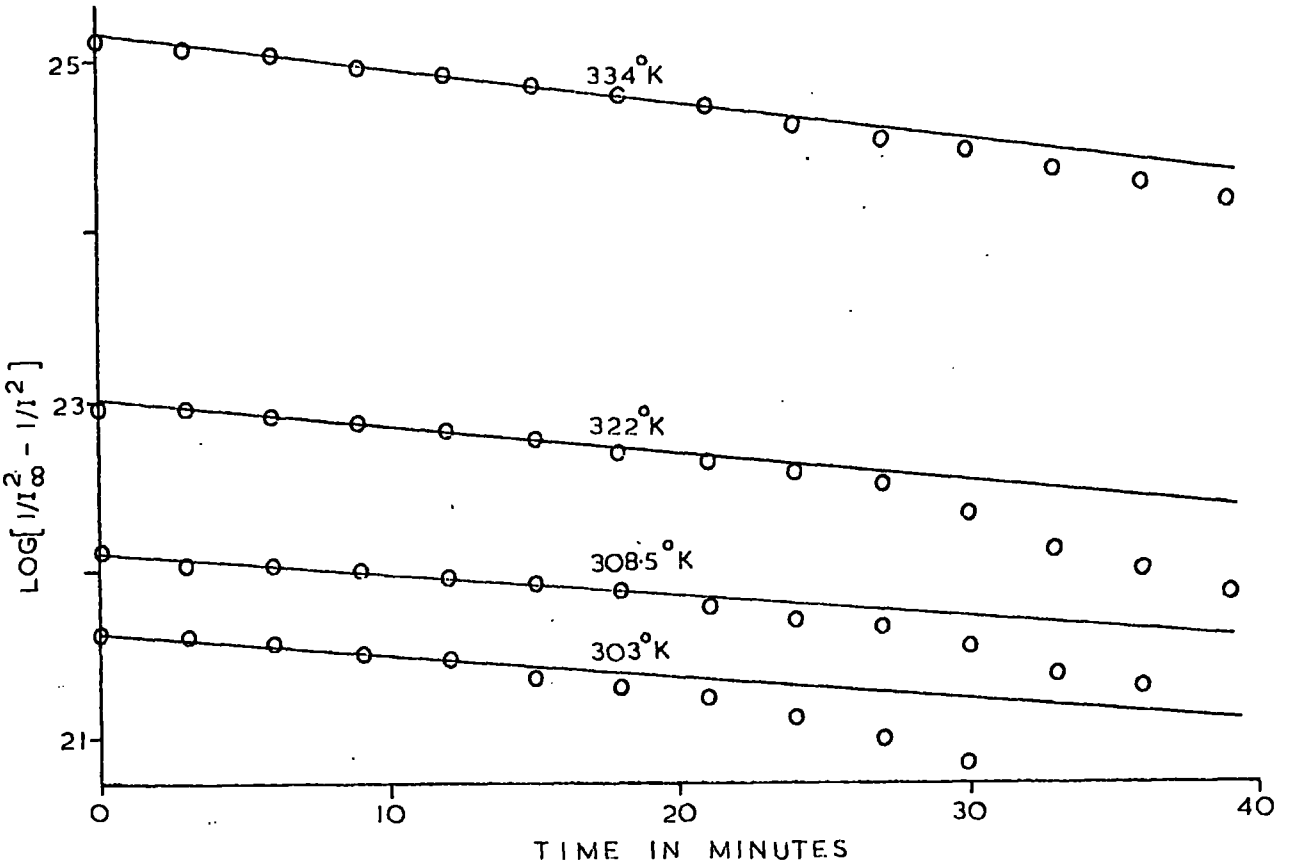

FIGURE 7.3.10 ISOTHERMAL DECAY OF PHOTOCURRENT FOR SAMPLE C, PLOTTED AS LOG$[1/I_{co}^2 - 1/I^2]$ VERSUS TIME

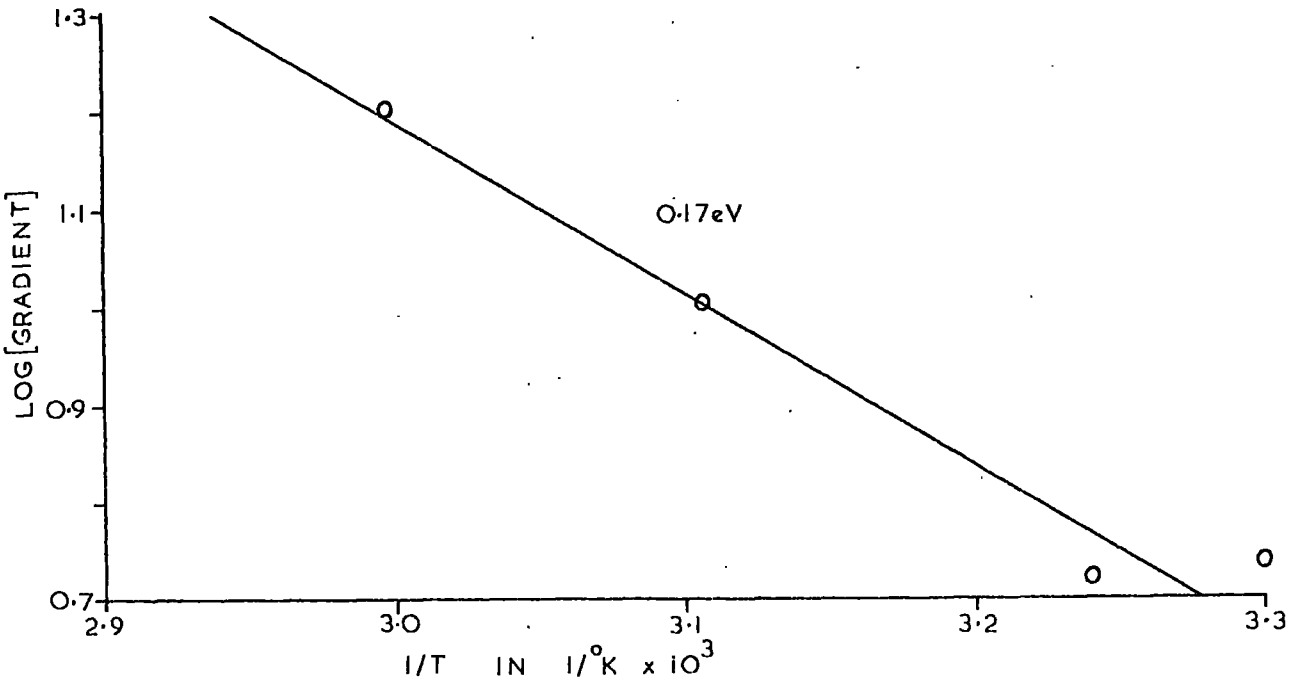

FIGURE 7.3.11 GRADIENTS OF THE CURVES SHOWN IN FIGURE 7.3.10, PLOTTED AS LOG[GRADIENT] VERSUS 1/T

photocurrent, and hence the free electron lifetime, is decreasing more rapidly with time than would be expected from the simple theory. The photocurrent versus temperature curves, illustrated in Figure 7.3.9, indicate that the onset of thermal quenching occurs at approximately 300°K. Under these conditions, the free electron lifetime is very sensitive to the position of the Fermi level for electrons. (In Chapter 2 it was demonstrated that thermal quenching occurs when the hole demarcation level for the sensitising Class 11 centres lies in the region of these centres. The electron Fermi level and hole demarcation level are intimately related, as may be seen by reference to Equation 8.3.1.) Thus the decay in photocurrent causes an additional decrease in the free electron lifetime due to the effect of thermal quenching. The dependence of the magnitude of thermal quenching on the free electron density can be clearly seen in Figure 5.9.4.

Following the argument of Zomov and Serdyuk, the temperature dependence of the decay can be found from the gradient, $S_t v N_{ct}$, of the curves shown in Figure 7.3.10 plotted in the form of log(gradient) as a function of 1/T. Here T is the temperature at which the decay was measured. Such a plot should yield the thermal activation energy of the traps which are filled during the decay, as $N_{ct} = N_c \exp(-E_t/kT)$.

Figure 7.3.11 shows log(gradient), from Figure 7.3.10 1/T yielding an activation energy of 0.17 eV. From earlier T.S.C. measurements, illustrated in Figure 7.3.6, it can be seen that the isothermal decay is associated with an increase in the density of the highest temperature trap (trap H), which has a thermal activation energy of 0.60 eV. There is a considerable difference between the value of E_t for trap H and the value of 0.17 eV, found from the temperature dependence of the decay. However, it has been shown in Chapter 6, that trap H is created

photochemically with an activation energy of between 0.20 eV and 0.27 eV. The similarity between the activation energy found here and the value found for trap H previously suggests that trap H is again produced photochemically, so that the density of traps, n_t, created under illumination at time t is given by

$$n_t = An_cN_t(1 - \exp(-B\exp(-E_a/kT)t)) \qquad 7.3.7$$

where A and B are constants, N_t is the maximum density of photochemically produced traps at temperature T, and E_a (=0.17 eV) is the activation energy for creation of the traps. (There is some error in the decay curves, and hence the value of E_a, due to the effect of thermal quenching described above. It is not possible to correct for the quenching of photocurrent, by recording the photocurrent as a function of light intensity at fixed temperature, because the decay itself would interfere with such measurements.)

7.3(d) Sample D

This sample was cut from a boule grown under sulphur rich conditions with T_S = 300°C. Figure 7.3.12 shows the variation of potential, measured between electrodes 2 and 3, during the course of a T.S.C. run, Figure 7.3.13, made after illuminating the sample during cooling from 388°K with an infrared filtered tungsten lamp. The potential can be seen to be essentially constant, although a minimum occurs at approximately 200°K corresponding to trap E (E_t = 0.44 eV) which is more prominent in sulphur rich samples. The potential between electrodes 2 and 3 decreases at high temperatures, where the dark current is relatively high. A thermally stimulated conductance curve is also presented in Figure 7.3.13, which corresponds to the T.S.C. spectra. The two curves can be seen to be similar.

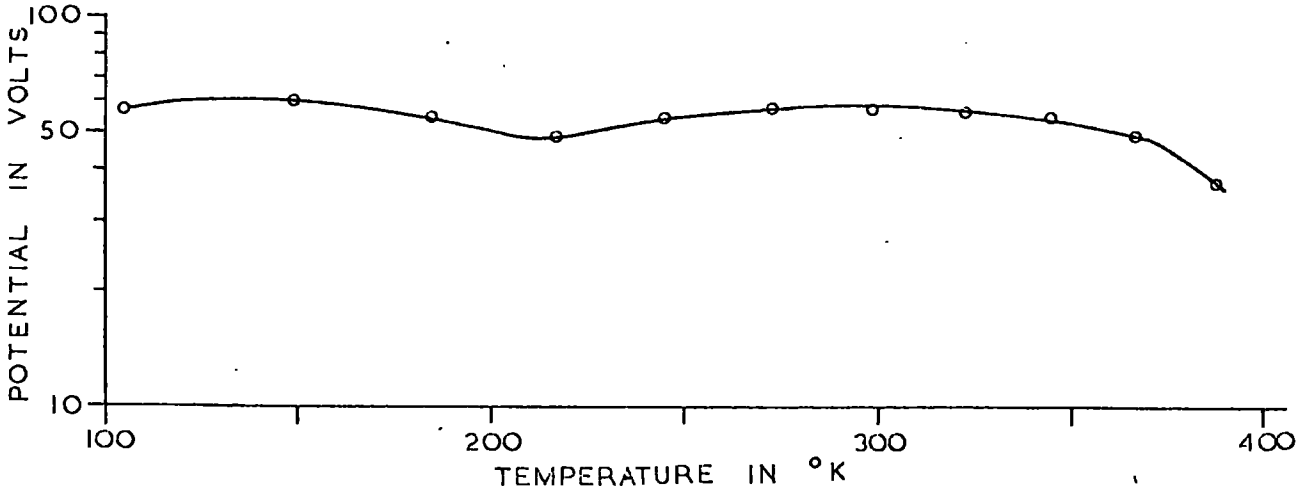

FIGURE 7.3.12 THE VARIATION IN THE POTENTIAL MEASURED BETWEEN ELECTRODES 2 AND 3 DURING THE T.S.C. MEASUREMENT SHOWN BELOW

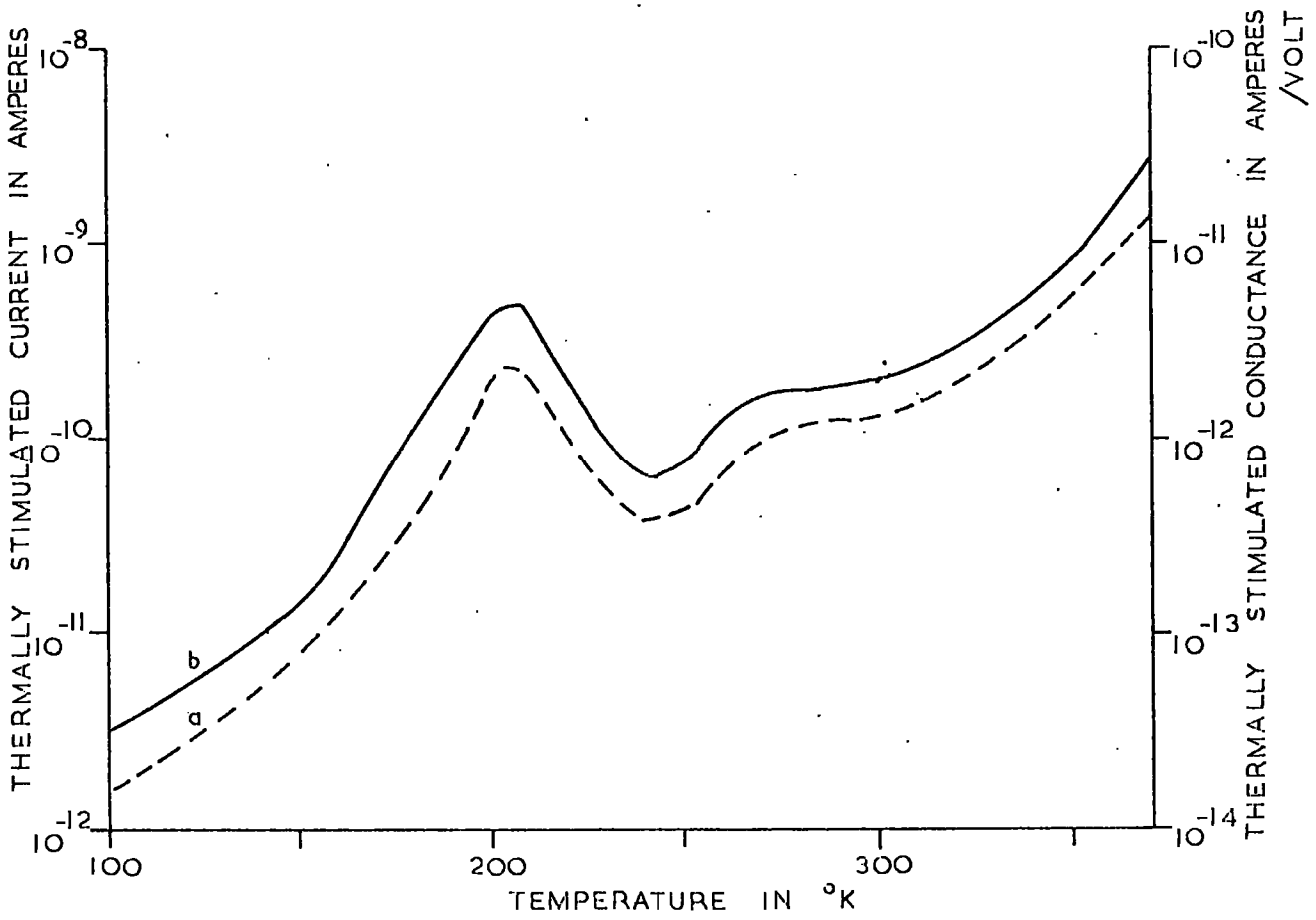

FIGURE 7.3.13 T.S.C. AND THERMALLY STIMULATED CONDUCTANCE CURVES FOR SAMPLE D FOLLOWING ILLUMINATION FROM 381°K

a T.S.C. CURVE

b CORRESPONDING CONDUCTANCE CURVE

7.4. Three Probe Measurements

Three probe measurements were made on samples which had already been used for the investigations described in Chapters 5 and 6. A guard ring arrangement of electrodes was used in an attempt to show whether surface trapping centres affect the T.S.C. The preparation of three probe specimens is presented in Chapter 4, where two types of electrode configuration are described.

Essentially, samples of the type shown in Figure 4.3.2 were platelets approximately 1 mm thick, with an irregular shaped cross-section, the area of which was of the order of 25 mm^2. On one side of the platelet an evaporated indium disc, 1.2 mm in diameter, was surrounded by an evaporated indium guard ring with an internal diameter of 2.3 mm and an outside diameter of 3.5 mm. A third indium contact, again disc shaped, was evaporated on to the side of the platelet opposite that of the guard ring. This contact was approximately 3.5 mm in diameter.

The second arrangement of three electrodes is shown in the insert in Figure 7.4.5. In this case the samples were bar-shaped some 6 mm long, with a rectangular cross-section of approximately 1 mm^2. Indium contacts were evaporated on to both ends, and a ring contact 1 mm in thickness was deposited some 1 mm distance from one of the end contacts.

Electrical measurements were carried out by holding the anode and guard ring at a similar potential with respect to the cathode. Because the d.c. amplifier had to be interposed in the required channel to make current measurements (either guard ring to cathode or anode to cathode), the potentials of the guard ring and anode were not exactly equal. The voltage drop across the d.c. amplifier was 1 volt for a maximum meter deflection. The influence of this disparity of potential between the guard ring and anode

was investigated in two ways.

(a) Three probe T.S.C. measurements were made using potentials of 10 volts, 50 volts and 100 volts across the sample for the same illumination schedule. Apart from the expected changes in the magnitude, the T.S.C. curves were essentially the same.

(b) A known voltage was applied to one of the channels, using a Tinsley Potentiometer, whilst the current was monitored through the other channel. In addition, during these measurements, made at room temperature under illumination, 100 volts was applied across the sample. For a variation in potential of $\pm$ 1 volt applied to the anode, the current in the guard ring to cathode circuit showed negligible variation, though the same change in potential applied to the guard ring caused a variation of approximately $\pm$ 20% in the current flowing between the anode and the cathode.

This last observation indicates that the three probe measurements, made for current flow through the anode, are in error by a maximum of 20% due to the disparity between the anode and guard ring potentials. A number of the experimental results presented in this section show that the current flowing through the anode circuit is at least a factor 2 larger when the guard ring is floating, than when the measurements are made using three electrodes. Such effects cannot, therefore, be attributed to the anode-guard ring potential difference. (The error in the anode current, under three probe conditions, is however a source of error in the analysis of a T.S.C. curve when trapping parameters are required. The samples used here had already been studied in depth as described in Chapters 5 and 6. The similarity of the T.S.C. spectra made using both two and three probe electrode

arrangements shows that the same trapping centres are present. Thus, detailed analysis of the T.S.C. curves is not required.) During the three probe measurements, described below, either 50 or 100 volts were applied to the sample.

To study surface traps, it would appear instructive to compare the current monitored through the guard ring circuit with that flowing through the anode, using three probe measurements made following the same illumination schedule. However, the differences in the electrode geometry for the two measurements makes analysis difficult. Figure 7.4.1 shows the T.S.C. spectra for a T_{Cd} = 350°C platelet sample, monitored after cooling under illumination from 388°K with an infrared filtered tungsten lamp. Curves (a) and (b) are the anode and guard ring curves respectively, using three probes and with 100 volts applied to the sample. Curve (c) shows the two probe measurement made between the anode and cathode, again with 100 volts applied to the sample. Curves (b) and (c) are essentially the same in basic structure, although their magnitudes are considerably different. This indicates that the T.S.C. monitored in the guard ring circuit is structurally similar to two probe measurements made between the anode and cathode. For this reason, and also because of the large difference in the magnitudes of the anode (curve (a)) and guard ring (curve (b)) T.S.C., due to electrode geometry, the results which follow will show comparison of the current flowing via the anode, with and without the guard ring held at a similar potential (e.g. curves (a) and (c) respectively).

Figure 7.4.2 shows the spectral response of photocurrent of a T_{Cd} = 350°C platelet sample. These measurements were made at 95°K, after cooling the sample in the dark from 388°K. Curve (a) shows the photocurrent measured between the cathode and anode with

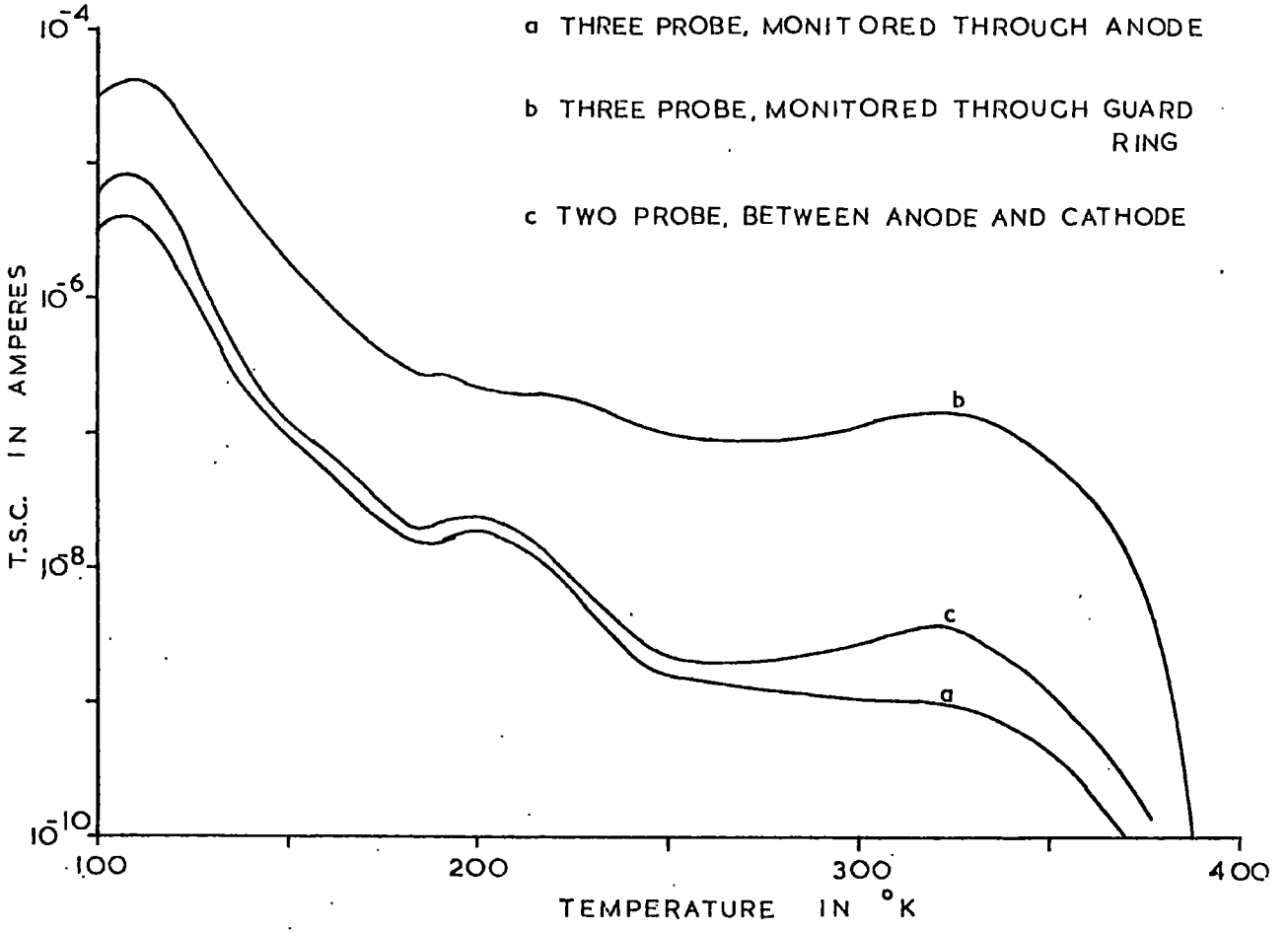

FIGURE 7.4.1 T.S.C. SPECTRA FOR A T_{Cd} = 350°C THREE PROBE PLATELET FOLLOWING ILLUMINATION FROM 388°K

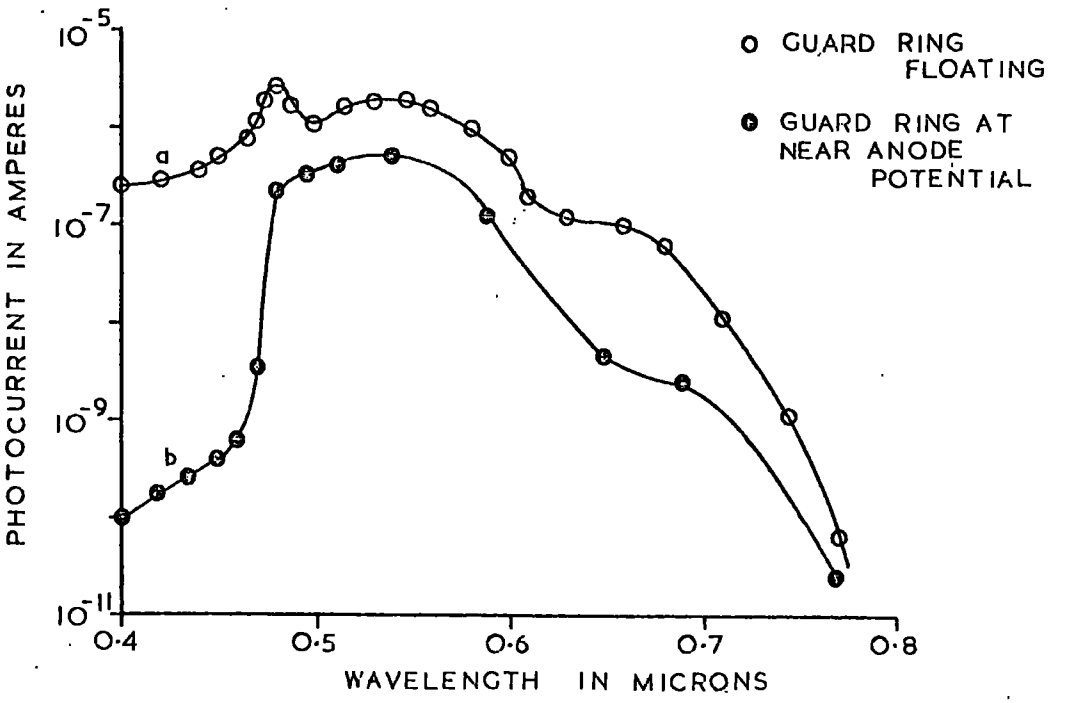

FIGURE 7.4.2 SPECTRAL RESPONSE OF PHOTOCURRENT FOR A T_{Cd} = 350°C THREE PROBE PLATELET

the guard ring floating, and curve (b) shows the response when the guard ring was held at 100 volts (i.e. approximately anode potential). The spectral response has not been corrected for the spectral distribution of the tungsten lamp, however the same slit settings and lamp intensity were used in both cases. A more detailed study of the spectral response of a variety of samples is reported in Chapter 8. In these experiments, the lamp current was adjusted for each monochromator setting to provide constant light energy incident upon the samples.

The most important conclusion to be drawn from the results shown in Figure 7.4.2 is that for wavelengths less than about 0.5 μm, the majority of the free carriers are generated close to the surface. The results indicate, therefore, that the effects of fluorescent-induced bulk photocurrent and exciton DIFFUSION from the surface are small in the present sample. The observation of the large decrease in the bulk photocurrent (Figure 7.4.2 curve (b)) for wavelengths shorter than 0.5 μm, also shows that the guard ring configuration conforms to its expected role, i.e. measurements made between the anode and cathode, with the guard ring held at near anode potential, are a measure of the bulk conduction.

The two T.S.C. curves obtained after illuminating the above $T_{Cd} = 350^{\circ}C$ sample during cooling, with a narrow band of light centred on 0.65 μm, are shown in Figure 7.4.3. Curve (a) was measured with the guard ring floating, and curve (b) with the guard ring held at 100 volts. The structure of the two curves can be seen to be essentially the same, though the magnitude of the T.S.C. is different.

The T.S.C. was also monitored following illumination with light centred on 0.48 μm during cooling from $388^{\circ}K$. Curve (a), Figure 7.4.4 shows the T.S.C. measured in the anode lead with the

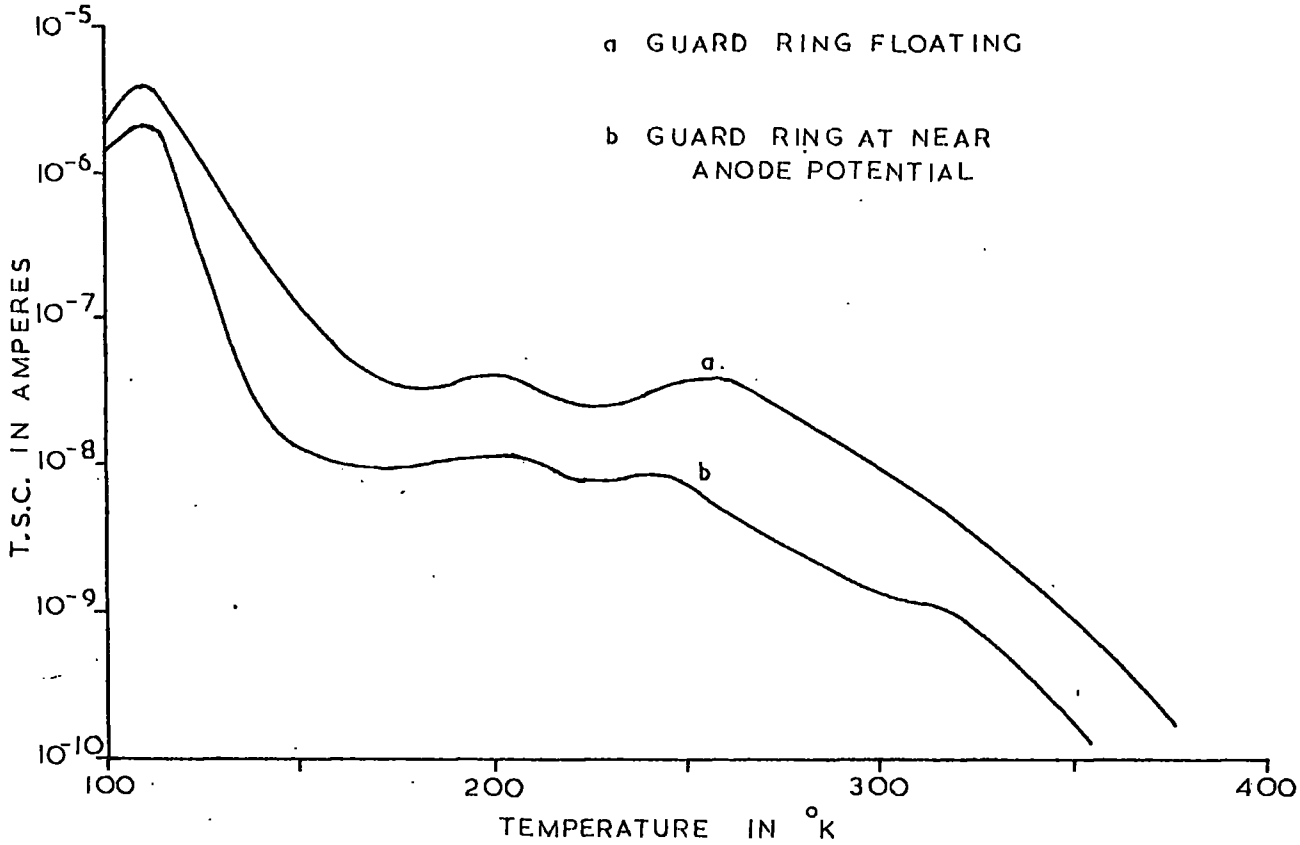

FIGURE 7.4.3 T.S.C. SPECTRUM FOR A T_{Cd} = 350°C THREE PROBE PLATELET ILLUMINATED WHILST COOLING FROM 388°K WITH λ = 0·65 μm

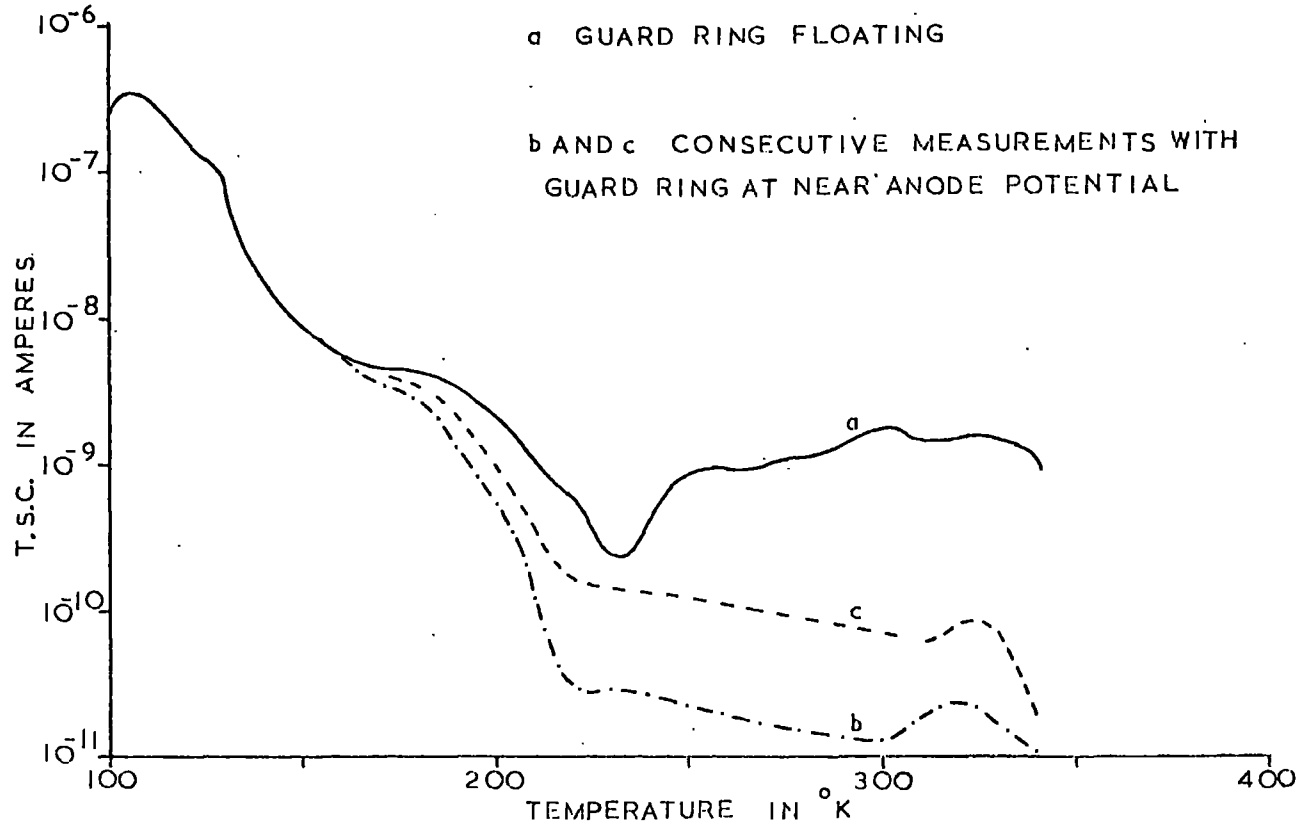

FIGURE 7.4.4 T.S.C. SPECTRUM FOR A T_{Cd} = 350°C THREE PROBE PLATELET ILLUMINATED WHILST COOLING FROM 388°K WITH λ = 0·48 μm

guard ring floating. Curves (b) and (c) are for consecutive runs with the guard ring held at 100 volts, and show that the T.S.C. level of the high temperature traps is less than that observed during two probe measurements. The significance of this observation will be discussed together with the following three probe measurements made on a bar-shaped sample.

The T.S.C. of a bar-shaped T_{Cd} = 350°C sample, with three electrodes, was also measured and is shown in Figure 7.4.5. Curves (a) and (b) were obtained when the guard ring was floating, and curves (c) and (d) when the guard ring was held at a similar potential to that of the anode. In all four sets of measurements the anode was held at a potential of 100 volts with respect to the cathode, and illumination was switched on at 388°K during cooling. Curves (a) and (c) were obtained following excitation with a 750 watt tungsten lamp filtered by two Chance HA 1 filters and a one centimetre path length of 10 % copper sulphate solution, together with a Barr and Stroud interference filter centred on 0.4358 μm. Curves (b) and (d) were measured using the same copper sulphate and Chance filters and a Barr and Stroud interference filter centred on 0.5460 μm. The T.S.C. monitored after irradiation with this latter 'green' light showed a much more pronounced structure of the three highest temperature traps. The T.S.C. level of the high temperature traps, during the three probe measurements shown in Figure 7.4.5, can be seen to be greater by two orders of magnitude when green light was used to fill the traps, than when blue light was used.

Some of the differences in the current level, and T.S.C. spectra, in Figures 7.4.4 and 7.4.5 are due to the differences in contact configurations. The essential similarity is that, following illumination with blue light, the T.S.C. level of the

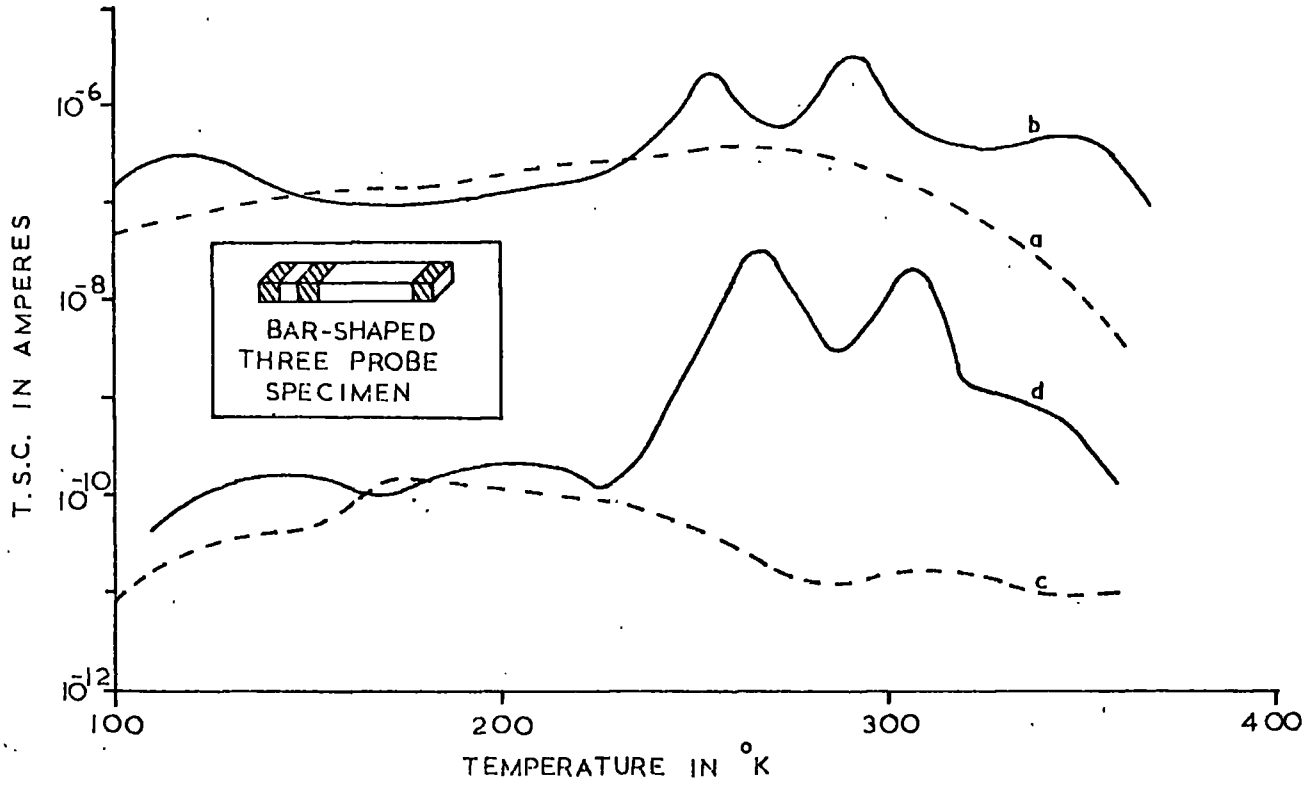

FIGURE 7.4.5 T.S.C. SPECTRA FOR A $T_{Cd} = 350°C$ BAR-SHAPED SAMPLE WITH THREE PROBES, FOLLOWING ILLUMINATION FROM 388°K

a λ=0·4358 μm GUARD RING
b λ=0·5460 μm FLOATING
c λ=0·4358 μm GUARD RING AT NEAR
d λ=0·5460 μm ANODE POTENTIAL

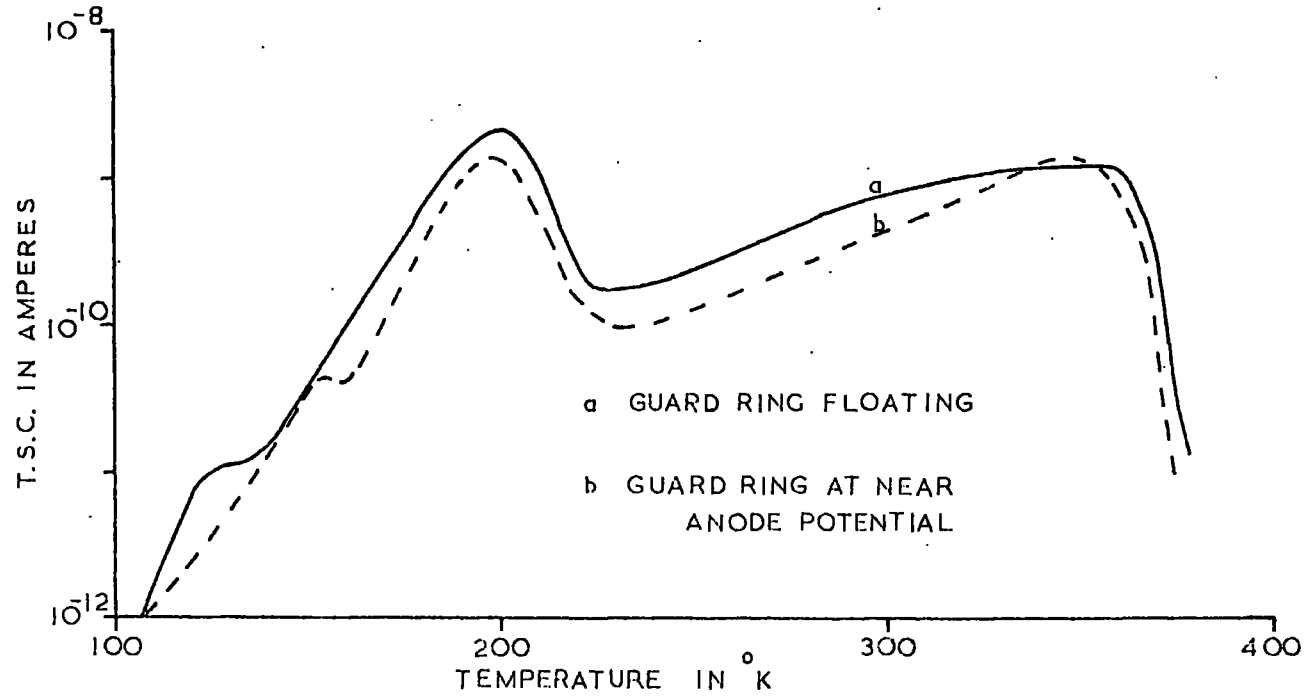

FIGURE 7.4.6 T.S.C. SPECTRA FOR A $T_S = 300°C$ THREE PROBE PLATELET, FOLLOWING ILLUMINATION FROM 388°K

high temperature traps is relatively low during bulk measurements. The results for the spectral response of photocurrent, Figure 7.4.2, show that blue light is strongly absorbed at the crystal surface. Hence one would expected that mainly surface traps would be filled under blue irradiation. This is substantiated by the three probe measurements in Figure 7.4.5, where green illumination causes a greater number of traps to be filled than blue irradiation. Comparison of the curves shown in Figure 7.4.5 indicates that the ratio of the high to low temperature traps, from curves (c) and (d), is greater for the bulk than for the two probe measurements. This implies that the shallow traps, which are observed at low temperature, are present at the surface in greater concentration than the deep, high temperature centres.

Illumination with broad band visible radiation from a 750 watt tungsten lamp, filtered with two Chance HA 1 filters and a one centimetre path length of 10% copper sulphate solution to remove infrared quenching radiation, yielded T.S.C. spectra very similar to those observed using narrow band green light.

Two sulphur rich platelets (T_S = 300°C) were investigated using the infrared filtered, wide band radiation as defined above. Figure 7.4.6 shows the T.S.C. obtained after cooling under illumination from 388°K. Curve (a) was monitored with the guard ring floating and curve (b) with the guard ring held at anode potential. Following these measurements, the sample was subjected to bombardment by 2 KV hydrogen ions for 165 minutes. From the area of the discharge glow and the ion current, an estimated ion flux density of $10^{16} cm^{-2} sec^{-1}$ was used. The T.S.C. measurements made after this treatment are shown in Figure 7.4.7, where curves (a) and (b) were measured under the same conditions as curves (a) and (b) in Figure 7.4.6.

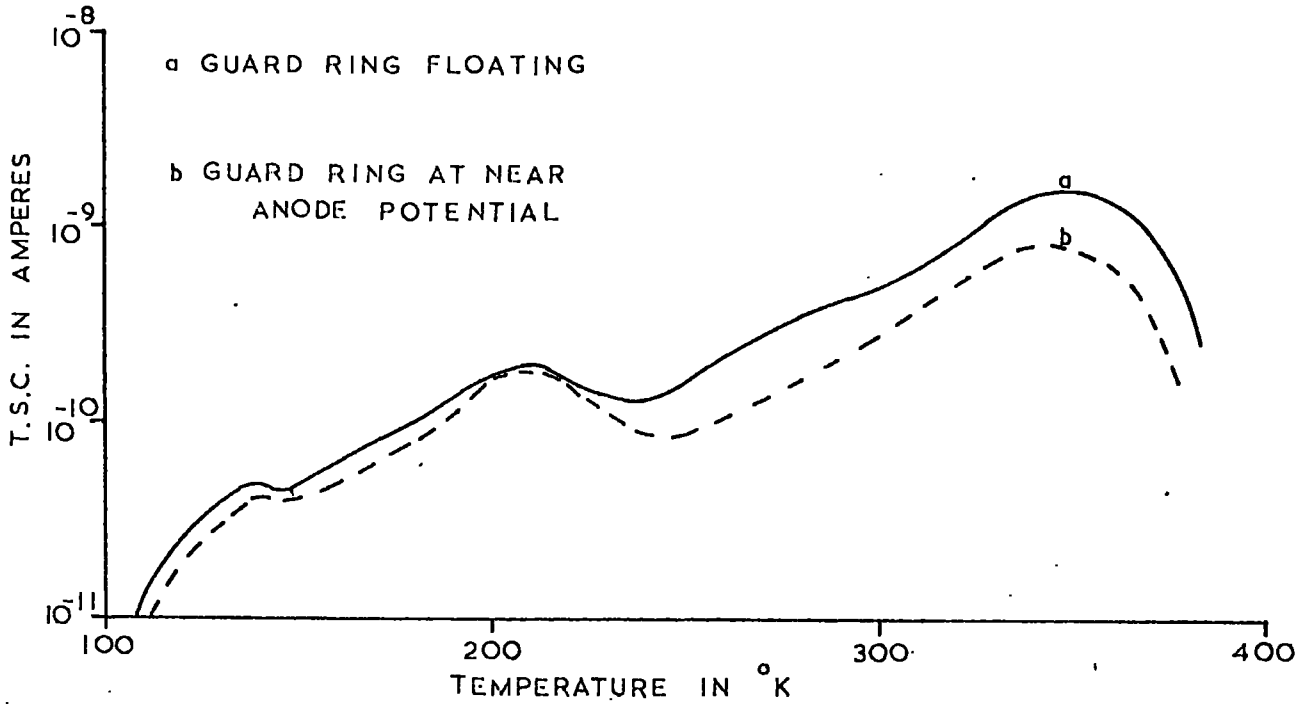

FIGURE 7.4.7 T.S.C. SPECTRA, AFTER HYDROGEN ION BOMBARDMENT, FOR A T_S= 300°C FOLLOWING ILLUMINATION FROM 388°K

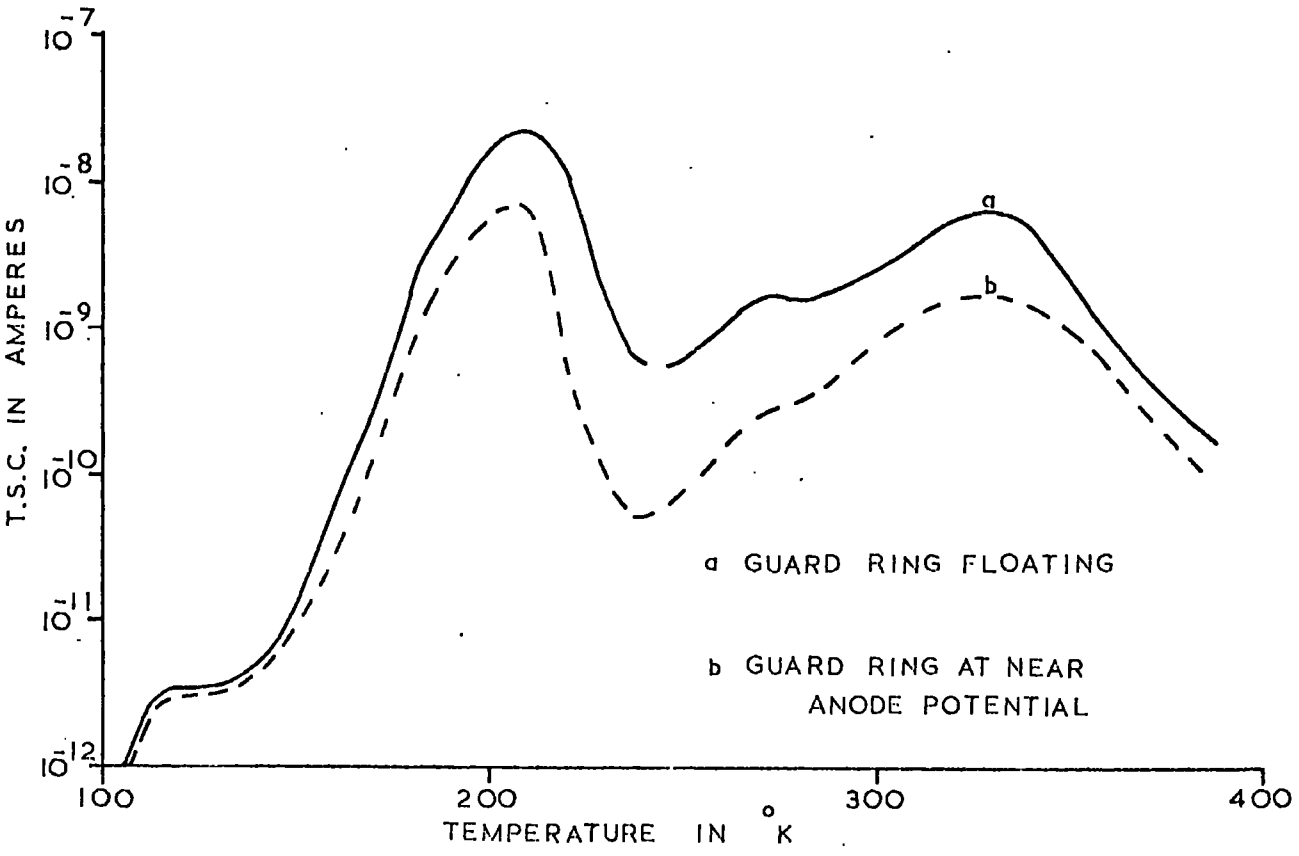

FIGURE 7.4.8 T.S.C. SPECTRA FOR A T_S= 300°C SAMPLE, FOLLOWING ILLUMINATION FROM 388°K. SAMPLE LAPPED BUT NOT ETCHED

In Figure 7.4.7 (as in Figure 7.4.6) the two and three probe measurements are similar and so demonstrate that the bombardment did not affect the conductivity of the surface. Comparison of Figures 7.4.6 and 7.4.7 shows, however that ion bombardment did decrease the T.S.C. in the region of the maximum at approximately 200°K. The two and three probe measurements in Figure 7.4.7 indicate that the trap associated with the 200°K maximum is a bulk entity. Hence the change in the apparent magnitude of this trap could be due to bombardment-induced surface states which affect the lifetime. (The hydrogen ion would be expected to affect the crystal only in the surface region.)

The second sulphur rich platelet was cut from the same (T_S = 300°C) boule as the sample discussed above. Both of the flat surfaces were ground using 600 L.C. carborundum powder in water. The sample was then washed in distilled water, but no attempt was made to etch the surfaces. The T.S.C. measured after irradiation while cooling from 388°K is shown in Figure 7.4.8. Curve (a) was obtained with the guard ring floating, and curve (b) with the guard ring held at 100 volts.

It was thought that the surface grinding might well create trapping centres which would show up under three probe T.S.C. measurement. This was clearly not the case as the curves in Figure 7.4.8 demonstrate. The structure of the T.S.C. spectra are similar for both two and three probe measurement, and are typical of other samples taken from this boule. However, the difference in the current level between the two and three probe curves suggests that the surface treatment created a more highly conducting surface.

7.5. Effect of Ambient Pressure on the T.S.C. Spectra

During the course of the present work a number of samples

were studied using the same irradiation conditions, in air pressures of approximately $5x10^{-5}$ torr and 10^{-2} torr. The effect on the T.S.C. was found to be negligible for all samples.

A number of workers have observed marked changes in the T.S.C. and spectral response of photocurrent associated with the sorption of oxygen and water vapour by CdS samples, using ambient pressures similar to those reported here. Bube (1953) has studied the effects of water vapour on the spectral response of CdS samples, and Reed and Scott (1964) and Mark (1965 (a) and (b)) considered the effects of oxygen absorption. In all cases, higher pressures of these ambients decreased the surface lifetime.

In the following chapter it will be demonstrated that the spectral response of photocurrent for a cadmium rich sample (T_{Cd} = 350°C) was slightly sensitive to ambient pressure, when a range of pressure was used which was larger than that for T.S.C. measurement. When the response measurements were made at 388°K, a change in air pressure from atmospheric pressure to $5x10^{-5}$ torr caused less than a factor 2 increase in the photocurrent level. Thus, an effect due to ambient may have been seen in the T.S.C. measurements had they been made on the present samples under ultra high vacuum conditions.

7.6. Discussion

Three main features of the work presented in this chapter are of direct relevance to the two probe T.S.C. measurements which were discussed in Chapters 5 and 6.

(a) The four probe measurements indicate that the use of the three criteria for ohmic contacts give adequate protection against the inadvertent use of non-ohmic contacts. However, in all the samples examined, some variation in the potential dropped

between the central electrodes (2 and 3) occurred during the four probe T.S.C. studies, so that measurement of thermally stimulated conductance should yield more accurate results.

The use of the four probe configuration of electrodes also demonstrated the existence of crystal inhomogeneity, which has also been observed by Islam and Woods (1970) in samples grown in a similar manner to those measured here. In only one case was an isothermal variation of photocurrent with time observed during the course of two probe measurements. Thus, it may be assumed that inhomogeneities, of the type found in sample C (Section 7.3(c)), did not play a significant detrimental role in the present two probe studies.

(b) With the CdS samples investigated here, excitation with broad band visible light, with the infrared quenching element removed, yields T.S.C. spectra which are not greatly influenced in structure by surface states, although the carrier lifetime is almost certainly governed in part by the crystal surface. Even when a deliberate attempt was made (by ion bombardment and by measuring a lapped and unetched sample) to induce surface states, the three probe technique revealed no significant change in the structure of the T.S.C. spectra.

(c) No large change in carrier lifetime was observed when the ambient pressure was changed by three orders of magnitude.

Thus the two probe T.S.C. measurements appear to be representative of the bulk material. However, the three probe measurements made using narrow band visible illumination seem to indicate that the shallow traps occur in greater density at the crystal surface.

Three probe measurements on cadmium and sulphur rich platelets show that the surface states have a significant effect on the

surface conduction for cadmium rich samples, where there is a large difference in the T.S.C. levels for two and three probe measurement. The sulphur rich samples, when etched, do not show such large changes. This supports the spectral response measurements to be reported in the following chapter, where a cadmium rich sample was found to be more sensitive to ambient pressure than a sulphur rich sample.

References to Chapter 7

Bube, R.H., 1953, J. Chem. Phys. 21, 1409.

Islam, M.N. and J. Woods, 1970, J. Phys. D. (Brit. J. Appl. Phys.) Series 2, 3, 1297.

Mark, P., 1965(a), J. Phys. Chem. Solids 26, 959.

Mark, P., 1965(b), J. Phys. Chem. Solids 26, 1767.

Reed, C.E. and C.G. Scott, 1964, Brit. J. Appl. Phys. 15, 1045.

Serdyuk, V. and R.H. Bube, 1967, J. Appl. Phys. 38, 2399.

Smith, R.W., 1955, Phys. Rev. 79, 1525.

Stewart, P.A.M. and R.B. Wilson, 1967, Brit. J. Appl. Phys. 18, 1657.

Zomov, V.V. and V.V. Serdyuk, 1969, Sov. Phys. Solid State 10, 2936.

CHAPTER 8

SPECTRAL RESPONSE AND INFRARED QUENCHING OF PHOTOCURRENT

8.1. Introduction

The spectral response and infrared quenching was measured for representative samples taken from among those on which T.S.C. measurements had been made (see Chapter 5). Significant differences were found between samples grown in a cadmium rich atmosphere and those grown under sulphur rich conditions. Where impure starting material was used to grow the boule crystals anomalous results were obtained.

The spectral response and infrared quenching measurements will be interpreted in terms of a model, shown in Figure 8.1.1, which contains two sets of Class 11 centres (11_a and 11_b) together with a set of Class 1 centres. Infrared quenching results from the optical excitation of electrons to the Class 11_a centres either from the valence band (Transition 1) or from the Class 11_b centres (Transition 2). Transition 2 also involves a thermal step so that holes are freed to the valence band. The photocurrent is quenched when the resulting freed holes are captured at the Class 1 centres.

8.2. Spectral Response Measurements

These measurements were made on bar-shaped samples having an indium contact at each end. The experimental arrangement has been described in Chapter 4.

It was found necessary to prolong the illumination at each wavelength for some time (about 15 minutes) to enable the photocurrent to reach equilibrium, so that continuous variation of the

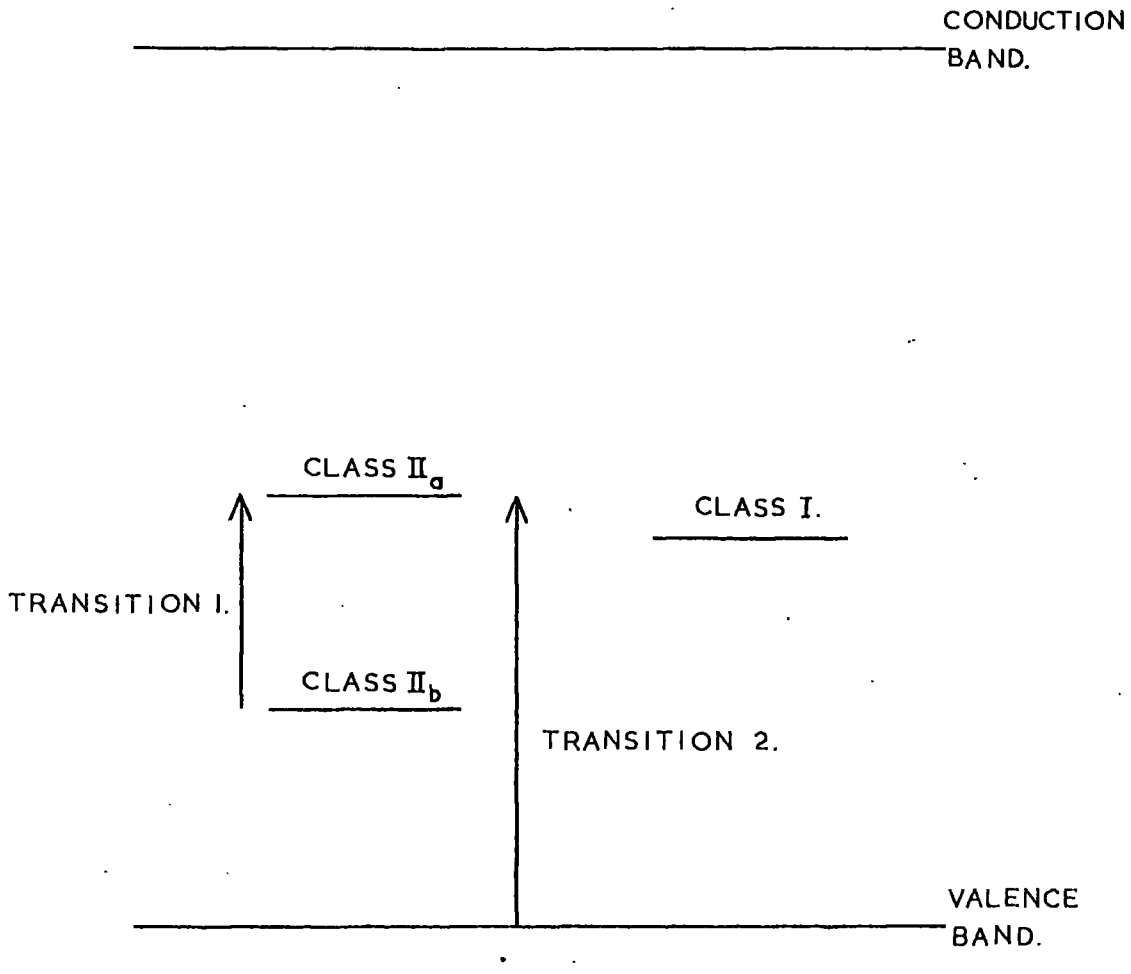

FIGURE 8.1.1. MODEL SHOWING ELECTRON TRANSITIONS TO EXPLAIN INFRARED QUENCHING DATA.

exciting wavelength was not used. Instead, the photocurrent was measured at a number of fixed wavelengths after equilibrium had been reached. By adjusting the tungsten lamp current, the exciting radiation from the monochromator was arranged to give the same response on a thermopile at each wavelength. From the sensitivity of the thermopile and the gain of the Barr and Stroud amplifier, the energy density of the exciting radiation in the region of the sample was calculated to be $5.10^{-9}\mu Wcm^{-2}$.

8.2.1. Dependence of the Spectral Response on the Conditions of Crystal Growth

Figure 8.2.1 shows the spectral response measured at $90^{o}K$, after cooling in the dark from $388^{o}K$, for five samples taken from different boule crystals grown from Optran starting material. Curves (a) and (b) were obtained from two samples grown with T_{Cd} = $350^{o}C$. Curves (c), (d) and (e) were monitored for samples grown with sulphur reservoirs held at 50, 300 and $450^{o}C$ respectively. All the samples were of approximately the same dimensions, i.e. with a 1 mm^2 cross-sectional area and with 2 mm to 3 mm between contacts.

Three significant observations can be made from these curves.

(a) The response at approximately 0.48 μm is two orders of magnitude greater with cadmium rich samples than with sulphur rich samples.

(b) The response for cadmium rich samples is markedly greater in the region 0.50 μm to 0.70 μm.

(c) The short wavelength response decreases rapidly with decreasing wavelengths for the more sensitive cadmium rich samples.

Bube (1956) reported a similar family of spectral response

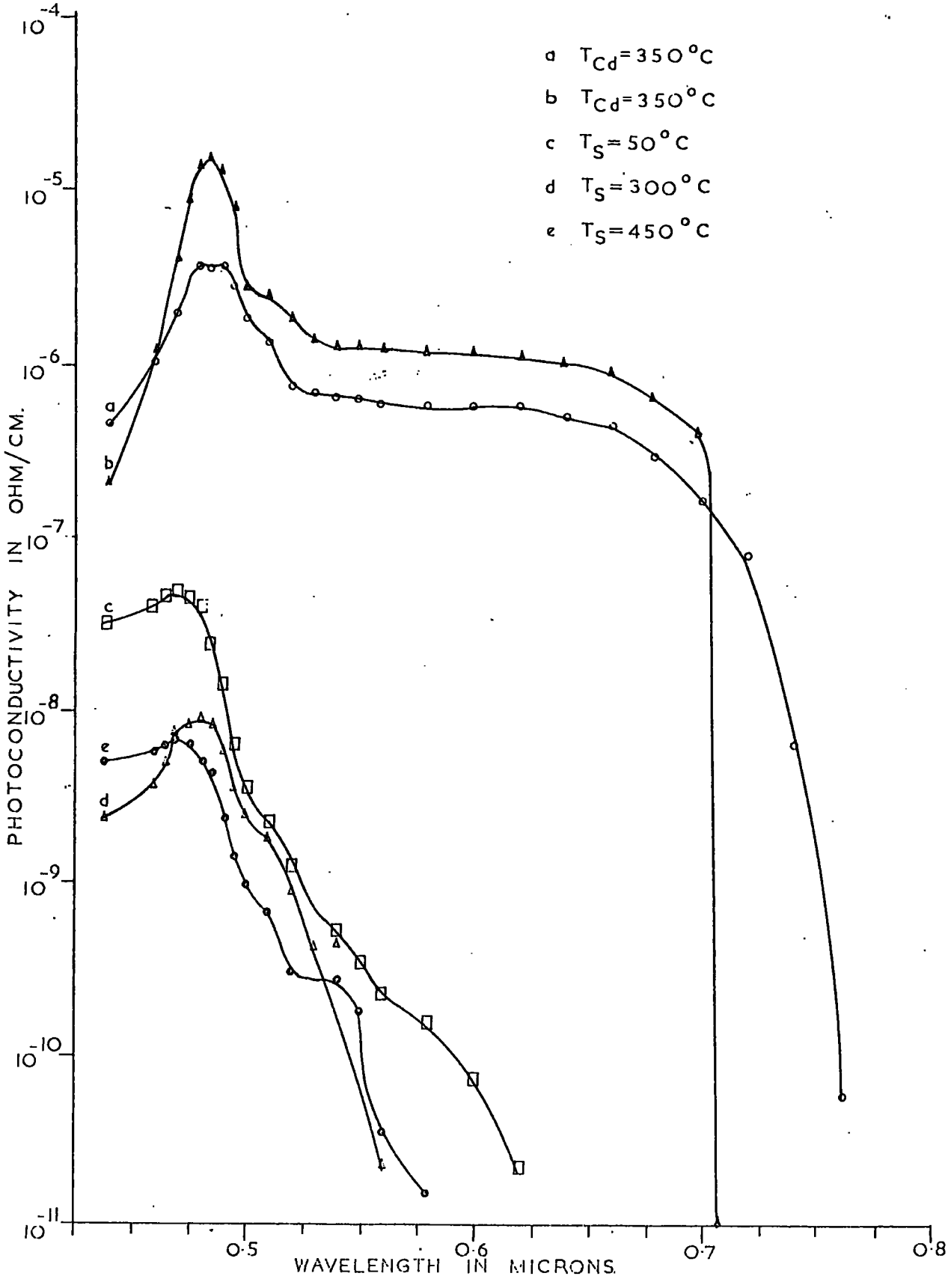

FIGURE 8.2.1. SPECTRAL RESPONSE OF PHOTOCONDUCTIVITY AT 90°K FOR FIVE SAMPLES GROWN IN DIFFERING SULPHUR AND CADMIUM AMBIENTS.

curves for CdS which showed these three features. He interpreted the variation in sensitivity in terms of changes in stoichiometry or impurity concentration during the growth of his crystals. The present observations indicate that the increase in sensitivity, with increasing cadmium content, is due to changes in stoichiometry though it is by no means certain that the process is governed by simple native defects.

The threshold of photoconductivity for the cadmium rich samples occurs at approximately 0.75 μm, whereas that for sulphur rich samples occurs at approximately 0.60 μm. Thus, in the dark at 90°K the cadmium rich samples contain centres filled with electrons up to approximately 0.85 eV from the valence band. In sulphur rich samples under the same conditions, centres are only filled up to an energetic separation of 0.43 eV from the valence band.

The response in the short wavelength region has been shown by Reed and Scott (1968) to vary considerably with electrode configuration. They found that the response was greatest where two contacts were made to their crystal platelets on the same side as the incident illumination. The present contact arrangement is very similar to this optimum condition. Reed and Scott also showed that their short wavelength response could be fitted to theoretical contributions from surface photocurrent and a bulk photocurrent excited by fluorescence from the surface region. The spectral response of a cadmium rich sample with three probes is shown in Figure 7.4.2. Although this sample had a somewhat different electrode configuration, the large ratio between the surface and bulk response for wavelengths shorter than the band gap suggests that fluorescence-induced bulk photocurrent, and also exciton diffusion from the surface, is comparatively small in the

present samples. The decrease in the spectral response is therefore indicative of the presence of surface states with a short free electron lifetime.

8.2.2. Effect of Illumination on the Low Temperature Spectral Response

The spectral response measurements described in Section 8.2.1 were obtained after each of the samples had been heated to 388°K and cooled in the dark to 90°K. Because changes in the T.S.C. and photocurrent with temperature were observed in some samples, following previous illumination at different temperatures, the effect of illuminating the sample with a 250 watt tungsten lamp (filtered to remove the infrared quenching radiation) prior to the response measurement was also studied.

The two sulphur rich samples, grown with $T_S = 300°C$ and $T_S = 450°C$, showed no significant variation in the spectral response after the illumination treatment. The two cadmium rich samples showed a marked increase in response after illumination. Figure 8.2.2 shows the spectral response of a cadmium rich sample monitored immediately after cooling in the dark to 90°K (curve (a)) and the response following five minutes illumination at 90°K (curve (b)). (After illuminating cadmium rich samples at 90°K, it was necessary to heat the samples to approximately 150°K and then cool in the dark to 90°K. Without this treatment, the isothermal emptying of the shallower traps yielded a background current of the order of 10^{-9} amperes which obscured the long wavelength threshold of photocurrent.)

In Section 6.2, it was shown that a few samples exhibited a large change in photocurrent with temperature at about 200°K (see

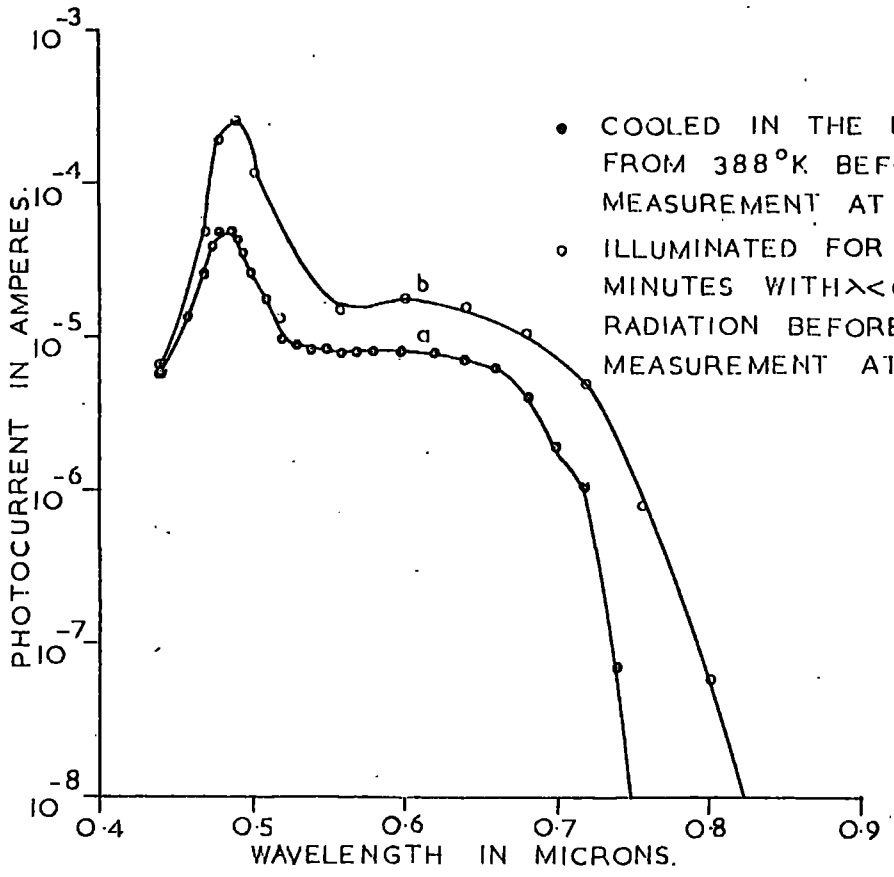

FIGURE 8.2.2. SPECTRAL RESPONSE FOR A SAMPLE GROWN WITH $T_{Cd} = 350\,^{\circ}C$.

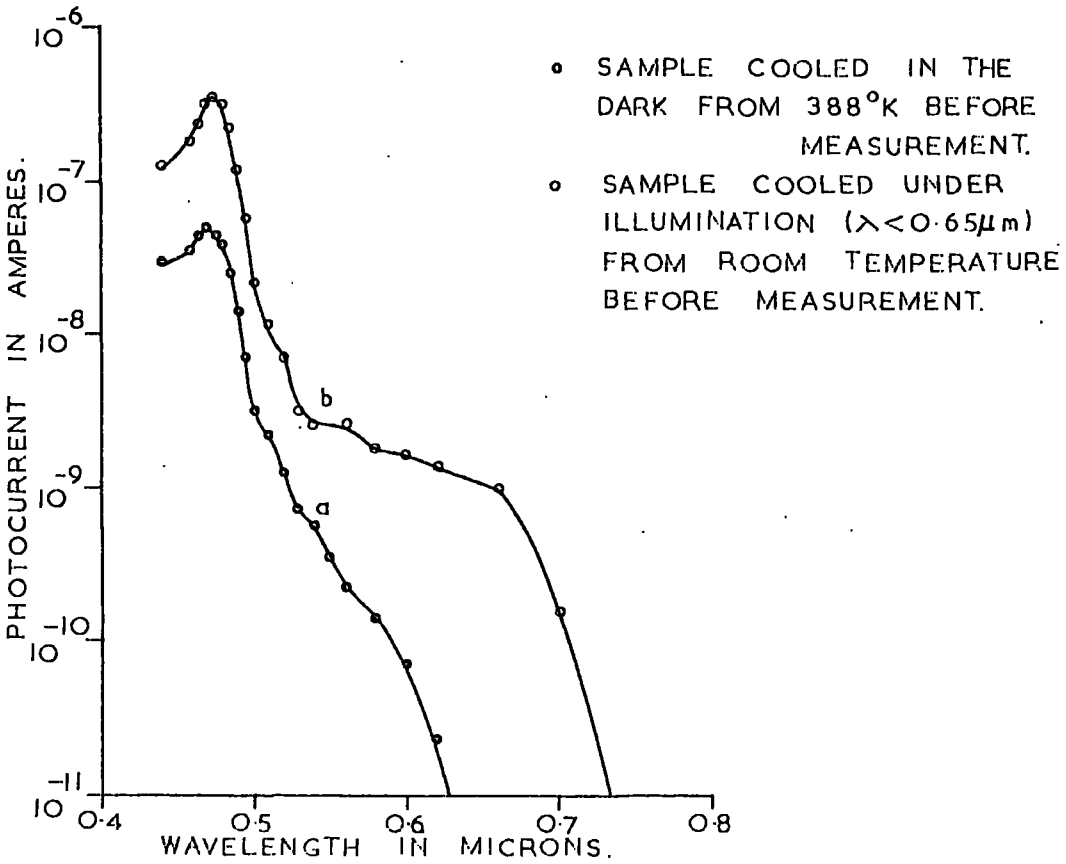

FIGURE 8.2.3. SPECTRAL RESPONSE AT 90°K FOR A SAMPLE GROWN WITH $T_S = 50\,^{\circ}C$.

Figure 6.2.2) when they had been cooled in the dark before excitation. Figure 8.2.3 shows the spectral response of such a sample (T_S = 50°C) at 90°K, where curve (a) was monitored after the sample had been cooled in the dark from 388°K, and curve (b) obtained after cooling from room temperature under illumination. Again, the increase in sensitivity was associated with an increase in the contribution to the photocurrent on the long wavelength side of the band edge, though for the sample to which Figure 8.2.3 refers, this has been achieved simply by illumination.

The infrared quenching of the sample grown with T_S = 50°C also showed considerable changes when it was monitored at 90°K (see Figure 8.3.3) following the two illumination treatments used in Figure 8.2.3. The spectral response and infrared quenching measurements will be discussed in Section 8.5.

8.2.3. The Effect of the Ambient Pressure on the Spectral Response

Attempts to measure the effect of air pressures of 10^{-5} torr and one atmosphere, on the spectral response of one of the sulphur rich samples and one of the cadmium rich samples, were made at room temperature and 388°K. Previous measurements of the T.S.C. in air pressures of 10^{-2} and 10^{-5} torr showed negligible differences with all the samples investigated. Spectral response measurements at 90°K and room temperature, for the five samples discussed in Section 8.2.1, were also unaffected by changes in ambient pressure between 10^{-2} and 10^{-5} torr.

With the sulphur rich sample, no difference was observed between the photocurrents measured at pressures of 10^{-5} torr and one atmosphere either at room temperature or 388°K. Although the cadmium rich sample was unaffected by changes in ambient pressure

at room temperature, there was an increased response at 388°K for a pressure of 10^{-5} torr compared with atmospheric pressure. The increase in sensitivity at the lower pressure was by less than a factor two. Figure 8.2.4 curves (a) and (b) are the spectral response curves for the cadmium rich sample measured at pressures of 10^{-5} torr and one atmosphere respectively. The current at long wavelengths is associated with the dark current, which becomes significant at 388°K.

It has been shown in Section 8.2.1 that cadmium rich samples are more sensitive than sulphur rich samples, and in Chapter 7 it was also demonstrated that the surface of a cadmium rich crystal carried a significant proportion of the free electrons. In addition, samples grown in cadmium rich conditions should have a greater density of sulphur vacancies than sulphur rich ones. The sulphur vacancy would be an ideal site for substitution of an iso-electronic oxygen ion, or other negative ions (e.g. OH^-). The effect of surface adsorption would therefore be expected to be greater in cadmium rich samples.

For completeness, it should be noted that a greater effect, due to ambient pressure, may have been recorded had the present measurements been extended to ultra high vacuum conditions.

8.2.4. Anomalous Spectral Response

In Section 5.11, the T.S.C. spectra of two samples grown from Derby Luminescent grade material were shown to be significantly different from those recorded with Optran material. Figure 8.2.5 shows the photocurrent as a function of wavelength for the two Derby samples. The measurements were made at 90°K after cooling in the dark from 388°K. Curve (a) was obtained from a boule crystal, which was grown with T_{Cd} = 300°C. Curve (b) is for a

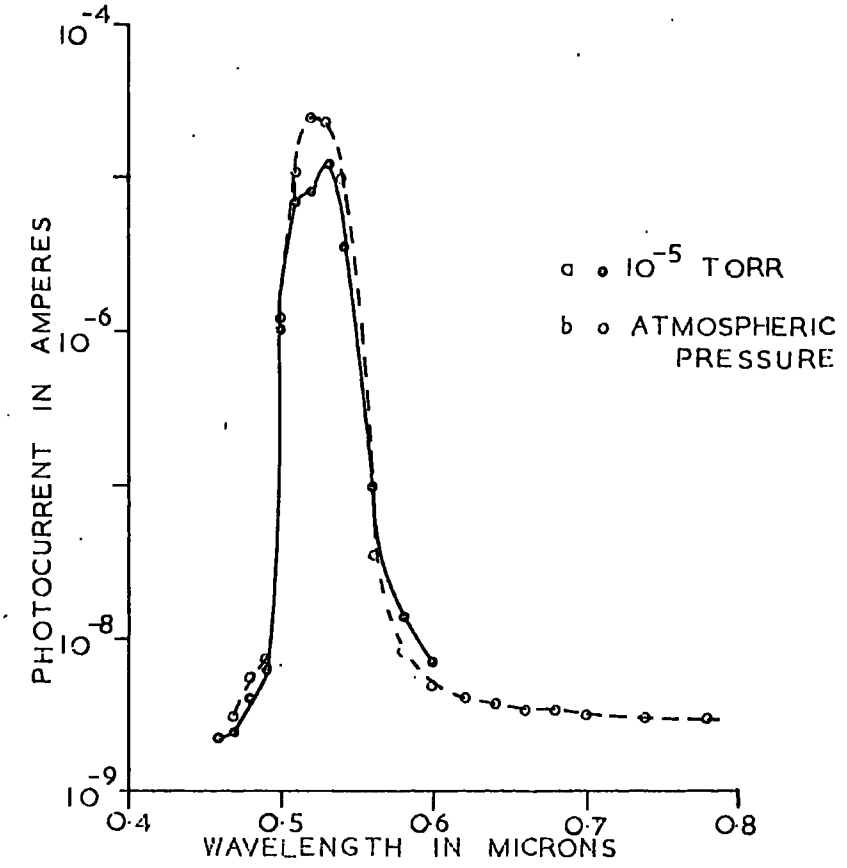

FIGURE 8.2.4. EFFECT OF AMBIENT PRESSURE ON THE SPECTRAL RESPONSE AT 388°K FOR A SAMPLE GROWN WITH T_{Cd}=350°C

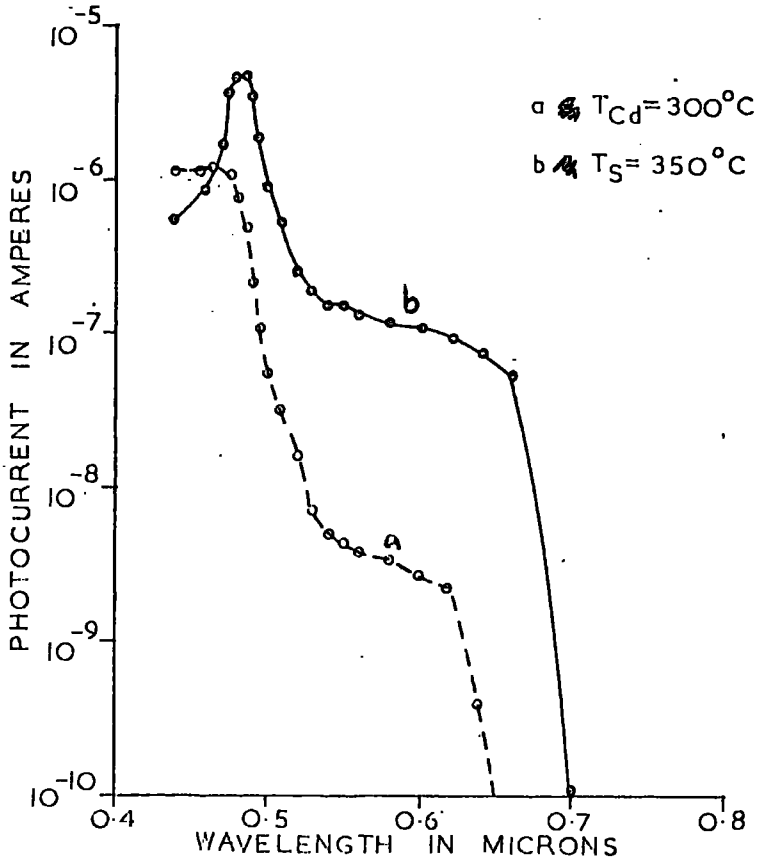

FIGURE 8.2.5. SPECTRAL RESPONSE OF TWO DERBY LUMINESCENT SAMPLES AT 90 °K

crystal grown with T_S = 350°C. The large difference in sensitivity, which was observed between Optran samples grown in cadmium and sulphur ambients, was not evident in the Derby crystals. The spectral responses of the Derby samples are anomalous because the sulphur rich Derby sample, which was more sensitive than the cadmium rich sample, also showed a greater response at long wavelength. With Optran grown boules, cadmium rich samples were more sensitive and their response was greater at long wavelength. The effects of stoichiometry were presumably swamped by impurities introduced with the starting material.

8.3. Infrared Quenching

The infrared quenching of the photocurrent was measured with the samples illuminated with primary excitation supplied by a tungsten lamp, filtered by two Chance HA 1 infrared absorbing filters and a one centimetre path length of 10% copper sulphate solution. The quenching radiation was derived from the output slits of a Barr and Stroud double prism monochromator. The quenching radiation was such that its energy density was held constant at $4.10^{-7}\mu Wcm^{-2}$ at each wavelength.

For all the samples investigated it was necessary to reduce the primary light intensity, using a 1% Barr and Stroud neutral density filter, so that appreciable quenching could be observed. This represented a flux of approximately 10^2 lumens/(metre)^2 incident on the sample from the primary excitation.

Quenching measurements were made at 90°K and at room temperature on the samples discussed in Sections 8.2.2 and 8.2.4. The measure of quenching used is the percentage decrease in the primary excited photocurrent.

8.3.1. Crystals Grown from Optran Material

The infrared quenching data for the two samples grown with T_{Cd} = 350°C were similar. Figure 8.3.1. curve (a) shows the quenching spectrum obtained at 90°K, and curve (b) that at room temperature for one of these samples.

The curves in Figure 8.3.2 illustrate the infrared quenching at liquid nitrogen and room temperatures for the sample grown with T_S = 450°C. The sample grown with T_S = 300°C showed a similar basic structure to that depicted in Figure 8.3.2, though the two room temperature bands were not so well defined.

By comparison of Figures 8.3.1 and 8.3.2, it may be seen that the long wavelength band, which was only observed at room temperature in cadmium rich samples, also occurred at low temperature in sulphur rich samples.

In Section 8.2.2 it was demonstrated that the sensitivity and long wavelength spectral response at 90°K for the sample grown with T_S = 50°C could be increased by illumination from room temperature prior to the response measurement (see Figure 8.2.3). Figure 8.3.3 curve (a) shows the quenching spectrum, measured at 90°K, after cooling the sample in the dark from 388°K. Curve (b) shows the low temperature quenching after excitation of the sample with primary irradiation during cooling from 388°K. Curve (c) is the room temperature spectrum.

Thus, in the less sensitive state, curve (a), the low temperature quenching is similar to that obtained from the less sensitive sulphur rich samples, and in the more sensitive state, curve (b), the low temperature quenching resembles that observed in cadmium rich samples.

The experimental results presented in this section are

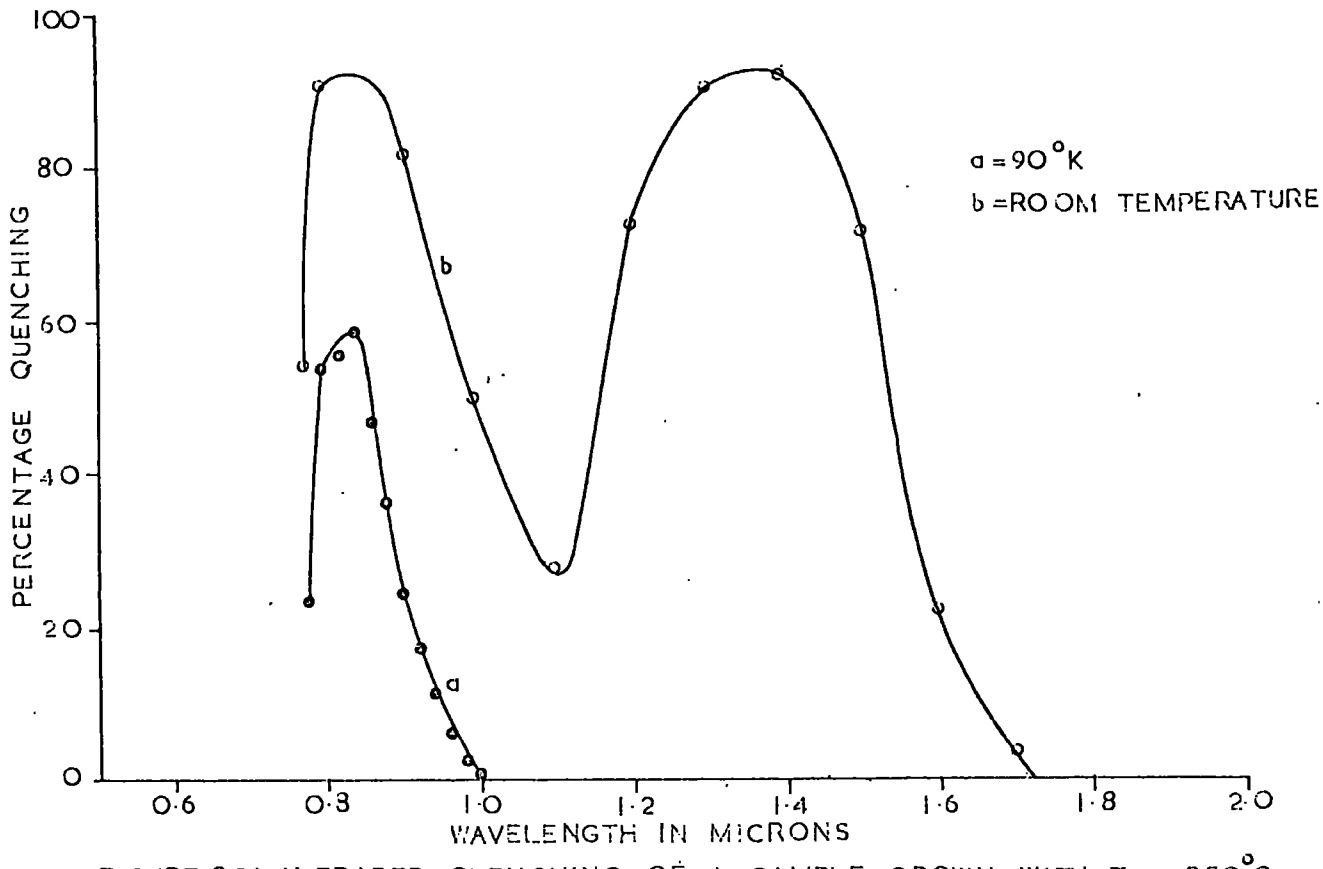

FIGURE 8.3.1 INFRARED QUENCHING OF A SAMPLE GROWN WITH T_{Cd}=350°C

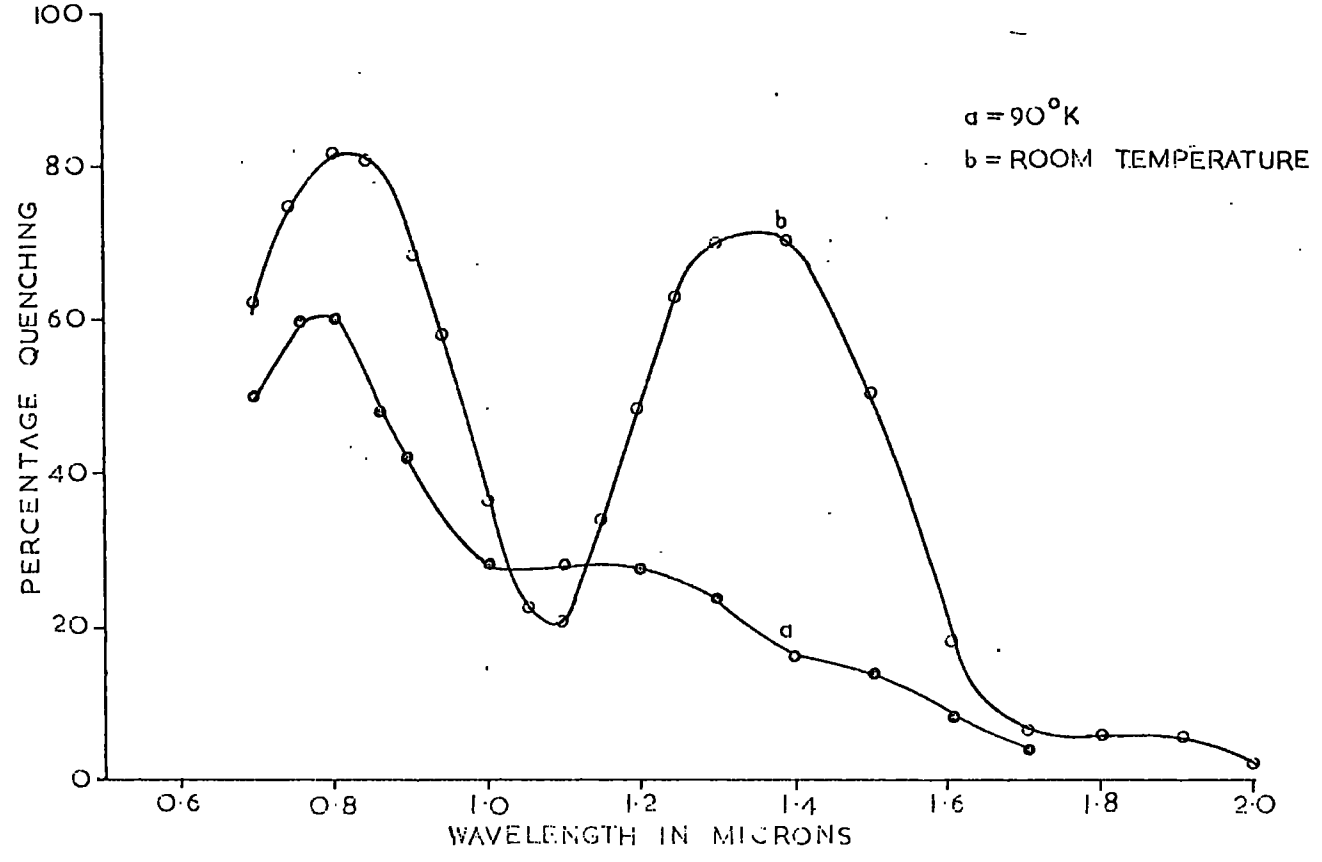

FIGURE 8.3.2 INFRARED QUENCHING OF A SAMPLE GROWN WITH T_S=450°C

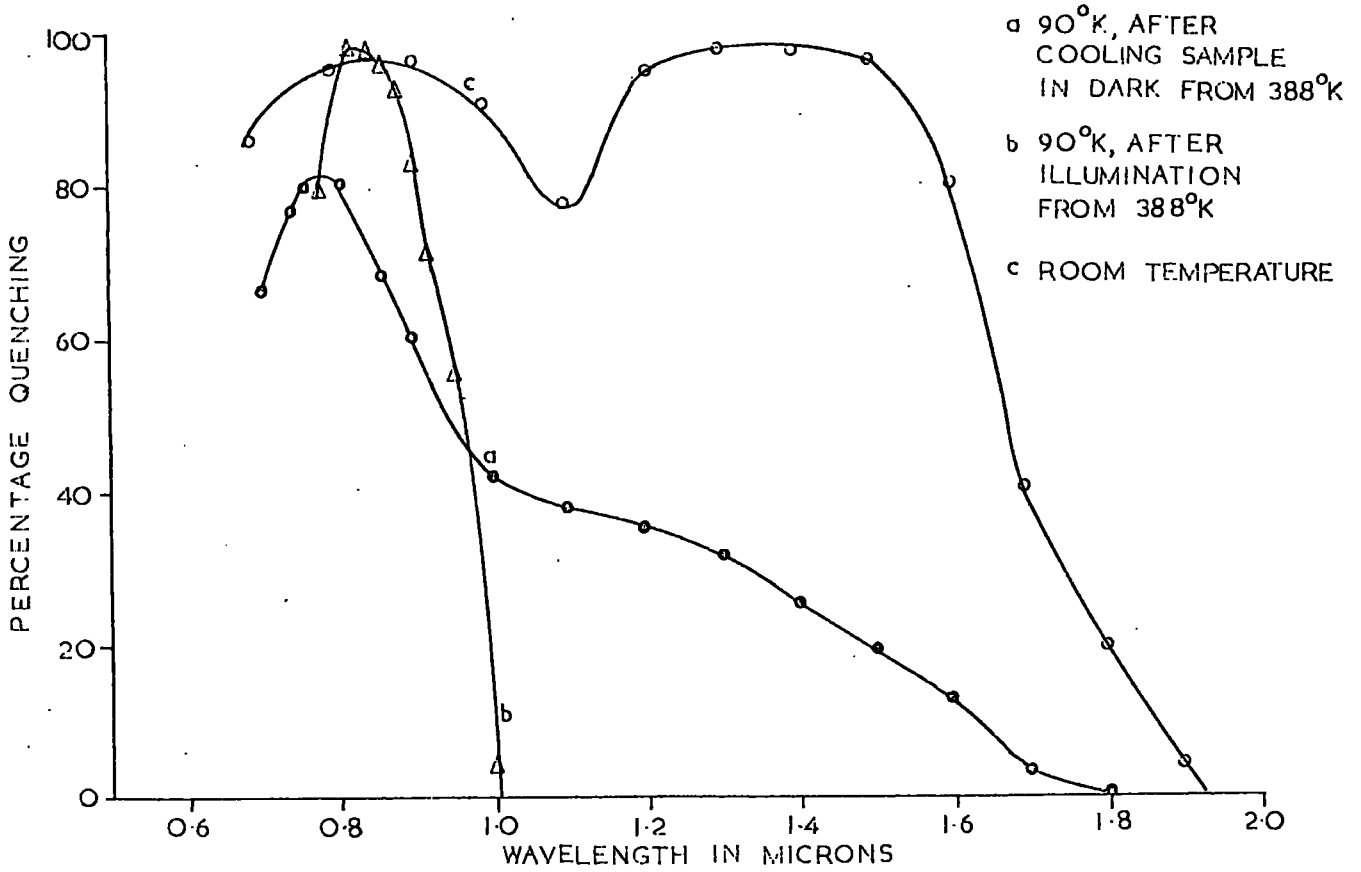

FIGURE 8.3.3 INFRARED QUENCHING FOR A SAMPLE GROWN WITH T_S=50°C

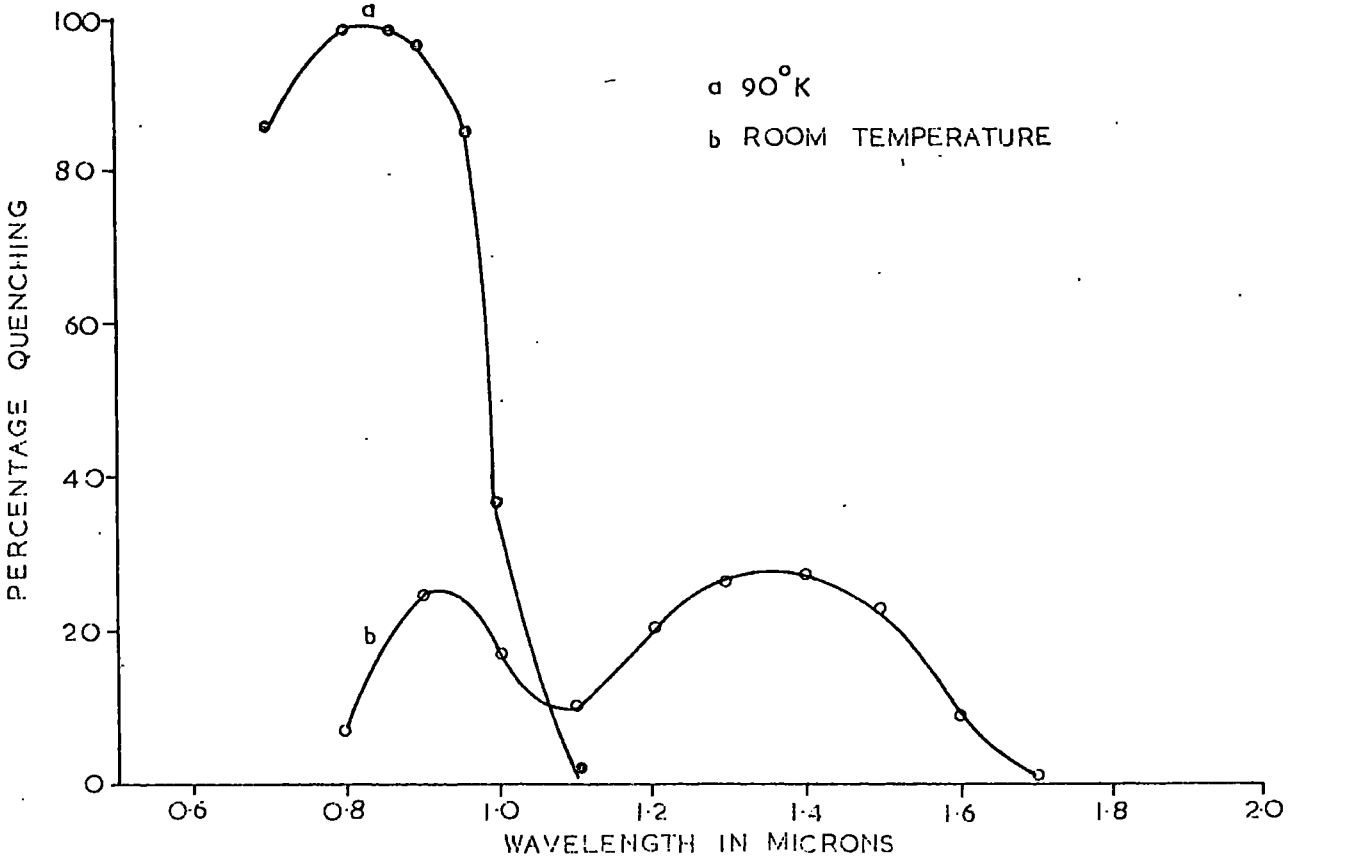

FIGURE 8.3.4 INFRARED QUENCHING FOR A DERBY LUMINESCENT SAMPLE GROWN WITH T_S=350°C

indicative of two main quenching bands, which is in agreement with other workers. The similarity of the room temperature bands suggests that the same quenching mechanism occurs in both cadmium and sulphur rich samples. The model which accounts for these two bands has been shown in Figure 8.1.1, where the long wavelength band is caused by Transition 1 and the short wavelength band by Transition 2. From the quenching data in this section the optical Transition 1 is approximately 0.92 eV using the maximum of the long wavelength band (1.35 μm). The threshold of the short wavelength band (1.05 μm) yields a value of 1.2 eV for Transition 2. These are substantially the same values (0.89 eV and 1.1 eV) as given by Bube (1960), who discussed this model in detail. Bube is of the opinion that the long wavelength band is not seen at low temperatures, though both bands are seen at room temperature (as in Figure 8.3.1). He assumed that the thermal ionisation of holes from the Class 11_b centres (Figure 8.1.1) only becomes significant at elevated temperatures.

The hole demarcation level (H.D.L.) for centres 11_b is the key parameter which determines whether or not there is a significant thermal ionisation of holes to the valence band. When the H.D.L. lies below the centres, electron recombination is more probable (see Section 2.5). The present results suggest that, during infrared quenching at $90^{\circ}K$, the H.D.L. for centres 11_b lies above these centres in sulphur rich samples and below them in cadmium rich samples.

A value of the H.D.L., D_p, (for a centre with a capture cross-section S_p for holes when filled with electrons, and a capture cross-section S_n for electrons when filled with holes) has been given in Section 2.5. The H.D.L. may also be expressed in the form

$$D_p = E_{fn} + kT\log(S_p/S_n)$$

$$+ (3/2)kT\log(m_h/m_e') \qquad 8.3.1$$

To a first approximation $m_h/m_e' = 1$, so that D_p depends on the electron Fermi level and the ratio S_p/S_n.

Values of E_{fn} were calculated for the samples discussed in this section from their photoconductivity at 90°K, when they were illuminated with the primary excitation used for the infrared quenching measurements. E_{fn} was 0.14 eV for both of the more sensitive cadmium rich samples. The less sensitive sulphur rich samples yielded values of E_{fn} of 0.17 eV and 0.19 eV. The sample grown with T_S = 50°C gave values of E_{fn} equal to 0.16 eV and 0.2 0.2 eV when in its more and less sensitive states respectively.

According to the argument advanced above, the H.D.L. for centres 11_b lies in the region of these centres for values of E_{fn} between 0.16 eV and 0.18 eV, under the above conditions of measurement. Assuming that S_p/S_n for centres 11_b is between 1 and 10^5, then centres 11_b are separated from the valence band by 0.16 eV to 0.27 eV. From the optical energies of Transitions 1 and 2, the centres 11_b lie 0.28 eV above the valence band. Thus there is qualitative agreement between the thermal and optical separations of the centres 11_b from the valence band. (The thermal and optical positions of a centre are not necessarily equal, as will be demonstrated in Section 8.4.)

8.3.2. Derby Luminescent Material

The infrared quenching of samples grown from Derby powder also gave anomalous results when compared with the data recorded for Optran material. As stated earlier (Section 8.2.4), the

spectral response at 90°K for these two samples was anomalous, in that the cadmium (sulphur) rich Derby sample resembled Optran sulphur (cadmium) rich samples. The low energy quenching band, a at low temperatures, again follows this pattern.

Figures 8.3.4 and 8.3.5 show the low temperature and room temperature quenching for the samples grown with T_S = 350°C and T_{Cd} = 300°C respectively. The low temperature quenching of the sulphur (cadmium) rich Derby sample is similar to that shown for cadmium (sulphur) rich Optran samples.

Values of E_{fn} were again calculated for the Derby samples at 90°K under irradiation from the infrared quenching primary source. The sulphur rich sample yielded a value of 0.16 eV, and the cadmium rich sample an energy of 0.19 eV. These energies are similar to those found for Optran samples when they showed the same low temperature quenching behaviour.

8.4. Optical Trap Emptying

Optical trap emptying was studied at 90°K using the same experimental arrangement as that employed to determine the spectral response. The illumination to fill the traps was supplied by a tungsten lamp, filtered to remove infrared quenching radiation.

A cadmium rich sample, grown with T_{Cd} = 350°C, was chosen for measurements of the optical trap emptying of the three highest temperature traps, as this sample showed most of the trapping centres during the measurement of T.S.C. First it was necessary to empty the shallow traps, as their thermal emptying contributed considerably to the measured current.

A sample grown with T_S = 450°C was also investigated. The

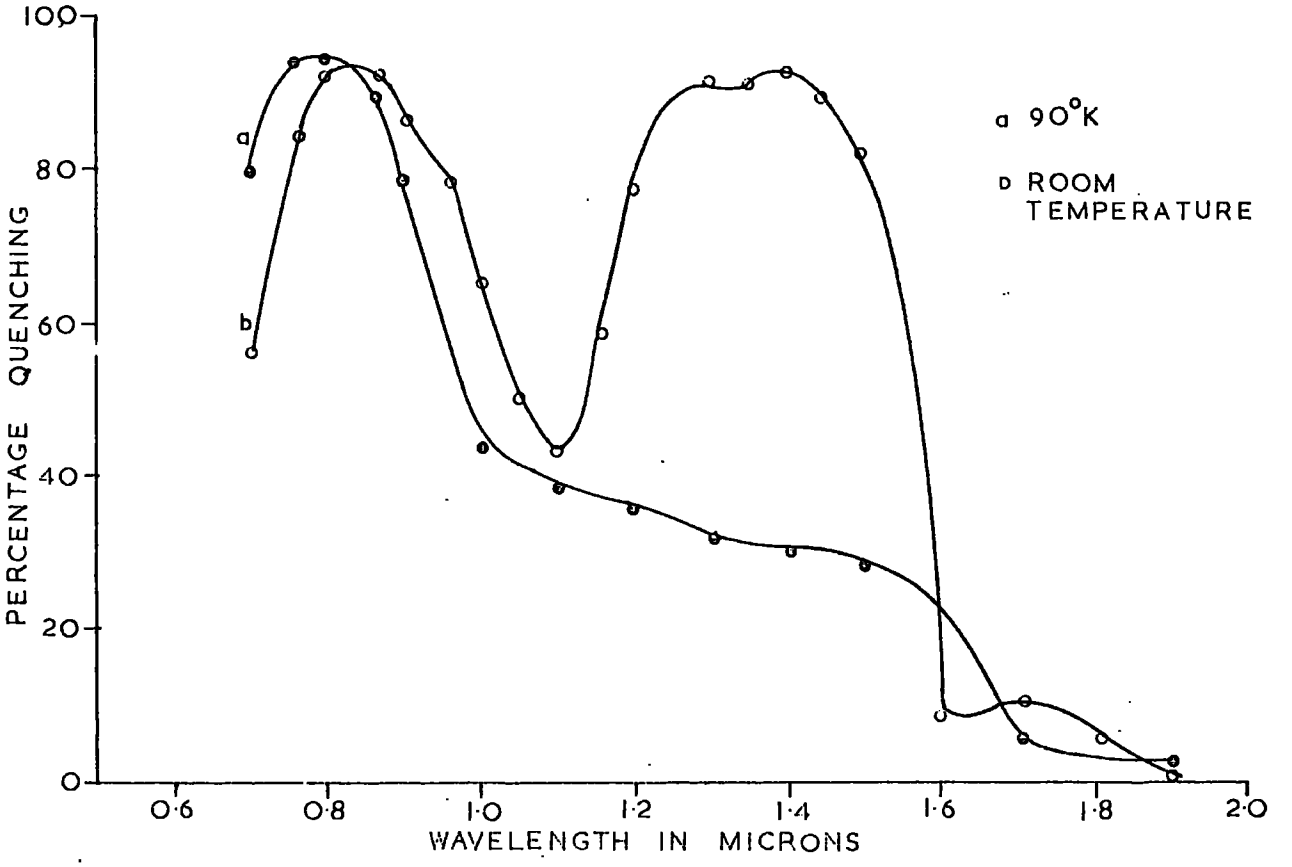

FIGURE 8.3.5. INFRARED QUENCHING FOR A DERBY LUMINESCENT SAMPLE GROWN WITH T_{Cd}=300°C.

lower density of the shallow traps in this sample greatly reduced the interference associated with their thermal emptying. After a period of approximately 30 minutes in the dark, the current associated with the thermal emptying of the shallow traps was only 3.10^{-13} amperes. The T.S.C. measurements of such samples showed a dominant trap emptying at approximately 200°K, it is concluded therefore that the threshold for optical emptying was associated with this centre.

Figure 8.4.1 curves (a) and (b) show the typical variation of photocurrent with wavelength for optical trap emptying. Previous measurements of the low temperature spectral response of both samples yielded no detectable current (i.e. $< 10^{-14}$ amperes) for wavelengths greater than the impurity response (i.e. in the region 0.5 μm to 0.8 μm) when the samples were cooled in the dark from 388°K. It follows therefore that the longer wavelength thresholds discussed in this section are associated with trapped electrons. In the present work, the optical trap depth was measured, somewhat arbitarily, as the energy at which the response was 1.10^{-13} amperes above the background current.

The spectral response measurements illustrated in Figure 8.4.1(a) were obtained after the cadmium rich sample had been illuminated whilst cooling from 388°K, and then heated in the dark to 246°K to empty all but the three highest temperature traps. Two separately measured curves are shown in Figure 8.4.1(a), which yielded a mean value of 0.75 eV for the optical trap depth. The same trap depth was found from T.S.C. analysis of this trap.

The three spectra shown in Figure 8.4.1(b) were monitored in a similar manner, excepting that all but the two highest temperature traps were emptied before the response was measured, by heating the sample to 268°K in the dark. The photocurrent at

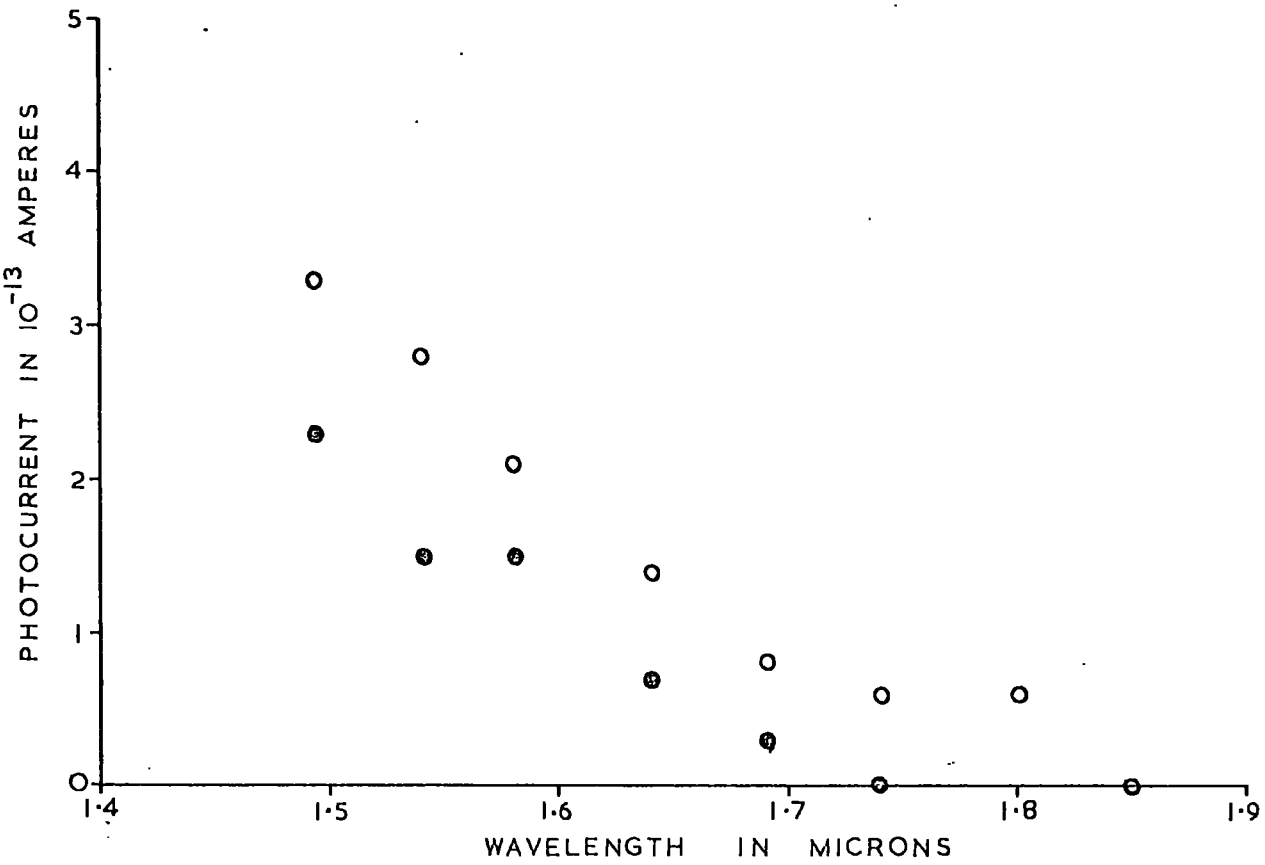

FIGURE 8 4 1(a) SPECTRAL RESPONSE AT 90°K DUE TO OPTICAL TRAP EMPTYING, FOR A T_{Cd} = 350°C SAMPLE HEATED TO 246°K IN THE DARK PRIOR TO MEASUREMENT

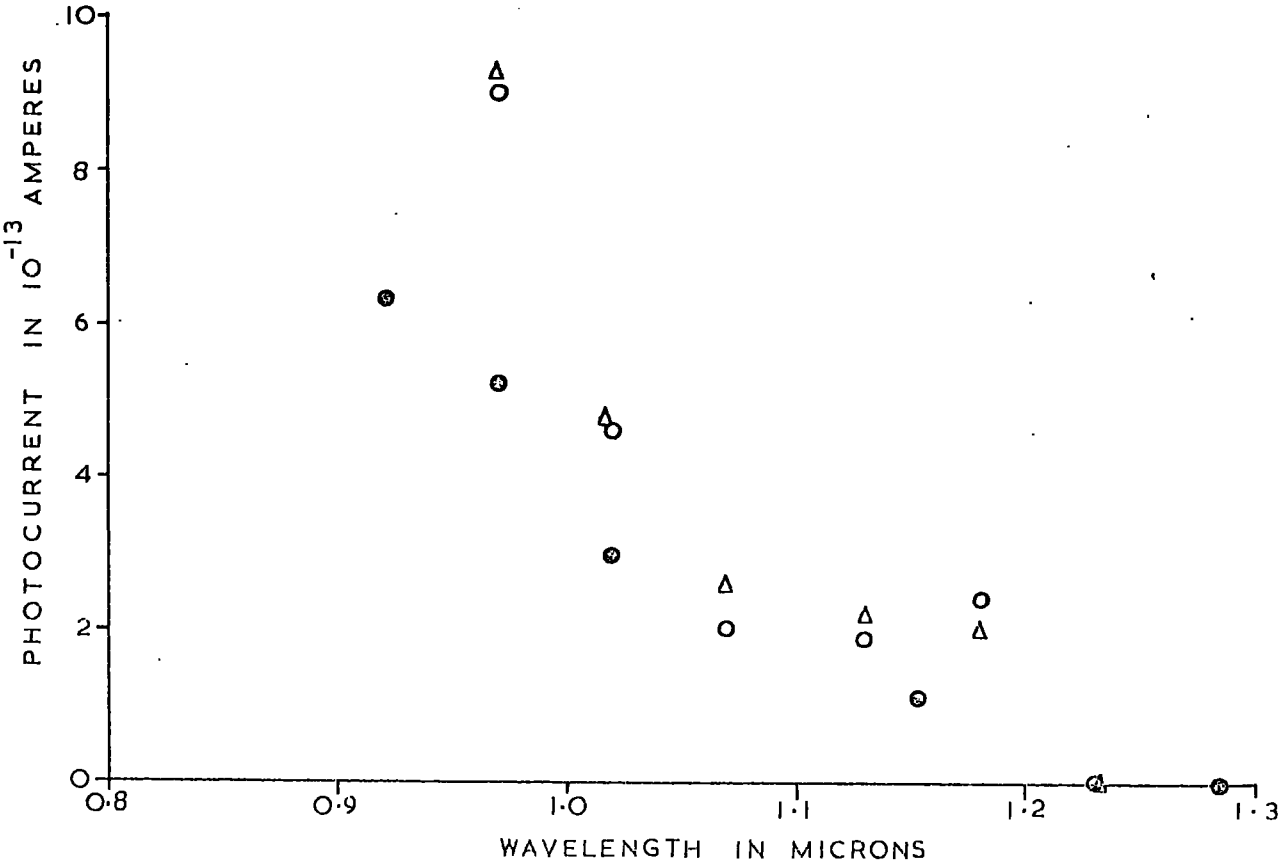

FIGURE 8 4 1(b) SPECTRAL RESPONSE AT 90°K DUE TO OPTICAL TRAP EMPTYING FOR A T_{Cd} = 350°C SAMPLE HEATED TO 286°K IN THE DARK PRIOR TO MEASUREMENT

1.10^{-13} amperes yielded a mean value of 1.13 eV for the optical trap depth of the centre for which the thermal activation energy was 0.53 eV.

In a further experiment, the cadmium rich sample was heated to 310°K, and then cooled to 90°K, leaving only the highest temperature trap occupied by electrons. From the mean value of three separate determinations of the threshold at 1.10^{-13} amperes, the optical trap depth of this centre was 1.21 eV compared with a thermal trap depth of 0.60 eV.

The sulphur rich sample was illuminated at 90°K for five minutes, and then left in the dark for a further thirty minutes prior to measurement. Assuming the response to be associated with the dominant trap observed in sulphur rich samples, which empties at approximately 200°K during T.S.C. measurement, the optical trap depth was 0.60 eV. This value was obtained from the mean of three separate determinations of the response threshold, at a current level 1.10^{-13} amperes above the background. The thermal activation energy of this centre was 0.44 eV.

The results given in this section are shown in Table 8.4.1, together with the values found by Arkad'eva (1964) for a shallow trap. It can be seen that, except for the trap yielding a value of 0.75 eV for both optical trap depth (E_{op}) and thermal trap depth (E_{th}), the ratio E_{op}/E_{th} is greater than unity. Such a result is not unexpected for polar crystals containing electron traps which are positively charged when empty. Because the charged trap distorts the surrounding lattice, the minimum of the electron energy-coordinate system of the centre does not correspond to the position of the electron energy minimum in the surrounding lattice. Figure 8.4.2 shows a qualitative picture of the

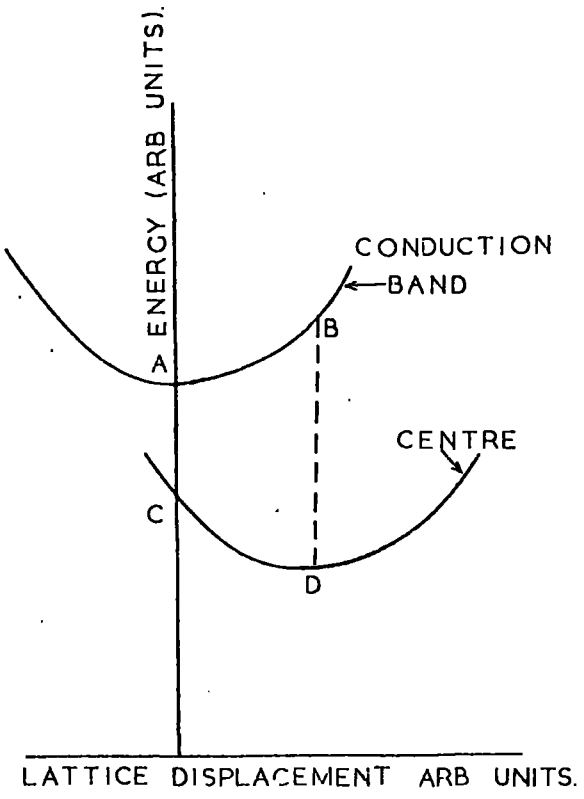

FIGURE 8.4.2 SCHEMATIC ENERGY-CONFIGURATION DIAGRAM FOR THE CONDUCTION BAND AND A POSITIVELY CHARGED CENTRE CONTAINING AN ELECTRON.

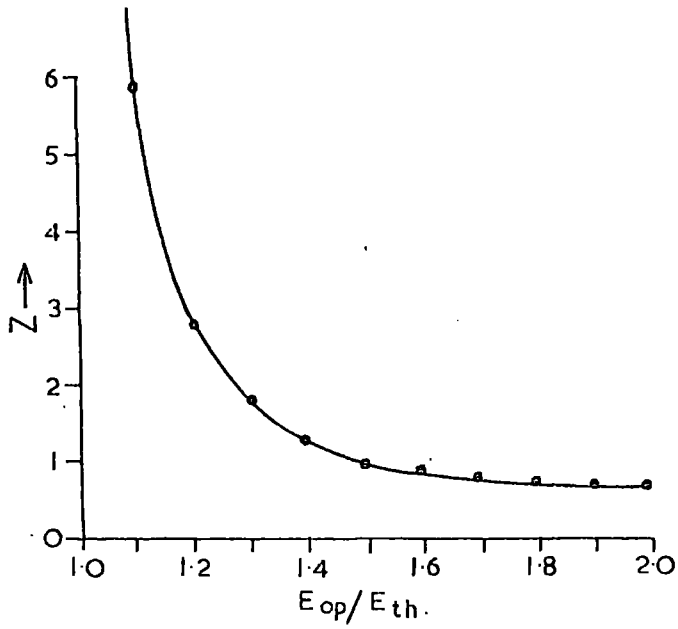

FIGURE 8.4.3 A PLOT OF THE CHARGE (Z) OF AN EMPTY ELECTRON TRAP VERSUS E_{op}/E_{th}.

TABLE 8.4.1

The Optical and Thermal Trap Depths of five Electron Traps

	Present Work				Arkad'eva (1964)
Optical Trap Depth in eV	0.60	0.75	1.13	1.21	0.32
Thermal Trap Depth in eV	0.44	0.75	0.53	0.60	0.18

energy-coordinate arrangement of the centre and the conduction band in the surrounding lattice, where A, B, C and D are cardinal points. A and D are the energy minima of the electrons in the conduction band and the centre respectively. B (C) is the point on the energy-coordinate system for the conduction band (centre) which corresponds to the same coordinate point as the centre (conduction band) energy minimum. Transitions DA, DB and AC correspond to the energies for thermal emptying (E_{th}), optical emptying (E_{op}) and emission (E_{em}) respectively.

Hoogenstraaten (1958) has considered such a model, and from a semi-classical analysis of the polarisation caused by a charged centre in polar crystals, derived the following expressions :-

$$E_{th} = (1/2)m_e'[z/\epsilon + 5c/16]^2 \qquad 8.4.1$$

$$E_{op} = (1/2)m_e'[z/\epsilon + 15/16][z/\epsilon + 5c/16] \qquad 8.4.2$$

$$E_{em} = (1/2)m_e'[z/\epsilon]^2 \qquad 8.4.3$$

where m_e' is the electron effective mass, z is the charge on the centre, and ϵ and ϵ_o are the static and optical dielectric constants respectively such that c is given by

$$c = 1/\epsilon_o + 1/\epsilon \qquad 8.4.4$$

(The above equations are expressed in units which were originally proposed by Hartree (1928) such that e = m = h = 1, and where the unit of length, a_o, = 0.529 A^o and the unit of energy is 17.2 eV.)

From the above equations E_{op}/E_{th} = R may be written in the

form

$$z/\epsilon c = (5/16)\ (3 - R)/(R - 1) \qquad 8.4.5$$

Assuming that $\epsilon_o = 5.85$ and $\epsilon = 11.6$ for CdS, a plot of z versus R is shown in Figure 8.4.3. Thus for a centre which is singly positively charged, R = 1.45, $E_{th} = 0.034$ eV, $E_{op} = 0.049$ eV and $E_{em} = 0.020$ eV (where $m_e' = 0.2\ m_e$).

For the traps shown in Table 8.4.1, z lies between 0.6 and 1, excepting the centre which gave both thermal and optical energies of 0.75 eV. However, this centre has been shown to be unusual as in some cases its density can vary with illumination treatment prior to T.S.C. measurement (see Section 6.3), moreover it has a higher thermal activation energy (from T.S.C. measurement) than would be expected from the temperature at which the T.S.C. maximum occurs.

8.5. Discussion

It has been demonstrated in this chapter that samples grown in cadmium rich conditions are more photosensitive than those grown in sulphur rich conditions. The long wavelength spectral response extends to longer wavelengths in cadmium rich samples. The infrared quenching of sulphur rich samples shows both quenching bands at liquid nitrogen temperatures, where cadmium rich samples show only the short wavelength band.

The simple model shown in Figure 8.1.1 is sufficient to explain qualitatively the infrared quenching phenomena. The similarity of the infrared quenching data at room temperature, for all the samples investigated, suggests that the quenching mechanism is basically the same. The upper lying Class 11_a centres lie

optically 1.2 eV above the valence band. Optical measurements also show that the Class 11_b centres lie 0.28 eV above the valence band. Calculations, which are described in Section 8.3.1, suggest that the thermal ionisation energy of the Class 11_b centre centres lies in the region 0.16 eV to 0.27 eV (assuming that S_p/S_n for these centres is between 1 and 10^5 and $m_h/m'_e = 1$).

An estimate of the thermal position of the Class 11_a centres above the valence band may be obtained from a knowledge of the position of the Fermi level at the onset of thermal quenching of photocurrent. (Under these conditions, the H.D.L. for the Class 11_a centres will lie in the region of these centres.) Using Equation 8.3.1, and assuming that S_p/S_n for the Class 11_a centres is 10^7, and $m_h/m'_e = 1$, the H.D.L. was calculated at the onset of thermal quenching for a cadmium rich sample grown with $T_{Cd} = 350^oC$ and for a sulphur rich sample grown with $T_S = 450^oC$. In both cases the calculations yielded a value for the H.D.L. in the region of 0.85 eV. (It has been reported by Dussel and Bube (1966) that, for certain trap distributions, such a calculation can be in error. However, the effect of the traps causes a decrease in the estimated thermal activation energy of the sensitising centres. In the example cited by Dussel and Bube the decrease was from 0.74 eV, which is substantially the value given above, to a value of 0.41 eV.)

It follows that the thermal and optical position of the Class 11_a centres are not the same. From Figure 8.4.3, which shows the ratio of E_{op}/E_{th} for centres in CdS with a charge z, the ratio 1.41 is commensurate with a centre having approximately a single negative charge. (Although the curve depicted in Figure 8.4.3 was calculated for the analysis of electron traps, the expressions from which it was derived contain only the optical and static

dielectric constants, so that it is equally well applicable to hole traps.) The difference between the optical and thermal separation of the Class 11_a centres from the valence band implies that their position when filled with electrons will also be different from that when they are empty.

The long wavelength threshold of photoconductivity indicates the energetic level to which centres are filled by electrons in the dark. For cadmium rich samples this energy was approximately 0.85 eV (above the valence band) and for sulphur rich samples the value was approximately 0.43 eV. Of particular interest is the occupancy of the Class 1 and Class 11 centres. From the values found for E_{th} and E_{op} for the Class 11_a centres it is concluded that $z = 1$. Equation 8.4.3 was used used to calculate E_{em}, the emission energy for electrons from the Class 11_a centres to the valence band, The hole effective mass was obtained from Equation 8.4.1, and yielded a value of E_{em} of approximately 0.6 eV. Where it is assumed that the optical excitation of electrons from the Class 11_a centres to the conduction band corresponds to an energy of $E_g - E_{em}$ (1.9 eV), then it must be presumed that the Class 11_a centres are substantially filled with electrons in cadmium rich samples, and substantially empty in sulphur rich samples. Such a situation would explain the greater sensitivity of the cadmium rich samples.

The increase in sensitivity of the two samples discussed in Section 8.2.2 may also be qualitatively explained in terms of the occupancy of the Class 11_a centres. For the samples grown with $T_S = 50^oC$ (Figure 8.2.3) there is a marked increase in the impurity response (curve (b)) following the illumination treatment which caused the sensitisation. This indicates that the sensitisation was achieved by decreasing the number of available centres

for the recombination of electrons. (A possible explanation of the sensitisation phenomenon of the T_S = 50°C sample has been given in Section 6.2, where a set of hole traps was postulated, such that each trap was surrounded by a potential barrier. Under illumination at low temperatures only, the hole traps cannot capture a significant number of holes, because they have to surmount the barrier. Following illumination from elevated temperatures, the hole traps will be filled. Where holes are distributed between the hole traps and the Class 11_a centres, illumination at high temperatures will decrease the occupancy of the Class 11_a centres by holes and thus increase the free electron lifetime by reducing recombination via the Class 11_a centres.)

The cadmium rich samples grown with T_{Cd} = 350°C did not show such a pronounced increase in the long wavelength response after sensitisation. However, reference to Figure 8.2.2 shows that after sensitisation (curve (b)) there is a relative increase at 0.62 μm (marked A in the figure) compared with the response at 0.52 μm (B). Where the response in the region A is due to optical excitation of electrons from the Class 11_a centres, and the region B due to optical excitation of electrons from a shallow centre lying near to the valence band, the sensitisation may be explained in terms of the redistribution of electrons from the shallow centres to the Class 11_a centres.

The low temperature infrared quenching observed in sulphur rich samples (see Figure 8.3.2) does not show the two main bands clearly. It would appear that a third band is present with a maximum in the region of 1.2 μm, which corresponds to an optical transition of 1.05 eV. This places the centre from which the electron is excited at 0.15 eV above the valence band. Such a

centre may be that which was used to explain the sensitisation of the cadmium rich samples after illumination, discussed in the previous paragraph.

The observation of optical quenching involving two main centres (e.g. Transition 1 in Figure 8.1.1) presumes that the centres are in close proximity, because the transition does not involve a carrier entering either the conduction or valence bands. The two quenching bands have been interpreted, by Boyn (1968) and other workers, in terms of the Class 11_b centre being an excited state (for a hole) of the Class 11_a centre. The present observations are consistent with such a model. (In this case, the optical quenching radiation for the long wavelength band excites holes from the Class 11_a centres to the Class 11_b centres. Quenching is observed when the optically excited holes can be thermally stimulated to the valence band.)

The precise nature of the Class 11 centres in CdS is not known at the present time. Boyn (1968) has studied the optical absorption of CdS heat treated in cadmium and sulphur, and concluded that cadmium interstitials and vacancies are the dominant native defects. He suggested that the cadmium vacancy containing a single electron is the sensitising recombination centre. Absorption corresponding to the two infrared quenching bands was only found in sulphur rich samples, which supports his argument that the Class 11 centre is a cadmium vacancy. In this chapter it has been shown that the occupancy of the Class 11_a centres by electrons is greater in cadmium rich samples. This again indicates that the observation of the quenching bands in absorption should be more likely in sulphur rich samples.

Bube and Cardon (1964) found that the electron capture cross-section for the sensitising centres is of the order of 10^{-21} cm^2.

Because of the weak temperature dependence of the capture cross-section, they suggested that the likely recombination mechanism was radiative recombination at a neutral centre. Later work by Hemila and Bube (1967) suggests that the Class 11 centres are complex in nature, and also that more than one centre may be involved.

The calculations described earlier in this section, relating to the ratio of the optical and thermal separation of the Class 11_a centres from the valence band, are compatible with the Class 11_a centre having a single negative charge when occupied by an electron. When the Class 11_a centre is behaving as a recombination centre for electrons, it will be approximately neutral in charge, which agrees with the hypothesis of Bube and Cardon. It is not possible to explain the small capture cross-section for this neutral centre, though it would appear unlikely that the centre is simple in nature.

The thermoelectric power measurements made by Lawrance and Bube (1968) (see Section 2.10), under conditions of illumination corresponding to those used for the infrared quenching of the photocurrent, are also explicable in terms of the present model for the Class 11_a centres. Their observation of an increase in the negative thermoelectric power with optical quenching radiation suggests a polarisation effect, which would occur with sensitising centres of the type discussed above.

The anomalous spectral response and infrared quenching of the boule crystals grown from Derby material can only be interpreted in terms of the presence of other recombination centres and hole traps associated with impurities. Yoshizawa (1968) found a further quenching band at 0.575 μm (2.15 eV) in CdS doped with

phosphorous. (The observation of such quenching during the present work would have been obscured by the increase in the photocurrent, due to impurity response, at such wavelengths.) He suggested that the phosphorous substituted for sulphur.

In Figure 8.3.5, a third quenching band may be seen in the spectral range 1.60 μm to 2.00 μm. Because of the number of impurities present, it is not possible to assign this to any particular impurity from this result alone. However, this sample was intentionally doped with sodium to a level of 2 p.p.m. The sulhpur rich sample shown in Figure 8.3.2 also shows this band, and mass spectrographic analysis indicated a similar concentration of sodium. Thus, the third quenching band may be associated with sodium.

References to Chapter 8

Arkad'eva, E.N., 1964, Sov. Phys. Solid State 6, 798.

Boyn, R., 1968, Phys. Stat. Sol. 29, 307.

Bube, R.H., 1956, Phys. Rev. 101, 1668.

Bube, R.H., 1960, Photoconductivity of Solids, published by John Wiley and Sons, Inc. New York, P. 348.

Bube, R.H. and F. Cardon, 1964, J. Appl. Phys. 35, 2712.

Dussel, G.A. and R.H. Bube, 1966, J. Appl. Phys. 37, 13.

Hartree, D.R., 1928, Proc. Cambr. Phil. Soc. 24, 89.

Hemila, S.O. and R.H. Bube, 1967, J. Appl. Phys. 38, 5258.

Hoogenstraaten, W., 1958, Thesis, University of Amsterdam, submitted February 1958.

Lawrance, R. and R.H. Bube, 1968, J. Appl. Phys. 39, 1807.

Reed, C.E. and C.G. Scott, 1968, J. Phys. D. (Brit. J. Appl. Phys.) Series 2, 1, 1125.

Yoshizawa, M., 1968, Japanese J. Appl. Phys. 7, 182.

CHAPTER 9

INFRARED LUMINESCENCE

9.1. Introduction

The infrared luminescence (I.R.L.) in the spectral range 0.65 μm to 2.50 μm was measured at liquid nitrogen temperatures for a number of samples for which the T.S.C. and photoconductivity had also been studied. In addition, a few semi-conducting samples and some lightly doped samples were investigated. In all the samples the change in the intensity of each of the main luminescent bands was monitored, as the temperature was increased from 85°K to 388°K.

The experimental arrangement for the measurement of I.R.L. is described in Chapter 4.

9.2. I.R.L. from Photoconducting Optran Samples

Figure 9.2.1 curves (a) and (b) show the I.R.L. emission, observed at 85°K, from two cadmium rich samples grown with T_{Cd} = 350°C. Figures 9.2.2 and 9.2.3 show the I.R.L., at 85°K, from two sulphur rich samples grown with sulphur reservoirs at 300°C and 450°C respectively.

All the photoconducting samples showed the band with a maximum at 1.02 μm, and the structured luminescence in the region 1.60 μm to 2.00 μm, which comprised two peaks at 1.60 μm and 1.83 μm together with a shoulder at approximately 2.00 μm. The cadmium rich samples also yielded an emission centred on 0.70 μm which was not observed with sulphur rich crystals. The replica of the 1.60 μm to 2.00 μm emission, which was located at 2.00 μm to 2.50 μm (Figure 9.2.3), was only observed to a marked extent in

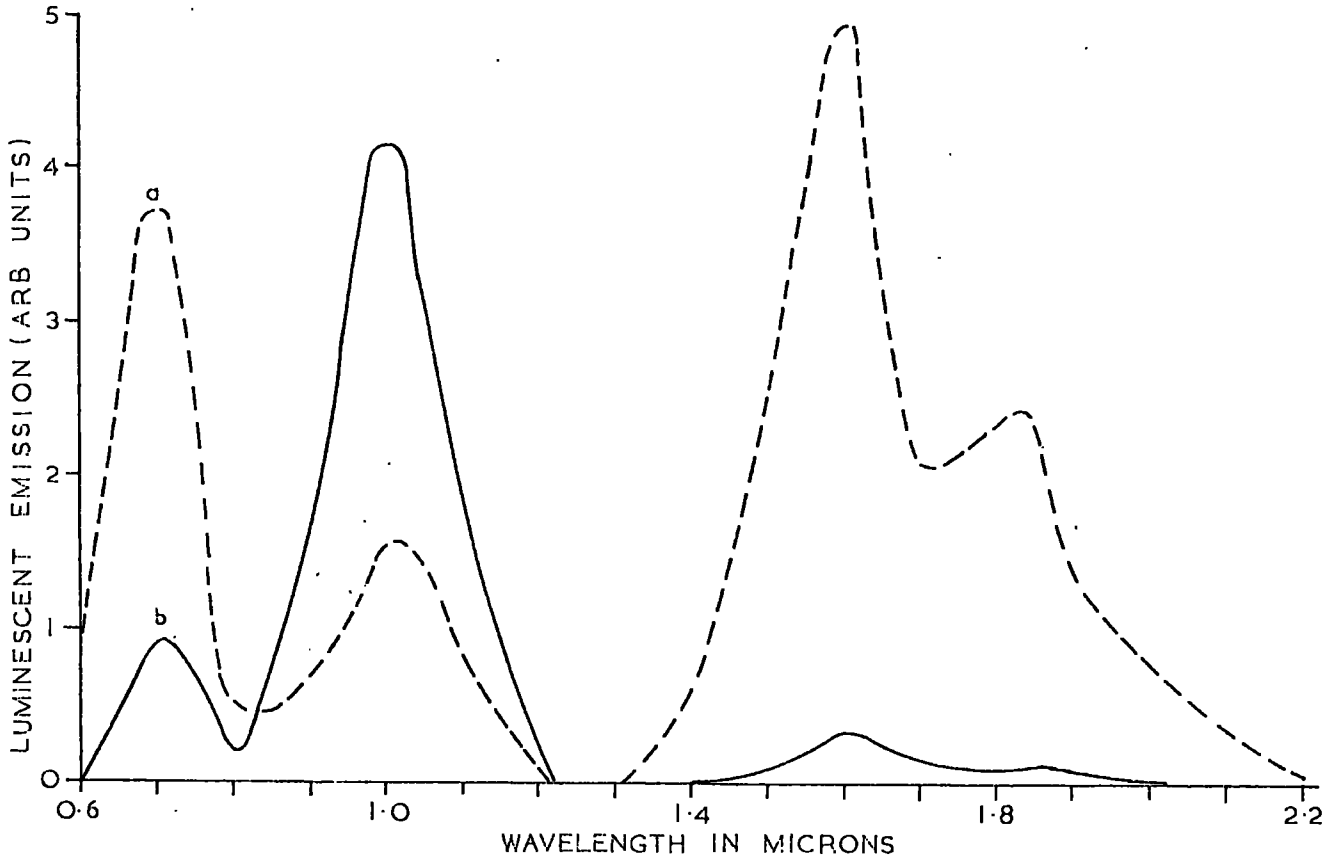

FIGURE 9.2.1 INFRARED LUMINESCENCE AT 85°K FROM TWO SAMPLES GROWN WITH $T_{Cd} = 350°C$

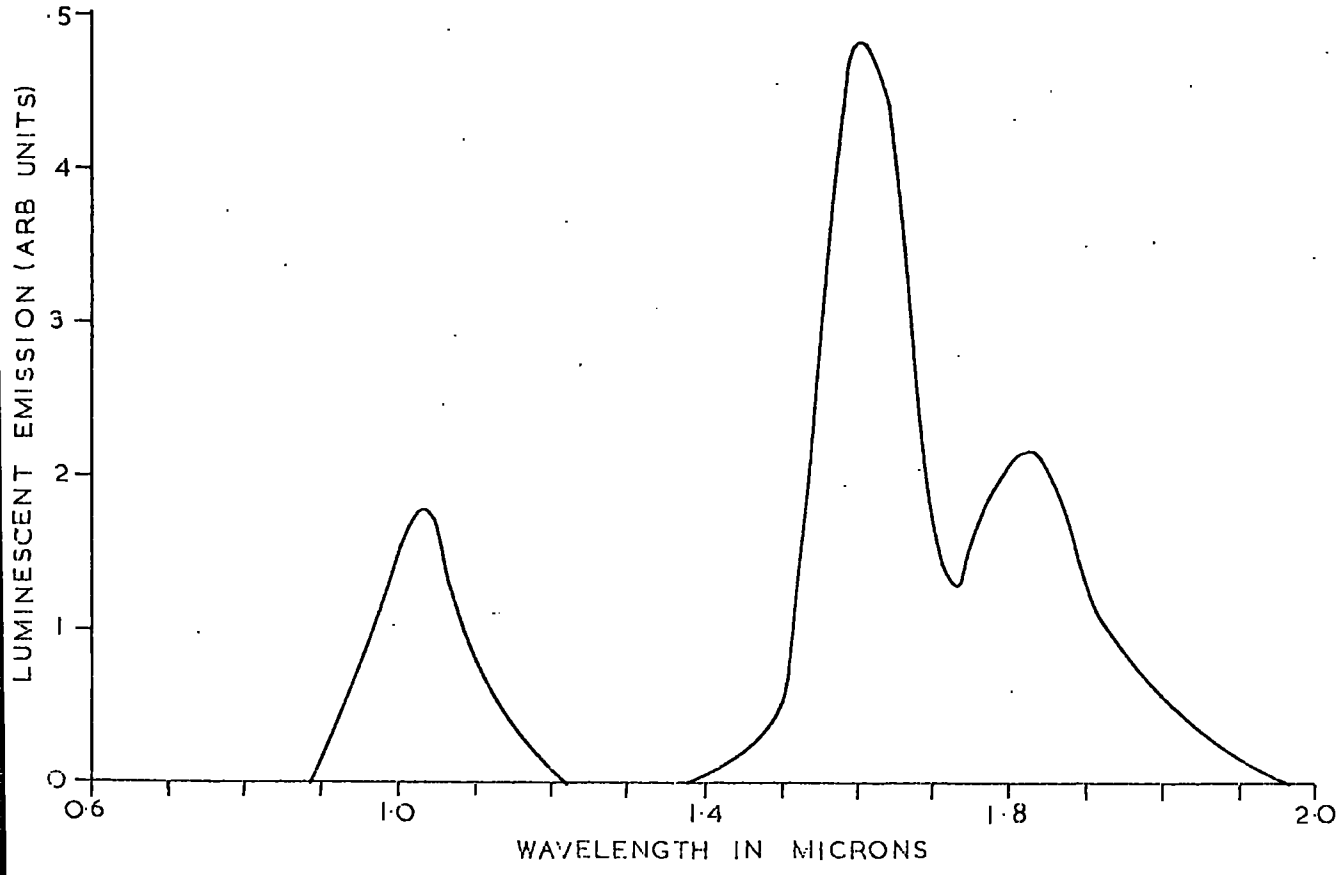

FIGURE 9.2.2 INFRARED LUMINESCENCE AT 85°K FROM A SAMPLE GROWN WITH $T_S = 300°C$

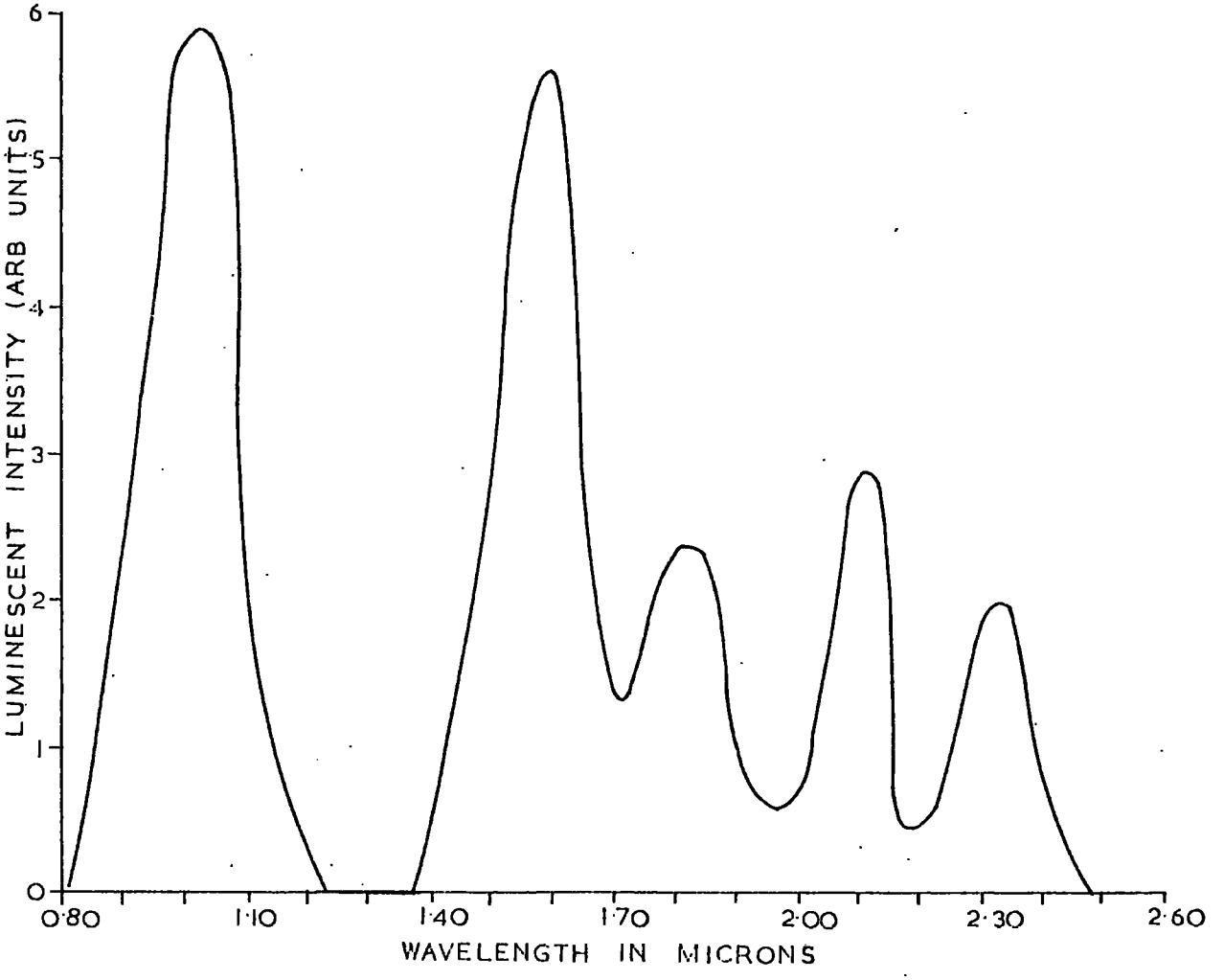

FIGURE 9.2.3. INFRARED LUMINESCENCE AT 85°K FROM A SAMPLE GROWN WITH $T_S = 450°C$

one undoped sample (T_S = 450°C) and in one impure sample which is described in Section 9.4. The replica emission contained two peaks centred on 2.12 μm and 2.33 μm. Similar long wavelength I.R.L. has been reported by Bryant and Cox (1966), and is discussed at the end of this chapter.

Two simple models to explain the temperature quenching of luminescence are illustrated in Figure 9.2.4 (a) and (b). The quenching in Figure 9.2.4(a) results from the thermal excitation of an electron from the valence band to an empty luminescent centre situated at an energy E_A above the valence band. As a result, recombination of conduction electrons with the centre is reduced. In the second model, the emission associated with an electron transition from a localised level to a luminescent centre may be quenched, as shown in Figure 9.2.4(b), when the electron in the excited state is thermally ionised to the conduction band. For both transitions, the dependence of the luminescent efficiency, η_L, on temperature may be expressed as

$$\eta_L = 1/(1 + C\exp(E_i/kT)) \qquad 9.2.1$$

where $E_i = E_A$ for the first model and $E_i = E_t$, the trap or excited state ionisation energy in the second. The variation of η_L with temperature, according to Equation 9.2.1, is shown in Figure 9.2.4(c). The intensity of luminescent emission, I, will obviously vary in a similar manner.

Curves (a) to (d) in Figure 9.2.5 are the intensities of the 0.70 μm, 1-02μm, 1.60 μm and 1.83 μm emissions respectively plotted against temperature for one of the cadmium rich (T_{Cd} = 350 350°C) samples. The thermal quenching of the 0.70 μm emission in the cadmium rich samples above 300°K approximates to the simple

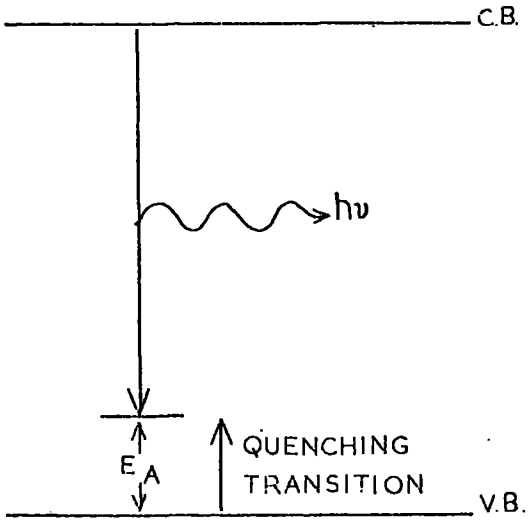

FIGURE 9.2.4(a) QUENCHING OF LUMINESCENT EMISSION BY THERMAL EXCITATION OF AN ELECTRON FROM THE VALENCE BAND TO A LUMINESCENT CENTRE

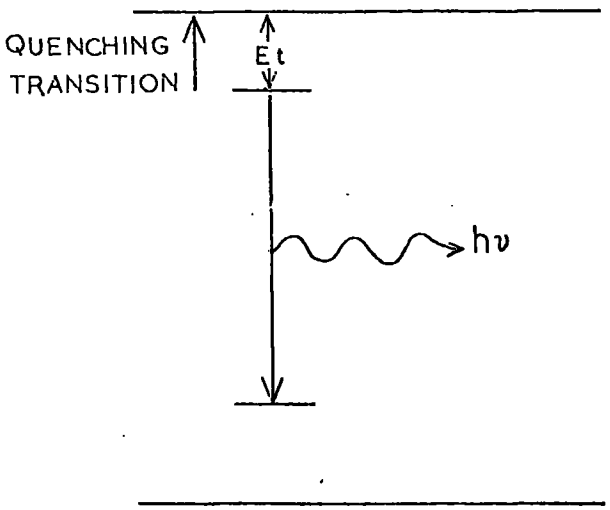

FIGURE 9.2.4(b) QUENCHING OF LUMINESCENT EMISSION DUE TO THERMAL IONISATION OF A TRAPPING CENTRE

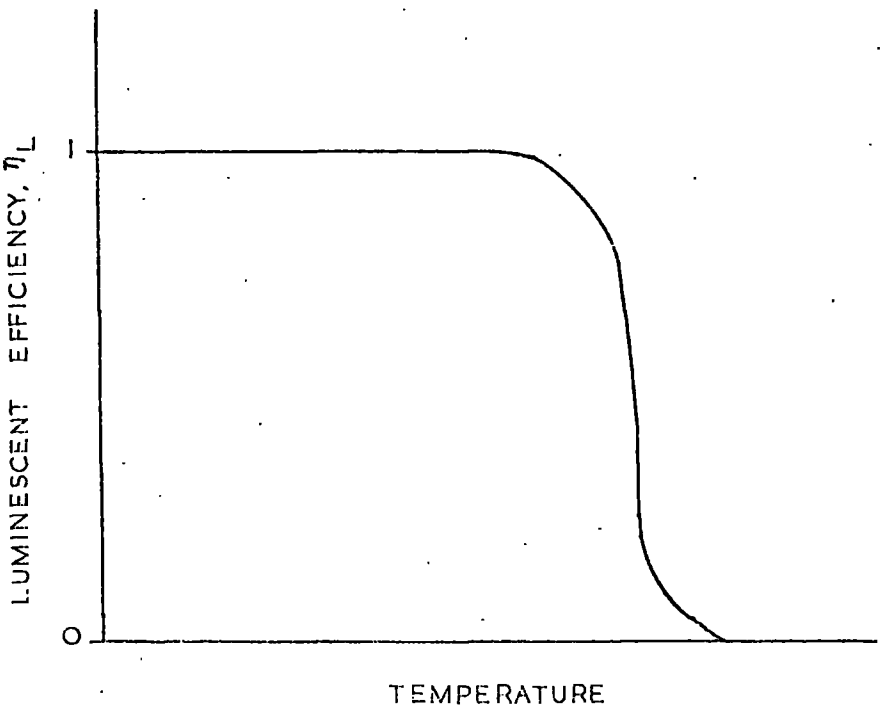

FIGURE 9.2.4(c) VARIATION OF LUMINESCENT EFFICIENCY WITH TEMPERATURE FOR THE MODELS SHOWN ABOVE

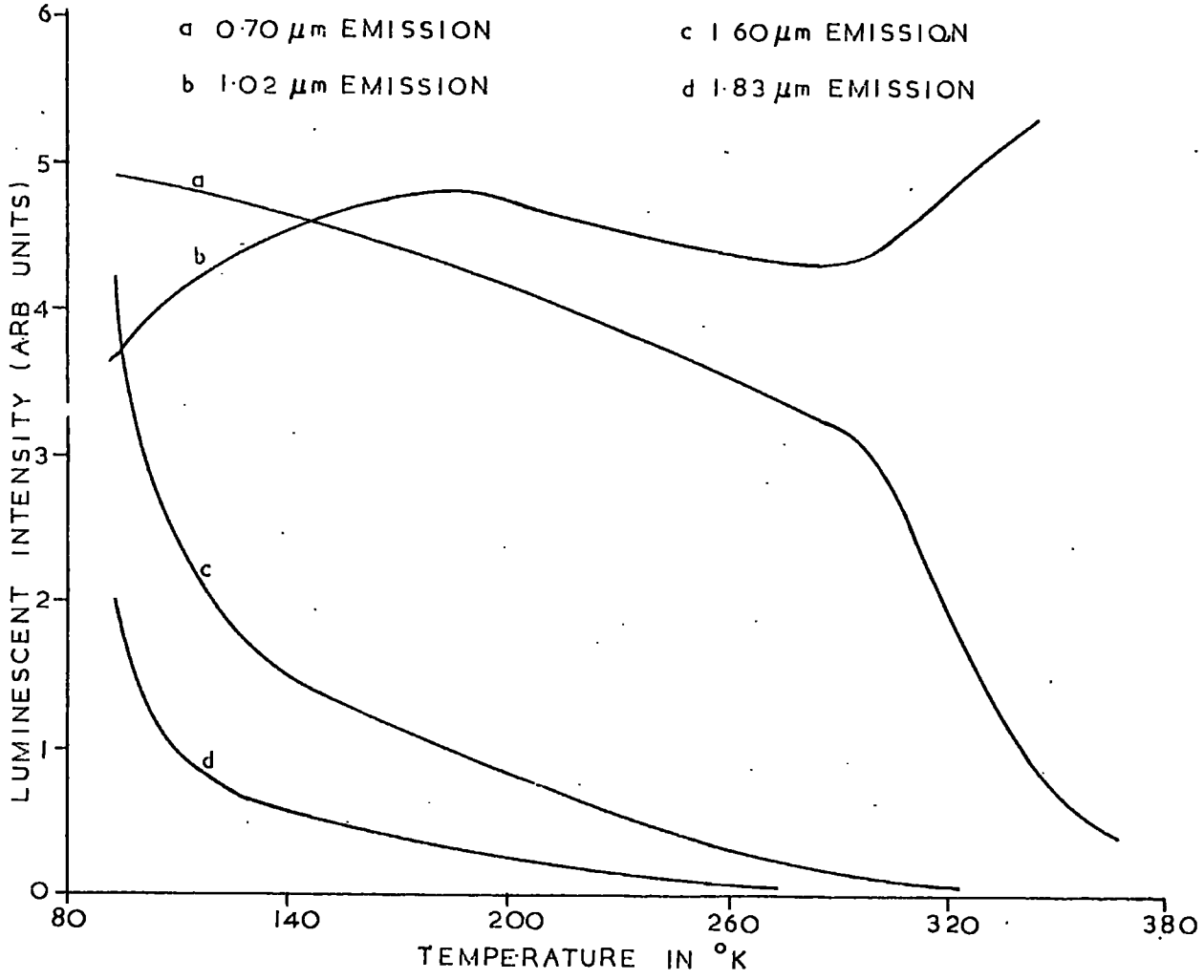

FIGURE 9.2.5. THERMAL QUENCHING OF INFRARED LUMINESCENCE FROM A SAMPLE GROWN WITH $T_{Cd} = 350\,^{\circ}C$

relationship, Equation 9.2.1, so that a plot of $\log[(I_{max} - I_T)/I_T]$ versus the reciprocal of temperature should yield a straight line, from which the activation energy of the quenching process can be obtained. Figure 9.2.6 curves (a) and (b) are two such plots for the 0.70 μm emission from different cadmium rich boules. The slopes of the lines yield activation energies of 0.56 eV and 0.58 eV.

In contrast, the 1.02 μm emission was found to increase in intensity, with increasing temperature, in the range where the 0.70 μm emission was quenched in cadmium rich samples (Figure 9.2.5).

The similarity of the thermal quenching of the I.R.L. bands centred on 1.60 μm and 1.83 μm can be seen in Figure 9.2.5. Their intensity decreased as the temperature was raised from 85°K, so that a true value of I_{max} could not be measured. However, from Equation 9.2.1, when $1 + C\exp(-E_i/kT) >> 1$, then the luminescent emission intensity at temperature T can be expressed as

$$I_T \propto \exp(E_i/kT) \qquad 8.2.2$$

Thus a plot of $\log(I_T)$ versus 1/T should yield an activation energy for the quenching process.

Figure 9.2.7 shows this plot for the 1.60 μm emission from two cadmium rich samples (T_{Cd} = 350°C). In the first case, curve (a), a single activation energy of 0.06 eV was obtained. Curve (b) shows two straight line regions leading to an activation energy of 0.03 eV at low temperatures and 0.17 eV at high temperature. Similar changes in activation energies for the thermal quenching of the analogous structured luminescence in ZnS phosphors (which occurs at 1.20 μm to 1.50 μm) have been reported

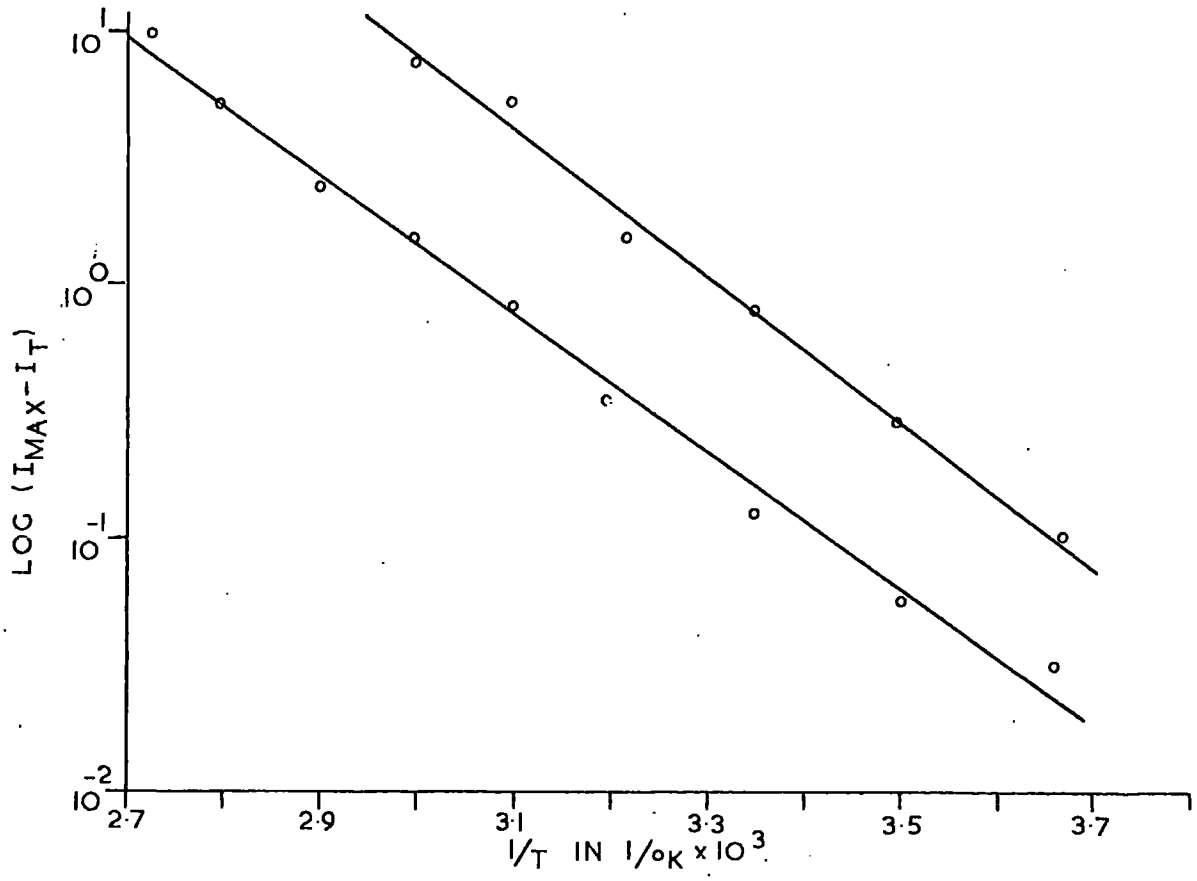

FIGURE 9.2.6 LOG $[(I_{MAX}-I_T)/I_T]$ VERSUS $1/T$ FOR THE 0·70 μm EMISSION FROM TWO T_{Cd}=350°C SAMPLES.

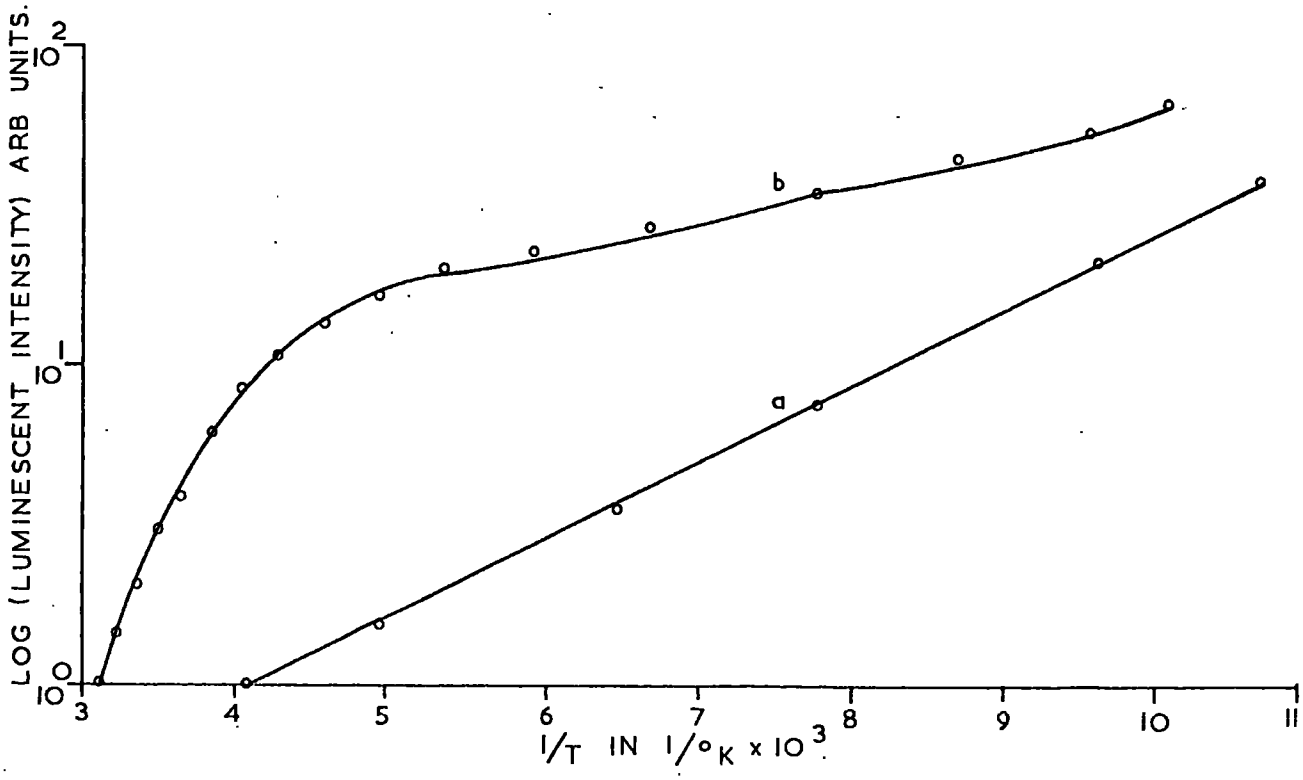

FIGURE 9.2.7 PLOT OF LOG (LUMINESCENT INTENSITY) VERSUS $1/T$ FOR THE 1·60 μm EMISSION FROM TWO T_{Cd}=350°C SAMPLES.

by Browne (1956).

The 0.70 μm luminescent band was not observed in the sulphur rich samples grown with T_S = 300°C and 450°C. Also, the intensity of the 1.02 μm emission did not increase at temperatures above 300°K, as was the case for the cadmium rich samples. Figure 9.2.8 shows the variation of the 1.02 μm and 1.60 μm peaks with temperature, for the sample grown with a sulphur reservoir at 300°C. The 1.60 μm peak yielded an activation energy of 0.06 eV.

The quenching of the 1.60 μm, 1.83 μm, 2.12 μm and 2.33 μm emissions of the 450°C sulphur rich sample is shown in Figure 9.2.9, curves (a) to (d) respectively. It is particularly interesting to note that although the 1.60 μm and 1.83 μm peaks are quenched in a similar manner, the 2.12 μm and 2.33 μm emissions are not. The 2.12 μm emission does, however, vary in a somewhat similar manner to the 1.60 μm and 1.83 luminescence. (Bryant and Cox (1966) have discussed the structured luminescence (1.60 μm to 2.00 μm). They attributed both to radiative recombination from electrons from a centre with holes in the upper branches of the valence band. In all cases during the present work, the 1.60 μm and 1.83 μm emissions were quenched in a similar manner. If the replica emission results from a similar recombination mechanism, then the 2.12 μm and 2.33 μm emissions might also be expected to be similarly quenched.) A plot of log(luminescent intensity) versus 1/T for the four curves shown in Figure 9.2.9 yielded activation energies in the region of 0.4 eV above 220°K.

9.3. Variation of the I.R.L. from Photoconducting Optran Samples with Conditions of Illumination

It has been demonstrated in earlier chapters, that the temperature at which illumination is commenced, during the cooling

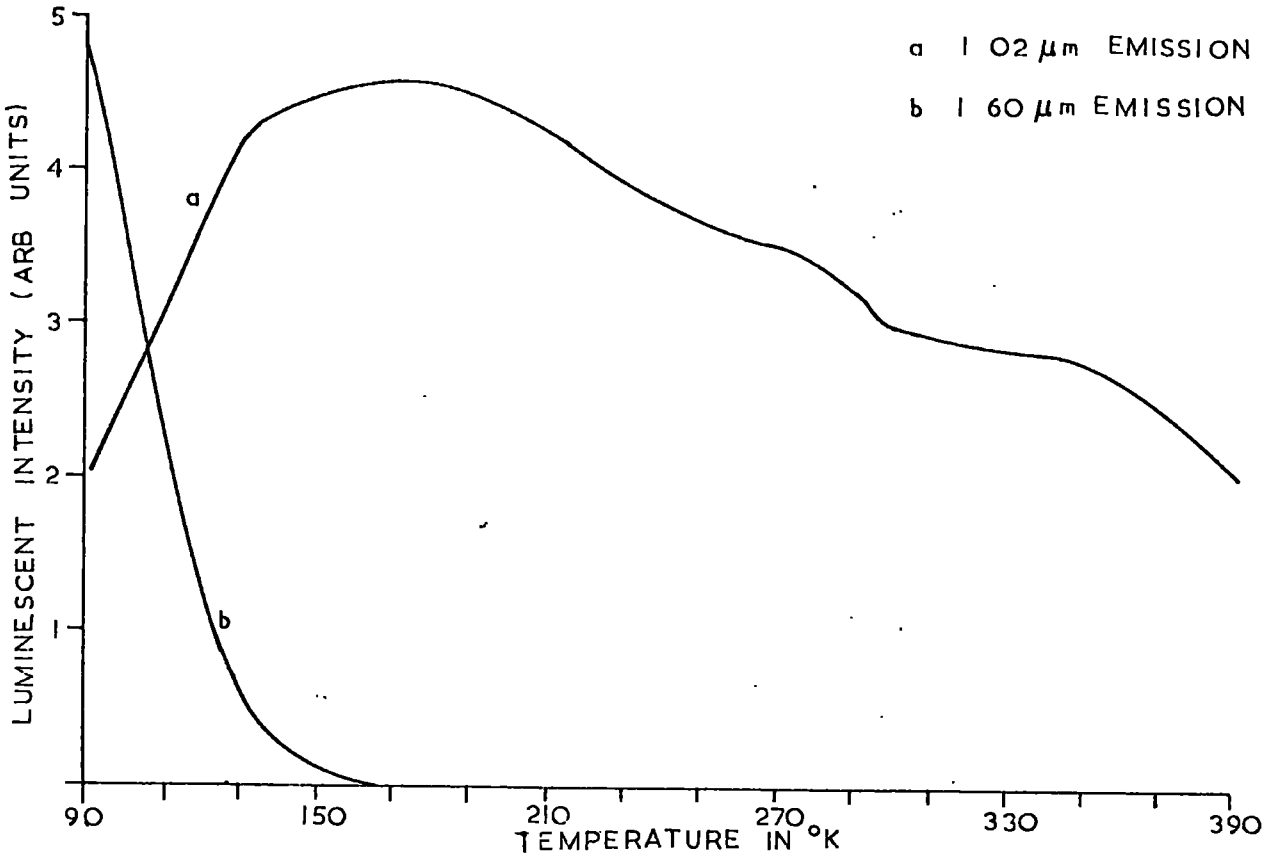

FIGURE 9.2.8 VARIATION OF THE INFRARED LUMINESCENT INTENSITY WITH TEMPERATURE FOR A SAMPLE GROWN WITH $T_S = 300\,^{\circ}C$

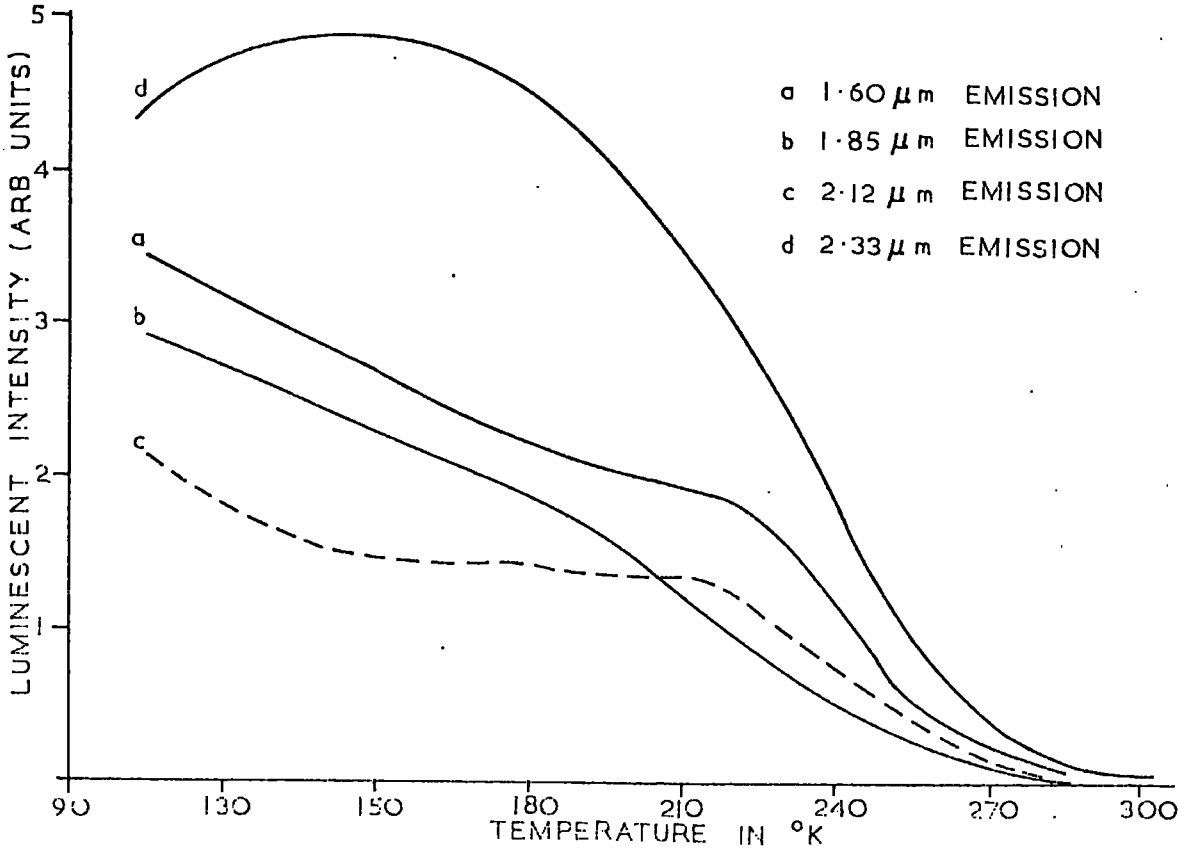

FIGURE 9.2.9 THERMAL QUENCHING OF INFRARED LUMINESCENCE FROM A SAMPLE GROWN WITH $T_S = 450\,^{\circ}C$

of a sample, prior to the measurement of the T.S.C., photocurrent etc. can have a marked effect on the ensuing measurement. It was found, in some cases, that changes in the intensities of the I.R.L. bands also occurred when comparison was made between spectra obtained after cooling the sample in the dark from 388°K and after illumination during cooling. In most samples the intensity change was less than a factor of two.

In Sections 6.2, 8.2.2 and 8.3.1 the photocurrent versus temperature, spectral response and infrared quenching respectively are described for a sample grown with T_S = 50°C. This sample showed a large change in free electron lifetime when it was illuminated during cooling from temperatures in the region of 200°K. When it was irradiated below this temperature region, a large change in photocurrent was observed at approximately 200°K (see Figure 6.2.2). It was found that the intensity of the 1.06 μm to 2.00 μm emission was also associated with this lifetime change.

Figure 9.3.1 shows the spectral distribution of the I.R.L., at 85°K, for the T_S = 50°C sample. Curve (a) was obtained after illumination at 85°K only, whereas curve (b) was measured after illumination during cooling from 388°K. In curve (a) the emission at 0.70 μm is seen together with a maximum at 1.15 μm. (No I.R.L. was observed in the region of 1.02 μm). Curve (b) shows no emission at 0.70 μm, though the 1.02 μm maximum is present. The structured luminescence has increased in intensity by over one order of magnitude.

Cowell and Woods (1967) studied the relationship between the intensity of the structured luminescence and the magnitude of the T.S.C. spectrum following similar pre-illumination treatments. They suggested that the recombination of free electrons

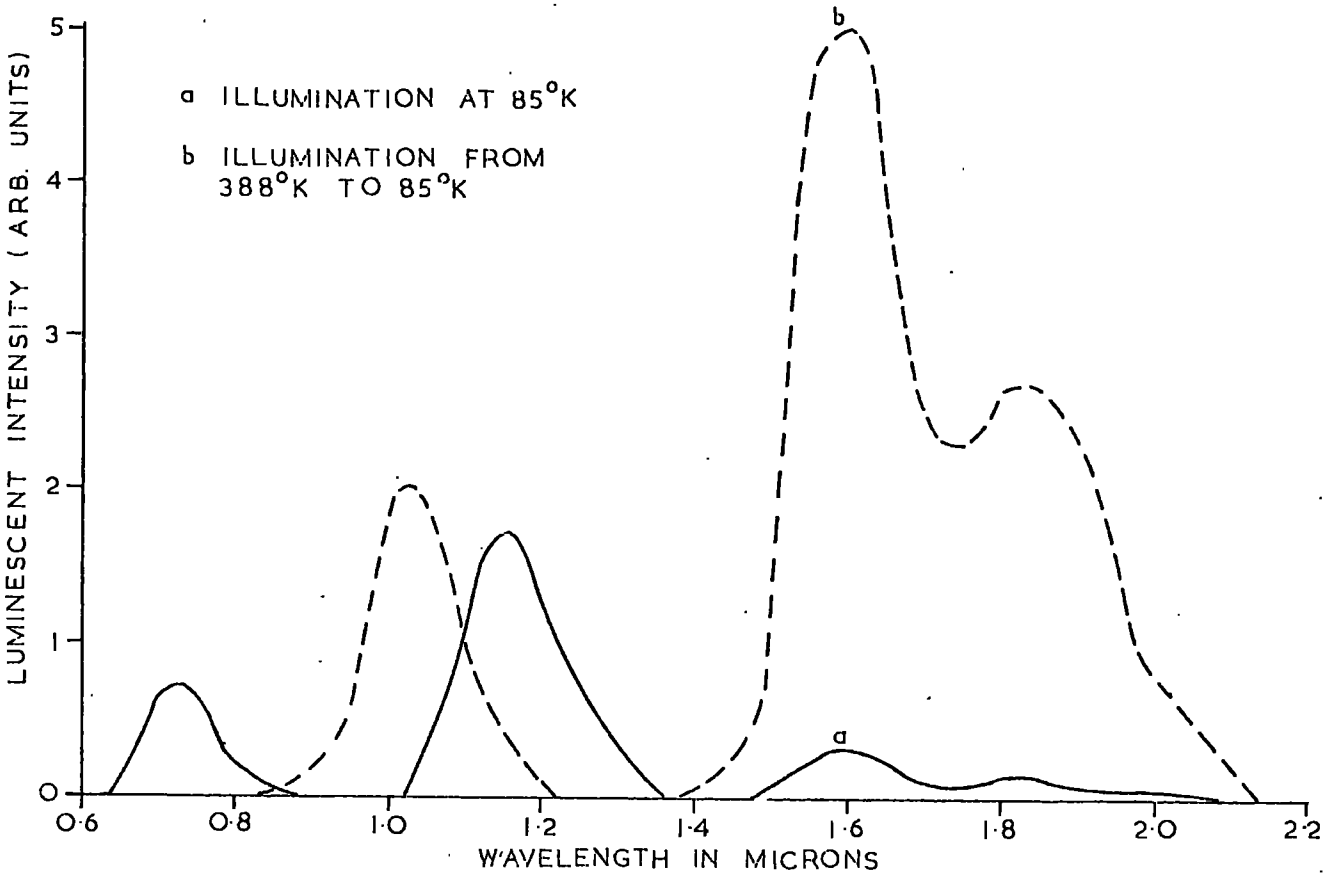

FIGURE 9.3.1 INFRARED LUMINESCENCE AT 85°K FROM A SAMPLE GROWN WITH $T_S = 50°C$

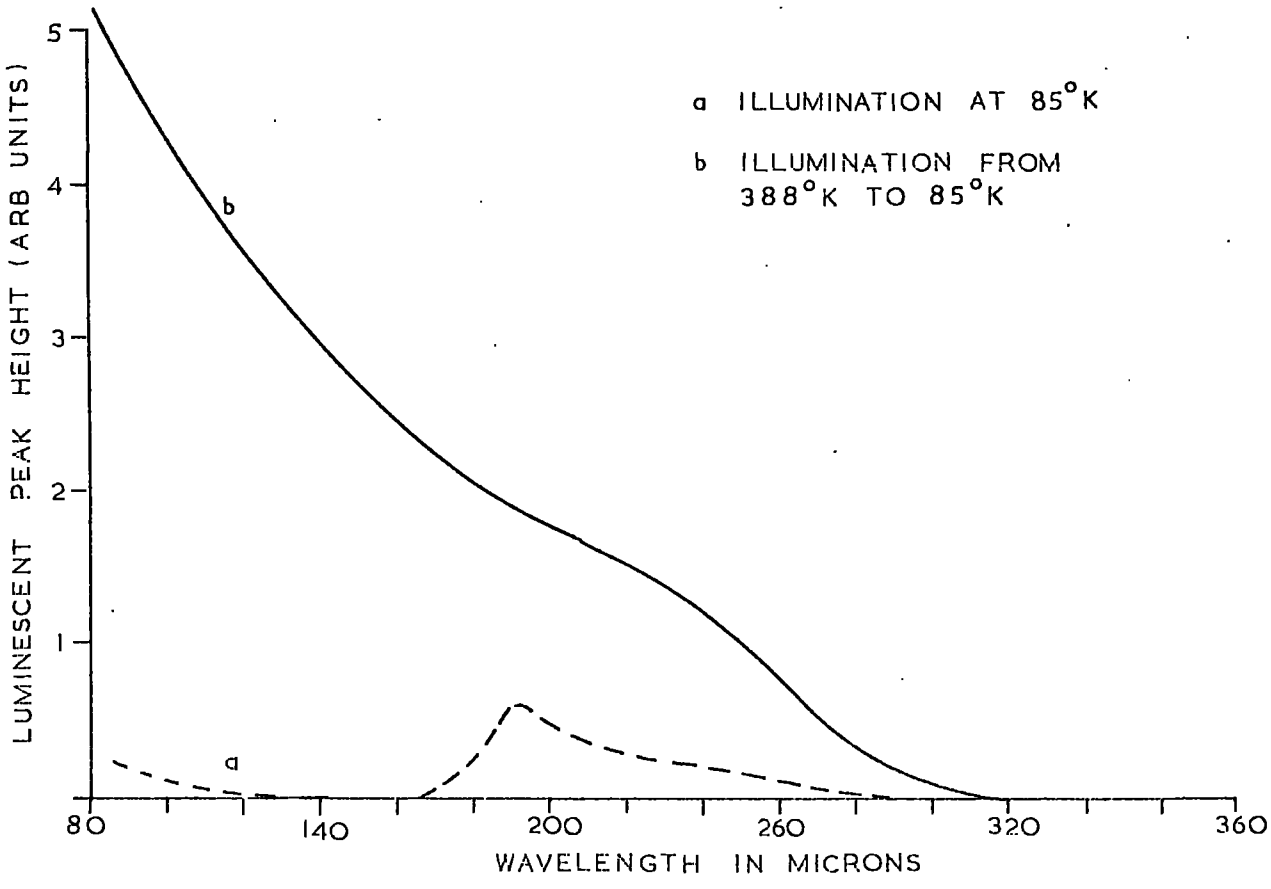

FIGURE 9.3.2 THERMAL QUENCHING OF THE 1·60 mm EMISSION FOR A SAMPLE GROWN WITH $T_S = 50°C$

in their samples occurred at a centre with a level lying approximately 0.70 eV above the valence band. The structured luminescence resulted from radiative recombination of electrons from this centre with holes in the valence band. This model was chosen because the structured luminescence intensity was greater when the free electron lifetime was longer (i.e. the occupancy of the recombination centres was greater).

Although the present sample showed an increase in free electron lifetime in the temperature range 85°K to 200°K, whereas Cowell and Woods observed changes for the whole of their T.S.C. spectrum (85°K to 390°K), the structured luminescence was again of greater intensity when the sample was more photosensitive.

Figure 9.3.2 shows the variation of the intensity of the 1.60 μm emission maximum with increasing temperature from 85°K. In curve (a) the magnitude of the emission is lower where the sample was irradiated at 85°K only, however a marked increase in emission is seen at approximately 200°K corresponding to the steep rise in photocurrent which is illustrated in Figure 6.2.2. When the sample was continuously illuminated during cooling from 388°K a continuous decrease in the intensity of the 1.60 μm emission was observed with increasing temperature (Figure 9.3.2 curve (b)).

The measurements of spectral response of photocurrent and infrared quenching, discussed in Chapter 8, suggest that the recombination of free electrons is associated with two centres (Class 11_a and Class 11_b in Figure 8.1.1) lying 1.2 eV and 0.28 eV above the valence band. The upper of these centres (Class 11_a) is the sensitising centre, the thermal activation

energy of which was calculated, from the onset of thermal quenching, to be 0.85 eV. Luminescent emission by recombination of electrons from the Class 11_a centre with holes in the conduction band will correspond to an energy of approximately 0.6 eV (using the above values of thermal and optical activation energies and Equations 8.4.1 to 8.4.5). The structured luminescence yields three emission bands centred on 1.60 μm, 1.83 μm and 2.00 μm. The 2.00 μm (0.62 eV) band is close to the calculated emission energy (0.6 eV) for electrons from the Class 11_a centres with holes in the valence band. The simple model described in Chapter 8 considers a single valence band only, so that the 1.60 μm and 1.83 μm emission bands could result from the recombination of electrons from the Class 11_a centres with holes in the deeper lying valence bands. (An account of the theoretical work of Birman (1959) and the exciton studies of Thomas and Hopfield (1959) has been given in Section 1.3, where it is shown that the upper branches of the CdS valence band comprise three separate bands.)

Cox et al. (1968) have studied the decay time with temperature of the structured luminescence and from practical and theoretical considerations conclude that the emission stems from radiative recombination of electrons, from a singly negatively charged cadmium vacancy, with holes in the valence band. Such a centre could well be the Class 11_a centre observed during measurements of photoconductivity.

The 1.15 μm emission observed after illumination of the $T_S = 50^{\circ}C$ sample at low temperatures (curve (a) in Figure 9.3.1) was monitored with increasing temperature as shown in Figure 9.3.3 curve (a). The emission centred on 1.02 μm was also measured with increasing temperature after low temperature

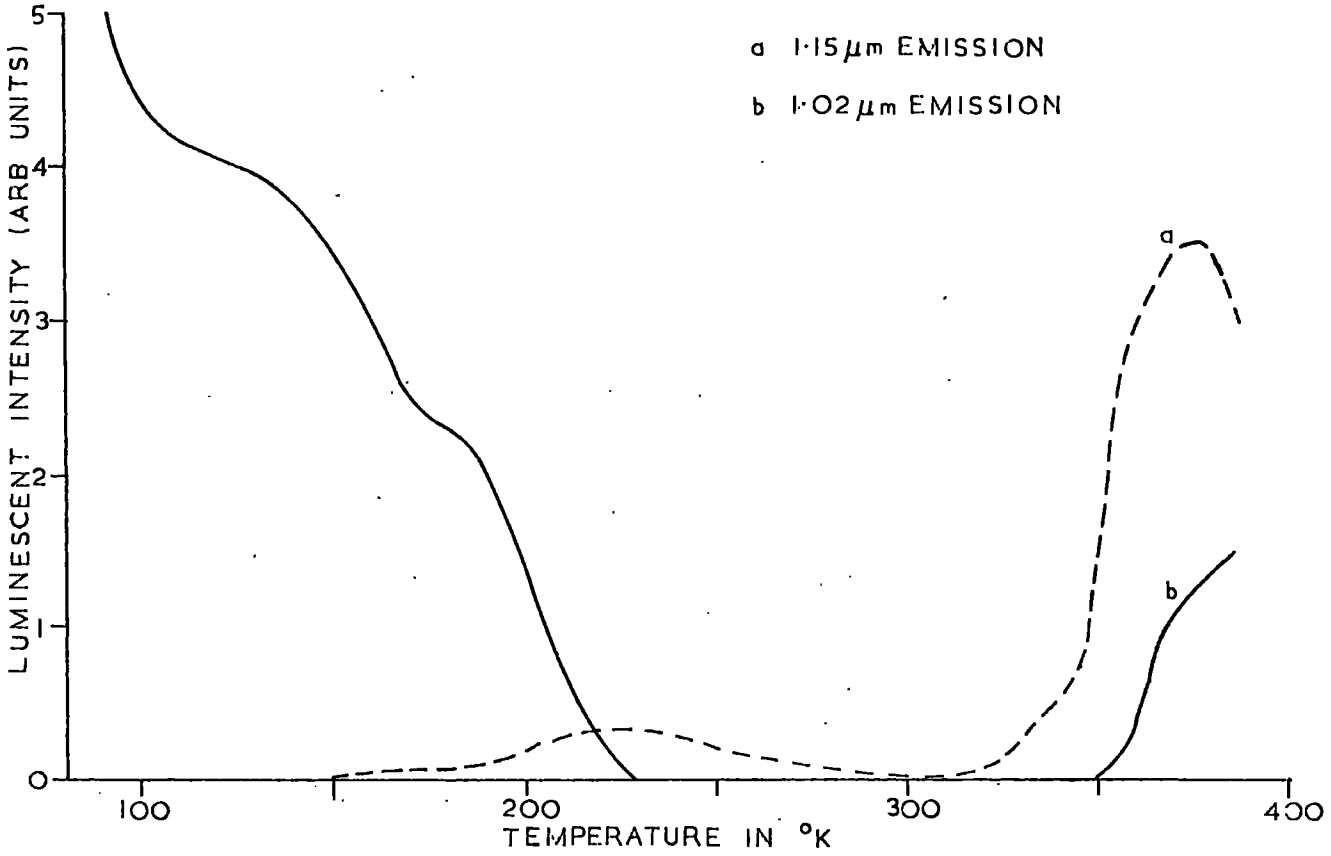

FIGURE 9.3.3. VARIATION OF THE 1·02μm AND 1·15μm EMISSIONS WITH TEMPERATURE, FOLLOWING THE COOLING OF A T_S= 50°C SAMPLE FROM 388°K IN THE DARK

irradiation and is shown in Figure 9.3.3 curve (b). The reason for making this second measurement was to investigate the possibility that the observation of the 1.02 μm peak after high temperature illumination and a 1.15 μm peak after low temperature illumination might result from a continuous shift of the emission maximum between two extrema depending on the condition of sensitisation of the sample. From Figure 9.3.3 this is clearly not the case, partly because the decrease in the 1.15 μm emission does not correspond to the increase of the 1.02 μm emission, and in particular because both emissions are seen above 345°K.

The nature of the 1.15 μm emission is not clear, though from Figure 9.3.3 it can be seen to occur at low temperatures where the sample is in its less sensitive state, and also above 345°K where thermal quenching of photocurrent usually occurs. The 1.02 μm emission also increases above 345°K and so the two emissions may be associated with each other in some way.

9.4. I.R.L. from Photoconducting Derby Material

The photoconductive properties of two boule crystals, grown from Derby Luminescent starting powder, have been shown to differ considerably from those of samples taken from boule crystals grown from Optran material. The luminescent spectra obtained from these two samples also reflect these differences.

The sample grown with T_{Cd} = 450°C showed a single I.R.L. maximum at 2.07 μm. The green edge emission from this sample, when excited with blue and ultraviolet light, was easily detected with the PbS cell and was the most intense of all the samples investigated.

The I.R.L. from the sample grown with T_S = 350°C is shown in Figure 9.4.1. Here curve (a) was monitored after the sample had been cooled under illumination from 388°K and curve (b) where the I.R.L. was measured following cooling of the sample from 388°K in the dark. The emission spectrum differs from that seen in sulphur rich Optran material because the 0.70 μm peak was not observed in these samples. Also two shoulders can be seen on either side of the 1.02 μm maximum, at approximately 1.15 μm and 0.87 μm. The 1.15 μm emission was also observed in the sample from which the curves in Figure 9.3.1 were obtained, though the 0.87 μm peak was not observed in any other sample investigated.

The observation of a single I.R.L. maximum in the Derby sample grown with T_{Cd} = 450°C and a luminescent spectrum containing all the emission maxima (seen in Optran samples) plus an additional peak centred on 0.87 μm for the Derby sample grown with T_S = 350°C is difficult to explain. The data for the sulphur rich sample suggests that the same luminescent centres occur in this sample as for Optran material. The cadmium rich Derby sample showed none of the usual emission bands from 0.70 μm to 2.00 μm, so that in this case it may be tentatively concluded that impurities in the starting material create non-radiative recombination paths.

9.5. I.R.L. from Conducting and Lightly Doped Samples

A number of samples taken from boule crystals were found to be semi-conducting and not photoconductive so that they were not amenable to the measurements described in earlier chapters, however their luminescent properties could be studied.

The cadmium rich samples showed very similar I.R.L. to that observed in photoconducting Optran samples grown in a similar way.

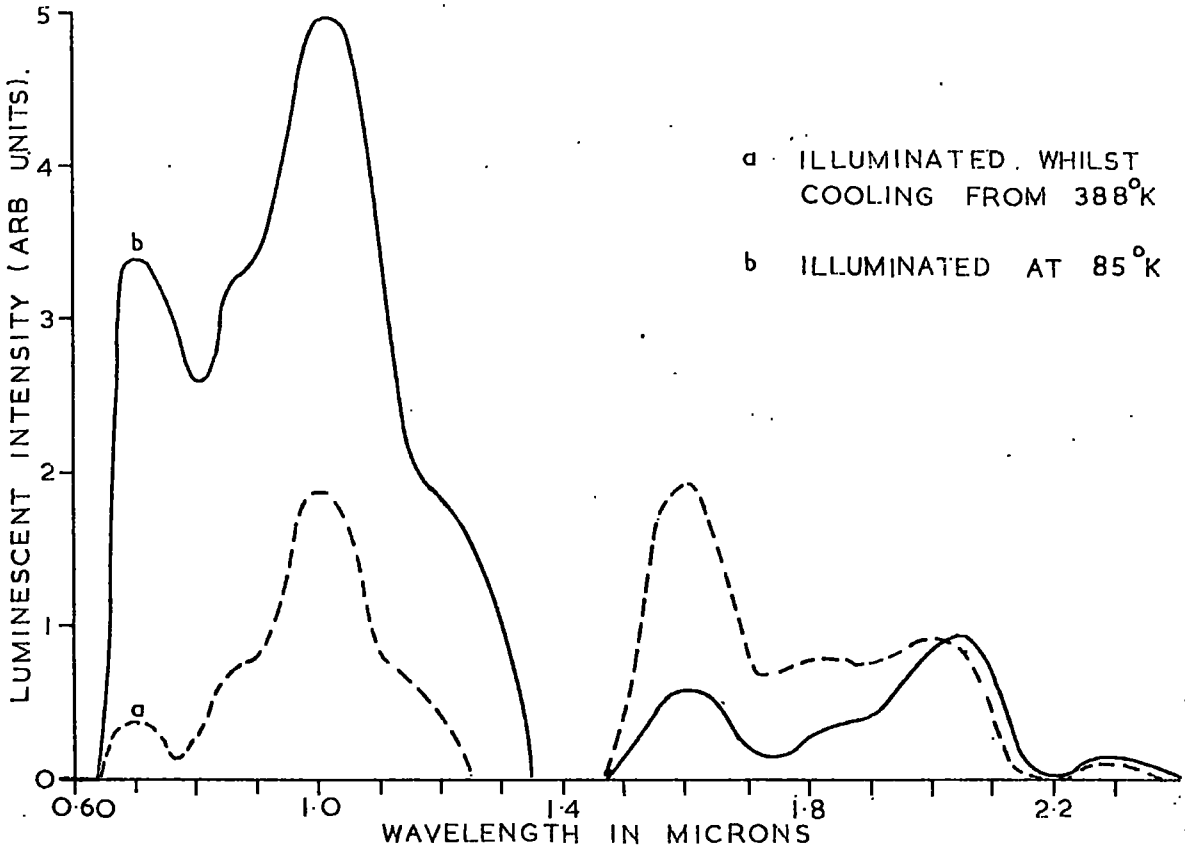

FIGURE 9.4.1 INFRARED LUMINESCENCE AT 85°K FROM A DERBY LUMINESCENT SAMPLE GROWN WITH $T_S = 350°C$

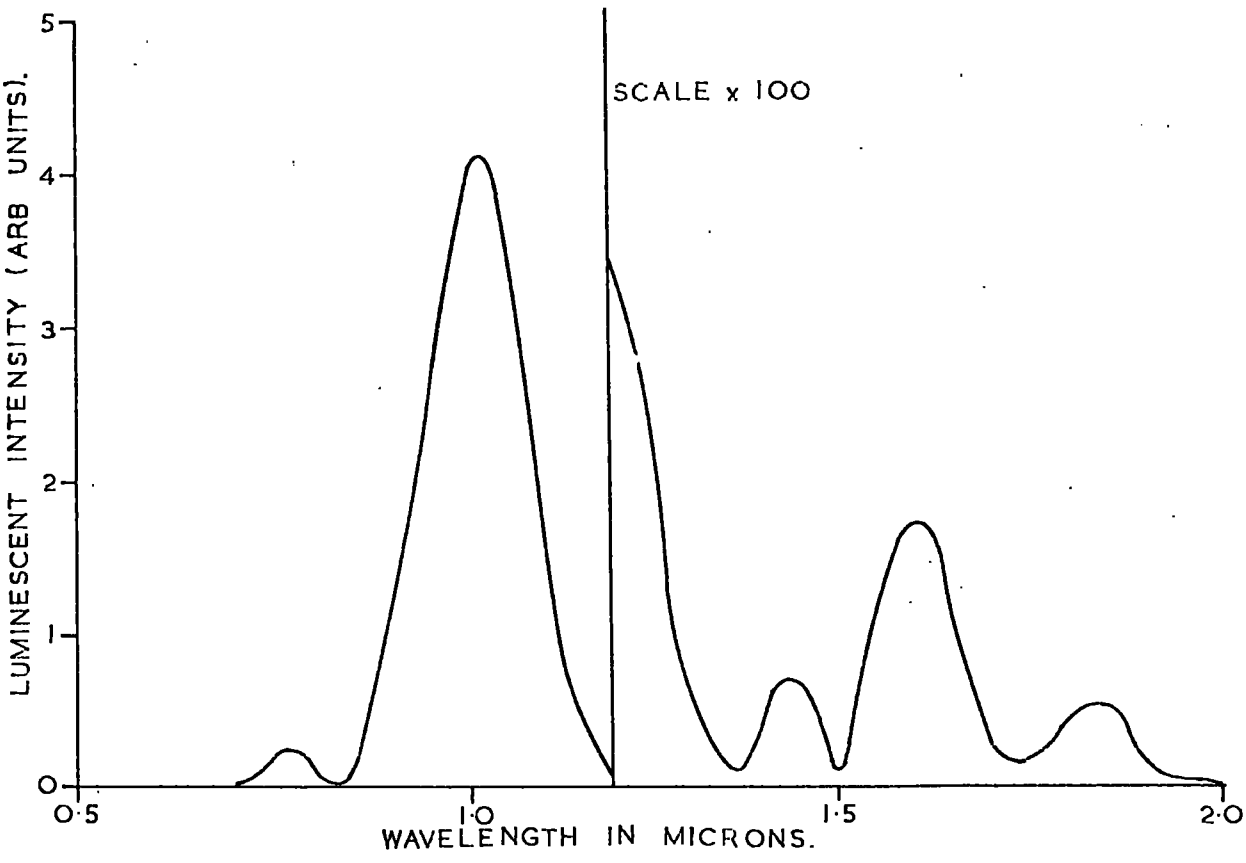

FIGURE 9.5.1. INFRARED LUMINESCENCE AT 85°K FOR A COPPER DOPED SAMPLE GROWN WITH $T_{Cd} = 650°C$ FOLLOWING ILLUMINATION FROM 388°K

Some variation was found in the maximum near to 0.70 μm. This was observed to vary between 0.70 μm and 0.76 μm. The '0.70 μm' emission was again quenched above room temperature, and in most cases there was a corresponding increase in the 1.02 μm emission.

One semi-conducting sample grown with T_S = 450°C showed a maximum at 0.76 μm together with the 1.02 μm and structured emissions. The 0.76 μm emission was more intense than the 1.02 1.02 μm peak by more than an order of magnitude, and was quenched above room temperature with a thermal activation energy of 0.57 eV.

The thermal quenching of the structured luminescence of the semi-conducting samples gave the thermal activation energy in the region of 0.1 eV.

In addition, five lightly doped samples were studied. Two of these were doped with copper and grown with T_S = 350°C and T_{Cd} = 650°C, while two others were doped with chlorine under the same growth conditions as the copper doped samples. The copper doping was achieved by the addition of approximately 0.5 mgm of Cu_2S to the charge of the growth tube, and chlorine was added by placing 0.3 mgm of $CdCl_2$ with the charge. An antimony doped sample was also studied, and was grown with T_{Cd} = 650°C, and 20 mgm of antimony was introduced into the tail before growth.

Mass spectrographic analysis indicated that copper was introduced in concentrations of approximately 0.2 p.p.m. and chlorine in concentrations of approximately 1 p.p.m. The antimony sample was doped to a level of 1.2 p.p.m. with antimony. These impurity concentrations were similar to those found in the Optran starting material.

In all cases, the 1.02 μm emission appeared together with the

the structured luminescence, though the 0.70 μm emission was not observed in the chlorine doped cadmium rich sample. The 0.70 μm luminescence was quenched above room temperature in all samples where it could be detected, and was accompanied by an increase in the 1.02 μm emission maximum. No significant trend could be seen in the intensity of the I.R.L. with conditions of growth. The copper doped sample grown in cadmium rich conditions did, however, show an additional luminescence maximum at approximately 1.43 μm, as may be seen in Figure 9.5.1. The emission at 1.43 μm was only observed when the sample was cooled under illumination from 388°K, though the other maxima were of similar intensity for both illumination from 388°K and illumination at 85°K only.

9.6. Discussion

During the course of the present work, two main emission maxima have been observed in the region of 0.70 μm and 1.02 μm, together with a structured luminescence in the region 1.60 μm to 2.00 μm. Additional luminescent peaks were seen in some samples at 0.87 μm, 1.15 μm and 1.43 μm, and a structured luminescence which occurred in the region 2.00 μm to 2.50 μm (this has been described as a replica of the 1.60 μm to 2.00 μm structure). Emission spectra similar to that shown in Figure 9.2.1 have been observed by many workers and analogous emission is seen in ZnS, with a shift of each of the peak maxima to shorter wavelengths.

In the cadmium rich (Optran) photoconducting samples, where the 0.70 μm and 1.02 μm emissions occurred together, the 0.70 μm emission was quenched above room temperature. The thermal activation energy for quenching of the 0.70 μm peak was found to be close to a value of 0.57 eV. In a number of samples the 1.02 μm emission increased in intensity as the 0.70 μm emission

was quenched. In contrast, the sulphur rich photoconducting samples did not show the 0.70 μm peak.

Cox et al. (1968) have discussed the 0.70 μm and 1.02 μm emissions in CdS, and the analogous 'copper blue' and 'copper green' emissions in ZnS, and interpreted these in terms of electron recombination at cation vacancies. They proposed that the 0.70 μm emission resulted from an electron, in an excited state of the centre, recombining with the ground state of a singly negatively charged cadmium vacancy (V'_{Cd}). The 1.02 μm emission occurs when an electron in an excited state of a doubly negatively charged cadmium vacancy (V''_{Cd}) recombines at the ground state.

The fact that the 0.70 μm emission is quenched where the 1.02 μm emission increases in intensity is qualitatively in agreement with the model proposed by Cox et al. If the 0.70 μm emission occurs at a V'_{Cd} and the 1.02 μm at a V''_{Cd} centre, then quenching of the 0.70 μm emission would convert the V'_{Cd} to V''_{Cd} with an increase in the 1.02 μm emission.

The Class 11_a sensitising centre may be associated with a V'_{Cd} when filled with an electron. Although photoconductivity measurements indicated two main levels (Class 11_a and Class 11_b in Figure 8.1.1) Cox et al. showed that such a centre should comprise a number of levels. The 0.70 μm band could result from electron recombination at one of these levels which was not observed during photoconductivity measurements. (The quenching of the 0.70 μm emission (0.57 eV) does not correspond to the calculated thermal separation from the valence band of either the Class 11_a (0.85 eV) or the Class 11_b (0.16 eV to 0.27 eV)).

The 0.70 μm emission was not detected in sulphur rich photoconducting Optran samples. This might result from the lesser

occupancy of the Class 11_a centres by electrons, though intuitively one would expect a greater density of cadmium vacancies in sulphur rich samples. One possible explanation is that the 0.70 μm emission occurs when electrons from the shallow trap, observed with a thermal activation energy of 0.15 eV by T.S.C. measurement, recombine at a level in a neutrally charged cadmium vacancy. This trap, which yielded a T.S.C. maximum at approximately 115°K, was associated with cadmium interstitials (see Section 5.12) and was some four orders of magnitude greater in density in cadmium rich samples compared with sulphur rich samples.

The structured luminescence was observed in all but one of the samples investigated, and the similarity of the thermal quenching of the two major peaks suggests that it is the result of three associated transitions. It has been proposed by a number of workers that the structured luminescence is associated with copper impurities, as the intensity of the emission increases with the addition of copper.

For the analogous emission in ZnS, Broser et al. (1965) attributed the luminescence to internal transitions of a $(3d)^9$ configuration of copper ions, and Broser and Franke (1965) showed that the luminescence increased with time following irradiation of ZnS with neutrons. Broser and Franke interpreted the increase in the intensity of the structured luminescence in terms of the increase of ^{65}Cu ions on zinc sites, as the ^{65}Cu isotope is the decay product of the ^{65}Zn created during neutron bombardment.

It has been demonstrated by Cox et al. (1968) that 98% of the transitions from ^{65}Zn to ^{65}Cu involve energies sufficient to displace the ^{65}Cu to an interstitial site. Thus the final product of the decay could be a zinc vacancy and a copper

interstitial, or an interstitial copper-vacancy defect centre, as well as the simpler explanation given by Broser and Franke. The work of Cox et al. suggests that the luminescent decay time is commensurate with the structured luminescence resulting from recombination of electrons from a level in a V'_{Cd} centre with holes in the valence band.

The thermal quenching of the structured luminescence is difficult to explain in terms of either of the above models, as the activation energy of the quenching process is comparatively small and broadly similar for all the samples investigated.

The increase in the intensity of the structured luminescence, which was accompanied by an increase in the free electron lifetime, has been discussed in Section 9.3. The results indicate that the structured luminescence occurs when electrons from the Class 11_a centres recombine with holes in the upper branches of the valence band. The ratio of the thermal and optical positions of the Class 11_a centres (above the valence band) suggest that the Class 11_a centres are approximately singly negatively charged when filled with electrons. They could therefore be levels in a V'_{Cd} which would agree with the proposal of Cox et al.

The 'replica' emission (of the 1.60 μm to 2.00 μm emission), which occurred in the region of 2.00 μm to 2.5 μm, has been reported by Bryant and Cox (1966) and was only seen in two samples. The thermal quenching of the emission maxima at 2.12 μm and 2.33 μm were not similar, as is the case for the 1.60 μm and 1.83 μm maxima observed in the structured luminescence. This therefore casts some doubt on the similarity of the recombination mechansims of the structured luminescence and its replica, which was suggested by Bryant and Cox.

References to Chapter 9

Birman, J.L., 1959, Phys. Rev. 115, 1493.

Birman, J.L., 1959, Phys. Rev. Letters 2, 157.

Broser, I. and K.H. Franke, 1965, J. Phys. Chem. Solids, 26, 1013.

Broser, I., H. Maier and H.J. Schulz, 1965, Phys. Rev. 140, A2135.

Browne, P.F., 1956, J. Electron. 2, 1.

Bryant, F.J. and A.F.J. Cox, 1966, Phys. Stat. Sol. 14, 427.

Cowell, T.A.T. and J. Woods, 1967, Phys. Stat. Sol. 24, K37.

Cox, A.F.J., W.E. Hagston and C.J. Radford, J.Phys. C. (Proc. Phys. Soc.) Series 2, 1, 1746.

Thomas, D.G. and J.J. Hopfield, 1959, Phys. Rev. 116, 573.

CHAPTER 10

CONCLUSION

10.1. Introduction

It has been demonstrated in this thesis that the properties of samples grown in excess cadmium are significantly different from those of samples grown in excess sulphur. In addition, it has also been shown that where the relatively impure Derby Luminescent Grade material was used to grow boule crystals, their photoconductive and luminescent properties were anomalous by comparison with boules grown from the purer Optran starting powder.

10.2. Thermally Stimulated Current Measurements

The crystals examined contained up to eight discrete electron traps, with thermal activation energies of 0.15, 0.16, 0.18, 0.31, 0.44, 0.53, 0.60 and 0.75 eV. Comparison of trap depths calculated on the assumption of monomolecular recombination and by Bube's method (Bube 1955) suggests that the traps with activation energies of 0.44, 0.53 and 0.60 eV empty under fast retrapping conditions. The 0.60 eV trap also exhibited a change in the position of the temperature maximum of the T.S.C. curve, which is to be expected for a fast trap.

The density of the 0.15 eV trap decreased by four orders of magnitude with inceasing sulphur pressure during growth. Boyn (1968) observed two absorption bands in samples heat treated in cadmium, which were not observed in samples annealed in sulphur. The two bands, at energies of 0.32 eV and 0.4 eV, were attributed to singly ionised cadmium interstitials. Arkad'eva (1964) reported the observation of a trap, which yielded a thermal

activation energy of 0.18 eV, from T.S.C. measurements, and an optical trap depth of 0.32 eV. Arkad'eva's optical trap depth and Boyn's lower energy absorption band have the same energy. The activation energy of 0.15 eV, found for the present trap, is similar to Arkad'eva's value of 0.18 eV. This suggests that the 0.15 eV trap is associated with singly ionised cadmium interstitials.

It has been shown that the magnitude and structure of T.S.C. curves can vary with the conditions of illumination prior to measurement. In some cases, the free electron lifetime can change in such a manner as to severely modify the observed T.S.C. spectrum. The two traps, with E_t = 0.53 eV and 0.60 eV, were associated with changes in the T.S.C. level which indicate that they are photochemically created. The 0.60 eV trap yielded a consistent variation of trap density with illumination conditions, from sample to sample, which led to an activation energy for creation of approximately 0.25 eV. The 0.53 eV trap varied in density in a comparatively few samples. Analysis yielded an activation energy of 0.32 eV for the creation of these traps, and an activation energy of 0.16 eV for their destruction.

Four probe T.S.C. measurements have been reported, which show that the three criteria, listed in Section 7.2, provide adequate protection against the inadvertent use of non-ohmic contacts. It should be noted, however, that some variation of the potential distribution along the samples was observed during four probe T.S.C. measurements, and so use of the four electrode arrangement should yield more accurate results.

Three probe studies indicated that the surfaces of the CdS samples did not significantly modify the structure of the T.S.C. spectrum, although the surfaces of cadmium rich samples appear to

be more highly conducting than those of sulphur rich samples. When deliberate attempts were made to damage the surface, by hydrogen ion bombardment and surface lapping, the T.S.C. structure was not affected, although the lapping treatment did increase the surface conductivity.

10.3. Spectral Response and Infrared Quenching of Photocurrent

The spectral response measurements showed that the cadmium rich samples were considerably more photosensitive than sulphur rich samples. The optical quenching has been interpreted in terms of a model containing two centres, which lie optically 0.28 eV and 1.2 eV above the valence band. The structure of the infrared quenching at liquid nitrogen temperatures was significantly different for cadmium rich samples than sulphur rich samples. This difference has been explained in terms of the position of the hole demarcation level for the shallow (0.28 eV) quenching centres. Calculations indicate that the thermal activation energy of the shallow centres lies between 0.16 and 0.27 eV.

From the position of the electron Fermi level at the onset of thermal quenching, a value of 0.85 eV has been calculated for the thermal activation energy of the upper Class 11 centres. The disparity between the optical (1.2 eV) and thermal (0.85 eV) separation of the upper Class 11 centres from the valence band suggests that they are neutrally charged when unoccupied by electrons, using the analysis proposed by Hoogenstraaten (1958). Such an observation is in agreement with Bube and Cardon (1964) who also concluded that the Class 11 centres were charge neutral.

The apparently anomalous measurements of the infrared quenching of thermoelectric power, reported by Lawrance and Bube (1968), can also be explained in terms of the present model for the

upper Class 11 centres. Under conditions of illumination which correspond to those used for the measurement of the infrared quenching of photocurrent, Lawrance and Bube observed an increase in the negative thermoelectric power. It might be expected that the thermoelectric power would become more positive, under infrared quenching conditions, due to the greater density of free holes. However, during optical quenching of the Class 11 centres described above, the centres will become negatively charged and so polarise the surrounding lattice. Lawrance and Bube also invoked polarisation effects to explain the phenomenon which they observed.

The spectral response due to the optical emptying of the traps, with thermal activation energies of 0.44, 0.51, 0.60 and 0.75 eV, were also studied. The ratio of thermal to optical trap depth for the 0.75 eV centre was unity. The other three traps yielded optical trap depths which indicated that they were positively charged, with effective charges lying between 0.6 and 1.

10.4. Infrared Luminescence

It is not possible to make a reliable assignment of the centres involved in all the luminescent transitions observed during the course of the present work. However, the structured luminescence, in the region 1.6 μm to 2.0 μm, can be explained in terms of radiative recombination of electrons from the sensitising Class 11 centres with holes in the valence band.

The difference between the thermal and optical positions of the upper Class 11 centres implies that the emission energy, for electrons from the Class 11 centres to the valence band, is considerably smaller than the optical energy required to fill the Class 11 centres with electrons. Calculations indicate that radiative recombination of electrons from the Class 11 centres

with holes in the valence band corresponds to an energy of approximately 0.6 eV. The lowest energy band in the structured luminescence occurs at about 2.0 μm (0.62 eV). It was also shown that the intensity of the structured luminescence increased when the free electron lifetime increased, i.e. when the occupancy of the Class 11 centres by electrons was greater. The similarity in the structure of the infrared quenching of photocurrent and the excitation spectrum for the structured luminescence is also consistent with this model.

10.5. Suggestions for Further Work

The four probe studies, described in Chapter 7, demonstrate that some variation of the potential distribution along a crystal occurred during T.S.C. measurements. Although there was no serious change in potential, greater accuracy would be obtained using the four probe configuration of electrodes.

The thermopower measurements made by Lawrance and Bube (1968) indicated that hole traps were present in the CdS crystals they studied, A more detailed appraisal on a range of samples, similar to that employed here, would be an obvious advantage for the understanding of the role that hole traps play during T.S.C. measurements,

A number of the samples taken for the present studies were found to be semi-conducting and were not amenable to electrical measurements of the type described in this thesis. Recently, Weisberg and Schade (1968) demonstrated that T.S.C. measurements can be made on p-n junctions and Schottky diodes fabricated on semi-conducting $GaAs_{0.5}P_{0.5}$. These measurements were made under constant reverse bias. The fabrication of p-n junctions from CdS

appears to be a fundamental impossibility, except by employing ion implantation techniques, due to autocompensation effects. However, Schottky diodes can be made by evaporating gold onto the surface of CdS samples (Goodman 1963). Semi-conducting CdS crystals are often annealed in sulphur to incease the resistivity and photosensitivity. The use of the Schottky-T.S.C. technique allows the measurement of trapping parameters without the introduction of other traps, which may occur during doping treatments used to increase the material resistivity.

References to Chapter 10

Arkad'eva, E.N., 1964, Sov. Phys. Solid State, 6, 798.

Boyn, R., 1968, Phys. Stat. Sol. 29, 307.

Bube, R.H. and F. Cardon, 1964, J. Appl. Phys. 35, 2712.

Goodman, A.M., 1963, J. Appl. Phys. 34, 329.

Hoogenstraaten, W., 1958, Thesis, University of Amsterdam, submitted February 1958.

Lawrance, R. and R.H. Bube, 1968, J. Appl. Phys. 39, 1807.

Weisberg, L.R. and H. Schade, 1968, J. Appl. Phys. 39, 5149.

APPENDIX 1

COMPUTOR PROGRAMME USED FOR T.S.C. CURVE FITTING

The following programme was used to generate theoretical points for T.S.C. curves under conditions of slow retrapping (IT1) (IT1), fast retrapping (IT2) and bimolecular recombination (IT3). The theoretical points were normalised to the experimental results using the measured values of the temperature maximum (TTS) and the current maximum (IMAX). The temperature, in ^{o}K, has been written as TT, and the trap depth, in eV, as EP.

```
//DAP 01(1601,68),M.A.CARTER
//EXEC NPL1FCLG
//SYSIN DD *
 TSC: PROCEDURE OPTIONS(MAIN);
 DCL (A,B,C,D,A1,B1,IT1,IT2,IT3,IMAX,TS,EP,T,K,TT,TTS) FLOAT;
 Q: GET LIST(N,M,IMAX,TTS);
 BEGIN; DCL AA(N) FLOAT;
 GET LIST(AA); PUT SKIP(3) DATA(TTS,IMAX); PUT SKIP(2);
 L: DO I=1 TO M BY 1;
 GET LIST(EP); PUT DATA(EP); PUT SKIP(2);
 LL: DO II=1 TO N BY 1;
 TT=AA(II);
 K=8.61E-05;
 T=EP/(K*TT); TS=EP/(K*TTS);
 B=EXP(TS)*TS**(2); D=EXP(TS)*TS**(7/2);
 B1=TS**(2)*EXP(TS)/((-3/(2*TS+3))+2*TS**(-1)-6*TS**(-2)
 +24*TS**(-3));
 A1=IMAX*TS**(3/2)*EXP(TS)*(1+B1*EXP(-TS)*TS**(-2)*(1-2*TS**(-1)
 +6*TS**(-2)-24*TS**(-3)));
```

```
A=IMAX*EXP(TS+B*EXP(-TS)*TS**(-2)*(1-2*TS**(-1)+6*TS**(-2)
-24*TS**(-3)));
C=IMAX*EXP(TS+D*EXP(-TS)*TS**(-7/2)*(1-7/2*TS**(-1)
+1.575E01*TS**(-2)-8.663E01*TS**(-3)));
IT1=A*EXP(-T-B*EXP(-T)*T**(-2)*(1-2*T**(-1)+6*T**(-2)
-24*T**(-3)));
IT2=C*EXP(-T-D*EXP(-T)*T**(-7/2)*(1-7/2*T**(-1)+1.575E01*T**(-2)
-8.663E01*T**(-3)));
IT3=A1*T**(-3/2)*EXP(-T)/(1+B1*EXP(-T)*T**(-2)*(1-2*T**(-1)
+6*T**(-2)-24*T**(-3)));
PUT DATA(TT,IT1,IT2,IT3); PUT SKIP(2); END LL;
PUT DATA(B,D,B1,A1,A,C); PUT SKIP(2): END L;
END;
GO TO Q;
END TSC;
/*
```

The data for each set of curves was presented in the following manner

```
//G. SYSIN DD *
 N,M,IMAX,TTS,
 TT1, ..... TTN,
 EP1, ..... EPM,
/*
```

N and M are integers, where N is the number of values of temperature, TT, and M is the number of values of trap depth, EP. Except for N and M, all data must be written in the form X.YZEUV, e.g. 12.1 = 1.21E01, and 0.121 = 1.21E-01.